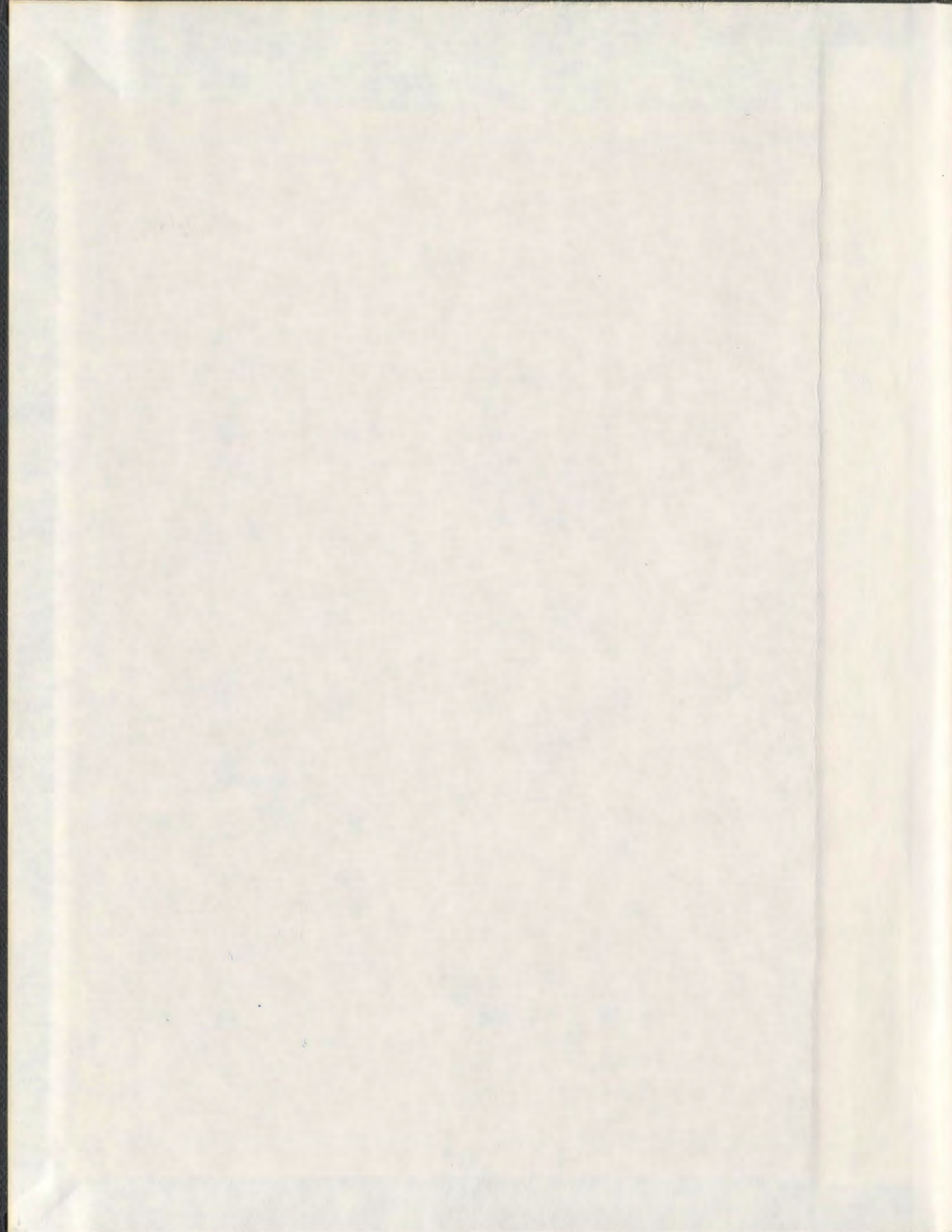


SEDIMENTARY RECORDS OF CLIMATEALLY
CONTROLLED RIVER AND SEDIMENT DISCHARGE
IN HUDSON BAY AND LABRADOR SINCE
10,000 YR BP

PETER HÜLSE



**SEDIMENTARY RECORDS OF
CLIMATICALLY CONTROLLED RIVER AND SEDIMENT DISCHARGE
IN HUDSON BAY AND LABRADOR SINCE 10,000 YR BP**

by

© Peter Hülse

A thesis submitted to the School of Graduate Studies
in partial fulfillment of the requirements for the degree of Philosophiae Doctor

Department of Earth Sciences

Memorial University of Newfoundland

October 2012

St. John's

Newfoundland

Abstract

In order to evaluate possible effects of climate change on freshwater discharge in northeastern Canada, and to place recently observed changes in freshwater discharge in an appropriate temporal and global framework of change, the sedimentary record offshore the Great Whale River (GWR) in Hudson Bay and in Nachvak and Saglek Fjords, Labrador, were analyzed in terms of climatic and river discharge proxies.

Results of AMS¹⁴C mass accumulation rates at the GWR suggest that a warming climate may lead to increasing water and sediment discharge. An inferred offshore shift in sediment deposition during the past ~150 yr (determined from ²¹⁰Pb and ¹³⁷Cs sediment radiochemistry) was related to a more energetic marine environment as a result of decreased sea-ice coverage and may already be a signal of global warming. Additionally, a fluctuation in the magnetic susceptibility (MS) record of 195–263 years is inferred to be a signal of terrestrial mineralogenic input related to variability in the hydrologic cycle. Overall, consistent TOC, TN, C/N, and δ¹³C values suggest that no major changes in paleoenvironmental processes controlling carbon and nitrogen burial conditions occurred during the past ~2000 yr.

The sediment cores from Nachvak and Saglek Fjords date to ~9,800 yr BC and ~5,400 yr BC, respectively. Ice-rafted debris contents implies a continuous net decrease in sea-ice cover until the end of the Holocene Thermal Maximum (~2,000 yr BC). After 2000 yr BC, sea-ice cover increased again during the Neoglacial cooling. This trend is accompanied by increasing productivity (determined from TOC, TN, TOC, and δ¹³C). These trends are likely related to orbitally-forced Milankovitch-scale variations in

insolation. Relatively low sedimentation during the Temperate Period, which was of supposedly high meltwater discharge, is inferred to the presence of glacial lakes, trapping sediment and rerouting freshwater discharge. Higher frequency variability in the MS record appears to be related to a solar forced ~1000 yr cyclicity and in Nachvak Fjord rates of input of terrestrial minerogenic matter appear to increase during warmer intervals relative to colder periods. This is interpreted as a sign of increased precipitation and river discharge during warm periods (the same trend like at the Great Whale River). Similar cyclicity is apparent in Saglek Fjord. Dating uncertainties, however, preclude precise correlations between the fjords or Labrador, and Hudson Bay. In Saglek Fjord, however, an increase in sediment accumulation rate (SAR) was recorded during the Little Ice Age (LIA) (the opposite trend to that of the Great Whale River). More detailed dating would improve the understanding of the ancient climate-river discharge interactions of NE Canada.

ACKNOWLEDGEMENTS

I would like to thank my supervisor Dr. Samuel J. Bentley for his guidance, support, and the chance to travel to spectacular places in Hudson Bay and Labrador. I thank Dr. Duncan McIlroy and Dr. Susan Ziegler for their scientific advice and for serving on my supervisory committee.

Further, I would like to thank the captains and crews of the CCGS Amundsen the CCGS Radisson, and the What's Happening for their help in the field in 2007 and 2009. Many thanks go to Erlangga Septama, Robin Haworth, Ryan Binder, Thomas Richerol, Lina Stolze, Kendra Carrigan, and Joey, Leo, and Dorothy Angnatok, who assisted during field- and laboratory work. Inside Memorial University of Newfoundland, I would like to thank Keir Hiscock for his help with any fieldwork related problems. I thank Michelle Miskell and Claudette Kennedy for their organizational support throughout my time as student at MUN. I would also like to thank the International Student Advising Office for their help with study permits.

Finally, I would like to thank my family, my father Dr. Knut Hülse, my mother Brigitte Hülse, and my brother Kristian Hülse for their advice, financial and mental support. Special thanks go to Elisabeth Kahlmeyer for her patience and mental support through all that time.

TABLE OF CONTENTS

Abstract	ii
Acknowledgements	iv
Table of Contents	v
List of Tables	xii
List of Figures	xiii
List of Appendices	xvi
Co-authorship statement	xviii

Chapter 1 – Introduction

1. Project Overview and Incentive	1 – 1
1.1 Background and overview	1 – 1
1.2 Current understanding of river discharge in the Hudson Bay Region	1 – 4
1.3 Funding	1 – 5
2. Study areas	1 – 7
2.1 The Great Whale River in Hudson Bay	1 – 7
2.2 Saglek and Nachvak Fjords in Northern Labrador	1 – 8
3. Objectives and Methods	1 – 10
References	1 – 12

**Chapter 2 – A ^{210}Pb sediment budget and granulometric record of sediment fluxes in
a subarctic deltaic system: the Great Whale River, Canada**

Abstract.....	2 – 1
1. Introduction.....	2 – 2
2. Regional setting.....	2 – 4
2.1 Deglacial and postglacial history.....	2 – 4
2.2 Drainage basin properties.....	2 – 5
2.3 Oceanographic setting.....	2 – 6
2.4 Sea-ice formation.....	2 – 7
2.5 Freshwater and sediment discharge.....	2 – 7
2.6 Marine basin physiography.....	2 – 8
3. Methods.....	2 – 10
3.1 Seafloor geomorphology and sample collection.....	2 – 10
3.2 Radiochemistry.....	2 – 11
3.3 Physical sedimentological properties.....	2 – 13
3.3.1 Granulometry.....	2 – 13
3.3.2 X-radiography.....	2 – 14
3.4 Sediment mass flux calculations.....	2 – 14
4. Results.....	2 – 15
4.1 Sediment and mass accumulation rates.....	2 – 15
4.2 Sediment discharge and dispersal.....	2 – 17
4.3 Physical sedimentological properties.....	2 – 19
4.3.1 Sedimentary structures.....	2 – 19

4.3.2 Granulometry.....	2 – 20
5. Discussion.....	2 – 21
5.1 Sediment and mass accumulation rates.....	2 – 21
5.2 Modern sediment mass fluxes / budget.....	2 – 24
5.3 Temporal sediment depositional patterns.....	2 – 26
6. Conclusion.....	2 – 29
Acknowledgements.....	2 – 31
References.....	2 – 31

Chapter 3 – Climatically controlled sediment and water discharge during the past two millennia: the subarctic Great Whale River, Hudson Bay, Canada

Abstract.....	3 – 1
1. Introduction.....	3 – 2
2. Study Area.....	3 – 5
2.1 Deglacial and postglacial history.....	3 – 5
2.2 Oceanographic setting and climate.....	3 – 5
2.3 Drainage basin geology.....	3 – 6
2.4 Marine sedimentary basin.....	3 – 7
3. Methods.....	3 – 7
3.1 Bathymetry, subsurface stratigraphy and core sampling.....	3 – 7
3.2 Radiocarbon analyses.....	3 – 8
3.3 River discharge estimates.....	3 – 10
3.4 Physical sedimentary properties.....	3 – 11

3.4.1 X-radiography.....	3 – 11
3.4.2 Granulometry.....	3 – 11
3.4.3 Magnetic susceptibility and bulk density.....	3 – 11
3.5 Sedimentary organic matter.....	3 – 12
4. Results.....	3 – 13
4.1 Subsurface stratigraphy and total fluvio-deltaic sediment thickness.....	3 – 13
4.2 Core lithology.....	3 – 13
4.3 Geochronology and sediment accumulation rates.....	3 – 15
4.4 Physical sediment properties.....	3 – 18
4.5 Magnetic susceptibility.....	3 – 20
4.6 Carbon and nitrogen geochemistry.....	3 – 22
5. Discussion.....	3 – 24
5.1 Total fluvio-deltaic sediment budget.....	3 – 24
5.2 Sediment mass flux variability since ~2000 yr BP.....	3 – 26
5.3 River discharge variability and global climatic change.....	3 – 27
5.4 Short term discharge variability and climatic forcings.....	3 – 28
5.4.1 Magnetic susceptibility – Short term variability in discharge and/or weathering.....	3 – 28
5.4.2 Climatic forcings of MS variabilities.....	3 – 30
5.4.3 Palaeo-environmental implications.....	3 – 31
6. Conclusion.....	3 – 32
Acknowledgements.....	3 – 33
References.....	3 – 34

**Chapter 4 – A sedimentary record of climatically forced Holocene river discharge in
NE-Canada: Saglek and Nachvak Fjords**

Abstract	4 – 1
1. Introduction	4 – 2
2. Study Area	4 – 5
2.1 Deglacial and postglacial history	4 – 5
2.2 Climate and oceanography	4 – 6
2.3 Basin properties Saglek Fjord	4 – 8
2.4 Basin Properties Nachvak Fjord	4 – 8
3. Methods	4 – 9
3.1 Core sampling	4 – 9
3.2 Laboratory methods	4 – 10
3.2.1 Radiocarbon analyses	4 – 10
3.2.2 Granulometry	4 – 11
3.2.3 X-radiography	4 – 11
3.2.4 Magnetic susceptibility and bulk density	4 – 12
3.2.5 Sedimentary organic matter	4 – 13
4. Results	4 – 13
4.1 Geochronology and sediment accumulation rates	4 – 13
4.2 Core lithology	4 – 18
4.3 Granulometry	4 – 20
4.4 Magnetic susceptibility and bulk density	4 – 21
4.5 Sedimentary organic matter	4 – 22

5. Discussion	4 – 25
5.1 Geochronology – Holocene sediment mass fluxes	4 – 25
5.2 Sedimentary textures – Holocene depositional environments and sea-ice variability	4 – 28
5.3 Magnetic susceptibility – Holocene climate and discharge variability	4 – 31
5.4 Sedimentary organic matter – Holocene environmental change	4 – 34
6. Conclusion	4 – 35
Acknowledgements	4 – 37
References	4 – 37

Chapter 5 – Summary

1. Review of objectives	5 – 1
2. Summary of methods	5 – 2
3. Summary of conclusions	5 – 3
3.1 Modern (<150 yr) sediment and river discharge at the Great Whale River, Hudson Bay	5 – 3
3.2 Ancient sediment and river discharge at the Great Whale River, Hudson Bay	5 – 4
3.3 Ancient sediment and river discharge in Nachvak and Saglek Fjords, NE-Labrador	5 – 5
4. Significance of research	5 – 7
5. Open questions and future directions	5 – 8

LIST OF TABLES

Chapter 2

Table 1 2 – 17

Summary of $^{210}\text{Pb}_{\text{XS}}$ and ^{137}Cs SARs and MARs, T_r , and L_b

Table 2 2 – 18

Sediment load and sediment bypass estimations (BQART-model)

Chapter 3

Table 1 3 – 16

a) ^{14}C calibration

b) ^{14}C apparent SARs and MARs

Chapter 4

Table 1 4 – 14

a) ^{14}C calibration

b) ^{14}C apparent SARs and MARs

LIST OF FIGURES

Chapter 1

Figure 1	1 – 9
Overview map of the study areas at the Great Whale River (GWR) in Hudson Bay and in Nachvak and Saglek Fjords, Labrador	

Chapter 2

Figure 1	2 – 6
Overview map of the GWR study area in Hudson Bay	
Figure 2	2 – 9
Detailed map displaying bathymetry, coring locations, and mass accumulation rates at the GWR	
Figure 3	2 – 16
Graphs displaying $^{210}\text{Pb}_{\text{XS}}$ and ^{137}Cs activities at the GWR	
Figure 4	2 – 19
X-radiographic images of box cores from the GWR	
Figure 5	2 – 21
Grain diameter frequencies for box and gravity cores from the GWR	
Figure 6	2 – 22
Mean grain diameter profiles for box and gravity cores at the GWR	
Figure 7	2 – 24

Cross correlations of SAR, MAR, mean grain diameter, $^{137}\text{Cs}/^{210}\text{Pb}_{\text{XS}}$ SAR,
distance to river mouth, and water depth

Figure 8 2 – 28

Down-core grain diameter frequency distributions for box and gravity cores
at the GWR

Chapter 3

Figure 1 3 – 4

Overview map of the Great Whale River (GWR) study area, Hudson Bay

Figure 2 3 – 14

Subbottom profiles from the GWR study area

Figure 3 3 – 15

^{14}C age-depth profiles of gravity cores from the GWR

Figure 4 3 – 17

Down-core profiles for SAR, MAR, M, Q_{S} , and Q

Figure 5 3 – 19

Physical properties and mean grain diameter for core RA09-GW-7-P10

Figure 6 3 – 20

Physical properties and mean grain diameter for core RA09-GW-5-P5

Figure 7 3 – 21

Physical properties and mean grain diameter for core RA09-GW-4-P3

Figure 8 3 – 24

Geochemical properties for gravity cores from the GWR

Chapter 4

Figure 1	4 – 3
Overview maps of the study areas in Nachvak and Saglek Fjords, Labrador	
Figure 2	4 – 15
¹⁴ C age-depth profiles of gravity cores from Nachvak and Saglek Fjords	
Figure 3	4 – 16
Physical sediment properties granulometry, SARs, and MARs of core	
AM09-PC-N-606	
Figure 4	4 – 17
Physical sediment properties granulometry, SARs, and MARs of core	
AM09-PC-S-618	
Figure 5	4 – 19
X-radiographic images for cores AM09-PC-N-606 and AM09-PC-S-618	
Figure 6	4 – 23
Geochemical properties for core AM09-PC-N-606	
Figure 7	4 – 24
Geochemical properties for core AM09-PC-S-618	

LIST OF APPENDICES

Appendix A	Appendix – 1
Radiochemistry data for box cores 2007 and gravity cores 2009, Hudson Bay	
Appendix B	Appendix – 10
Granulometric data for box cores 2007 and gravity cores 2009, Hudson Bay	
Appendix C	Appendix – 59
Physical sediment properties for gravity cores 2009, Hudson Bay	
Appendix D	Appendix – 90
Geochemical data for gravity cores 2009, Hudson Bay	
Appendix E	Appendix – 95
Subbottom profiles Hudson Bay	
Appendix F	Appendix – 98
X-radiographic images for gravity cores 2009, Hudson Bay	
Appendix G	Appendix – 102
Granulometric data for pistoncores 2009, Labrador	

Appendix H	Appendix – 111
Physical properties for piston cores 2009, Labrador	
Appendix I	Appendix – 197
Geochemistry data for piston cores 2009, Labrador	
Appendix J	Appendix – 202
X-radiographic images for piston cores 2009, Labrador	

CO-AUTHORSHIP STATEMENT

The following thesis chapters are presented in manuscript format. Chapters 2, 3, and 4 have been developed in collaboration between me (the author of this thesis) and others. As the author of this thesis, the work is predominantly my own, with guidance from my supervisor and co-author Dr. Samuel J. Bentley.

Chapters 2 and 3 evaluate marine records of Late Holocene fluvial sediment supply to a fluvio-deltaic system in eastern Hudson Bay. Sample collection was performed during two fieldworks in the summers of 2007 (four weeks) and 2009 (two weeks). It was undertaken by me and my supervisor Dr. Samuel J. Bentley in 2007, and by me and Erlangga Septama in 2009. Chapter 2 has been reviewed, revised, and resubmitted to Estuarine, Coastal, Shelf Sciences.

Chapter 4 evaluates marine records of Holocene fluvial sediment supply to two fjords in northern Labrador. Sample collection was performed during one fieldwork in autumn 2009 (two weeks). It was undertaken by me and my supervisor Dr. Samuel J. Bentley.

All of the authors were involved in the logistics and planning of the field season. As the primary author of these manuscripts, I performed all data collection and analytical work for this project. My supervisor Dr. Samuel J. Bentley provided guidance and editorial comments. Funding for this work was provided in the form of a grant from ArcticNet, a Network of Centres of Excellence of Canada, to Dr. Samuel Bentley, with additional support from the Canada Research Chair Secretariat, the Canada Foundation for Innovation, Memorial University of Newfoundland, and the Harrison Chair in Sedimentary Geology at Louisiana State University.

Chapter 1

Introduction

This Ph.D. thesis is written in manuscript format. It is subdivided into five chapters. Chapter 1 provides the context for the dissertation research. This will be accomplished by giving a review on research background to date, an outline of the dissertation objectives, and a brief review of the study areas. Chapters 2 to 4 are written as research papers and present the research completed as part of my Ph.D. thesis. Each research paper includes an introduction to the study areas, objectives and methods, a description of results, a discussion and conclusions. Chapter 5 summarizes the conclusions, discusses their significance and outlines objectives to future work.

1. Project Overview and Incentive

1.1 Background and overview

As summarized in the Arctic Climate Impact Assessment (ACIA, 2005), the Arctic is the region of the globe that will be impacted first and most severely by the present warming of Earth's lower atmosphere. Many of the symptoms of a warming Arctic anticipated by climate models are already verified by observations on land, at sea and from space. Rising surface temperatures lead to: 1) a decreasing thickness and duration of the snow cover; 2) a warming and thawing of the permafrost; 3) and increasing storminess and precipitation (e.g., Curtis et al., 1998; Stieglitz et al., 2003).

General circulation models forecast that the Hudson Bay Basin (HBB) (including northern Labrador, Fig. 1) and its surroundings will experience some of the more dramatic environmental changes in the coming century (Gagnon and Gough, 2005). Furthermore, HBB is expected to be affected sooner and more strongly by the consequences of climate change than the Arctic Ocean due to its close association with terrestrial systems (Gough and Wolfe, 2001; ACIA, 2005; Gagnon and Gough, 2005).

Recent studies on freshwater discharge discovered a 13 % (96 km^3) decrease in the total annual freshwater discharge into the HBB between 1964 and 2000 (Déry et al., 2005). Further, annual peak discharges from snowmelt advanced by 8 days during this period and decreased by $0.036 \text{ km}^3 \text{d}^{-1}$ in intensity. More recent evaluations, however, suggest greater variability and question the existence of a real decrease in river runoff (Déry, 2008). A strong anticorrelation between the Arctic Oscillation and Hudson Bay Basins fluvial discharge, suggests that the observed variability in river discharge is driven by large-scale atmospheric anomalies (Déry and Wood, 2004). There is a close inter-relationship between climate, land use, vegetation cover density and erosion rates. The response of the hydrologic cycle to climate change will depend on the duration of the climatic fluctuation, the variability in spatial properties such as relief, geology, and hydrological processes (Syvitski, 2003). Variations in river discharge have implications for the transport of nutrients, sediments and other trace species, such as pollutants, to high-latitude oceans (Anderson et al., 2004), sea-ice formation, marine salinity (Saucier et al., 2004), and thermohaline circulation (Aagaard and Carmack, 1989). Déry et al. (2005) suggested that variations and trends in precipitation, snowcover, and thus river runoff into HBB may play a key role in governing the state of the upper layers of the Arctic Ocean

and northwestern Atlantic Ocean. Since the HBB is the most southerly extension of the Arctic Ocean, and contributes with 30 % to the total Canadian runoff (ACIA, 2005; Déry et al., 2005), it is of great importance to understand, how HBB watersheds may respond to global climatic changes. This can be accomplished by understanding past responses of freshwater and sediment discharge to global climatic change and will improve the understanding, detection and projection of already ongoing climate change consequences in HBB and its surrounding terrestrial systems (Johannessen et al., 2004; Déry et al., 2005; Gagnon and Gough, 2005; Lawrence and Slater, 2005).

The Arctic may be the only terrestrial region where the effects of climate change dominate over direct human effects because human impact still is relatively low. The evaluation of hydro-ecological sensitivity including the study of climate change and associated impacts on water resources of northern areas in Canada is complicated by poor spatial distribution and short length-of-record of hydrometric monitoring stations (Prowse, 1990). A clear understanding of past climatic and hydrologic conditions is therefore a fundamental requirement, if we are to understand present conditions and to prepare for potentially adverse affects of future changes. The best places to study such conditions are fluvially-derived marine sedimentary archives, since the variations in river runoff can be reflected by the amount and type of sediment transported to the ocean (Syvitski et al., 2003). Because river runoff is controlled by processes in the atmosphere and the land surface, such as air temperature, precipitation, snowcover, or permafrost (Déry et al., 2005), changes in river runoff are sensitive indicators for changes in climate and are recorded in the fluvial sediments accumulated in marine basins (Syvitski and Shaw, 1995). Nearshore marine basins reflect variations in both the marine and the

terrestrial environment, and are thus especially suitable for paleoclimatic and palaeoenvironmental reconstructions (Karageorgis et al., 2005).

Two such localities are: 1) a sedimentary basin offshore of the Great Whale River at the eastern coast of Hudson Bay and 2) Saglek and Nachvak Fjords in northern Labrador. These basins are closely associated to terrestrial riverine sources and hold valuable sedimentary records, which were exploited on past climate-discharge conditions in my Ph.D.-project.

This Ph.D. thesis contributes to a better understanding of: 1) sediment dispersal in high-latitude coastal systems; 2) the expression of modern climatic conditions in the marine sedimentary record; 3) the effects of historical climatic changes on freshwater runoff recorded in marine sediments at chosen key localities in Hudson Bay and northern Labrador. This is important because predicted warming in the HBB and surrounding watersheds may alter the amount and timing of runoff and thus the load of suspended solids, dissolved organic matter and other major nutrients, and heat delivered to the marine system (ArcticNet, 2010). Ultimately, this will help to place recently observed variations in freshwater discharge into a historical framework of global climatic change.

1.2 Current understanding of climate change and river discharge in the Hudson Bay Region

Recent studies of the Hudson Bay watershed in northern Canada have shown that modern export of freshwater into Hudson Bay is highly variable, possibly decreasing, and strongly influenced by climatic forcing (Déry and Wood, 2004; Déry et al., 2005). This suggests that global climatic variations have an impact on river discharge into Hudson

Bay. Much effort has been placed on the paleoenvironmental reconstruction of large scale climate changes during the transition from the last glacial period to the Holocene of the subarctic Hudson Bay system (Barber et al., 1999; Hall et al., 2001; Alley and Ágústsdóttir, 2005; Lajeunesse and St-Onge, 2008; Haberzettl et al., 2010). Over shorter timescales studies have included environmental records spanning the last century (Hare et al., 2008; Kuzyk et al., 2010), to several millennia (Gonthier et al., 1993; Jenner and Piper, 2002; Haberzettl et al., 2010). These millennial-scale studies have suggested the potential for sub-century-scale paleoenvironmental preservation at the Great Whale River, but did not attempt to resolve environmental patterns within the strong climatic variations from the Medieval Warm Period to the Little Ice Age to the present.

Studies on climatic variations in northern Labrador are few. Most studies concentrated on larger scale climatic variations, such as the last deglaciation (e.g., Evans and Rogerson, 1986; Bell et al., 1988; Jansson, 2003; Carlson et al., 2007). High-resolution data relating to freshwater discharge variations from the marine sedimentary record on sub-millennial timescales are lacking completely. However, the central basins of Nachvak and Saglek Fjords are excellent traps for postglacial fluvio-marine sediments with temporal resolutions of in the order of decades (Bentley and Kahlmeyer, 2012). Thus, the sediments in these two fjords provide an excellent archive for paleo-discharge patterns of centennial to decadal timescale.

1.3 Funding

This Ph.D. project is funded by ArcticNet, Memorial University of Newfoundland, the Canada Foundation for Innovation, and funds granted to Samuel J. Bentley by the

Lousiana State University. ArcticNet is supported by the Government of Canada through the Networks of Centres of Excellence programs, a joint initiative of the Natural Sciences and Engineering Research Council, the Canadian Institutes of Health Research, the Social Sciences and Humanities Research Council and Industry Canada (ArcticNet, 2010). The aim of the Networks of Centres of Excellence is to turn Canadian research and entrepreneurial talent into economic and social benefits for all Canadians (ArcticNet, 2010). ArcticNet projects are grouped into Integrated Regional Impact Studies (IRIS) according to geographical areas in Canada. This Ph.D. project spans both IRIS 3 and IRIS 4. The following overview on the sites IRIS 3 and IRIS 4 is summarized from ArcticNet (2008; 2010).

IRIS 3 focuses on Hudson Bay. The large freshwater input into Hudson Bay is one of the key features that make this region particularly significant. The Hudson Bay watershed is the largest in the country, stretching in the north from Nunavut and Northwest Territories to Minnesota, North Dakota, South Dakota and Montana in the south. The Nelson River in Manitoba and the Great Whale River in Québec are the two major fresh waterways into Hudson Bay. Annual average air temperature around the Bay is heavily influenced by the presence of ice. Temperatures in January range between -16°C and -27°C. Summer temperatures range in the mid to high single digits. The Bay is generally ice-free from mid to late August until late October. Ice fills the Bay by January and remains mainly frozen until May. Precipitation in the region can range from as much as 600-800 mm annually in the southern areas to 200-400 mm in the northern extremes of the Bay. Warmer average annual temperatures in association with later freeze-ups and earlier melting of the ice in Hudson Bay have been recorded in the recent past and will

have implications on all physical systems within the Bay. The Hudson Bay coastal area is known to be a large store of methane, an effective greenhouse gas. Warmer temperatures in the region have allowed a portion of the permafrost layer to begin to melt, not only allowing for the release of methane, but also the deterioration of social infrastructure and natural habitat.

IRIS 4 is focused on Canada's Eastern sub-Arctic including the Inuit territories of Nunavik (northern Quebec) and Nunatsiavut (northern Labrador). Geographically IRIS 4 is bound by Hudson Bay to the west, Hudson Strait and Ungava Bay to the north, and the Labrador Sea to the east. The climate of this area is continental with high precipitation (mainly snow). It is expected to warm by 3-4 °C and have precipitation increase by 10 to 25% by the middle of the century (ArcticNet, 2008).

2. Study areas

2.1 The Great Whale River in Hudson Bay

The field locality in Hudson Bay is the Great Whale River at Hudson Bay's eastern coast (Fig. 1). The Great Whale River was chosen due to its pristine environment and because it is statistically representative of eastern Hudson Bay in terms of river discharge trends in the Hudson Bay Region (Déry et al., 2005). Further, the Great Whale River has a marine sedimentary basin offshore from the river mouth on the southeastern coast of Hudson Bay. Deposition in the sedimentary basin includes fluvio-deltaic muds averaging 16 m in thickness with decadal-scale resolution potential (Gonthier et al., 1993; this study) which will provide an archive of undisturbed river runoff history into the Hudson Bay.

2.2 Saglek and Nachvak Fjords in northern Labrador

In northern Labrador, Nachvak and Saglek Fjords (Fig. 1) were chosen due to their pristine environments and deep marine basins providing excellent archives for paleoenvironmental studies. Further, a modern sediment budget is available for these fjords (Bentley and Kahlmeyer, 2012), providing a baseline for the paleoenvironmental studies central to this Ph.D. thesis. Compared to the Great Whale River in the central part of the Hudson Bay Region, Saglek and Nachvak Fjords sit in the northeastern part of the Hudson Bay Region. Comparison between these two study areas will help to elucidate if observed patterns are of local character, or regional trends that can be traced across the Quebec-Labrador Peninsula.

The mouth of Saglek Fjord is located at approximately 58.58° N, 62.78° W, 230 km north of Nain, Labrador. Saglek Fjord is well protected from oceanic influences by a relatively shallow sill at -95 m water depth (this study). A major source of sediment to Saglek Fjord is Nachvak Brook, an un-glaciated catchment of 809 km² size. Sediment accumulation in Nachvak Fjord was estimated to 39,000 t/yr (Bentley and Kahlmeyer, 2012).

The mouth of Nachvak Fjord is located at approximately 59.10° N, 63.40° W, 300 km north of Nain, Labrador. The main basin of Nachvak Fjord receives 43,000 t/yr of sediment. Most of its sediments come from the glacierized McCornick River catchment (77 km²). In comparison to the marine basin of Saglek Fjord, the marine basin of Nachvak Fjord lacks a distinct separation from the basin seaward of the basin studied due to a relatively deep sill at -175 m (this study).

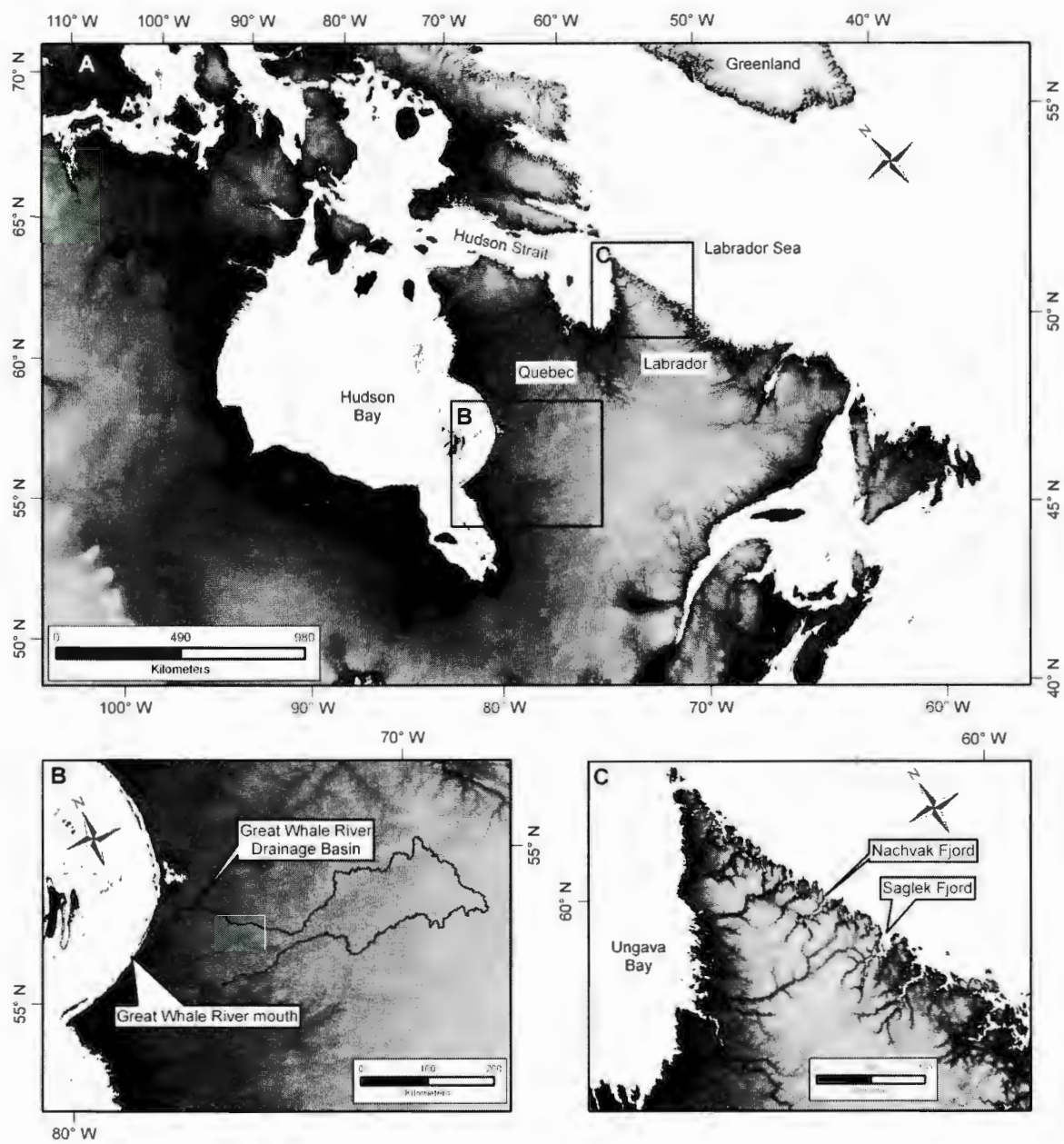


Figure 1: Map A displays the locations of the Hudson Bay and Labrador study areas. Map B displays the location of the study area at the Great Whale River mouth and the Great Whale River drainage basin at the eastern coast of Hudson Bay. Map C displays the locations of Nachvak and Saglek Fjords in northern Labrador.

3. Objectives and methods

The goal of this Ph.D. project was to use marine sedimentary records to determine the roles of climate change on freshwater discharge into Hudson Bay and the Labrador Fjords. This objective was accomplished by placing recent climate process and changes in freshwater discharge in an appropriate temporal and global framework of global climatic change, by addressing as follows:

Modern sediment discharge, dispersal, and deposition:

In the course of this study, sediment dispersal processes were studied at the Great Whale River study site, because there is a knowledge gap in the sediment dispersal patterns of higher latitude sediment dispersal systems due to their remoteness, relative to much better understood marine dispersal systems from lower latitudes. It was hypothesized, that cold periods will result in lower water and sediment discharge, but more deposition closer to the river mouth, whereas warm periods will result in greater water and sediment discharge, but perhaps greater wave mixing, resulting in broader dispersal of sediment, even if sea-ice cover is still complete at the time of spring floods (e.g. Wright and Nittrouer, 1995).

As a first step, the relation between modern climatic conditions, freshwater discharge and its expression in the sedimentary record was studied, to create a baseline against which paleoenvironmental change can be measured.

Ancient sediment discharge, dispersal, and deposition:

Further, past responses of river discharge to historical periods of climatic change were studied to identify possible consequences of modern global warming in the eastern Canadian sub-Arctic. An analogue to the present warming was the Medieval Warm Period (MWP), which was of similar temperature like the mid 20th century and separated from the Modern Optimum by the relative cooler Little Ice Age (LIA) (Crowley and Lowery, 2000; Bond et al., 2001; Wanner et al., 2011). By studying proxies for variability in the Holocene river discharge since the last deglaciation ~10 kyr BP, the ongoing processes were placed in a large scale climatic context that also incorporates orbitally forced climatic controls, which caused the disintegration of the Laurentide Ice Sheet, the Temperate period, the Holocene Thermal Maximum and the Neoglacial (e.g. Wanner et al., 2011).

The following approaches were used to address the above objectives:

1. To elucidate the relationship(s) between modern climatic conditions, freshwater discharge and its expression in the marine sedimentary record by creating a modern marine sediment budget for the Great Whale River. This is addressed by the study of sedimentation rates and patterns at the Great Whale River over the past ~200 years using ²¹⁰Pb geochronology, the granulometric proxy record and physical sedimentary structures. These data can be used as baseline for comparison of sub-modern and ancient climatic changes that are recorded in older parts of the GWR sedimentary succession.

2. To place historical and Holocene river discharge variations at the Great Whale River and in northern Labrador in a global framework of climatic change. This was achieved by creating a total Holocene sediment budget for the study areas from sub-bottom sonar data and river discharge proxy data from the sedimentary record from long cores. Sediment mass fluxes were studied using AMS ^{14}C geochronology. Short term climate and river discharge variability since the deglaciation was studied using granulometry, magnetic susceptibility and sediment geochemistry (TOC, TN, C/N, $\delta^{13}\text{C}$) as proxies for variations in weathering, terrestrial minerogenic input and marine paleoenvironmental conditions. By comparing the two study sites at the Great Whale River in eastern Hudson Bay and Nachvak and Saglek Fjords in northern Labrador, we evaluated whether or not the observed responses of river discharge to climatic drivers are of local character or can be traced across the eastern Canadian sub-Arctic.

References:

- Aagaard, K. and Carmack, E.C., 1989. The role of sea ice and other freshwater in the Arctic circulation. *Journal of Geophysical Research*, 94: 14485-14498.
- ACIA, 2005. Impacts of a Warming Arctic: Arctic Climate Impact Assessment. Cambridge University Press, Cambridge.
- Alley, R.B. and Ágústsdóttir, A.M., 2005. The 8 k event: cause and consequences of a major Holocene abrupt climate change. *Quaternary Science Reviews*, 24: 1123-1149.
- Anderson, L.G., Jutterström, S., Kaltin, S., Jones, E.P. and Björk, G., 2004. Variability in river runoff distribution in the Eurasian Basin of the Arctic Ocean. *Journal of Geophysical Research*, 109.
- ArcticNet, 2008. Rational. <http://www.arcticnet.ulaval.ca/index.php?fa=ArcticNet.aboutUs>.

ArcticNet, 2010. Impacts of Environmental Change in the Canadian Coastal Arctic: A Compendium of Research Conducted during ArcticNet Phase I (2004-2008), ArcticNet Inc., Québec City, Canada.

Barber, D.C., Dyke, A., Hillaire-Marcel, C., Jennings, A.E., Andrews, J.T., Kerwin, M.W., Bilodeau, G., McNeely, R., Southon, J., Morehead, M.D. and Gagnon, J.-M., 1999. Forcing of the cold event of 8200 years ago by catastrophic drainage of Laurentide lakes. *Nature*, 400: 344-348.

Bell, T., Rogerson, R.J. and Mengel, F., 1988. Reconstructed ice-flow patterns and ice limits using drift pebble lithology, outer Nachvak Fiord, northern Labrador. *Canadian Journal of Earth Sciences*, 26: 577-590.

Bentley, S.J. and Kahlmeyer, E., 2012. Patterns and mechanisms of fluvial sediment flux and accumulation in two sub-arctic fjords: Nachvak and Saglek Fjords, Nunatsiavut, Canada. *Canadian Journal of Earth Sciences*, submitted.

Bond, G., Kromer, B., Beer, J., Muscheler, R., Evans, M.N., Showers, W., Hoffmann, S., Lotti-Bond, R., Hajdas, I. and Bonani, G., 2001. Persistent Solar Influence on North Atlantic Climate During the Holocene. *Science*, 294: 2130-2136.

Carlson, A.E., Clark, P.U., Raisbeck, G.M. and Brook, E.J., 2007. Rapid Holocene Deglaciation of the Labrador Sector of the Laurentide Ice Sheet. *Journal of Climate*, 20: 5126-5133.

Crowley, T.J. and Lowery, T.S., 2000. How Warm Was the Medieval Warm Period? *Journal of the Human Environment*, 29(1): 51-54.

Curtis, J., Wendler, G., Stone, R. and Dutton, E., 1998. Precipitation decrease in the western Arctic, with special emphasis on Barrow and Barter Island, Alaska. *Int. J. Climatol.*, 18: 1687-1707.

Déry, S.J. and Wood, E.F., 2004. Teleconnection between the Arctic Oscillation and Hudson Bay river discharge. *Geophysical Research Letters*, 31, L18205, doi:10.1029/2004GL020729.

Déry, S.J., Stieglitz, M., McKenna, E.C. and Wood, E.F., 2005. Characteristics and Trends of River Discharge into Hudson, James, and Ungava Bays, 1964-2000. *Journal of Climate*, 18: 2540-2557.

Déry, S.J., 2008. Recent trends and variability of river discharge in northern Canada, ArcticChange, Québec City.

- Evans, D.J.A. and Rogerson, R.J., 1986. Glacial geomorphology and chronology in the Selamiut Range - Nachvak Fiord area, Torngat Mountains, Labrador. Canadian Journal of Earth Sciences, 23: 66-76.
- Gagnon, A.S. and Gough, W.A., 2005. Climate change scenarios for Hudson Bay, Canada, from general circulation models. Climatic Change, 69: 269-297.
- Gonthier, N., d'Anglejan, B. and Josenhans, H.W., 1993. Seismo-stratigraphy and sedimentology of Holocene sediments off Grande Rivière de la Baleine, southeastern Hudson Bay, Québec. Géographie physique et Quaternaire, 47(2): 147-166.
- Gough, W.A. and Wolfe, E., 2001. Climate Change Scenarios for Hudson Bay, Canada, from general circulation models. Arctic, 54 (2): 142-148.
- Haberzettl, T., St-Onge, G. and Lajeunesse, P., 2010. Multi-proxy records of environmental changes in Hudson Bay and Strait since the final outburst flood of Lake Agassiz-Ojibway. Marine Geology, 271: 93-105.
- Hall, F.R., Andrews, J.T., Kerwin, M. and Smith, L.M., 2001. Studies of sediment colour, whole-core magnetic susceptibility, and sediment magnetism of the Hudson Strait-Labrador Shelf region: CSS Hudson Cruise 90023 and 93034. Marine Geology of Hudson Strait and Ungava Bay. Eastern Arctic Canada: Late Quaternary Sediments, Depositional Environments, and Late Glacial-Deglacial History Derived from Marine and Terrestrial Studies: Geological Survey of Canada Bulletin, 566, 161-170 pp.
- Hare, A., Stern, G.A., Macdonald, R.W., Kuzyk, Z.Z. and Wang, F., 2008. Contemporary and preindustrial mass budgets of mercury in the Hudson Bay marine system: the role of sediment recycling. Science of the Total Environment, 406: 190-204.
- Jansson, K.N., 2003. Early Holocene glacial lakes and ice marginal retreat pattern in Labrador/Ungava, Canada. Palaeogeography, Palaeoclimatology, Palaeoecology, 193: 473-501.
- Jenner, K.A. and Piper, D.J.W., 2002. Grande Riviere de la Baleine, Hudson Bay, Quebec - 1000 years of sedimentation. Geological Survey of Canada, 2002-E10.
- Johannessen, O.M., Bengtsson, L., Miles, M.W., Kuzmina, S.I., Semenov, V.A., Alekseev, G.V., Nagurny, A.P., Zakharov, V.F., Bobylev, L.P., Pettersson, L.H., Hasselmann, K. and Cattle, H.P., 2004. Arctic climate change: observed and modelled temperature and sea-ice variability. Tellus, 56 (A): 328-341.

- Kahlmeyer, E., 2011. Marine Records of Riverine Water and Sediment Discharge in Fjords of Nunatsiavut, Memorial University of Newfoundland, St. John's, 158 pp.
- Karageorgis, A.P., Anagnostou, C.L. and Kaberi, H., 2005. Geochemistry and mineralogy of the NW Aegean Sea surface sediments: implications for river runoff and anthropogenic impact. *Applied Geochemistry*, 20: 69-88.
- Kuzyk, Z.Z.A., Macdonald, R.W., Tremblay, J.-E. and Stern, G.A., 2010. Elemental and stable isotopic constraints on river influence and patterns of nitrogen cycling and biological productivity in Hudson Bay. *Continental Shelf Research*, 30 (2): 163-176.
- Lajeunesse, P. and St-Onge, G., 2008. The subglacial origin of the Lake Agassiz-Ojibway final outburst flood. *Nature Geoscience*, 1: 184-188.
- Lawrence, D.M. and Slater, A.G., 2005. A projection of near surface permafrost degradation during the 21st century. *Geophysical Research Letters*, 32 (L24401 doi: 10.1029/2005GL025080).
- Prowse, T.D., 1990. Northern Hydrology: an overview. In: T.D. Prowse and C.S.L. Ommenney (Editors), *Northern Hydrology: Canadian Perspectives*. National Hydrology Research Institute, Environment Canada, Saskatoon, Canada, pp. 1-36.
- Saucier, F.J., Senneville, S., Prinsenberg, S., Roy, F., Smith, G., Gachon, P., Caya, D. and Laprise, R., 2004. Modelling the sea ice-ocean seasonal cycle in Hudson Bay, Foxe Basin and Hudson Strait, Canada. *Canadian Climate Dynamics*, 23: 303-326.
- Stieglitz, M., Déry, S.J., Romanovsky, V.E. and Osterkamp, T.E., 2003. The role of snowcover in the warming of Arctic permafrost. *Geophysical Research Letters*, 30: 1721.
- Syvitski, J.P., Peckham, S.D., Hilberman, R. and Thierry, M., 2003. Predicting the terrestrial flux of sediment to the global ocean: a planetary perspective. *Sedimentary Geology*, 162: 5-24.
- Syvitski, J.P.M. and Shaw, J., 1995. Sedimentology and Geomorphology of Fjords. *Geomorphology and Sedimentology of Estuaries. Developments in Sedimentology*, 53: 113-178.
- Syvitski, J.P.M., 2003. Supply and flux of sediment along hydrological pathways: research for the 21st century. *Global and Planetary Change*, 39: 1-11.

Wanner, H., Solomina, O., Grosjean, M., Ritz, S.P. and Jetel, M., 2011. Structure and origin of Holocene cold events. Quaternary Science Reviews, 30: 3109-3123.

Wright, L.D. and Nittrouer, C.A., 1995. Dispersal of River Sediments in Coastal Seas: Six Contrasting Cases. Estuaries, 18: 494-508.

Chapter 2

A ^{210}Pb sediment budget and granulometric record of sediment fluxes in a subarctic deltaic system: the Great Whale River, Canada

Abstract

To elucidate how modern river discharge conditions of the Great Whale River (GWR) are represented in the marine sedimentary record, eight box and gravity cores were examined in terms of ^{210}Pb and ^{137}Cs radiochemistry, granulometry and physical sedimentary structures. These data were analyzed to provide insights into sedimentary processes and patterns at the study site. Sediment accumulation in the study area appears to be a relatively steady process over time-scales of 50 – 100 yr, allowing biological activity to overprint the primary depositional fabric. Subtle differences between ^{137}Cs and ^{210}Pb sediment accumulation rates (SARs) suggest an offshore shift in the locus of fine sediment deposition during the past ~150 yr, which may be a result of ongoing climatic warming leading to decreasing sea-ice coverage and a more energetic marine environment. Under present day conditions 23 % (40,000 t/yr) of the discharged sediment appear to accumulate in a 25 km² area off the river mouth. The remaining 77 % (136,000 t/yr) are either deposited further offshore, possibly along the northeastern shore as a result of Hudson Bay's counterclockwise circulation, or dispersed into the Hudson Bay system. Grain diameter frequency analyses suggest that environmental processes controlling sediment transport and deposition vary over decadal time scales. Although, we cannot

define an exact cause for this pattern, these shifts may be related to variations in river discharge, wave climate, possibly due to windier conditions or less sea-ice dampening, bioturbation or a combination of all. This also suggests that longer term river discharge signals are preserved in the marine sedimentary record offshore of the Great Whale River. In summary, no major change in sediment discharge over the past ~150 yr was observed. However, the offshore shift in the locus of sediment deposition suggests, that a warming climate will lead to more energetic marine conditions, less sea-ice coverage, and an increased offshore transport of terrestrial matter.

1. Introduction

Recent studies of the Hudson Bay watershed have shown that export of freshwater into Hudson Bay is highly variable and possibly decreasing (13 % between 1964 and 2000), and is strongly influenced by climatic oscillations, such as the Arctic Oscillation, El Niño Southern Oscillation and the Pacific Decadal Oscillation (Déry and Wood, 2004; Déry et al., 2005). In contrast to other Arctic and sub-Arctic regions of the northern hemisphere (e.g., Mueller-Lupp et al., 2000; Schuster et al., 2000; Stein et al., 2004), river discharge patterns and histories of the Canadian Arctic and subarctic, especially Hudson Bay, have been understudied. The understanding of Arctic watersheds is of crucial importance to the marine environment, because rivers discharge nutrients, organic matter and other trace species, such as pollutants, into the marine system (Anderson et al., 2004). River water discharge also tends to stratify the water column, exerts control on mixing and thus has an effect on primary production, the basic component of the Hudson Bay food web (Kuzyk et al., 2010; Sibert et al., 2011). River water discharge influences

marine salinity, thereby influencing both sea-ice formation (Saucier et al., 2004) and thermohaline circulation in Arctic Regions (Aagaard and Carmack, 1989). With a total freshwater discharge of $635 \text{ km}^3/\text{yr}$ (Déry et al., 2009), equaling 12 % of the total pan-Arctic runoff (Lammers et al., 2001), Hudson Bay is a significant freshwater contributor to the Labrador Shelf (Straneo and Saucier, 2008). There is a critical need to create a recent historical context to evaluate the impact of modern global warming processes on the Hudson Bay system, including the integrated study of its watershed and the marine environment. This work aims to provide this integration through the study of the nearshore marine sedimentary record.

Nearshore marine environments are especially suitable for paleoclimatic reconstructions because they reflect variations in both the marine realm and terrestrial environments. Because most of the sediment adjacent to larger rivers entering the ocean comes from rivers (e.g., Karageorgis et al., 2005) such settings are excellent repositories of data relating to climate change. Sediment budgets not only describe the fate of particulate matter in the marine realm, but also can be used as proxies to estimate the amount of freshwater and sediment input to the marine environment (Wheatcroft and Sommerfield, 2005).

The marine sedimentary basin associated with the Great Whale River contains up to 3500 years of river-discharge history (Gonthier et al., 1993), and provides an ideal site in which to analyze variations in a subarctic watershed as recorded in the nearshore environments of eastern Hudson Bay. The GWR is statistically representative of “average” Hudson Bay river discharge (Déry et al., 2005) over the past ~four decades. The sediments analyzed in this study accumulated in a fluvial-marine depocenter

extending to 11 km offshore with a maximum age of 3500 yr based on a marine shell ^{14}C age just below the boundary between the underlying marine muds and the overlying fluvio-deltaic muds (Gonthier et al., 1993).

Detailed knowledge of the inter-relationship between freshwater and sediment discharge patterns and sediment dispersal of the Great Whale River during the younger Holocene (<3500 yr BP) is not available. The sediment budget presented here elucidates the relation between modern climatic conditions, freshwater discharge and its expression in the marine sedimentary record. These data can be used as baseline for comparison of sub-modern and ancient climatic changes that are recorded in older parts of the GWR sedimentary succession. The specific objectives of this study are to: 1) study sedimentation rates and patterns at the Great Whale River over the past ~200 years; 2) establish a modern sediment budget for the study area in order to assess fluvial sediment discharge and its dispersal to the Hudson Bay system; and 3) detect possible effects of ongoing climatic change on sediment discharge.

2. Regional Setting

2.1 Deglacial and postglacial history

During the most recent glaciation, Hudson Bay was covered by the Laurentide Ice Sheet (Dyke and Prest, 1987). As a result, the land surface was glacio-isostatically depressed by up to ~250 m (Lavoie et al., 2008). During deglaciation the ice-dammed, large proglacial Lake Agassiz-Ojibway built up along the southern edge of the Laurentide Ice Sheet (Lajeunesse and St-Onge, 2008). Around 8500 cal yr BP, the collapse of the Laurentide Ice Sheet caused a catastrophic northward drainage of this lake into the North

Atlantic (Barber et al., 1999; Lajeunesse and St-Onge, 2008). Subsequently, the Tyrrell Sea invaded the glacio-isostatically depressed Hudson Bay Basin from the north (Hillaire-Marcel, 1976; Lajeunesse and St-Onge, 2008). Between 8000 yr BP and 2800 yr BP, the rate of isostatic rebound fell from about 10 cm/yr to about 1 cm/yr and has remained more or less constant since then (Hillaire-Marcel and Fairbridge, 1978; Allard and Tremblay, 1983; Gonthier et al., 1993; Lajeunesse and Allard, 2003; Sella et al., 2007).

2.2 Drainage Basin Properties:

The Great Whale River enters southeastern Hudson Bay at 55.29°N and 77.59°W (Fig. 1). The surrounding shorelines are forested, low-lying rocky coasts with discontinuous permafrost (Goldstein and Jacobsen, 1988). A high resolution digital elevation model was created from NASA's 3 arc-seconds Shuttle Radar Topography Mission data using the hydrologic modeling software RiverTools by RIVIX, LLC. The drainage basin was estimated to ~43,200 km² with a maximum elevation of 608 m. At the river mouth, a subaqueous mouth bar limits water depth to 1-1.5 m (Ingram, 1981).

Rivers on the eastern coast of Hudson Bay flow typically over bedrock or deposits of glacial origin. In the lower parts of river-valley fills, fine-grained marine silty clays date from the marine invasion of the Tyrrell Sea (Hydro-Québec, 1993) and are inferred to result from 8100 to 8000 yr BP (Hillaire-Marcel, 1976; Dyke and Prest, 1987). Further upstream, flavioglacial sands and till deposits provide easily erodible material(Hydro-Québec, 1993). Raised beaches and riverine sands are incised by up to 15 m along the modern river, and provide direct evidence for ongoing relative sea-level fall.

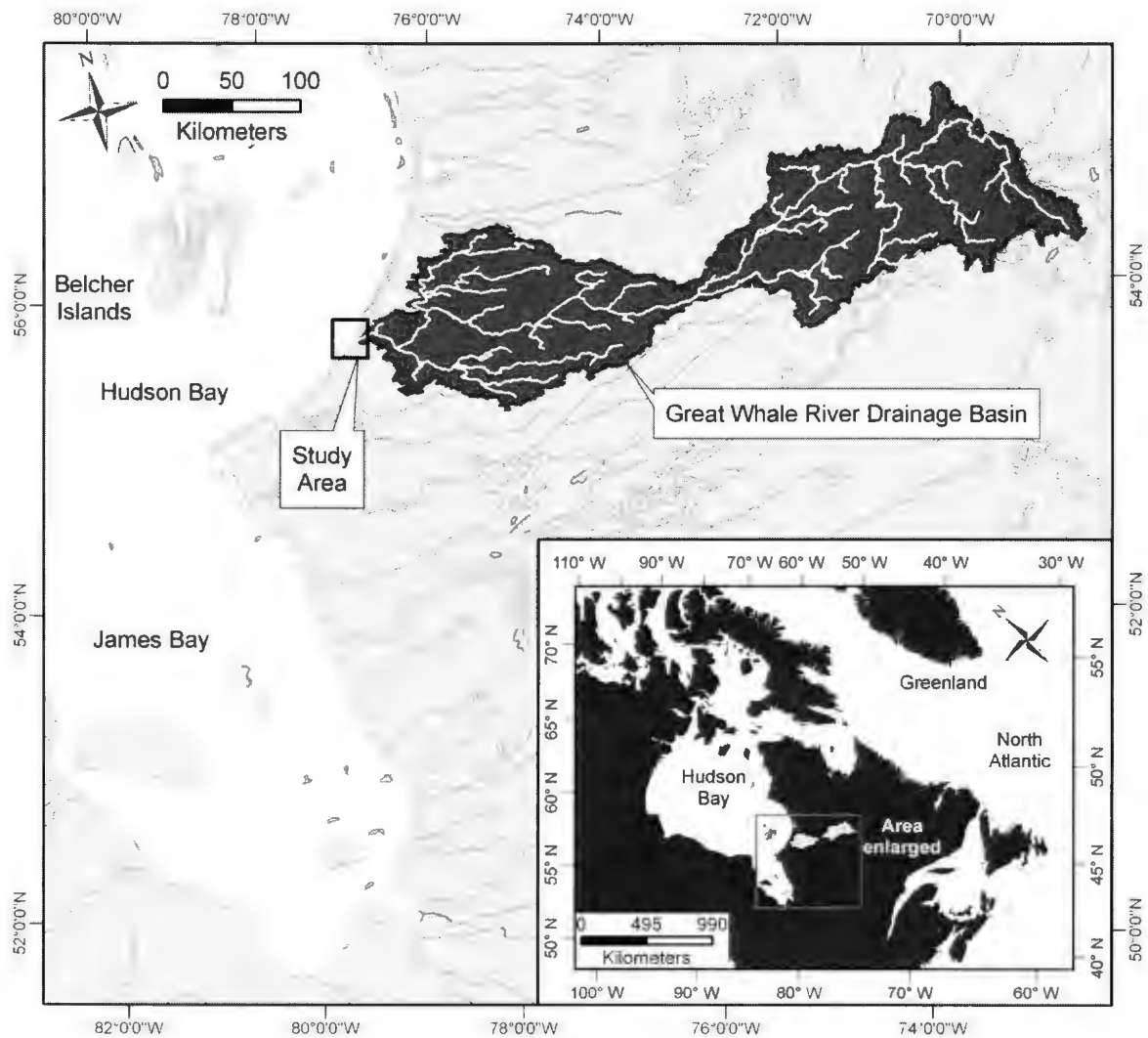


Figure 1: The small map displays the location of the drainage basin (light-grey) of the Great Whale River at the eastern coast of Hudson Bay, Canada. The larger map gives an overview of the rivers drainage basin (black) and the location of the marine study area (black frame). The study area is enlarged in Figure 2.

2.3 Oceanographic setting

Circulation in Hudson Bay is counterclockwise, with dense, cold, saline Arctic water flowing in from the northwest and outflow of relatively warm and fresh water to the northeast through Hudson Strait (Prinsenberg, 1986; Jones and Anderson, 1994; Saucier

et al., 1994; Saucier et al., 2004). Average surface currents are 5 cm/s in summer and 2-3 cm/s in winter. Along the east coast, sea-surface circulation is mainly controlled by wind forcing (predominantly northwesterly) with semidiurnal tides of a range of about 2 m and tidal currents <10 cm/s (Ingram, 1981). Today, Hudson Bay receives 30 % of the total Canadian freshwater runoff (Déry et al., 2005), and it does not receive North-Atlantic water (Hare et al., 2008).

2.4 Sea-ice formation

Ice formation in Hudson Bay usually begins in late October, coverage is typically complete in December, with maximum extent and thickness usually being reached in April. Melting season is May, June and July until open water conditions return in early August (Markham, 1986). The shore of Hudson Bay can be rimmed with land-fast ice throughout the year and offshore areas can be covered by mobile ice 9/10ths of the year (Prinsenberg, 1988). Since the mid-1990s eastern Canada and Hudson Bay experienced negative trends in sea-ice extent and duration (Gagnon and Gough, 2005; Hochheim et al., 2011). The eastern portion of Hudson Bay does not show significant changes in sea-ice extent and duration, most likely due to the advection of sea-ice by currents and wind forcing (Gagnon and Gough, 2005).

2.5 Freshwater and sediment discharge

Freshwater discharge ranges from < 200 m³/s in March to > 1300 m³/s in June (Ingram, 1981; Déry et al., 2005). The mean annual freshwater discharge is 600 m³/s, sufficient to modify local coastal water mass characteristics (Ingram et al., 1996). Due to

seasonal ice coverage, surface conditions vary through the year, resulting in a distinct freshwater plume of about 100 km² with 1-2 m thickness in summer and a significantly thicker and more extensive freshwater plume during winter, despite much lower river discharge at this time (Ingram, 1981). Ingram (1981) further suggests that the outer boundary of the plume may be a zone of frontal convergence of fresh river and saline marine waters. An observed change in offshore surface current velocity further suggests mixing of the surface plume water in this frontal convergence zone to accommodate the large offshore transport of plume water (Ingram et al., 1996). Sediment concentration data for the modern GWR plume is not currently available.

Limited data on sediment load of the GWR are available from Hydro-Québec (1993). Measurements of suspended sediment concentration reveal a substantial increase in downstream direction. This increase is related to erosion of the fine-grained deposits left by the Tyrrell Sea (Hydro-Québec, 1993). Generally, the suspended load is fairly low and rarely exceeds 20 mg/L (Hydro-Québec, 1993), but direct correlations between peak river discharge and sediment concentrations are not currently available. The total average sediment load of the Great Whale River was calculated to be 176,000 t/yr, of which 45,000 t/yr are sand fraction and 131,000 t/yr silt and clay fractions(Hydro-Québec, 1993).

2.6 Marine basin physiography

The slope break of the wave dominated Great Whale River delta occurs between 5 and 10 m water depth, and the prodelta slope extends to approximately 40 m water depth, where it merges with the basin floor (Hill et al., 2003). The basin reaches over 60 m water

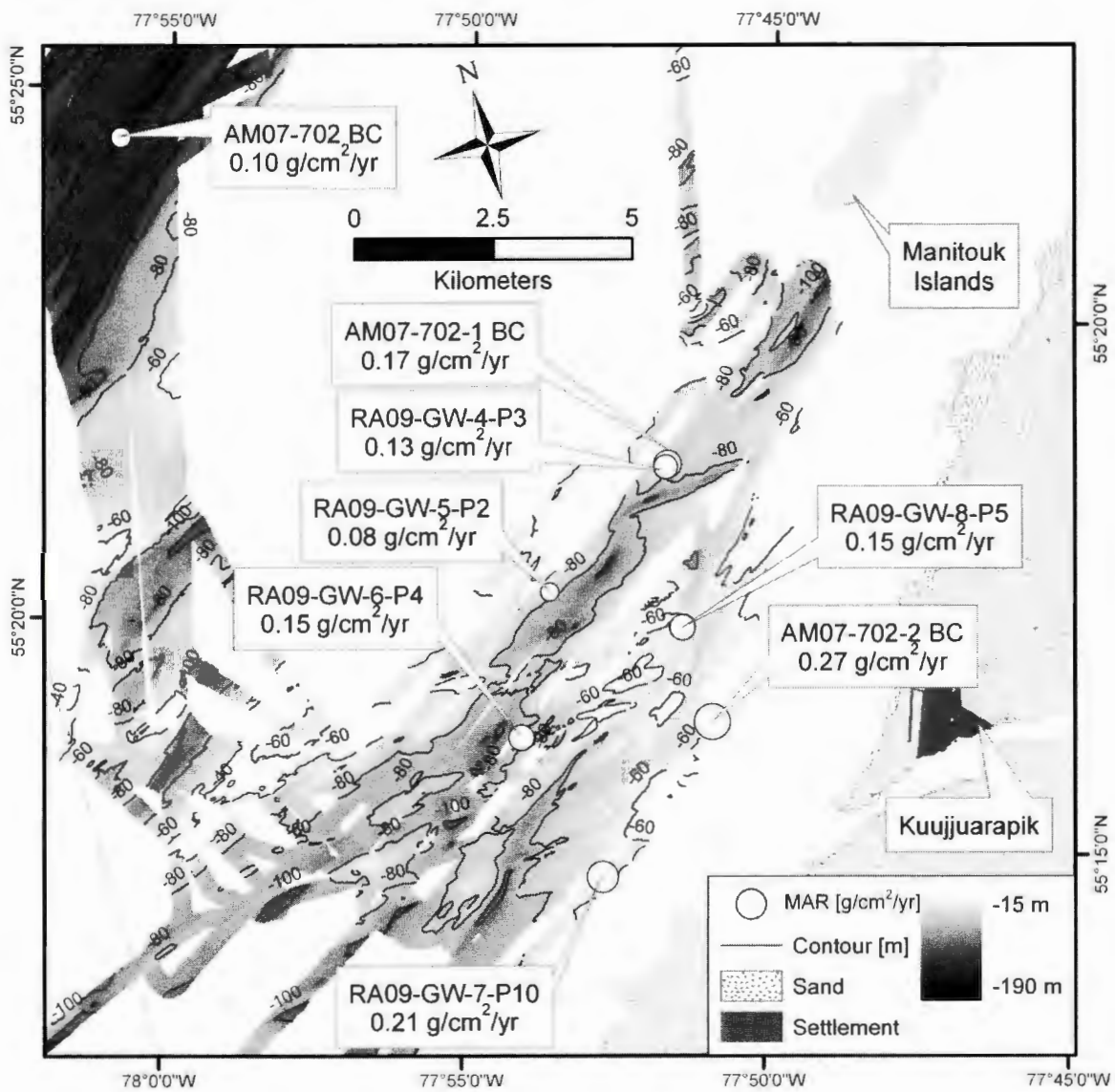


Figure 2: This map displays bathymetry, coring sites, and mass accumulation rates (circles, scaled proportional) in g/cm²/yr. The depositional basin is located right offshore the river mouth and bound to the NW by the subaqueous continuance of the Manitounuk Islands.

depth within 3 km of the shore but rarely exceeds 100 m depth (Figure 2). Approximately 8 km from the river mouth the seafloor rises to water depths of less than 20 m, thereby forming a small sedimentary basin in front of the river mouth. The bedrock topography offshore of the Great Whale River is generally similar to the physiography of the

Manitounuk Islands to the NE of the Great Whale River mouth, forming discontinuous ridges and troughs trending parallel to the modern coastline (Gonthier et al., 1993).

3. Methods

3.1 Seafloor geomorphology and sample collection

Box cores were collected in summer 2007, and gravity cores were collected in summer 2009 from the CCGS Amundsen and the CCGS Pierre Radisson, respectively. Sample locations were chosen by studying subbottom profiles and seafloor geomorphology. Bathymetrical data was collected between 2007 and 2010 using the CCGS Amundsen's Simrad EM 300 multibeam echosounder at an operating frequency of 30 kHz (data processed by the Ocean Mapping Group at the University of New Brunswick, Fredericton, NB, Canada). Sub-surface data were collected using a hull-mounted Knudsen Chirp 3200 echosounder with a frequency of 3.5 kHz. Data were visualized using Knudsen PostSurvey and ArcGIS softwares. The box cores were subsampled aboard ship by inserting 10 cm diameter PVC tubes to provide material for radioisotopic analyses and granulometry. The tubes were extruded onboard in 1 cm intervals, and samples sealed in watertight bags. Vertical slabs were collected from box cores for X-radiography by first inserting 2 cm thick three-sided rectangular Plexiglas trays and then the forth side to avoid compression. All samples were stored at 4-6 °C. Gravity cores were cut in 1 m sections, sealed and remained closed and cooled during transport.

3.2 Radiochemistry

Linear sediment accumulation rates (SAR) and mass accumulation rates (MAR) were estimated by analyzing activities of the naturally occurring radionuclide ^{210}Pb and the nuclear fallout isotope ^{137}Cs . ^{210}Pb is a product of the ^{238}U decay series and has been widely applied to study sedimentary processes on centennial timescales. ^{210}Pb has a half-life of $t_{1/2} = 22.3$ years and a decay constant of $\lambda = 0.031 \text{ yr}^{-1}$ (Hohndorf, 1969), and is produced in the atmosphere by decay of the radioactive gas ^{222}Rn , and by the *in situ* decay of particulate ^{226}Ra and its daughter ^{222}Rn in sediments and bedrock. The resulting products for the atmospheric and terrestrial sources of ^{210}Pb are referred to as supported ^{210}Pb and excess $^{210}\text{Pb}_{\text{XS}}$ (Goldberg, 1963). Once reaching the water column, $^{210}\text{Pb}_{\text{XS}}$ is scavenged by suspended sediment particles, settles to the seafloor and decays with progressive burial. Below the depth in sediment influenced by bioturbation (L_b), $^{210}\text{Pb}_{\text{XS}}$ activities can be used to calculate apparent SARs (e.g., Nittrouer et al., 1984/1985), assuming that mixing below L_b can be neglected (e.g., Nittrouer et al., 1979).

Samples were weighed wet, dried for 24 hours at 60 °C, dry weighed, ground, and $\geq 10 \text{ g}$ of dried sample material were sealed in $0.7 \times 5 \text{ cm}$ petri dishes, and sealed to allow ingrowth of the ^{210}Pb grandparent ^{222}Rn . Weighed samples were counted for 24 hours in Canberra GL-3825 detectors and analyzed with Genie 2000 gamma acquisition and analysis software. Total ^{210}Pb activities were measured by counting of the 46.5 keV gamma peak of ^{210}Pb , and were evaluated for sample absorption of gamma emission by comparison to standards of known activity and absorption (Cutshall et al., 1983). Supported activities of ^{210}Pb were determined by measuring the ^{226}Ra granddaughters ^{214}Pb (295 and 352 keV) and ^{214}Bi (609 keV). Excess activities of ^{210}Pb were calculated

by subtracting the supported ^{210}Pb activities from the total ^{210}Pb activities. All activities are reported in dpm/g (decays per minute/gram, with 1 dpm/g = 60 Bq), and were decay corrected to the time of collection. Assuming constant depositional rates for sediment and $^{210}\text{Pb}_{\text{XS}}$, a with time constant thickness of the mixed layer L_b , and negligible bioturbation below depth L_b , apparent sediment accumulation rates (SARs) can be calculated by

$$A_z = A_0 e^{(-\lambda z/S)} \quad \text{Eq. 1}$$

where A_0 is the $^{210}\text{Pb}_{\text{XS}}$ activity [dpm/g] at the sediment surface, A_z is the $^{210}\text{Pb}_{\text{XS}}$ activity [dpm/g] at depth z [cm], λ [yr^{-1}] is the decay constant and S [cm/yr] is sediment accumulation rate (Krishnaswami et al., 1980). This method averages S over timescales of ~ 150 yr, or 5-6 half lives of ^{210}Pb . Sediment accumulation rates were calculated from least squares regressions of Eq. 1 to the $^{210}\text{Pb}_{\text{XS}}$ profiles. To relate sediment accumulation to fluvial supply, sediment mass accumulation rates (MAR) [$\text{g}/\text{cm}^2/\text{yr}$] were determined from

$$MAR = S(1 - \phi)\rho_S \quad \text{Eq. 2}$$

where S is sediment accumulation rate [cm/yr], ϕ is the average porosity of the core, determined from water loss at 90°C, and ρ_S is the assumed grain density of the sediment of 2.65 g/cm³ (e.g. Muhammad et al., 2008).

To validate $^{210}\text{Pb}_{\text{XS}}$ SARs, SARs were also calculated from activities of ^{137}Cs , which is an anthropogenic radioisotope, first introduced to the atmosphere in 1954 by nuclear bomb tests. Introduction to the atmosphere peaked in 1963-1964 and dropped to insignificant levels by 1980 (e.g., Anderson et al., 1988; Sommerfield et al., 2007). Activities of ^{137}Cs were determined directly by counting the ^{137}Cs 661 keV peak. SARs then were calculated using

$$S = (z_{\max} - L_b) / (T - 1954) \quad \text{Eq. 3}$$

with sediment accumulation rate S [cm/yr], maximum penetration depth z_{\max} [cm] of ^{137}Cs , mixing layer thickness L_b [cm], and the year of sample collection T (Nittrouer et al., 1983). Mixing layer thickness L_b was estimated from the thickness of the top interval with uniform $^{210}\text{Pb}_{\text{XS}}$ activities present in some cores and from burrow depth in x-radiographs. To constrain the temporal resolution for paleoenvironmental signals, the transit time or residence time T_r [yr] for sediment in the bioturbated zone (Wheatcroft et al., 2006) was estimated using:

$$T_r = L_b / SAR \quad \text{Eq.4}$$

3.3 Physical sedimentological properties

3.3.1 Granulometry

To study variations in depositional processes, grain size in cores was analyzed at 1 cm intervals. Subsamples were disaggregated in NaPO_3 (0.05 %) solution, placed in an

ultrasonic bath for one hour, left in solution overnight, then ensonified again for one hour before measurement. Analyses were performed using a HORIBA Partica LA-950 laser diffraction particle size analysis system, with a particle size range of 0.1-3000 μm . The presence of bimodal distributions discussed below was confirmed by analysis of selected replicates using a Micromeritics Sedigraph, and the disaggregation procedures described above.

3.3.2 X-radiography

To study sedimentary structures, sediment slabs were imaged X-radiographically using a Thales Flashscan 35 X-ray detector, illuminated with an Acoma PX15HF X-ray generator. Images were stored as 14-bit TIFFs and studied using ImageJ visualization software.

3.4 Sediment mass flux calculations

To evaluate how modern river discharge conditions are reflected in the marine sedimentary record, $^{210}\text{Pb}_{\text{xs}}$ -inferred MARs [$\text{g}/\text{cm}^2/\text{yr}$] are compared to fluvial sediment load [t/yr], by averaging MARs for the size of our study area. Total modern marine sediment mass accumulation M_{MO} [t/yr] then is estimated by applying

$$M_{MO} = MAR * A \quad \text{Eq. 5}$$

where A is area [km^2]. To compare this to modern fluvial sediment discharge, M_{MO} is compared to values for the mean annual fluvial sediment load of the Great Whale River.

The mean annual fluvial sediment load Q_s is estimated after the BQART-model for a basin average temperature $T < 2^\circ\text{C}$ using Syvitski and Milliman (2007):

$$Q_s = 2\omega B Q^{0.31} A^{0.5} R \quad \text{Eq. 6}$$

The model is based on a global dataset of 488 rivers and his highly representative of geology, climate and socioeconomic conditions. Input parameters to estimate Q_s are maximum relief R [km], drainage basin area A [km/yr], modern water discharge Q [km³/yr] and B, which accounts for important geological and human factors and will be explained in the discussion section. The factor and $\omega=600$ is used to receive units in t/yr (modified after Syvitski and Milliman, 2007).

4. Results

4.1 Sediment and mass accumulation rates

Profiles for $^{210}\text{Pb}_{\text{XS}}$ (Figure 3) reveal a mean sediment accumulation rate of 0.16 ± 0.05 cm/yr, with r^2 of 0.95 ± 0.07 (mean $\pm 1\sigma$, n=8) (Table 1). Top sections of homogeneous $^{210}\text{Pb}_{\text{XS}}$ activity (Figure 3) as well as bioturbated fabrics in X-radiographs (Figure 4) indicate a mixed layer thickness of $L_b = 5 \pm 1$ cm (mean $\pm 1\sigma$, n=4) (Table 1) in cores AM07-702 BC, AM07-702-1 BC, AM07-702-2 BC, and RA09-GW-7-P10. In most cores, $^{210}\text{Pb}_{\text{XS}}$ activities in the surface layer are above 10 dpm/g. Below the mixing layer L_b , $^{210}\text{Pb}_{\text{XS}}$ activities generally decrease exponentially with depth. Some cores, however, exhibit intervals of uniform activities or step-like patterns, such as core AM07-702-1 BC at depth 16-18 cm, in core A M07-702-2 BC at depth 12-13 cm, and in core

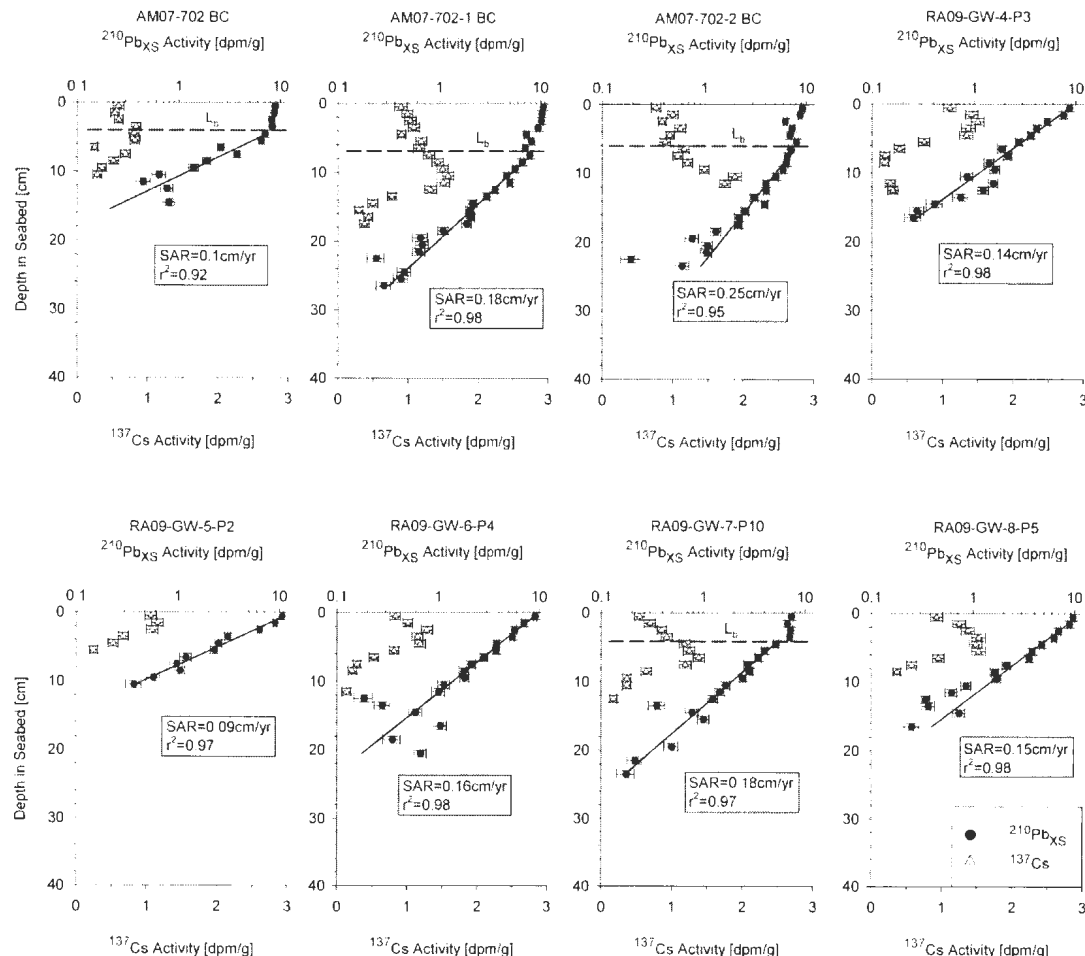


Figure 3: The graphs display downcore $^{210}\text{Pb}_{\text{XS}}$ (dots) and ^{137}Cs (triangles) activities. Sediment accumulation rates (SAR) were calculated by fitting regressions to $^{210}\text{Pb}_{\text{XS}}$ activities below the zone of biological homogenization and solving for S in Eq. 1. Biological homogenization depth L_b is marked with dashed lines.

RA09-GW-7-P10 at depth 8-10 cm (Figure 3). With SARs and Eq. 2 the mean mass accumulation rate (MAR) for the study area was calculated to be $0.16 \pm 0.06 \text{ g/cm}^2/\text{yr}$ (Table 1).

SARs were also calculated from ^{137}Cs penetration depth to a mean SAR of $0.16 \pm 0.06 \text{ cm/yr}$ (mean $\pm \sigma$, $n=8$) (Table 1). From ratios of $^{137}\text{Cs}/^{210}\text{Pb}$ SAR (Table 1), it is evident that cores closest to the river-mouth, in shallowest water, have ^{137}Cs SARs equal

to or lower than ^{210}Pb SAR for the same cores, whereas cores farther offshore in deeper water have ^{137}Cs SARs equal to or higher than ^{210}Pb SARs for the same cores (although results averaged for all cores show little difference).

Table 1: Summary of $^{210}\text{Pb}_{\text{XS}}$ and ^{137}Cs sediment accumulation rates (SAR), $^{210}\text{Pb}_{\text{XS}}$ apparent mass accumulation rates (MAR), mixing layer depth (L_b) and temporal resolution (T_r). The Cs/Pb ratio describes the level of correspondence between $^{210}\text{Pb}_{\text{XS}}$ and ^{137}Cs apparent SARs.

Core-ID	Water depth [m]	Distance to river [km]	$^{210}\text{Pb}_{\text{XS}}\text{-SAR}$ [cm/yr]	r^2	MAR [g/cm ² /yr]	$^{137}\text{Cs}\text{-SAR}$ [cm/yr]	Cs/Pb	L_b [cm]	T_r [yr]
AM07-702 BC	134	18.1	0.10	0.77	0.10	0.09	0.90	6	60
AM07-702-1 BC	74	7.3	0.18	0.98	0.17	0.26	1.44	4	22
AM07-702-2 BC	60	2.9	0.25	0.95	0.27	0.11	0.44	6	24
RA09-GW-8-P5	79	4.5	0.15	0.99	0.15	0.16	1.07	-	-
RA09-GW-4-P3	72	7.3	0.14	0.97	0.13	0.22	1.57	-	-
RA09-GW-7-P10	69	4.5	0.18	0.95	0.21	0.16	0.89	4	22
RA09-GW-6-P4	84	6	0.16	0.98	0.15	0.20	1.25	-	-
RA09-GW-5-P2	72	6.8	0.09	0.98	0.08	0.11	1.22	-	-
Mean			0.16	0.95	0.16	0.16	1.10	5	32
σ			0.05	0.07	0.06	0.06	0.34	1	16

4.2 Sediment discharge and dispersal

To evaluate how modern river discharge conditions are reflected in the marine sedimentary record, total modern marine sediment mass accumulation M_{MO} [t/yr] was estimated using Eq. 5. Area was measured in ArcGIS. With an area A of 25 km² and an aerially weighted average MAR of 0.16 g/cm²/yr, M_{MO} is estimated as 40,000 t/yr (Table 2). The mean annual fluvial sediment load Q_S was estimated to 153,891 t/yr (Table 2) using Eq. 6. Maximum relief R [m] was extracted from the DEM created for the study area. The value for river water discharge Q [km³/yr] (Table 2) was taken from

HydroQuébec (1993). For catchment properties (lithology, presence of glaciers, trapping efficiency) and human influences was accounted by applying $B = IL(1-T_E)E_h$ (Syvitski and Milliman, 2007). The Lithology Factor L was chosen after a map by Syvitski and Milliman (2007), who described the Canadian Shield of northeastern Canada as acid plutonic, high-grade metamorphic with a $L=0.5$. The anthropogenic factor was chosen to be $E_h=1$ for drainage basins with a low human footprint. Because the drainage basin is unglaciated, we used $I=1$ for unglaciated drainage basins. Due to lack of data on trapping efficiency T_E , we used an average value of 0.8 for the trapping efficiency term $1-T_E$ (Syvitski and Milliman, 2007).

Table 2: Table 2 displays results and values used to estimate riverine sediment load Q_{Sest} after the BQART-model (Syvitski and Milliman, 2007). The estimation of sediment bypass is displayed by Q_B .

Sediment load estimation (Q_{Sest})		Sediment bypass estimation (Q_B)	
Q_{Sest} [t/yr] = $2\omega B Q^{0.31} A^{0.5} R$	153,891	Q_B [t/yr] = $Q_S - M_{MO}$	136,000
ω (fort/yr)	600	Q_S (HydroQuebec, 1993; t/yr)	176,000
Q (km ³ /yr)	20.15	M_{MO} [t/yr]	40,000
A (km ²)	43,200		
R (km)	0.608		
$B=IL(1-T_E)E_h$	0.4		
I	1		
L	0.5		
E_h	1		
$1-T_E$	0.8		

4.3 Physical sedimentological properties

4.3.1 Sedimentary structures

X-radiographs of box cores AM07-702 BC, AM07-702-1 BC, and AM07-702-2 BC are shown in Figure 4. These boxcores have been chosen because they exhibit the best surface layer preservation, and represent the most proximal and distal cores relative to the river mouth. Cores AM07-702 BC, AM07-702-1 BC, and AM07-702-2 BC are located 18.1, 7.3, and 2.9 km from the river mouth, respectively (Table 1, Figure 2). Areas of lower density are represented by darker shading, areas of higher density by lighter shading. All cores generally exhibit a fairly similar, mottled texture with darker top

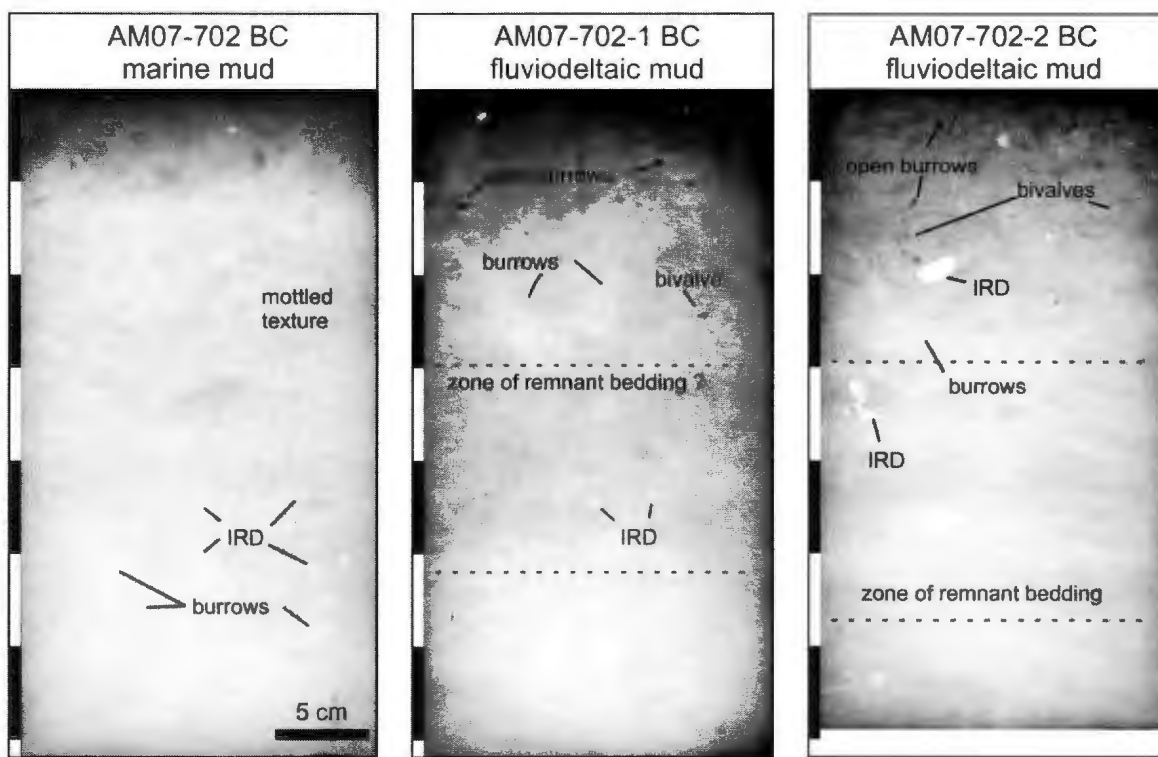


Figure 4: The images display X-radiographs of selected cores. Core AM07-702 BC is the most river distal core, while core AM07-702-2 BC is the most river proximal core. Brighter and darker colors represent areas of higher and lower density, respectively. Some examples for ice rafted debris (IRD), shell fragments, and burrows are marked. Vertical and horizontal scale bars equal 5 cm intervals.

sections, representing the mixing layer L_b with lower densities and higher porosities due to bioturbation. In cores AM07-702-1 BC and AM07-702-2 BC some open burrows are preserved. Bioturbation has destroyed most physical sedimentary structures in all cores. However, in cores AM07-702-1 BC and AM07-702-2 BC areas of remnant bedding are indicated by faint density contrasts in X-radiographs, while the most distal core, AM07-702 BC, is homogeneous. Small amounts of ice rafted debris (IRD) are present in all three cores, but the most proximal core, AM07-702-2 BC, exhibits the highest content and largest clasts (granule size). Also, the content of bioclasts is higher in the river-proximal cores AM07-702-1 BC and AM07-702-2 BC, relative to the most distal core AM07-702 BC.

4.3.2 Granulometry

Sediments from all cores generally consist of silt-rich and sandy mud, have a mean grain diameter of \sim 10-30 μm , and show a bi-modal grain-diameter frequency distribution (Figure 5). The most prominent mode at 7-15 μm corresponds to the fine silt fraction, and the second, lesser mode is at \sim 0.3-1 μm corresponds to the fine clay and colloidal fraction. The silt and clay/colloidal modes vary in proportion and are anticorrelated with each other (Figure 8). Both silt and clay/colloidal modes are present in all cores but the clay/colloidal mode increases in proportion with increasing distance to the river mouth. The clay/colloidal mode is most prominent in core AM07-702 BC, the most distal core, but is minor in core RA09-GW-7-P10 and almost absent in core AM07-702-2 BC, the most proximal cores (Figure 2 and 5). Proximal cores show more

variability in mean grain size (Figure 6). Cores AM07-702 BC, AM07-702-1 BC, RA09-GW-6-P4, and RA09-GW-7-P10 show subtle upward coarsening (Figure 6).

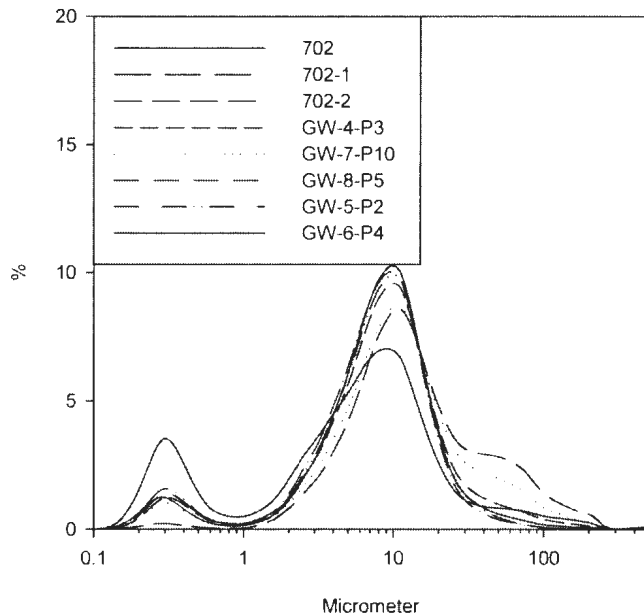


Figure 5: These graphs display average grain diameter frequencies for box and gravity cores offshore from the Great Whale River.

5. Discussion

5.1 Sediment and mass accumulation rates

To examine depositional patterns during the past ~150 yr, sediments were examined in terms of ^{210}Pb and ^{137}Cs radiochemistry, sedimentary structures and granulometry. According to the generally log-linear pattern of $^{210}\text{Pb}_{\text{xs}}$ decay below the biologically homogenized surface mixing layer L_b (Figure 3), sediment accumulation appears to be a relatively steady process over timescales of 10-100 yr. This is supported by the mottled sedimentary fabric seen in X-radiographs (Figure 4) and lack of physical

stratification, which suggests slow sediment accumulation at a rate that allows biological activity to overprint the primary depositional fabric (e.g., Bentley et al., 2006).

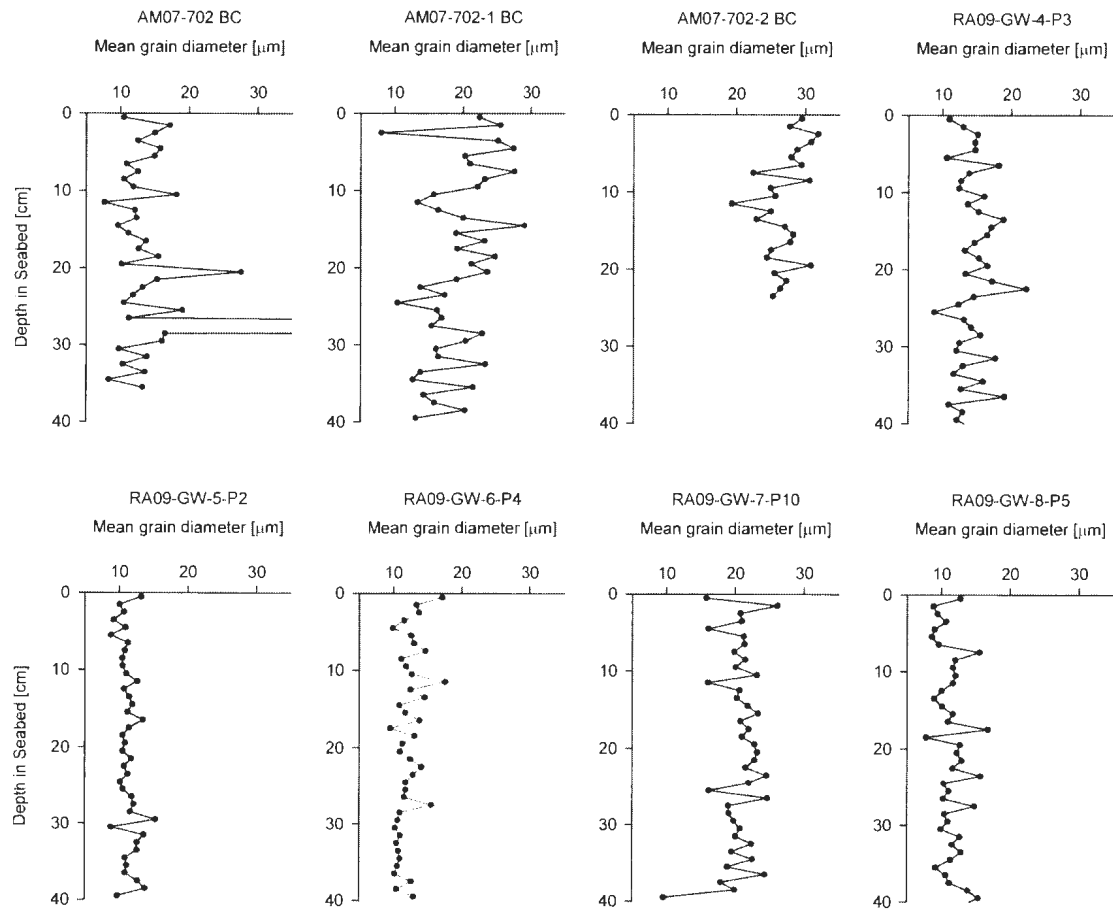


Figure 6: This figure shows depth profiles of mean grain diameter for all box and gravity cores offshore from the Great Whale River.

SAR estimates from ^{137}Cs and ^{210}Pb describe processes over different time intervals. ^{137}Cs averages accumulation over the past ~ 60 y. ^{210}Pb is supplied continuously, averaging SAR over a time interval >100 y, extending back in time from the age of sediment at the base of the bioturbated zone (Wheatcroft et al., 2006). Thus, changes in

ratios of $^{137}\text{Cs}/^{210}\text{Pb}$ SAR (Table 1) indicate change in SAR from 100-150 years ago relative to the most recent ~60 years. Results show that cores closest to the river mouth, in shallowest water, have ^{137}Cs SARs equal to or lower than ^{210}Pb SAR for the same cores, whereas cores farther offshore in deeper water have ^{137}Cs SARs equal to or higher than ^{210}Pb SARs for the same cores (Figure 7) (although results averaged for all cores show little difference). Collectively this suggests that there are no detectable changes in total sediment delivery over the last ~150 yr that can be inferred from our record. However, the locus of fine sediment deposition has shifted slightly offshore over the past century. This is indicative of a more energetic environment, which keeps fine-grained sediment in suspension for a longer period, thereby promoting offshore sediment transport. This may be a sign for ongoing climatic warming, leading to increased wave resuspension as a result of decreased sea-ice coverage.

Physical sedimentary structures are more easily destroyed by biological activity than are grain-size signals (Wheatcroft and Drake, 2003). Patterns and trends observed in the radiochemical and granulometric signal may hold information on time-scales shorter than T_r . Radiochemical profiles (Figure 3) in some cores (e.g. AM07-702-1 BC) show stair-step downcore patterns that could represent event deposition (cf. Bentley et al., 2002), however, these patterns are not reflected in mean grain-diameter trends (Figure 6) and X-radiographs (Figure 4). Sediment accumulation patterns show no strong correlation with distance to the river mouth (SAR, $r^2=0.47$; MAR, $r^2=0.6$) (Figure 7). However, SARs and MARs correlate inversely with mean grain diameter ($r^2=0.79$ and 0.82, respectively), which is weakly correlated with depth ($r^2=0.66$) but not with distance to the river mouth ($r^2=0.3$) (Figure 10). This suggests that sediment accumulation offshore of

the Great Whale River is more controlled by marine depth-dependent processes, such as wave activity and local current conditions, than purely by distance to the sediment source and particle settling rate.

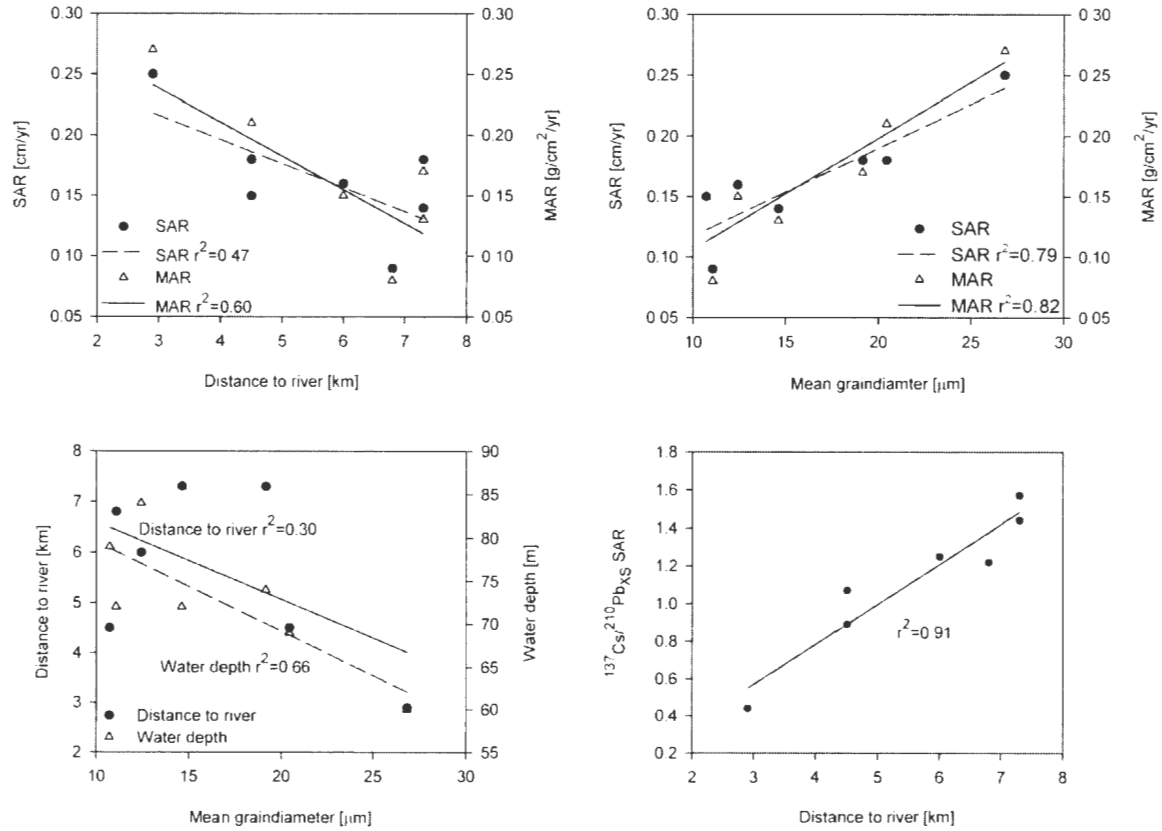


Figure 7: The upper graphs display correlations of sediment and mass accumulation rates (SAR, MAR) with distance to river mouth (top left) and mean grain diameter (top right). The lower left graph displays correlations of mean grain diameter with distance to the river mouth (dots, solid line) and water depth (triangles, dashed line). The graph to the lower right shows correlations of $^{137}\text{Cs}/^{210}\text{Pb}_{\text{XS}}$ ratios with distance to the river mouth.

5.2 Modern sediment mass fluxes / budget

To study how modern discharge conditions are reflected in the sedimentary record, M_{MO} was compared to Q_S . To validate our estimations for Q_{Sest} , we compared our

results to two values for sediment load from the literature. D'Anglejan and Biskham (1988) estimated fluvial sediment load to 500,000 t/yr, and HydroQuébec (1993) measured a fluvial sediment load of 176,000 t/yr. The BQART modeled annual sediment load $Q_{Sest} = 153,891$ t/yr of the Great Whale River is very close to the value of 176,000 t/yr measured by HydroQuébec (1993). Using slightly higher L values of 0.6-0.7 in our estimations might be reasonable due to the presence of tillites as well as clays from the Tyrrell Sea marine incursion in the lower part of the drainage basin. Doing so provides a slightly closer match to the Hydro-Québec estimate. We use the Hydro-Québec estimate for the discussion below, because of the similarity between it and the BQART estimate. Because the value by d'Anglejan and Biskham (1988) seems very high, relative to the other two values, we did not include this value for our study. Subtracting M_{MO} from Q_S , results in a sediment bypass of $M_B=136,000$ t/yr, equaling 77 % of the from the river discharged sediment load (Table 2). This means that, under present day climatic conditions with $Q = 20.15 \text{ km}^3/\text{yr}$, 23 % (40,000 t/yr) of the discharged sediments are deposited within the proximal study area. This is comparable to proximal marine-shelf deposition near many fluvial systems (Wright and Nittrouer, 1995; Stein et al., 2004). The remaining 77 % bypass the study area and are either deposited further offshore or dispersed into the Hudson Bay system. It should be noted, that all cores were taken from areas of active sedimentation. The freshwater plume described by Ingram (1981) covers an area of $\sim 100 \text{ km}^2$ and extends approximately 8 km offshore, where it rapidly mixes with the saline waters of Hudson Bay. Below the freshwater plume, currents are shore-parallel towards the northeast. Thus, it is likely that at least a part of the remaining 77 %

is being deposited further offshore within the 100 km² plume area or along the shore to the northeast of the river mouth.

5.3 Temporal sediment depositional patterns

Although the results from radiochemistry and X-radiography suggest relatively uniform sediment accumulation rate, there are patterns in the grain diameter frequency distributions (Figure 8), suggesting higher frequency variations in the properties of sediment deposited offshore of the Great Whale River. To better correlate between cores, depth was converted to Year AD using ²¹⁰Pb apparent SARs. A direct correlation among all peaks in all cores was not possible. However, at least in cores AM07-702-1 BC, RA09-GW-6-P4, RA09-GW-8-P5 and RA09-GW-4-P3, RA09-GW-5-P2 patterns in the upper 5-6 clay/colloidal peaks are very similar in shape and spacing (Figure 8), spanning approximately the past 100 yr. Due to lack of process related physical structures, it is impossible to relate the observed patterns to one process with certainty. This is further complicated by the fact that all signals formed during time periods shorter than T_r are likely to be altered during transit through the active layer, thus it is not surprising that there are differences in granulometric patterns among cores. The process causing these variations is not clear from our observations, but two possibilities exist. First, this fine fraction could represent a separate class of material transported in suspension. Second, this fine fraction could represent material desorbed from grain surfaces during analysis (but associated with larger grains during transport), in which case the difference would not be necessarily associated with particle size, but particle composition, and possibly source. Regardless of the type of material producing this record, the pattern does exist and

it has a periodicity that suggests changes in sediment delivery patterns over decadal timescales. Although, we cannot be certain about the exact cause of these patterns, four sedimentary processes able to create the patterns in Figure 8, sediment discharge variations, changing sediment source, winnowing, and bioturbation, are discussed below.

Assuming that all sediment in the study area is delivered by the river, if the mode represents a separate grain-size class, this peak is interpreted as settling of fine-grained suspended material from a river plume. Fine silt-grade material is at the boundary (McCave et al., 1995) between what can be transported in suspension versus bedload. Increases in silt concentration are interpreted to reflect rapid discharge from a turbid meltwater plume during spring melt. The observed variability thus may record river sediment discharge variations.

If the fine fraction does not represent a separate transported grain-size class, but is in fact material desorbed from larger grains during analysis, then results suggest variations in sediment composition, probably associated with the catchment source. The time scale of variation (decades) seems too short to be driven by weathering processes, but could be associated with spatially varying lithology and erosion within the catchment (Miller et al., 2005; Mukundan et al., 2010; Bernárdez et al., 2012).

Coarsening can also be caused by winnowing (e.g. Drake, 1997), thus the silt peaks may reflect variations in wave resuspension and thus may be a proxy for windier conditions and/or periods of less wave dampening due to decreased sea-ice coverage. In the latter (resuspension) scenario, anticorrelation between the colloidal and silt peaks then would reflect variations in the delivery of slightly coarser or finer fractions and/or wave climate, possibly accompanied by less sea-ice coverage.

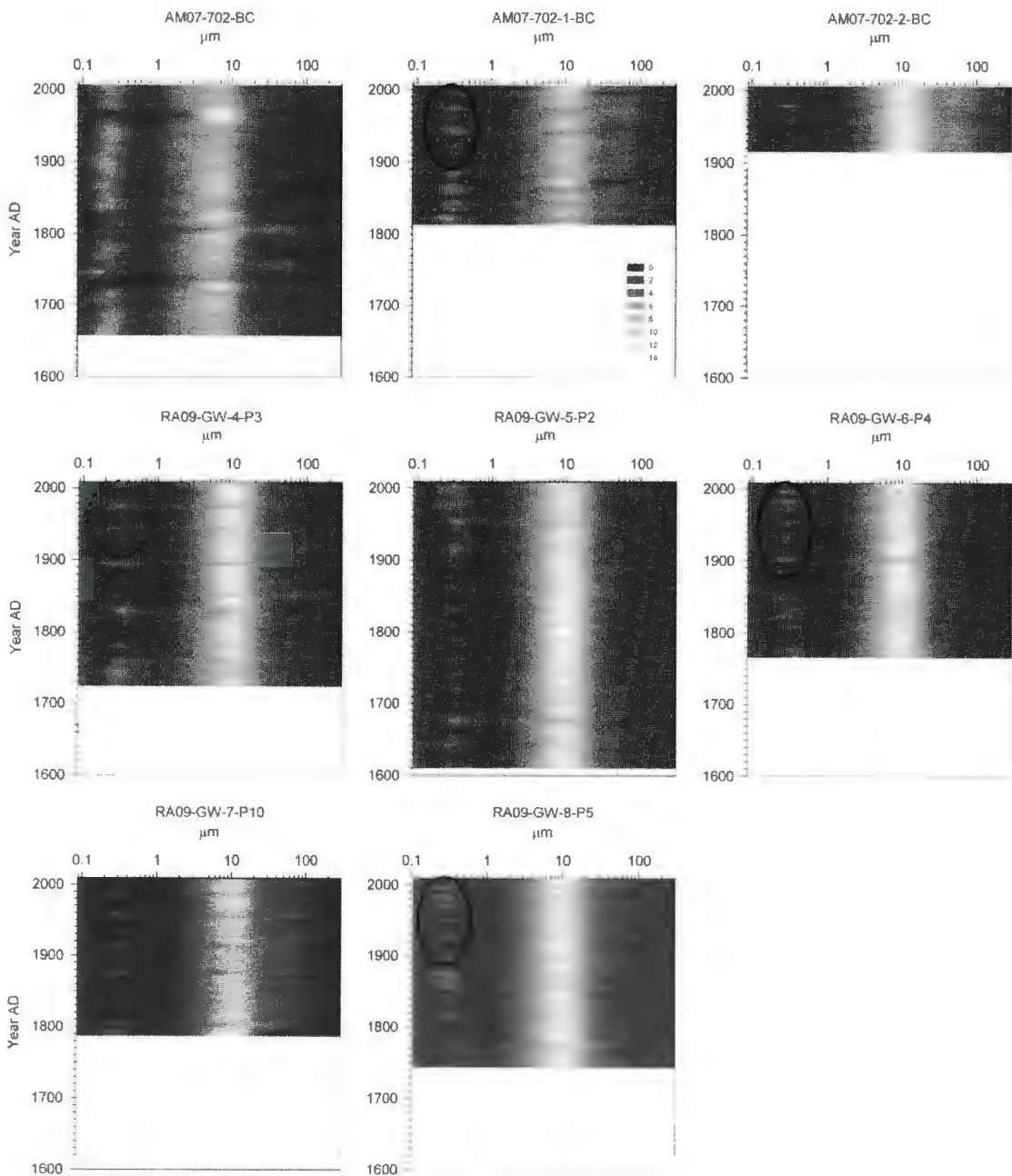


Figure 8: These graphs display downcore grain diameter frequencies for box and gravity cores offshore from the Great Whale River. Areas of clay peaks, which correlate between cores are marked with solid and dashed circles.

Bioturbation can produce graded bedding by selective feeding of burrowing organisms (Schäfer, 1962; Hansen, 1977). An alteration, as observed in our cores would require event-like deposition, forcing the burrowing organisms to rapidly move their feeding depth upward. Although SARs appear uniform on time-scales of 100-150 yr, event sedimentation cannot entirely be ruled out due to weak evidences from stair-step patterns in some $^{210}\text{Pb}_{\text{xs}}$ profiles and faint density differences in x-radiographs for event deposition.

Nevertheless, the observed patterns may be a sign for decadal-scale variations in environmental controls on sediment depositional and/or dispersal patterns. If and how these relate to climatic oscillations remains speculative. But decadal time-scale variations in physical sediment properties as a result of changes in atmospheric drivers such as the Arctic Oscillation, North Atlantic Oscillation or to solar cycles haven been observed before (e.g. Haug et al., 2001; Paetzel and Dale, 2010).

6. Conclusions

The major conclusions of our sedimentological study of the Great Whale River fluvial-marine depocenter are as follows:

Modern sediment accumulation rates in the study area vary between 0.09 and 0.26 cm/yr. Over time scales of 50-150 yr, sediment accumulation in the study area appears to be a relatively steady process, allowing biological activity to overprint the primary depositional fabric, but subtle differences between ^{137}Cs and ^{210}Pb SARs suggest an offshore shift in the locus of fine sediment deposition. This may be a sign of increased

wave resuspension due to a more energetic environment with less sea-ice as a result of a warming climate.

The modern (~200 yr) sediment budget reveals that under present day conditions 23 % of the discharged sediment accumulate in a 25 km² area off the river mouth. This is equal to 40,000 t/yr. The remaining 77 % or 136,000 t/yr are either deposited further offshore or dispersed into the Hudson Bay system, possibly along the eastern coast, as a result of Hudson Bay's counterclockwise circulation. Because all cores were taken from areas of active sedimentation, the 23 % are a minimum estimate. To elucidate the fate of the remaining 77 %, a larger grid of cores should be taken along the coastline.

Granulometric analyses suggest that processes controlling sediment transport and deposition vary over decadal time scales. Although we cannot define the exact causes of the observed patterns possible causalities could be variations in sediment plume intensity, sediment source, winnowing and wave resuspension, bioturbation or a combination of all three. These shifts may be related to variations in river discharge and/or variations in wave climate, possibly due to windier conditions or less sea-ice dampening, changes in sediment composition or a combination of all.

In summary, our findings suggest, that a warming climate may lead to decreased sea-ice coverage, more energetic marine conditions, and a greater offshore transport of terrestrial matter and that longer term river discharge signals should be preserved in the marine sedimentary record offshore the Great Whale River.

Acknowledgements

This project was funded by an ArcticNet grant to S. Bentley, the Canadian Center of Excellence in Canadian Arctic research, with additional support from the Canada Research Chair Secretariat, the Canada Foundation for Innovation, Memorial University of Newfoundland, and the Harrison Chair in Sedimentary Geology at Louisiana State University. Special thanks go to Robyn Haworth and Erlangga Septama, as well as the captains and crews of the CCGS Amundsen and CCGS Radisson, who were of indispensable help during the field seasons in 2007 and 2009. We would like to thank Duncan McIlroy for his helpful discussions and reviews. We thank Kendra Karrigan for her support in the laboratory.

References:

- Aagaard, K. and Carmack, E.C., 1989. The role of sea-ice and other freshwater in the Arctic Circulation. *Journal of Geophysical Research*, 94: 14485-14498.
- Allard, M. and Tremblay, G., 1983. La dynamique littorale des îles Manitoulin durant l'Holocène. *Zeitschrift für Geomorphologie*, 47: 61-95.
- Anderson, L.G., Jutterström, S., Kaltin, S., Jones, E.P. and Björk, G., 2004. Variability in river runoff distribution in the Eurasian Basin of the Arctic Ocean. *Journal of Geophysical Research*, 109 (1): pp. C01016 1-8.
- Anderson, R.F., Bopp, R.F., Buessler, K.O. and Biscaye, P.E., 1988. Mixing of particles and organic constituents in sediments from the continental shelf and slope off Cape Cod: SEEP I Results. *Continental Shelf Research*, 8: 925-946.
- Barber, D.C., Dyke, A., Hillaire-Marcel, C., Jennings, A.E., Andrews, J.T., Kerwin, M.W., Bilodeau, G., McNeely, R., Southon, J., Morehead, M.D. and Gagnon, J.-M., 1999. Forcing of the cold event of 8200 years ago by catastrophic drainage of Laurentide lakes. *Nature*, 400: 344-348.

- Bentley, S.J., Keen, T.R., Blain, C.A. and Vaughan, W.C., 2002. The origin and preservation of a major hurricane event bed in the northern Gulf of Mexico: Hurricane Camille, 1969. *Marine Geology*, 186: 423-446.
- Bentley, S.J., Sheremet, A. and Jaeger, J.M., 2006. Bioturbation, event sedimentation, and preserved sedimentary fabric: Field and model comparisons in three contrasting marine settings. *Continental Shelf Research*, 26: 2108-2124.
- Bernárdez, P., Prego, R., Giralt, S., Esteve, J., Caetano, M., Parra, S. and Francés, G., 2012. Geochemical and mineralogical characterization of surficial sediments from the Northern Rias: Implications for sediment provenance and impact of the source rocks. *Marine Geology*, 291-294: 63-72.
- Cutshall, N.H., Larsen, I.L. and Olsen, R., 1983. Direct analysis of ^{210}Pb in sediment samples: self-absorption corrections. *Nuclear Instruments and Methods in Physics Research B*, 206: 309-312.
- d'Anglejan, B. and Biskham, G., 1988. Late winter-early spring sedimentation off the Great Whale River, southeastern Hudson Bay. *Canadian Journal of Earth Sciences*, 25: 930-933.
- Déry, S.J. and Wood, E.F., 2004. Teleconnection between the Arctic Oscillation and Hudson Bay river discharge. *Geophysical Research Letters*, 31: pp. L18205 1-4
- Déry, S.J., Stieglitz, M., McKenna, E.C. and Wood, E.F., 2005. Characteristics and Trends of River Discharge into Hudson, James, and Ungava Bays, 1964-2000. *Journal of Climate*, 18: 2540-2557.
- Déry, S.J., Hernandez-Henriquez, M.A., Burford, J., E. and Wood, E.F., 2009. Observational evidence of an intensifying hydrological cycle in northern Canada. *Geophysical Research Letters*, 36: LI3402, pp. 5.
- Drake, D.E., 1997. Temporal and spatial variability of the sediment grain-size distribution on the Eel shelf: the flood layer of 1995. *Marine Geology*, 154: 169-182.
- Dyke, A.S. and Prest, V.K., 1987. Late Wisconsinan and Holocene History of the Laurentide Ice Sheet. *Géographie physique et Quaternaire*, 41: 237-263.
- Gagnon, A.S. and Gough, W.A., 2005. Trends in the dates of ice freeze-up and breakup over Hudson Bay, Canada. *Arctic*, 58 (4): 370-382.
- Goldberg, E.D., 1963. Geochronology with ^{210}Pb : Radioactive Dating, Conference Proceedings, November 19-23, 1962, Athens, IAEA, Vienna, pp. 121-131.

- Goldstein, S.J. and Jacobsen, S.B., 1988. REE in the Great Whale River estuary, NW Quebec. *Earth and Planetary Science Letters*, 88: 241-252.
- Gonthier, N., d'Anglejan, B. and Josenhans, H.W., 1993. Seismo-stratigraphy and sedimentology of Holocene sediments off Grande Rivière de la Baleine, southeastern Hudson Bay, Québec. *Géographie physique et Quaternaire*, 47(2): 147-166.
- Hansen, J.M., 1977. Sedimentary history of the island of Læsø, Denmark. *Bulletin of the Geological Society of Denmark*, 26: 217-236.
- Hare, A., Stern, G.A., Macdonald, R.W., Kuzyk, Z.Z. and Wang, F., 2008. Contemporary and preindustrial mass budgets of mercury in the Hudson Bay marine system: the role of sediment recycling. *Science of the Total Environment*, 406: 190-204.
- Haug, G.H.H., K.A., Sigman, D.M., Peterson, L.C. and Röhl, U., 2001. Southward Migration of the Intertropical Convergence Zone through the Holocene. *Science*, 293 (5533): 1304-1308.
- Hill, P.R., Meulé, S. and Longuépée, H., 2003. Combined-flow processes and sedimentary structures on the shoreface of the wave dominated Grande-Rivière-De-La-Baleine delta. *Journal of Sedimentary Research*, 73(2): 217-226.
- Hillaire-Marcel, C., 1976. La déglaciation et le relèvement isostatique sur la côte est de la Baie d'Hudson. *Cahiers de géographie de Québec*, 20(50): 185-220.
- Hillaire-Marcel, C. and Fairbridge, R.W., 1978. Isostacy and eustacy of Hudson Bay. *Geology*, 6: 117-122.
- Hochheim, K.P., Lukovich, J.V. and Barber, D.G., 2011. Atmospheric forcing of sea ice in Hudson Bay during the spring period, 1980-2005. *Journal of Marine Systems*, 88: 476-487.
- Hohndorf, A., 1969. Bestimmung der Halbwertszeit von ^{210}Pb . *Zeitschrift für Naturforschung*, 24A: 612-615.
- Hydro-Québec, 1993. Grande-Baleine Complex; Feasibility Study, Hydro-Québec.
- HydroQuebec, 1993. Grande-Baleine Complex; Feasibility Study, HydroQuebec.
- Ingram, R.G., 1981. Characteristics of the Great Whale River Plume. *Journal of Geophysical Research*, 86(C3): 2017-2023.

- Ingram, R.G., Wang, J., Lin, C., Legendre, L. and Fortier, L., 1996. Impact of freshwater on a subarctic coastal ecosystem under seasonal sea ice (southeastern Hudson Bay, Canada). I. Interannual variability and predicted global warming influence on river plume dynamics and sea ice. *Journal of Marine Systems*, 7: 221-231.
- Jones, E.P. and Anderson, L.G., 1994. Northern Hudson Bay and Foxe Basin: water masses, circulation and productivity. *Atmosphere-Ocean*, 32: 361-374.
- Karageorgis, A.P., Anagnostou, C.L. and Kaberi, H., 2005. Geochemistry and mineralogy of the NW Aegean Sea surface sediments: implications for river runoff and anthropogenic impact. *Applied Geochemistry*, 20: 69-88.
- Krishnaswami, S., Benninger, L.K., Aller, R.C. and Vondamm, K.L., 1980. Atmospherically-derived radionuclides as tracers of sediment mixing and accumulation in near-shore marine and lake sediments: Evidence from Be-7, Pb-210, and Pu-239, Pu-240. *Earth and Planetary Science Letters*, 47: 307-318.
- Kuzyk, Z.Z.A., Macdonald, R.W., Tremblay, J.-E. and Stern, G.A., 2010. Elemental and stable isotopic constraints on river influence and patterns of nitrogen cycling and biological productivity in Hudson Bay. *Continental Shelf Research*, 30 (2): 163-176.
- Lajeunesse, P. and Allard, M., 2003. Late Quaternary deglaciation, glaciomarine sedimentation and glacioisostatic recovery in the Rivière Nastapoka Area, Eastern Hudson Bay, Northern Québec. *Géographie physique et Quaternaire*, 57: 65-83.
- Lajeunesse, P. and St-Onge, G., 2008. The subglacial origin of the Lake Agassiz-Ojibway final outburst flood. *Nature Geoscience*, 1: 184-188.
- Lammers, R.B., Shiklomanov, A.I., Vörösmarty, C.J., Fekete, B.M. and Peterson, B.J., 2001. Assessment of contemporary Arctic river runoff based on observational discharge records. *Journal of Geophysical Research*, 106 (D4): 3321-3334.
- Lavoie, C., Hill, P.R., Allard, M., St-Onge, G. and Lajeunesse, P., 2008. High-resolution seismo-stratigraphy and sedimentological properties of late- and postglacial sediments in Lac Guillaume Delisle Estuary and Nastapoka Sound, eastern Hudson Bay. *Canadian Journal of Earth Sciences*, 45(427-441).
- Markham, W.E., 1986. The ice cover. *Canadian Inland Seas*. Elsevier, New York, 101-116 pp.

- McCave, I.N., Manighetti, B. and Robinson, S.G., 1995. Sortable silt and fine sediment size/composition slicing: parameters for palaeocurrent speed and palaeoceanography. *Palaeocenaography*, 10: 593-610.
- Miller, J.R., Lord, M., Yurkovich, Y., Mackin, G. and Kolenbrander, L., 2005. Historical trends in sedimentation rates and sediment provenance, Fairfield Lake, Western North Carolina. *Journal of the American Water Resources Association*, 41(5): 1053-1075.
- Mueller-Lupp, T., Bauch, H.A., Erlenkeuser, H., Heftet, J., Kassens, H. and Thiede, J., 2000. Changes in the deposition of terrestrial organic matter on the Laptev Sea shelf during the Holocene: evidence from stable carbon isotopes. *International Journal of Earth Sciences*, 89: 563-568.
- Muhammad, Z., Bentley, S.J., Febo, L.A., Droxler, A.W., Dickens, G.R., Peterson, L.C. and Opdyke, B.N., 2008. Excess ^{210}Pb inventories and fluxes along the continental slope and basins of the Gulf of Papua. *Journal of Geophysical Research*, 113: F01S17, pp. 14.
- Mukundan, R., Radcliff, D.E., Ritchie, J.C., Risso, L.M. and McKinley, R.A., 2010. Sediment Fingerprinting to Determine the Source of Suspended Sediment in a Southern Piedmont Stream. *Journal of Environmental Quality*, 39: 1328-1337.
- Nittrouer, C.A., Sternberg, R.W., Carpenter, R. and Bennett, J.T., 1979. Use of Pb-210 geochronology as a sedimentological tool: Application to the Washington continental-shelf. *Marine Geology*, 31: 297-316.
- Nittrouer, C.A., DeMaster, D.J., McKee, B.A., Cutshall, N.H. and Larson, I.L., 1983. The effect of sediment mixing on ^{210}Pb accumulation rates for the Washington continental shelf. *Marine Geology*, 54: 201-221.
- Nittrouer, C.A., DeMaster, D.J., Kuehl, S.A., McKee, B.A. and Thorbjarnarson, K.W., 1984/1985. Some questions and answers about the accumulation of fine-grained sediment in continental margin environments. *Geo-Marine Letters*, 4: 211-213.
- Paetzel, M. and Dale, T., 2010. Climate proxies for recent fjord sediments in the inner Sognefjord region, western Norway. *Geological Society, London, Special Publications*, 344: 271-288.
- Prinsenberg, S.J., 1986. The circulation pattern and current structure of Hudson Bay. *Canadian Inland Seas*. Elsevier, New York.

- Prinsenberg, S.J., 1988. Ice ridge contributions to the freshwater contents of Hudson Bay and Foxe Basin. *Arctic*, 41: 6-11.
- Saucier, F., Larouche, P., D'Astous, A. and Dionne, J., 1994. Moored physical oceanographic data from northeastern Hudson Bay between august 1992 and September 1993, Institut Maurice-Lamontagne.
- Saucier, F.J., Senneville, S., Prinsenberg, S., Roy, F., Smith, G., Gachon, P., Caya, D. and Laprise, R., 2004. Modelling the sea ice-ocean seasonal cycle in Hudson Bay, Foxe Basin and Hudson Strait, Canada. *Canadian Climate Dynamics*, 23: 303-326.
- Schäfer, W., 1962. *Aktuo-Paläontologie nach Studien in der Nordsee*. Kramer, Frankfurt am Main, 166 pp.
- Schoster, F., Behrends, M., Müller, C., Stein, R. and Wahsner, M., 2000. Modern river discharge and pathways of supplied material in the Eurasian Arctic Ocean: evidence from mineral assemblages and major and minor element distribution. *International Journal of Earth Sciences*, 89: 486-495.
- Sella, G.F., Stein, S., Dixon, T.H., Craymer, M., James, T.S., Mazzotti, S. and Dokka, R.K., 2007. Observation of glacial isostatic adjustment in "stable" North America with GPS. *Geophysical Research Letters*, 34(2): L02306, pp. 6.
- Sibert, V., Zakardjian, B., Gosselin, M., Starr, M., Senneville, S. and LeClainche, Y., 2011. 3D bio-physical model of the sympagic and planktonic productions in the Hudson Bay System. *Journal of Marine Systems*, 88: 401-422.
- Sommerfield, C.K., Ogston, A.S., Mulllenbach, B.L., Drake, D.E., Alexander, C.R., Nittrouer, C.A., Borgeld, J.C., Wheatcroft, R.A. and Leithold, E.L., 2007. Oceanic dispersal and accumulation of river sediment. In: C.A. Nittrouer, J.A. Austin, M.E. Field, J.H. Kravitz, J.P.M. Syvitski and P. Wiberg (Editors), *Continental-Margin Sedimentation: From Sediment Transport to Sequence Stratigraphy*. Blackwell Publishing, Oxford, UK, pp. 157-212.
- Stein, R., Dittmers, K., Fahl, K., Kraus, M., Matthiessen, J., Niessen, F., Pirrung, M., Polyakova, Y., Schoster, F., Steinke, T. and Fütterer, D.K., 2004. Arctic (palaeo) river discharge and environmental change: evidence from the Holocene Kara Sea sedimentary record. *Quaternary Science Reviews*, 23: 1485-1511.
- Straneo, F. and Saucier, F., 2008. The outflow from Hudson Strait and its contribution to the Labrador Current. *Deep-Sea Research Part I: Oceanographic Research Papers* 55 (8): 926-946.

Syvitski, J.P.M. and Milliman, J.D., 2007. Geology, Geography, and Humans Battle for Dominance over the Delivery of Fluvial Sediment to the Coastal Ocean. *The Journal of Geology*, 115: 1-19.

Wheatcroft, R.A. and Drake, D.E., 2003. Post-depositional alteration and preservation of sedimentary event layers on continental margins, I. The role of episodic sedimentation. *Marine Geology*, 199: 123-137.

Wheatcroft, R.A. and Sommerfield, C.K., 2005. River sediment flux and shelf sediment accumulation rates on the Pacific Northwest margin. *Continental Shelf Research*, 25: 311-332.

Wheatcroft, R.A., Wiberg, P.L., Alexander, C.R., Bentley, S.J., Drake, D.E., Harris, C.K. and Ogston, A.S., 2006. Post-depositional alteration and preservation of sedimentary strata. *Continental Margin Sedimentation*. Blackwell Publishing, 101-155 pp.

Wright, L.D. and Nittrouer, C.A., 1995. Dispersal of River Sediments in Coastal Seas: Six Contrasting Cases. *Estuaries*, 18: 494-508.

Chapter 3

Climatically controlled sediment and water discharge during the past two millennia: the subarctic Great Whale River, Hudson Bay, Canada

Abstract

To better understand the response of river discharge from the Great Whale River to global climatic changes, physical and geochemical proxies for fluvial and climatic variations have been studied in three gravity cores taken from a sedimentary basin within 7 km offshore of the river mouth. There is strong evidence that the Great Whale River responded to global climatic changes during the past 1500 to 2000 yr with decreased river discharge during the colder Little Ice Age (LIA) and increased river discharge, similar to modern values, during the warmer Medieval Warm Period (MWP). This is suggested by decreasing sediment mass accumulation rates (MAR) during the LIA, in contrast to increasing MAR during the MWP and Modern Optimum. MAR variations were strongest in the most distal core suggesting increased sediment retention in river proximal areas during the LIA, possibly due to increased sea-ice cover and associated wind-wave dampening. River discharge estimations are similar to modern values during the MWP but substantially lower during the LIA. A higher frequency signal is recorded in magnetic susceptibility (MS) records, suggesting river discharge variability with a period of 195–263 yr, which was persistent during the past ~2000 yr. Cyclicities of similar timescale from other studies from North America and the world suggest a relation to changes in the

hydrologic cycle due to North Atlantic sea surface temperature variability. If natural discharge variations occur with a period of 195-263 yr, they would be difficult to separate from anthropogenic influence in the existing 60-y instrumental discharge record. Despite the observed apparent discharge variability, no major changes were observed in marine burial of C and N during the past ~2000 yr. In summary, during the last ~2000y, warmer climates in eastern Hudson Bay produced increased river water and sediment discharge as well as stronger wave activity and increased sediment dispersal (due to decreased sea-ice coverage), while climatic cooling yielded the opposite effects. This implies that ongoing global climatic warming may lead to increasing river discharge from the Great Whale River.

1. Introduction:

Recent studies of the Hudson Bay watershed in northern Canada have shown that modern export of freshwater into Hudson Bay is highly variable, possibly decreasing, and strongly influenced by climatic forcing (Déry and Wood, 2004; Déry et al., 2005). Recently, much effort has been placed on paleoenvironmental reconstruction of the sub-Arctic Hudson Bay system (e.g., Haberzettl et al., 2010), especially on large scale climate changes during the transition from the last glacial period to the Holocene. The most prominent such example is the last outburst of the proglacial lake Agassiz-Ojibway around 8.5 cal kyr BP and its impact on global climate (e.g., Hall et al., 2001; Alley and Ágústsdóttir, 2005; Lajeunesse and St-Onge, 2008). Studies of environmental records from the Great Whale River (GWR)

spanning the last century (Hare et al., 2008; Kuzyk et al., 2010), to several millennia (Gonthier et al., 1993; Jenner and Piper, 2002; Haberzettl et al., 2010) suggest the potential for sub-century-scale paleoenvironmental preservation at the Great Whale River, but have not resolved environmental patterns within the strong climatic variations from the Medieval Warm Period to the Little Ice Age to the present, which set the context for conditions in the future. Hudson Bay is likely to be affected sooner and more strongly by climate change than the Arctic Ocean due to its close association with terrestrial systems (Gough and Wolfe, 2001; ACIA, 2005; Gagnon and Gough, 2005). Because Hudson Bay is the most southerly extension of the Arctic Ocean and because of its very high freshwater input (30 % of the total Canadian runoff) (ACIA, 2005; Déry et al., 2005), it is important to understand the impact of historical climate changes on river discharge to the bay as an analogue to ongoing climate-change consequences in Hudson Bay and its surrounding terrestrial systems (Johannessen et al., 2004; Déry et al., 2005; Gagnon and Gough, 2005; Lawrence and Slater, 2005).

To address this knowledge gap, this study presents continuous high-resolution records of paleoenvironmental proxies from marine sediment cores offshore the Great Whale River mouth in southeastern Hudson Bay (Fig. 1). The Great Whale River sediment dispersal system was chosen because: 1) it is statistically representative of the response of Hudson Bays rivers to modern climatic variations (Déry et al., 2005); 2) the proximal marine basin contains a thick Holocene sedimentary succession; and 3) a sediment budget reflecting modern discharge conditions (< 150 yr BP) is available for the

study area (Hulse and Bentley, 2012). In this study, geochemical and physical sedimentological proxies of sediment and water discharge and paleoenvironmental conditions were measured in order to: 1) create a total Holocene sediment budget for the

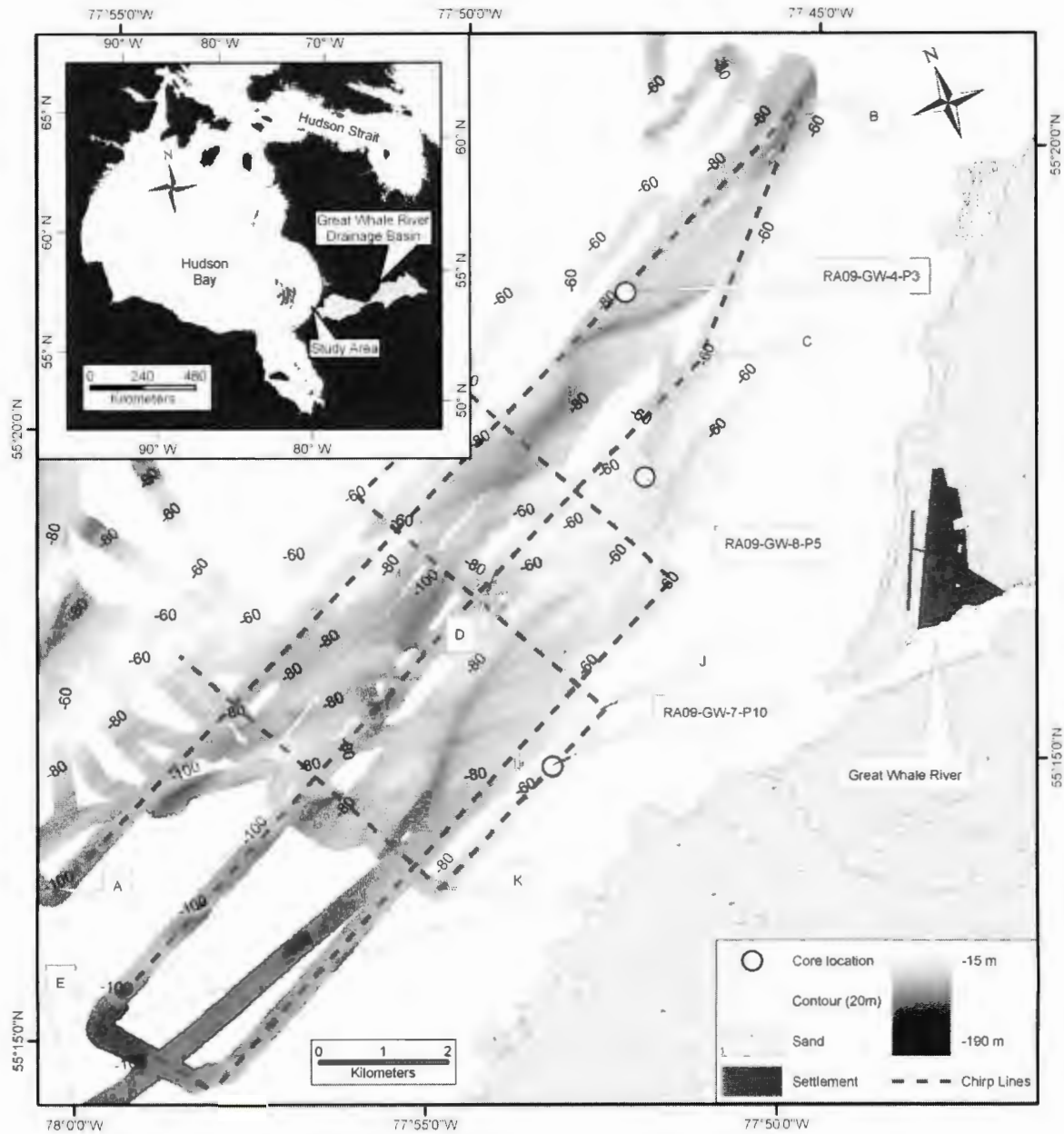


Figure 1: The small map displays the drainage basin of the Great Whale River and the location of the study area offshore the river mouth. The larger map shows bathymetry and the location of sub-bottom profiles (Chirp Lines, dashed) and coring locations (circles). Capital letters refer to sub-bottom profiles in Figure 2.

GWR; 2) study changes in sediment mass fluxes and their link to palaeoenvironmental change; 3) investigate short term variability in sediment discharge and climate during the past two millennia; and 4) place historical river discharge variations in the broader framework of climatic change.

2. Study area

2.1 Deglacial and postglacial history:

Hudson Bay and its surroundings were covered by the Laurentide Ice Sheet (LIS) during the last glaciation (Dyke and Prest, 1987), depressing the land > 315 m below the present land surface (Hillaire-Marcel, 1976; Shilts, 1986). Along the southern edge of the LIS a large ice-dammed proglacial lake developed (Lake Agassiz-Ojibway), which drained around 8500 cal yr BP, as a result of the collapse of the LIS (Barber et al., 1999; Lajeunesse and St-Onge, 2008). This catastrophic northward drainage was followed by the invasion of the Tyrell Sea into the glacio-isostatically depressed Hudson Bay Basin from the north (Hillaire-Marcel, 1976; Lajeunesse, 2008). Postglacial isostatic rebound of Hudson Bay occurred at rates of 10 cm/yr at 8000 BP (Allard and Seguin, 1987; Lajeunesse and Allard, 2003), decreasing to about 1 cm/yr since approximately 2800 yr BP (Gonthier et al., 1993).

2.2 Oceanographic setting and climate

Dense, cold, and saline Arctic water enters Hudson Bay from the northwest following a counterclockwise circulation eventually flowing out as relatively warm and fresh water through Hudson Strait (Prinsenberg, 1986; Jones and Anderson, 1994; Saucier

et al., 1994; Saucier et al., 2004). Average surface currents are 5cm/s in summer and 2-3 cm/s in winter. In coastal areas, sea-surface circulation is mainly controlled by wind forcing. Tides near the Great Whale River are semidiurnal with a range of about 2 m and tidal currents <10 cm/s (Ingram, 1981).

Sea-ice begins to form in late October and coverage is complete in December. Melting usually starts in May, until open water conditions are reached in early August (Markham, 1986). Landfast ice can rim the shore throughout the year and mobile ice can cover offshore areas 9/10ths of the year. Since the mid-1990s eastern Canada and Hudson Bay have experienced declining sea-ice extent and duration (Gagnon and Gough, 2005; Hochheim and Barber, 2010; Hochheim et al., 2011).

Hudson Bay receives 30 % of the total Canadian freshwater runoff (Déry et al., 2005). Mean annual freshwater discharge is 639 m³/s (HydroQuebec, 1993; Ingram et al., 1996). At the GWR a distinct 1-2 m thick freshwater plume of about 100 km² forms in summer and a significantly thicker and more extensive freshwater plume develops during winter due to seasonal ice coverage, despite a much lower river discharge at this time (Ingram, 1981).

2.3 Drainage basin geology:

The bedrock in the drainage basin consists mainly of Proterozoic metavolcanic and metasedimentary rocks (Shilts, 1986), overlain by Pleistocene glacial deposits. Fine silty clay deposits are found in the lower sections of the river valleys, dating back from the marine invasion of the Tyrell Sea (HydroQuebec, 1993) between cal 8100 and 8000

yr BP (Hillaire-Marcel, 1976; Dyke and Prest, 1987). The main part of easily erodible materials further upstream are fluvioglacial sands and tills (HydroQuebec, 1993).

2.4 Marine sedimentary basin:

The study area is a marine sedimentary basin offshore of the Great Whale River mouth on the southeastern coast of Hudson Bay (Figure 1) with fluvio-deltaic muds averaging 16 m in thickness (Gonthier et al., 1993; this study) preserving a sedimentary archive for “palaeo river discharge” studies. Within 3 km of the river mouth, a basin 60-100m deep is rimmed by shoals ~20 m deep, forming a natural sediment trap in front of the river mouth (Hülse and Bentley, 2012). The bedrock topography forms discontinuous ridges and troughs trending NE-SW, similar to the physiography of the Manitounuk Islands to the NE (Gonthier et al., 1993). Average sedimentation rates for the study area during the late Holocene were estimated to be 0.25 and 0.08 cm/yr, from a small number of radiocarbon dates by Gonthier et al. (1993) and Jenner and Piper (2002) respectively. A detailed study of Great Whale River sediment dispersal demonstrates an apparent $^{210}\text{Pb}_{\text{xs}}$ average sedimentation rate of 0.16 cm/yr over the past ~150 yr (Hülse and Bentley, 2012). Modern sediment load of the Great Whale River is 176,000 t/yr (HydroQuebec, 1993), of which 23 % (40,000 t/yr) are deposited in a 25 km² area within 7 km off the river mouth (Hülse and Bentley, 2012).

3. Materials and Methods:

3.1 Bathymetry, subsurface stratigraphy and core sampling

Bathymetric and subsurface data were collected with a Kongsberg-Simrad EM-300 multibeam echosounder and a hull-mounted 3.5 kHz Knudsen Chirp 3200 subbottom profiler during three ArcticNet research cruises between 2007 and 2010. The data were provided and processed by the Ocean Mapping Group at the University of New Brunswick, Fredericton, NB, Canada. Data were visualized using Knudsen PostSurvey and ArcGIS software. Subbottom profiles were used to create a Holocene sediment budget for the study area by measuring fluvio-deltaic sediment thickness and applying Eq.1,

$$M_T = (H_T * A * (1-\theta) * \rho_S) / T \quad \text{Eq. 1}$$

where M_T is total sediment accumulation over elapsed time T [yr], H [m] is average fluvio-deltaic sediment thickness of 16 m, A [km^2] = 25 km^2 is the size of our study area, θ is porosity of the sediment (0.65, taken from long cores in the area) and ρ_S is the assumed density of 2.65 g/cm³ of the sediment.

To characterize the sediment composition and its relation to river discharge, gravity cores were collected to sample fluvio-deltaic muds deposited off the river mouth of the Great Whale River. The cores were cut in 1 m sections shipboard and kept at 4°C during transport and storage. Sampling sites in depocentres were carefully chosen through the study of bathymetry and 3.5 kHz sub-bottom profiles.

3.2 Radiocarbon analyses

Radiocarbon dates are based on bulk organic carbon due to insufficient foraminifera, shells, and plant debris. Samples were taken as 1 cm slices of sediment, homogenized, treated with 10 % HCl to remove inorganic carbon, dried at 40° C and ground to fine powder. Four samples from each core were sent to the Radiochronology Laboratory at Laval University, Quebec City, Canada, for sample preparation, and inorganic carbon was removed by HCl treatment. Organic carbon was combusted to CO₂ and sent to the Keck Carbon Cycle AMS Facility, University of California, Irvine, CA, USA, to produce graphite targets and AMS measurements. Because all data will be discussed with reference to historical climatic periods, radiocarbon ages were calibrated to median calendar ages (Years BC/AD) using the online OxCal 4.1 calibration program (Bronk Ramsey, 2009) and the Marine09 correction curve (Reimer et al., 2009) with known ΔR values and ΔR errors of 107 (+/- 50) yrs from the area, corresponding to a reservoir effect of 370 (+/- 50) yrs (McNeely et al., 2006). The geochronological framework was used to produce age-depth diagrams in order to turn depth scales into age scales and to calculate sediment and mass accumulation rates (SARs, MARs). SARs [cm/yr] were calculated after Eq. 2, where $\Delta^{14}C_{cal}$ [yr] is the time elapsed between two radiocarbon dates and ΔD [cm] is the depth difference between the two sequential samples.

$$SAR = \Delta D / \Delta^{14}C_{cal} \quad \text{Eq. 2}$$

MARs [g/cm²/yr] were calculated after Eq. 3, where θ is porosity, taken from Geotek Multi-Sensor-Core-Logger (MSCL) measurements, averaged for the time intervals between radiocarbon dates, and ρ_S is the assumed sediment density of 2.65 g/cm³ (Muhammad et al., 2008).

$$MAR = SAR * (1 - \theta) * \rho_S \quad \text{Eq. 3}$$

3.3 River discharge estimates

To hindcast apparent freshwater discharge Q [km³/yr] variations, we inverted the BQART-model (Eq. 4) of Syvitski and Milliman (2007). The model is based on a global dataset of 488 rivers and is highly representative of geology, climate and socio-economic conditions.

$$Q = (Q_S / (2 \omega BA^{0.5} R))^{(1/0.31)} \quad \text{Eq. 4}$$

The values for drainage basin area A [km²] and maximum relief R [km] were taken from a digital elevation model of the drainage basin created using the hydrologic modeling software RiverTools software (Hulse and Bentley, 2012). The coefficient ω provides units in MT/yr. Coefficient B accounts for basin properties, such as lithology L , glacial erosion I , trapping efficiency T_E , and the anthropogenic factor E_h , and was calculated as $B = IL(I-T_E)E_h$ (Syvitski and Milliman, 2007). The value of the lithology factor L was chosen from observations of Syvitski and Milliman (2007), who described the Canadian Shield of northeastern Canada as acid plutonic, high-grade metamorphic with $L = 0.5$.

Results might be improved by using slightly higher L values between 0.6 and 0.7, which would account for the presence of soft glacial and postglacial sediments in the drainage basin. However, because the extent of soft sediments is unknown, we used $L = 0.5$ for this study, to provide the most conservative estimate. The anthropogenic factor was chosen to be $E_h = 1$ for drainage basins with a low human footprint. Because there is no information about sediment trapping efficiency in the drainage area, an average value of 0.8 was used for $(1-T_E)$ (Syvitski and Milliman, 2007). Sediment discharge Q_s [MT/yr] was calculated from MARs in the study area and assuming that 23% of the discharged sediment were deposited in our study area, which is characteristic of modern conditions (Hulse and Bentley, 2012).

3.4 Physical sedimentary properties

3.4.1 X-radiography

In order to study sedimentary structures, sediment cores were split longitudinally and imaged x-radiographically using a Thales Flashscan 35 X-ray detector, illuminated with a Lorad LPX160 X-ray generator. To account for variable exposure due to the semicircular cross-section, an aluminum compensator plate was designed to counterbalance decreasing core thickness towards the sides of the core. Images were stored as 14-bit TIFFs and studied using ImageJ software.

3.4.2 Granulometry

Grain-size distributions were measured at 5-cm intervals. Small amounts of wet samples were placed in 0.5 % NaPO₃ solution to disaggregate clay particles, sonicated for

half an hour, left in solution overnight, and then sonicated again before analyses. Analyses were performed using a HORIBA Partica LA-950 laser diffraction particle size analysis system, with a particle size range of 0.1-3000 μm .

3.4.3 Magnetic susceptibility and bulk density

Magnetic susceptibility (MS) was measured using a Geotek Multi-Sensor-Core-Logger (MSCL) (www.geotek.co.uk) equipped with a Bartington Meter Model MS2, loop sensor MS2C, and point sensor MS2E/1. The loop sensor was used for whole core measurements. It records average values for an approximately 20 mm thick slice of sediment. The point sensor delivers vertical resolution of ~4 mm with a horizontal sensor width of 10.5 mm. The resulting measurements are reported in volume-specific MS κ . Volume-specific MS κ then was corrected for density to mass-specific MS X [m^3/kg] using the Geotek MSCL processing software.

Bulk density was measured using the Geotek gamma densitometer. This sensor emits a narrow beam of ^{137}Cs gamma rays passing through the core, recorded by a NaI scintillation detector. Bulk density is reported in g/cm^3 .

3.5 Sedimentary organic matter

Bulk sedimentary organic matter was sampled at 5 cm intervals and measured as TOC at the CREATIT Network TERRA Facility Stable Isotope Laboratory at the Memorial University of Newfoundland. Wet sediment samples were acidified in 10 % HCl overnight to remove calcium carbonate. Residues were centrifuged three times and rinsed with distilled water, dried overnight at 50 °C and powdered for analysis.

Sedimentary total organic carbon (TOC), total nitrogen (TN), and the carbon isotope ratios ($\delta^{13}\text{C}$) of TOC were measured using a Carlo Erba NA 1500 Series 2 elemental analyzer interfaced to an isotope ratio mass spectrometer (ThermoElectron Delta V Plus) using a Conflo 2 interface (ThermoElectron). Mean deviations were calculated from duplicate measurements on ten samples, resulting in a mean error of $\mu \pm 1\sigma$ ($n=10$) for $\mu(\text{TOC}) = 0.01 \pm 0.01$ wt.%, $\mu(\text{TN}) = 0.001 \pm 0.001$ wt.%, $\mu(\text{C/N}) = 0.21 \pm 0.29$, and $\mu(\delta^{13}\text{C}) = 0.14 \pm 0.08$ ‰. Ratios of C/N are TOC over TN. Trends in data were evaluated with linear regressions and correlation coefficients (discussed in Results), but neither regression lines nor uncertainty estimates are shown on plots for the sake of clarity.

4. Results

4.1 Subsurface stratigraphy and total fluvio-deltaic sediment thickness

Subsurface stratigraphy was subdivided into different units according to acoustic properties and after descriptions given by Gonthier et al. (1993). In general, four stratigraphic units overlie bedrock in the study area, representing sub-glacial sediments, glacio-lacustrine, postglacial normal marine and fluvio-deltaic sediments, (Fig. 2). Our study focuses on the uppermost unit, the fluvio-deltaic sediments. The base of the internally well-stratified fluvio-deltaic muds (Fig. 2) is interpreted as the first strong reflector (α -reflector, Fig. 2) (Gonthier et al., 1993). Sediment thickness H [m] for the fluvio-deltaic muds was measured in 1-km intervals in subbottom profiles. The average thickness of this unit is 16 m but reaches 30 m in the CHIRP profiles closest to the river mouth. Acoustic properties of the fluvio-deltaic muds vary with distance to the river, showing strong internal reflectors close to the river mouth (line JK, Fig. 2) and weaker or

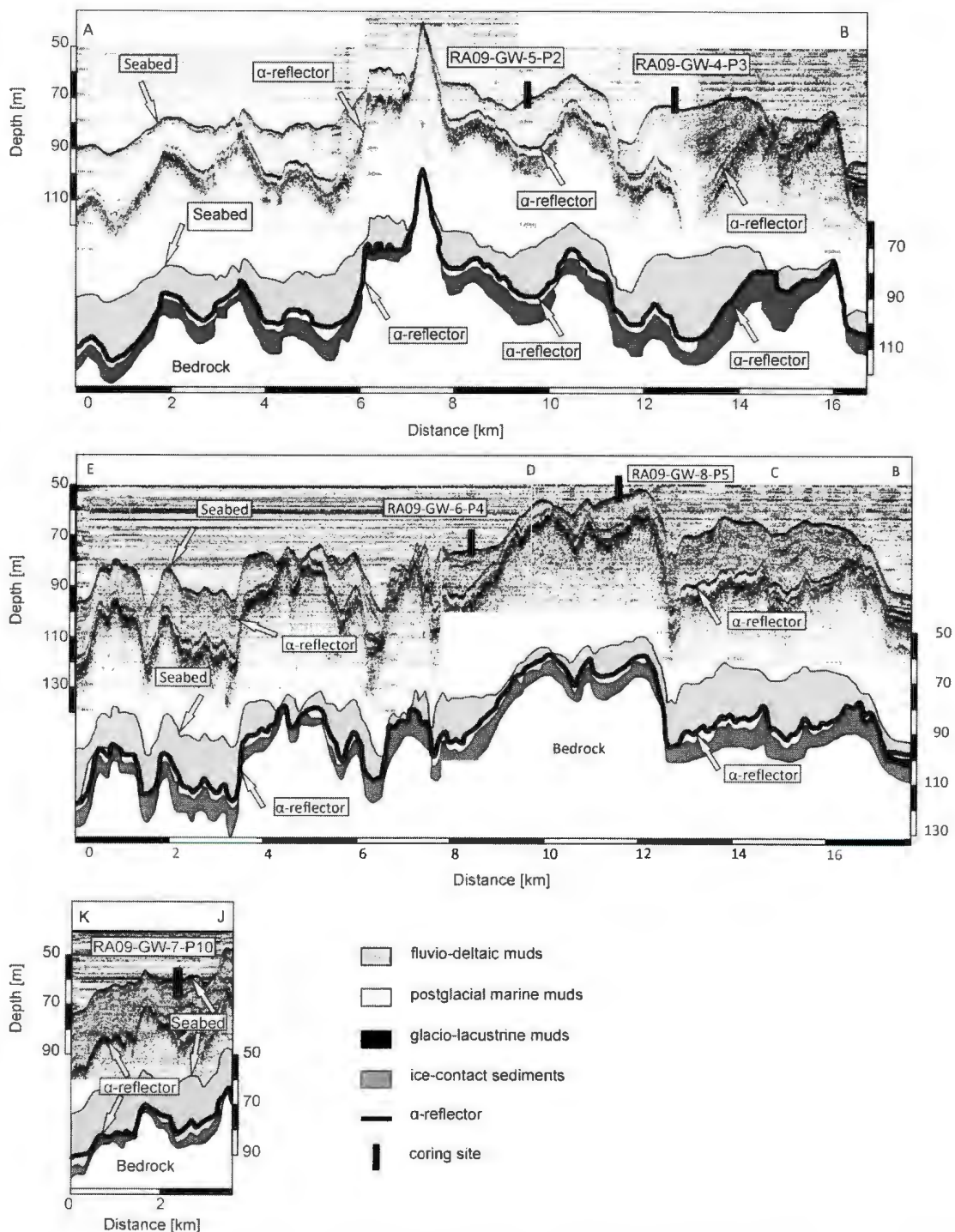


Figure 2: This figure shows 3.5 kHz CHIRP sub-bottom profiles from the Great Whale River site (dashed lines in Fig. 1) and the interpretation of stratigraphic units. Coring locations are marked with vertical black bars.

no internal reflectors more distal to the river (line AB, Fig. 2). On some local highs (e.g. between kilometer 3 and 4 in Line EDCB, Fig. 2) the internal reflector strength of the fluvio-deltaic muds increases upwards.

4.2 Core Lithology

Sediments of all three cores are composed of homogeneous marine mud of olive grey color and with numerous black flakes of degraded organic matter that disappeared due to oxidation after opening the cores. X-radiographs record homogeneous bioturbated fabrics with few preserved burrows but no physical sedimentary structures. Sparsely distributed dropstones of up to 5 cm and some broken shell fragments are present in all cores. All images are available for closer study in Appendix F (Hülse, 2012).

4.3 Geochronology and sediment accumulation rates

Twelve radiocarbon dates, four from each core, were used to establish a geochronological framework (Fig. 3). Radiocarbon dates represent maximum ages, because organic matter may be reworked or eroded from older sediments in the drainage basin of the GWR. Due to age reversal the lowermost sample of core RA09-GW-8-P5 was not used for interpretation (Fig. 3). All cores show a large age offset, which has been estimated from fitting regressions to the calibrated ^{14}C dates, extrapolating to the sediment surface and subtracting the year of the intersection with the sediment surface from the year of core collection. The resulting differences then were added to the calibrated ^{14}C ages, giving the calibrated and offset corrected $^{14}\text{C}_{\text{cal}}$ ages (Table 1). This is justified because all (except Ra09-GW-8-P5, 245.5 cm) ^{14}C ages display nearly linear

age-depth relationships (Fig. 3), and because measurements of $^{210}\text{Pb}_{\text{xs}}$ SAR shows modern sediment accumulation (Hülse and Bentley, 2012) is occurring at rates of the same magnitude as SARs in Figure 4.

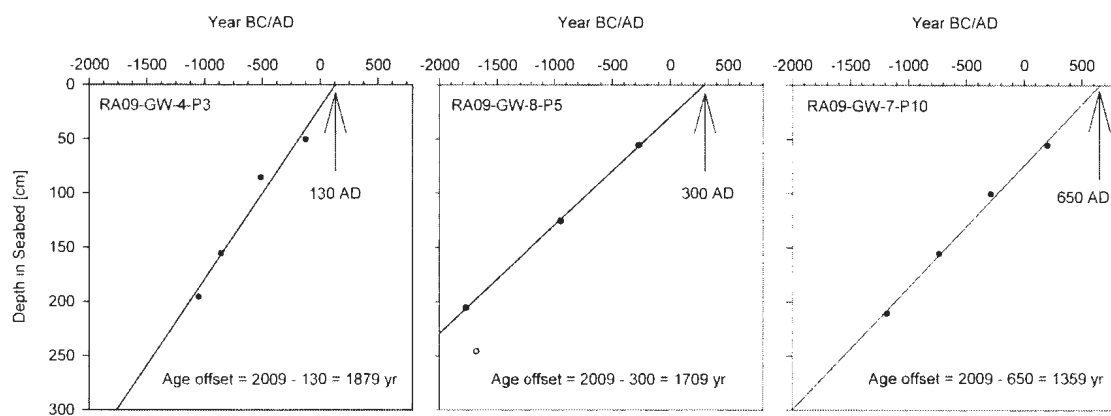


Figure 3: The graphs display age-depth plots of calibrated ^{14}C dates. The age-offset was corrected for by fitting regressions. The lowermost date in core RA09-GW-8-P5 was not considered for offset correction due to age reversal.

Sediment accumulation rates (SARs) were calculated using Eq. 2 and plotted versus time (yr BC/AD) (Table 1, Fig. 4). Core RA09-GW-4-P3 (solid line in Fig. 4) exhibited the highest SARs, reaching 0.21 cm/yr between 900 yr AD and 1100 yr AD. Between ~1100 yr AD and ~1400 yr AD SAR was 0.2 cm/yr. From 1400 yr AD to 1750 yr AD SAR was only 0.09 cm/yr and increased again to 0.19 cm/yr between 1775 yr AD and 2009 yr AD. In core RA09-GW-8-P5 (dotted line in Fig. 4) SAR was constant from core base to top over the time span 63 yr BC to 2009 yr AD. Due to the age reversal of the lowermost date in this core, SARs for sediments older than 63 yr BC were not calculated. In core RA09-GW-7-P10 (dashed line in Fig. 4) SAR was 0.12 cm/yr from ~200 yr AD to ~1100 yr AD. Between ~1100 yr AD and 1600 yr AD SAR was 0.09

cm/yr. After 1600 yr AD SAR was 0.12 cm/yr. MARs calculated after Eq. 3 generally followed the same trends as SARs.

Table 1: The Table a) shows ^{14}C sampling depth, uncalibrated ages ($^{14}\text{C}_{\text{uncal}}$), OxCal calibrated ages ($^{14}\text{C}_{\text{OxCal}}$), and the calibrated and offset corrected ages ($^{14}\text{C}_{\text{cal}}$), which were used for all interpretations in this study. Table b) shows the time intervals recorded between the $^{14}\text{C}_{\text{cal}}$ dates and resulting sediment accumulation rates (SAR). Mass accumulation rates (MAR) were calculated using porosity σ (from Geotek Multi-Sensor-Core-Logger) and the assumed mineral grain density.

a) ^{14}C age calibration

Core	Depth [cm]	$^{14}\text{C}_{\text{uncal}}$ [yr BP]	Error [+/- yr]	$^{14}\text{C}_{\text{OxCal}}$ [yr BC/AD]	Range [yr]	Offset	$^{14}\text{C}_{\text{cal}}$ [yr BC/AD]
RA09-GW-4-P3	50.5	2445	15	-127	75	1879	1753
	85.5	2750	15	-514	117	1879	1365
	155.5	3045	15	-858	60	1879	1022
	195.5	3195	15	-1053	91	1879	827
RA09-GW-8-P5	55.5	2545	15	-272	76	1709	1438
	125.5	3120	15	-948	78	1709	762
	205.5	3775	15	-1772	85	1709	-63
	245.5	3715	15	-1681	70	-	-
RA09-GW-7-P10	55.5	2275	20	200	140	1359	1559
	100.5	2690	15	-288	132	1359	1072
	155.5	3040	15	-736	148	1359	623
	210.5	3400	15	-1186	163	1359	174

b) Sediment and mass accumulation rates

Core	Time Interval	Porosity σ	Density [g/cm ³]	SAR [cm/yr]	MAR [g/cm ² /yr]
RA09-GW-4-P3	2009 to 1750	0.72	2.65	0.19	0.14
	1750 to 1360	0.67	2.65	0.09	0.08
	1360 to 1020	0.67	2.65	0.20	0.18
	1020 to 850	0.66	2.65	0.21	0.19
RA09-GW-8-P5	2009 to 1440	0.67	2.65	0.10	0.08
	1440 to 760	0.62	2.65	0.10	0.10
	760 to -63	0.63	2.65	0.10	0.10
	-63 to -495 ?	0.63	2.65	0.10	0.10
RA09-GW-7-P10	2009 to 1560	0.69	2.65	0.12	0.10
	1560 to 1070	0.65	2.65	0.90	0.90
	1070 to 620	0.64	2.65	0.12	0.12
	620 to 170	0.66	2.65	0.12	0.11

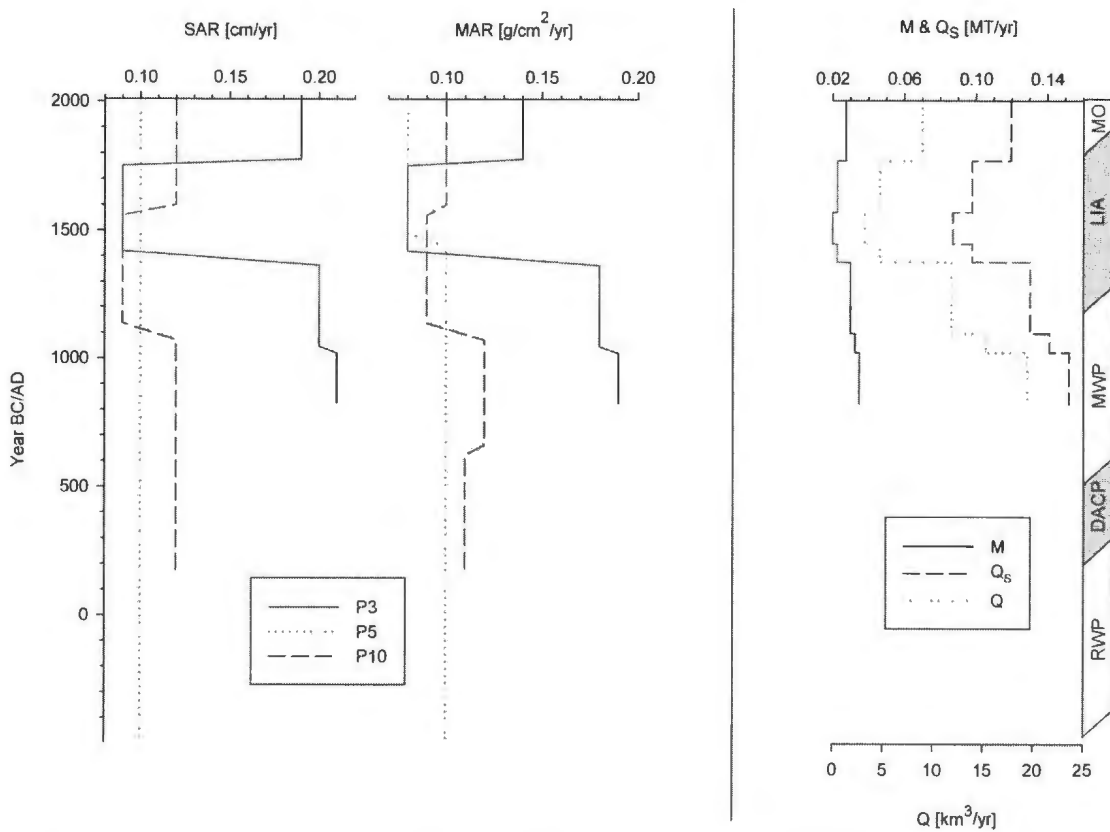


Figure 4: The left and middle graph display sediment and mass accumulation rates (SAR, MAR) of cores RA09-GW-4-P3 (black), RA09-GW-8-P5 (red) and RA09-GW-7-P10 (blue) plotted versus depth. The graph to the right displays average mass accumulation M in our study area, estimated sediment discharge Q_s and estimated river discharge Q . The vertical bar to the right shows the approximate duration of the Modern Optimum (MO), Little Ice Age (LIA), Medieval Warm Period (MWP) and Dark Ages Cold Period (DACP).

4.4 Physical sediment properties

In core RA09-GW-7-P10 mean grain diameter is approximately 20 μm (silt sized) throughout the core (Fig. 5). At the core base, between ~ 150 and ~ 350 yr AD, mean grain diameter is slightly lower, with lows $< 8 \mu\text{m}$. This is accompanied by low densities of $< 1.52 \text{ g/cm}^3$ during this time interval (Fig. 5). After ~ 350 yr AD average density is around 1.63 g/cm^3 and drops to $< 1.5 \text{ g/cm}^3$ after ~ 1850 yr AD (towards the sediment surface).

Density measurements are more variable between ~350 yr AD and ~1250 yr AD, compared to the time interval between ~1250 yr AD and ~1900 yr AD. The density patterns of core RA09-GW-7-P10 appear to correlate with changes in magnetic susceptibility (Fig.5).

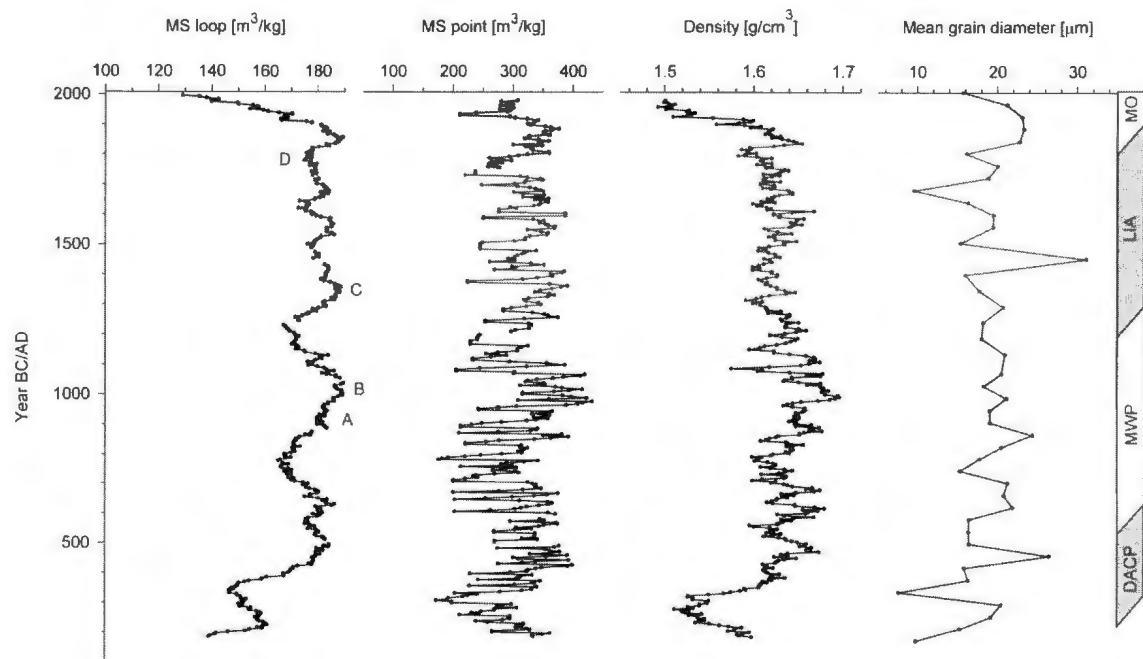


Figure 5: These graphs display variations through time in magnetic susceptibility (MS loop and point sensors), density, and mean grain diameter of core RA09-GW-7-P10. The vertical bar to the right shows the approximate duration of the climatic periods Modern Optimum (MO), Little Ice Age (LIA), Medieval Warm Period (MWP), Dark Ages Cold Period (DACP), and Roman Warm Period (RWP). The most recent cold period, LIA, is shaded in gray. Upper case letters A, B, C, and D indicate peaks that can be correlated to the cores in Figures 6 and 7.

In core RA09-GW-8-P5 (Fig. 6) mean grain diameter varies around 12 μm . Mean grain diameter is most variable between ~500 yr BC and ~650 yr AD. After ~650 yr AD

mean grain diameter appears less variable and increases from ~8 μm to ~17 μm until ~1400 yr AD. After ~1400 yr AD, mean grain diameter decreases to ~10 μm near the sediment surface, and variability is low. Density is relatively constant throughout the core with an average value of ~1.68 g/cm³ (Fig. 6). In sediments younger than ~1600 yr AD density slowly decreases and rapidly drops after ~1900 AD becoming ~1.57 g/cm³ at the sediment surface.

In core RA09-GW-4-P3 (Fig. 7) mean grain diameter is ~12 μm . Between ~800 yr AD and ~1400 yr AD mean grain diameter is variable but seems to increase from 10 μm to 17 μm . From ~1400 yr AD to ~1750 yr AD, mean grain diameter is relatively stable near ~15 μm , after which grain size becomes more variable. Average density is ~1.60 g/cm³ and decreases towards the sediment surface to ~1.3 g/cm³.

4.5 Magnetic Susceptibility

In core RA09-GW-7-P10 (Fig. 5), average MS-loop values are ~180 m³/kg. MS-loop values are lowest (<150 m³/kg) between ~150 and ~350 yr AD. Fluctuations in loop MS are evident in Figure 5, with magnitudes of 20-40 m³/kg. Based on apparent ages for MS maxima in Figure 5, the mean period for MS fluctuations in core RA09-GW-7-P10 is 232±97 yr (n=8 over 1625 yr).

In core RA09-GW-8-P5 (Fig. 6) MS-loop values vary around 145 m³/kg, with fluctuation magnitudes of 20-30 m³/kg (Fig. 6). Average MS-point values are ~180 m³/kg. Variability is highest (magnitudes >150 m³/kg) between ~500 yr BC and 0 yr AD. Between ~0 yr AD and ~900 yr AD MS-point values are very stable (magnitude ~50 m³/kg), followed by a period of more variable MS-point values from ~900 yr AD until

today. Based on apparent ages for MS maxima in Figure 6, the mean period for MS fluctuations in core RA09-GW8-P5 is 263 ± 71 yr (n=9 over 2100 yr).

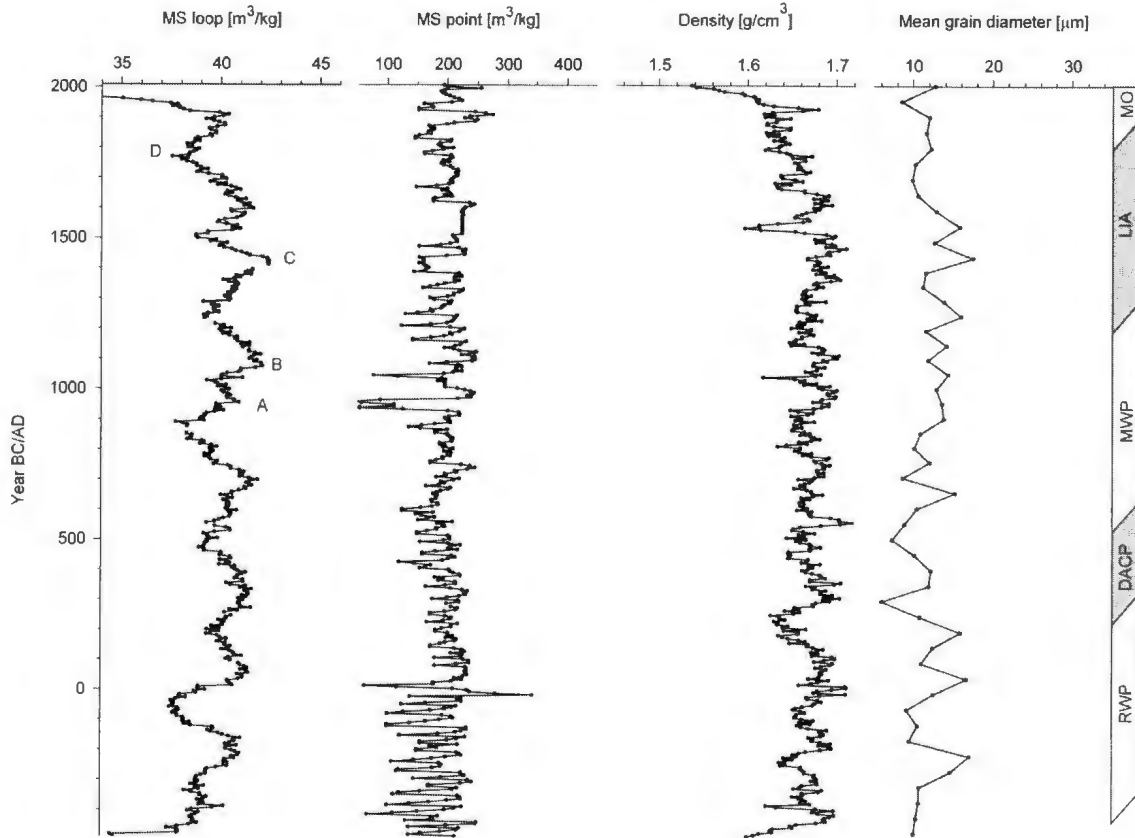


Figure 6: These graphs display variations through time in magnetic susceptibility (MS loop and point sensors), density, and mean grain diameter of core RA09-GW-8-P5. The vertical bar to the right shows the approximate duration of the climatic periods Modern Optimum (MO), Little Ice Age (LIA), Medieval Warm Period (MWP), Dark Ages Cold Period (DACP), and Roman Warm Period (RWP). Upper case letters A, B, C, and D indicate peaks that can be correlated to the cores in Figures 5 and 7.

In core RA09-GW-4-P3 MS-loop values vary around ~ 120 m³/kg (Fig. 7). MS-loop is most variable between ~ 800 yr AD and ~ 1200 yr AD with magnitudes of ~ 70 m³/kg. After ~ 1200 yr AD MS-loop values become more stable and are nearly uniform ~ 120 m³/kg between ~ 1400 yr AD and ~ 1800 yr AD. After ~ 1800 yr AD MS-loop values

decrease towards the sediment surface. MS-point values are $\sim 225 \text{ m}^3/\text{kg}$ and generally follow the patterns of the MS-loop values. Based on apparent ages for MS maxima in Figure 7, the mean period for MS fluctuations in core RA09-GW-4-P3 is $195 \pm 78 \text{ yr}$ ($n=6$ over 975 yr).

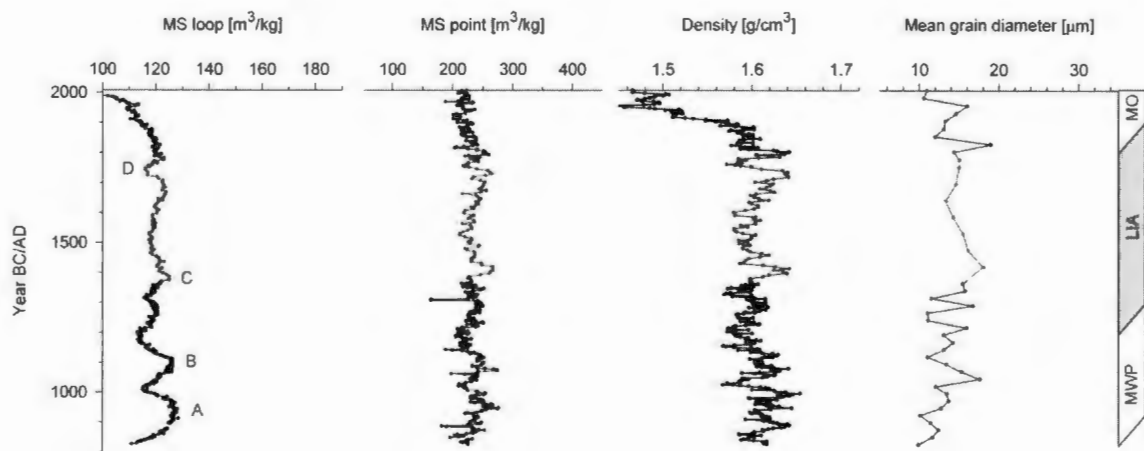


Figure 7: These graphs display variations through time in magnetic susceptibility (MS loop and point sensors), density, and mean grain diameter of core RA09-GW-4-P3. The vertical bar to the right shows the approximate duration of the climatic periods Modern Optimum (MO), Little Ice Age (LIA), and Medieval Warm Period (MWP). The most recent cold period, LIA, is shaded in gray. Upper case letters A, B, C, and D indicate peaks that can be correlated to the cores in Figures 5 and 6.

4.6 Carbon and nitrogen geochemistry:

In core RA09-GW-7-P10 average TOC is $\sim 0.56 \text{ wt.\%}$ (Fig. 8, dashed line). Overall, TOC increases from $\sim 0.52 \text{ wt.\%}$ between $\sim 150 \text{ yr AD}$ and $\sim 1100 \text{ yr AD}$ to $\sim 0.65 \text{ wt.\%}$ near the sediment surface (after $\sim 1680 \text{ yr AD}$ $r^2=0.6$). The lowest TOC of $\sim 0.3 \text{ wt.\%}$ is at $\sim 340 \text{ yr AD}$. Average TN is $\sim 0.055 \text{ wt.\%}$ and increases towards the sediment

surface, most distinctly after 1680 yr AD ($r^2=0.8$). Lowest TN of ~0.03 wt.% was measured at ~340 yr AD and two peaks of ~0.074 wt.% and ~0.071 wt.% occur at ~1360 yr AD and ~1600 yr AD, respectively. The resulting C/N (wt. %) profile does not follow any general trend. Average C/N is ~10.4. Two distinct lows of ~8.7 and ~9 occur at ~1360 yr AD and ~1600 yr AD, respectively. The highest C/N of ~11.7 was measured at ~1700 yr AD, after which C/N decreases ($r^2=0.84$) to ~10 at the sediment surface. The average $\delta^{13}\text{C}$ is ~-25 ‰. No general trend in $\delta^{13}\text{C}$ was observed. The lowest $\delta^{13}\text{C}$ of ~-25.8 occurs at ~340 yr AD and the highest values occur at ~1360 yr AD and ~1600 yr AD, respectively.

In core RA09-GW-8-P5 average TOC is ~0.62 wt.% (Fig. 8, dotted line). The core can be subdivided in two sections, which each appear to follow a weakly increasing trend. Between ~500 yr BC and ~800 yr AD TOC increases from ~0.57 wt.% to ~0.74 wt.%. An abrupt low of ~0.5 wt.% occurs at ~300 yr AD. At ~800 yr AD a shift to ~0.54 wt.% occurs, after which TOC varies around 0.58 wt.%. After ~1530 yr AD TOC follows a weakly increasing trend ($r^2=0.68$) to ~0.76 wt.% at the sediment surface. TN values vary around 0.053 wt.% between ~500 yr BC and ~1530 yr AD. After ~1530 yr AD TN gently increases ($r^2=0.67$) from 0.043 wt.% to 0.07 wt.%. Average C/N is ~11.9 and is slightly higher (~12.5) before ~800 yr AD. After ~800 yr AD C/N is variable and very weakly decreasing to ~10.9 at the sediment surface. The $\delta^{13}\text{C}$ values average around -25 ‰ and do not show any obvious patterns.

In core RA09-GW-4-P3 average TOC is ~0.62 wt.% (Fig. 8, solid line). TOC is lowest between ~840 yr AD and 960 yr AD, with values from 0.48 wt.% to 0.6 wt.%. Above 960 yr AD TOC values are relatively stable around 0.62 wt.% with a short episode

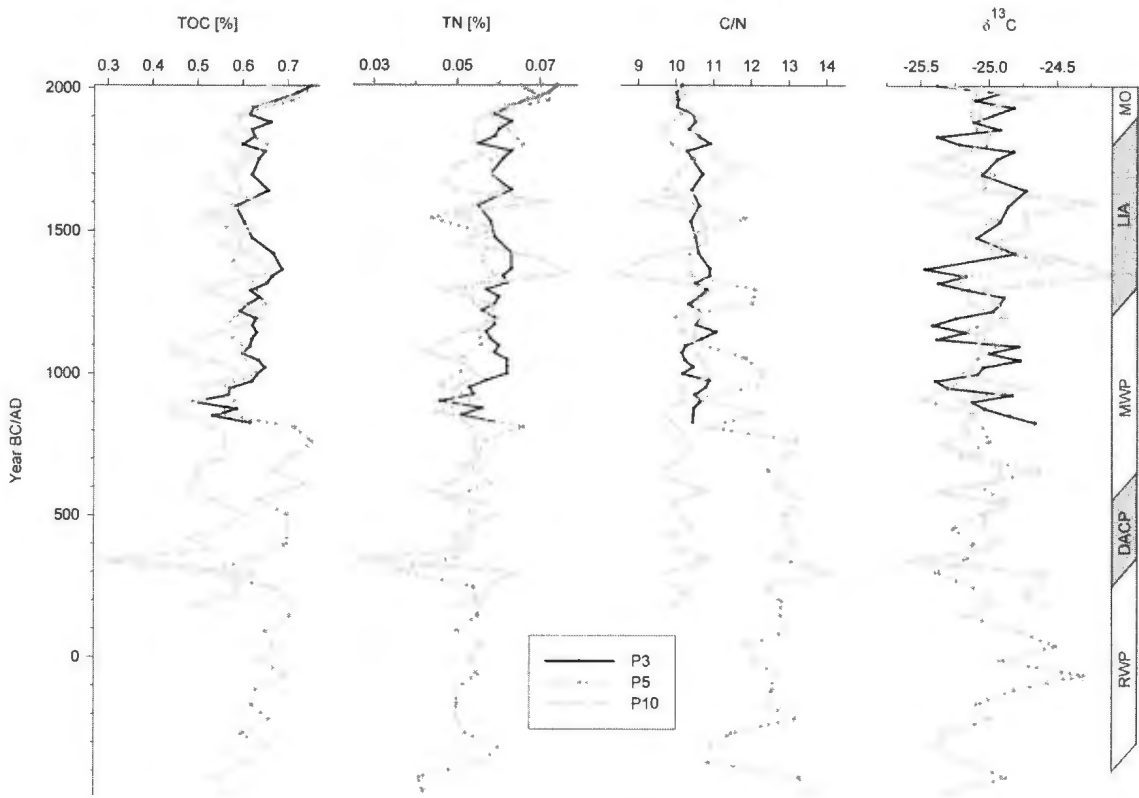


Figure 8: This figure displays variations in Total Organic Carbon (TOC, wt. %), Total Nitrogen (TN, wt. %), C/N (wt. %), $\delta^{13}\text{C}$ %, and of cores RA09-GW-4-P3 (solid black, P3), RA09-GW-8-P5 (dotted gray, P5) and RA09-GW-7-P10 (dashed gray, P10). The vertical bar to the right shows the approximate duration of the Modern Optimum (MO), Little Ice Age (LIA), Medieval Warm Period (MWP) and Dark Ages Cold Period (DACP), and Roman Warm Period (RWP).

of increasing ($r^2=0.85$) TOC values from ~0.58 wt.% to ~0.69 wt.% between ~1200 yr AD and ~1360 yr AD, respectively, followed by a short episode of decreasing ($r^2=0.97$) TOC from 0.69 wt.% to 0.58 wt.% between ~1360 yr AD and ~1600 yr AD. Above, TOC varies around ~0.6 wt.% before it increases ($r^2=0.98$) after ~1920 yr AD to 0.73 wt.% at the sediment surface. Average TN is ~0.06 wt.% and generally parallels the trends observed in TOC. TN is lowest between ~840 yr AD and 960 yr AD, with values from ~0.045 wt.% to ~0.055 wt%. Above, TN values vary around 0.6 wt.% with a short

episode of decreasing ($r^2=0.93$) TN from 0.063 wt.% to 0.055 wt.% between ~1360 yr AD and ~1600 yr AD. After ~1800 yr AD TN increases ($r^2=0.85$) from ~0.055 wt.% to ~0.076 wt.% at the sediment surface. Average C/N is ~10.5 and very stable throughout the core. A weak decrease ($r^2=0.75$) is observed after ~1800 yr AD from ~11 wt.% to 10 wt.%. The average $\delta^{13}\text{C}$ is ~-25.2 ‰. Except for an interval of slightly more stable $\delta^{13}\text{C}$ values between ~1400 yr AD and ~1730 yr AD no distinct trends are evident.

5. Discussion

5.1 Total fluvio-deltaic sediment budget

Apparent differences in mass accumulation ($M_{3500} \gg M_{MO}$) are inferred to be either the result of poor age models, decreasing sediment retention in the study area over time, decreasing sediment discharge (which could be driven by a combination of decreasing sediment yield or water discharge), or some combination of these factors.

Variability of river discharge was evaluated over a range of timescales using different approaches. We compared modern mass accumulation M_{MO} in our study area (Hülse and Bentley, 2012) with total fluvio-deltaic deposition since ~3500 yr BP (M_{3500}), inferred from seismic data. M_{3500} was calculated using Eq. 1, with age based on Gonthier et al. (1993). This resulted in $M_{3500} = 106,000 \text{ t/yr}$ for our proximal 25 km² study area. Compared to $M_{MO} = 40,000 \text{ t/yr}$ (Hülse and Bentley, 2012), this differs by a factor of 2.65, suggesting large decline in sediment delivery during the past 3500 years. This supports findings by Gonthier et al. (1993), who stated that sediment accumulation has been stable during the past 2800 years and was much higher before due to much faster rates of isostatic rebound between 3500 yr and 2800 yr BP. If sediment retention in the

study area was similar at 3500 yr BP to the present estimate of 23% yr (Hülse and Bentley, 2012), this suggests that total sediment discharge at 3500 yr BP was on the order of $Q_{S3500} = 460,870$ t/yr.

A decreasing sediment yield could be the result of decreasing availability of easily erodible sediments. With isostatic rebound, retreating sea-level, and continuous exposure, the amount of easily erodible glacial tillites and post-glacial marine clays should decrease. Decreasing sediment retention due to isostatic rebound could exert control on sediment accumulation because it continuously lowers relative sea-level, which leads to increased winnowing and wave resuspension of fine sediments. This may be supported by the observation of an upward change in reflector quality in some sub-bottom profiles. Further, climatic changes may exert control on the marine sediment dispersal system due to varying sea-ice and wave climate (e.g., Hass et al., 2010) and/or variation in sediment and freshwater discharge. These potential influences are addressed below in greater detail over a more recent time period (~2000 yr BP), using our core geochronologies.

5.2 Sediment mass flux variability since ~2000 yr BP

Results of sediment mass flux analysis suggests decreased terrestrial sediment discharge during the LIA and opposite effects during the MWP. This is most likely related to cooler and drier conditions during the LIA and warmer and wetter conditions with increased precipitation and runoff during the MWP.

The spatial and temporal variability of sediment flux to the marine basin offshore of the GWR were studied using core properties and AMS¹⁴C dates for each core. The changes in total mass accumulation M seem to be related to the Little Ice Age (LIA) (Fig.

4). The lowered total mass accumulation M between ~1400 yr AD and ~1750 yr AD (Fig. 4) suggests a decreasing sediment discharge during climatically cooler periods. This is supported by another weak decrease in MAR in core RA09-GW-7-P10 (Fig. 4, dashed line) during the cooler Dark Ages Cold Period (DACP). Further, SARs and MARs (Fig. 4) suggest that the biggest change in SAR and MAR occurred in the most river-distal core RA09-GW-4-P3 (Fig. 4, solid line). This suggests a weaker initial discharge speed due to decreased river discharge Q , and/or increased nearshore sediment retention related to less wave resuspension, during periods marked by decreased offshore mass accumulation M . Increased nearshore sediment retention could imply increased sea-ice coverage during the LIA, that would lead to increased wave dampening, less sediment resuspension, and more river-proximal accumulation of fluvial sediment. During the warmer Medieval Warm Period (MWP) in contrast, mass accumulation M seemed to increase in both cores P3 (distal) and P10 (proximal), suggesting a greater sediment discharge during this period. The overall relatively low and uniform SARs and MARs in core RA09-GW-8-P5 (Figure 4, dotted line) suggest a zone of relative sediment bypass at this coring location, consistent with the shallow water depth at this location, which could be close to wave base (thus allowing more sediment resuspension than in deeper water).

5.3 River discharge variability and global climatic change

Results of river discharge estimations imply that Great Whale River discharge decreases (increases) during colder and drier (warmer and wetter) climatic periods since ~2000 yr BP, although our method does not allow calculation of the exact magnitude of these changes.

Further, results suggest that Q was not stable between 3500 and 2000 yr BP, showing a net decrease from 3500 to 2000 yr BP, although the actual rate of the decline may not be accurately estimated by the model.

To elucidate changes in river discharge through the past ~2000 yr BP (0 yr BC/AD), M_T from core geochronology was used to estimate variations in Q during time (Figure 4). The resulting curve follows the patterns in M and Q_S and results in $Q_{MO} = 8.5 \text{ km}^3/\text{yr}$ for the most recent ~250 yr compared to a modern value of measured $Q_{HQ} = 20.15 \text{ km}^3/\text{yr}$ (HydroQuebec, 1993). This could either be caused by uncertainty in geochronology, by changes in catchment sediment yield, or by increasing Q since the LIA. Apparent Q was lowest in the LIA between 1420 yr AD and 1550 yr AD with $Q_{LIA} = 3 \text{ km}^3/\text{yr}$ (Figure 4) and highest during the MWP with $Q_{MWP} = 23 \text{ km}^3/\text{yr}$, which is very similar to the modern $Q_{HQ} = 20.15 \text{ km}^3/\text{yr}$.

Water discharge since ~3500 yr BP, Q_{3500} , was estimated using Eq. 4 (Syvitski and Milliman, 2007) with $Q_{S3500} = 460,870 \text{ t/yr}$. This infers an apparent river discharge of $Q_{3500} = 693 \text{ km}^3/\text{yr}$, which differs from modern measured water discharge of $Q_{HQ} = 20.15 \text{ km}^3/\text{yr}$ (HydroQuebec, 1993) by much more than model uncertainty (which is approximately 38% for the 488 rivers used to develop the model) (Syvitski and Milliman, 2007). The particularly large apparent $Q_{3500} = 693 \text{ km}^3/\text{yr}$ may indicate that the dispersal system has since evolved in ways not captured by the model, such as decreasing sediment yield in the catchment, decreasing sediment retention in the marine basin, or a combination of the two, either of which would cause a decrease in calculated apparent Q over time, using our approach.

5.4 Short term discharge variability and climatic forcings

5.4.1 Magnetic susceptibility - Short term variability in discharge and/or weathering

Magnetic susceptibility records (Figure 5-7) display apparently cyclical patterns, suggesting century-scale discharge and/or climate variability during the past ~2000 yr. Based on apparent ages for MS maxima in Figure 5, the mean period for MS fluctuations in core RA09-GW-4-P3 is 195 ± 78 yr (n=6 over 975 yr). In cores RA09-GW8-P5 and RA09-GW-7-P10, wherein MS fluctuations are more pronounced, MS fluctuation mean periods are 263 ± 71 yr (n=9 over 2100 yr) and 232 ± 97 yr (n=8 over 1625 yr), respectively. In addition to this centennial variability, magnitudes of fluctuations in cores RA09-GW-7-P10 and RA09-GW-4-P3 seem to decrease during the LIA by more than 50 % (Figs. 5 and 7). This suggests decreased sediment discharge and/or weathering and erosion in the drainage basin during the LIA and parallels the trends in MAR (Fig. 4). The relation between water discharge and sediment discharge however must not have been constant through time but may have varied as a function of changing weathering conditions and possibly physical characteristics of the basin, as it evolved morphologically. Changes in the MS signal thus may record a combination of river discharge and weathering conditions.

Further, trends in mean grain diameter suggest a relatively stable wave climate and may indicate retention of fine suspended material in the more river proximal areas during the LIA. Mean grain diameter exhibits a low stratigraphic variability during the LIA compared to the MWP and MO (Fig. 5-7), especially in the most distal core RA09-GW-4-P3 (Fig. 7), and is coarser grained on average during the LIA compared to the

MWP. At least in the latter half of the LIA, this is supported by a slow fining in grain size in cores RA09-GW8-P5 (Fig. 6) and RA09-GW-7-P10 (Fig. 5).

Because the periodicity of the MS change is shorter than our ^{14}C sampling resolution and longer than the ^{210}Pb time scale (Hulse and Bentley, 2012), we cannot identify any mass-flux changes associated with this MS signal. The duration of one half-cycle for the MS signal is comparable to the time scale of variability seen in the instrumental record of Great Whale River discharge (Déry et al., 2005; Déry et al., 2009). If MS variability is in fact associated with changing river discharge, this means that with 60 yr or less of instrumental records, it might be challenging to separate anthropogenic influence from natural variability.

5.4.2 Climatic forcings of MS variabilities

Due to similarities to comparable studies from the North Atlantic, we infer that the periodicities in our MS records of the GWR (195-263 yr) are not an isolated occurrence and may reflect century-scale variations in the hydrologic cycle due to environmental forcing.

Although our temporal resolution is limited by the number of AMS ^{14}C dates in each core, the 195-260 yr pattern in MS fluctuations is comparable to cyclical patterns from cores elsewhere in North America and the globe over this same period (Stocker and Mysak, 1992; O'Sullivan et al., 2002; Berner et al., 2011). Such variations have also been linked to sea surface temperatures in the Atlantic (White et al., 1996) and also seems to occur in the record of Holocene $\delta^{14}\text{C}$ (Stuiver and Braziunas, 1993; Stuiver and Braziunas, 1995) and thus are interpreted to be related to some form of solar cycle or

periodicity in Earth's magnetic field. Covariance of $\delta^{14}\text{C}$ production and $\delta^{18}\text{O}$ from Greenlandic ice core records and other North Atlantic data sets suggest sun-climate relations in a period range from 100-400 yr (Fisher, 1982; Stuiver and Braziunas, 1993; Stuiver and Braziunas, 1995; Stuiver et al., 1995). O'Sullivan (2002) and Stuiver et al. (1995) recorded a 213 yr cycle, which may be linked to variability in North Atlantic sea surface temperatures (White et al., 1996). Hoyt and Schatten (1997) identified this cycle as the solar Suess cycle (Suess, 1986), suggesting a relation to sea surface temperature variability in the North Atlantic. The larger scale climatic fluctuations (submillennial to millennial), such as the last cold period, the Little Ice Age (LIA), are believed to be caused by solar forcing (Bond et al., 2001) and reductions in the production of North Atlantic Deep Water (NADW) (Bianchi and McCave, 1999; Oppo et al., 2003).

Regardless of the exact causality, we thus conclude that the periodicities in our MS records of the GWR (195-263 yr) are not an isolated occurrence and may reflect century-scale variations in the hydrologic cycle due to environmental forcing. More detailed study of this signal and its impact on water and sediment flux is needed.

5.4.3 Palaeo-environmental implications

The relatively uniform patterns in C and N geochemistry (Fig. 8) suggest that no major environmental changes influencing C and N burial (i.e., net effects of production, deposition, and remineralization) have occurred during the past ~2000 yr at the GWR study site. Total organic carbon and nitrogen are widely used as proxies for paleoproductivity (e.g., Haberzettl et al., 2010). Stable carbon isotope ratios and carbon-nitrogen ratios have been used to reconstruct the sources of organic matter in different

depositional environments, based on marine and terrestrial end members (Meyers, 1994; St-Onge and Hillaire-Marcel, 2001; Lavoie et al., 2008; Haberzettl et al., 2010). Terrestrial organic matter usually shows a general depletion of ^{13}C ($\delta^{13}\text{C}$ values of approximately -25 ‰ to -29 ‰), relative to marine organic matter ($\delta^{13}\text{C}$ values near -20 ‰) (Meyers, 1994; Lamb et al., 2006).

The $\delta^{13}\text{C}$ values indicate a mixed marine-lacustrine composition of the organic matter at the study site. The weak decrease in TOC and TN in core RA09-GW-4-P3 between 1360 yr AD and 1600 yr AD, suggests a slight decrease in organic production during the LIA. During this time interval the two peaks in $\delta^{13}\text{C}$ and lows in C/N in the most river proximal core RA09-GW-7-P10 suggest a weak increase (in marine and/or decrease in terrestrial organic matter content, possibly related to a decreasing discharge of terrestrial organic matter due to decreasing river discharge and/or an increase in primary productivity. The most recent increase in TOC and TN after ~1850 yr AD may suggest an improvement of environmental conditions leading to increased primary productivity with onset of the MO.

6. Conclusions

The sediment cores analyzed in this study cover the past 2000 yr of river discharge history of the Great Whale River. The major findings of our proxy study on river discharge of the GWR are:

Average mass accumulation offshore the GWR during the past 3500 yr was substantially higher than compared to modern values and the last 2000 yr.

Sediment mass accumulation appears to decrease during climatic colder periods, such as the LIA. With this decrease, the locus of sediment mass accumulation appears to move to more river proximal areas during periods of climatic cooling, possibly in relation to increased wave dampening as a result of increased sea-ice coverage.

This is accompanied by a lower (higher) freshwater discharge during periods of global cooling (warming). River discharge during the MWP appears to have been similar to modern values, compared to much lower values during the LIA.

Superimposed on these climatic variations, a higher frequency signal of climatic change is recorded in MS with a period of 195-263 yr. This signal seems to be persistent through the past ~2000 yr, with decreased magnitude of fluctuations during the LIA. Comparison with other studies from North America and the world suggest a change in the hydrologic cycle due to sea surface temperature variability in the North Atlantic as a possible causative mechanism. Lower magnitudes in MS variations and a more stable mean grain diameter in the river distal areas during the LIA suggest more stable hydrodynamic conditions during the LIA compared to the MWP.

The similarity between the average half-period of MS fluctuations and the time scale of variability in the instrumental record of Great Whale River discharge, suggests that with 60 yr or less of instrumental records, it is not possible to separate anthropogenic influence from natural cycles.

A major change in paleoenvironmental processes controlling carbon and nitrogen burial conditions was not be observed during the past ~2000 yr in the sedimentary record of the Great Whale River.

In summary, in the past, warmer climate in eastern Hudson Bay seems to have increased precipitation, river water and sediment discharge, as well as wave activity and sediment resuspension as a result of decreased sea-ice coverage, while past climatic cooling is inferred to have the opposite effect.

Acknowledgements

This project was funded by an ArcticNet grant to S. Bentley, the Canadian Center of Excellence in Canadian Arctic research, with additional support from the Canada Research Chair Secretariat, the Canada Foundation for Innovation, Memorial University of Newfoundland, and the LSU Harrison Chair of Sedimentary Geology. Special thanks go to Robyn Haworth, Erlangga Septama, Thomas Richerol, as well as the captains and crews of the CCGS Amundsen and CCGS Radisson, who were of indispensable help during the field seasons in 2007 and 2009. We would like to thank Duncan McIlroy and Susan Ziegler for their helpful discussions and reviews. We thank Kendra Karrigan for her support in the laboratory.

References:

- ACIA, 2005. Impacts of a Warming Arctic: Arctic Climate Impact Assessment. Cambridge University Press, Cambridge.
- Allard, M. and Seguin, M.K., 1987. The Holocene evolution of permafrost near the tree line, on the eastern coast of Hudson Bay (northern Quebec). Canadian Journal of Earth Sciences, 24: 2206-2222.
- Alley, R.B. and Ágústsdóttir, A.M., 2005. The 8 k event: cause and consequences of a major Holocene abrupt climate change. Quaternary Science Reviews, 24: 1123-1149.

- Barber, D.C., Dyke, A., Hillaire-Marcel, C., Jennings, A.E., Andrews, J.T., Kerwin, M.W., Bilodeau, G., McNeely, R., Southon, J., Morehead, M.D. and Gagnon, J.-M., 1999. Forcing of the cold event of 8200 years ago by catastrophic drainage of Laurentide lakes. *Nature*, 400: 344-348.
- Berner, K.S., Koç, N., Godtliebsen, F. and Divine, D., 2011. Holocene climate variability of the Norwegian Atlantic Current during high and low solar insolation forcing. *Paleoceanography*, 26(PA2220): 15.
- Bianchi, G.G. and McCave, I.N., 1999. Holocene periodicity in North Atlantic climate and deep-ocean flow south of Iceland. *Nature*, 397: 515-517.
- Bond, G., Kromer, B., Beer, J., Muscheler, R., Evans, M.N., Showers, W., Hoffmann, S., Lotti-Bond, R., Hajdas, I. and Bonani, G., 2001. Persistent solar influence on North Atlantic climate during the Holocene. *Science*, 294: 2130-2136.
- Bronk Ramsey, C., 2009. Bayesian analysis of radiocarbon dates. *Radiocarbon*, 51 (1): 337-360.
- Déry, S.J. and Wood, E.F., 2004. Teleconnection between the Arctic Oscillation and Hudson Bay river discharge. *Geophysical Research Letters*, 31: pp. L18205 1-4
- Déry, S.J., Stieglitz, M., McKenna, E.C. and Wood, E.F., 2005. Characteristics and Trends of River Discharge into Hudson, James, and Ungava Bays, 1964-2000. *Journal of Climate*, 18: 2540-2557.
- Déry, S.J., Hernandez-Henriquez, M.A., Burford, J., E. and Wood, E.F., 2009. Observational evidence of an intensifying hydrological cycle in northern Canada. *Geophysical Research Letters*, 36: LI3402, pp. 5.
- Dyke, A.S. and Prest, V.K., 1987. Late Wisconsinan and Holocene History of the Laurentide Ice Sheet. *Géographie physique et Quaternaire*, 41: 237-263.
- Fisher, D.A., 1982. Carbon-14 Productions Compared to Oxygen Isotope Records from Camp Century, Greenland and Devon Island, Canada. *Climatic Change*, 4: 419-426.
- Gagnon, A.S. and Gough, W.A., 2005. Trends in the dates of ice freeze-up and breakup over Hudson Bay, Canada. *Arctic*, 58 (4): 370-382.
- Gonthier, N., d'Anglejan, B. and Josenhans, H.W., 1993. Seismo-stratigraphy and sedimentology of Holocene sediments off Grande Rivière de la Baleine, southeastern Hudson Bay, Québec. *Géographie physique et Quaternaire*, 47(2): 147-166.

- Gough, W.A. and Wolfe, E., 2001. Climate Change Scenarios for Hudson Bay, Canada, from general circulation models. *Arctic*, 54 (2): 142-148.
- Haberzettl, T., St-Onge, G. and Lajeunesse, P., 2010. Multi-proxy records of environmental changes in Hudson Bay and Strait since the final outburst flood of Lake Agassiz-Ojibway. *Marine Geology*, 271: 93-105.
- Hall, F.R., Andrews, J.T., Kerwin, M. and Smith, L.M., 2001. Studies of sediment colour, whole-core magnetic susceptibility, and sediment magnetism of the Hudson Strait-Labrador Shelf region: CSS Hudson Cruise 90023 and 93034. *Marine Geology of Hudson Strait and Ungava Bay. Eastern Arctic Canada: Late Quaternary Sediments, Depositional Environments, and Late Glacial-Deglacial History Derived from Marine and Terrestrial Studies: Geological Survey of Canada Bulletin*, 566, 161-170 pp.
- Hare, A., Stern, G.A., Macdonald, R.W., Kuzyk, Z.Z. and Wang, F., 2008. Contemporary and preindustrial mass budgets of mercury in the Hudson Bay marine system: the role of sediment recycling. *Science of the Total Environment*, 406: 190-204.
- Hass, H.C., Kuhn, G., Monien, P., Brumsack, H.-J. and Forwick, M., 2010. Climate fluctuations during the past two millennia as recorded in sediments from Maxwell Bay, South Shetland Islands, West Antarctica. *Geological Society, London, Special Publications*, 344: 243-260.
- Hillaire-Marcel, C., 1976. La déglaciation et le relèvement isostatique sur la côte est de la Baie d'Hudson. *Cahiers de géographie de Québec*, 20(50): 185-220.
- Hochheim, K.P. and Barber, D.G., 2010. Atmospheric forcing of sea ice in Hudson Bay during the fall period, 1980-2005. *Journal of Geophysical Research*, 115(C05009).
- Hochheim, K.P., Lukovich, J.V. and Barber, D.G., 2011. Atmospheric forcing of sea ice in Hudson Bay during the spring period, 1980-2005. *Journal of Marine Systems*, 88: 476-487.
- Hoyt, D.V. and Schatten, K.H., 1997. *The Role of the Sun in Climate Change*. Oxford University Press, Oxford, 279 pp.
- Hülse, P., 2012. Climatically controlled river discharge in the eastern Canadian sub-Arctic during the Holocene, Earth Sciences Department. Memorial University of Newfoundland, St. John's.
- Hülse, P. and Bentley, S.J., 2012. A ^{210}Pb sediment budget and granulometric record of sediment fluxes in a sub-Arctic deltaic system: the Great Whale River,

- Canada, Estuarine Coastal and Shelf Science. Memorial University of Newfoundland.
- HydroQuebec, 1993. Grande-Baleine Complex; Feasibility Study, HydroQuebec.
- Ingram, R.G., 1981. Characteristics of the Great Whale River Plume. *Journal of Geophysical Research*, 86(C3): 2017-2023.
- Ingram, R.G., Wang, J., Lin, C., Legendre, L. and Fortier, L., 1996. Impact of freshwater on a subarctic coastal ecosystem under seasonal sea ice (southeastern Hudson Bay, Canada). I. Interannual variability and predicted global warming influence on river plume dynamics and sea ice. *Journal of Marine Systems*, 7: 221-231.
- Jenner, K.A. and Piper, D.J.W., 2002. Grande Riviere de la Baleine, Hudson Bay, Quebec - 1000 years of sedimentation. Geological Survey of Canada, 2002-E10.
- Johannessen, O.M., Bengtsson, L., Miles, M.W., Kuzmina, S.I., Semenov, V.A., Alekseev, G.V., Nagurny, A.P., Zakharov, V.F., Bobylev, L.P., Pettersson, L.H., Hasselmann, K. and Cattle, H.P., 2004. Arctic climate change: observed and modelled temperature and sea-ice variability. *Tellus*, 56 (A): 328-341.
- Jones, E.P. and Anderson, L.G., 1994. Northern Hudson Bay and Foxe Basin: water masses, circulation and productivity. *Atmosphere-Ocean*, 32: 361-374.
- Kuzyk, Z.Z.A., Macdonald, R.W., Tremblay, J.-E. and Stern, G.A., 2010. Elemental and stable isotopic constraints on river influence and patterns of nitrogen cycling and biological productivity in Hudson Bay. *Continental Shelf Research*, 30 (2): 163-176.
- Lajeunesse, P. and Allard, M., 2003. Late Quaternary deglaciation, glaciomarine sedimentation and glacioisostatic recovery in the Rivière Nastapoka Area, Eastern Hudson Bay, Northern Québec. *Géographie physique et Quaternaire*, 57: 65-83.
- Lajeunesse, P., 2008. Early Holocene deglaciation of the eastern coast of Hudson Bay. *Geomorphology*, 99: 341-352.
- Lajeunesse, P. and St-Onge, G., 2008. The subglacial origin of the Lake Agassiz-Ojibway final outburst flood. *Nature Geoscience*, 1: 184-188.
- Lamb, A.L., Wilson, G.P. and Leng, M.J., 2006. A review of coastal palaeoclimate and relative sea-level reconstructions using $\delta^{13}\text{C}$ and C/N ratios in organic material. *Earth-Science Reviews*, 75: 29-57.

- Lavoie, C., Hill, P.R., Allard, M., St-Onge, G. and Lajeunesse, P., 2008. High-resolution seismo-stratigraphy and sedimentological properties of late- and postglacial sediments in Lac Guillaume Delisle Estuary and Nastapoka Sound, eastern Hudson Bay. *Canadian Journal of Earth Sciences*, 45(427-441).
- Lawrence, D.M. and Slater, A.G., 2005. A projection of near surface permafrost degradation during the 21st century. *Geophysical Research Letters*, 32 (L24401 doi: 10.1029/2005GL025080).
- Markham, W.E., 1986. The ice cover. *Canadian Inland Seas*. Elsevier, New York, 101-116 pp.
- McNeely, R., Dyke, A.S. and Southon, J.R., 2006. Canadian marine reservoir ages, preliminary data assessment. *Geological Survey of Canada, Open File 5049*, 3.
- Meyers, P.A., 1994. Preservation of elemental and isotopic source identification of sedimentary organic matter. *Chemical Geology*, 114: 289-302.
- Muhammad, Z., Bentley, S.J., Febo, L.A., Droxler, A.W., Dickens, G.R., Peterson, L.C. and Opdyke, B.N., 2008. Excess ^{210}Pb inventories and fluxes along the continental slope and basins of the Gulf of Papua. *Journal of Geophysical Research*, 113: F01S17, pp. 14.
- O'Sullivan, P.E., Moyeed, R., Cooper, M.C. and Nicholson, M.J., 2002. Comparison between instrumental, observational and high resolution proxy sedimentary records of Late Holocene climatic change - a discussion of possibilities. *Quaternary International* 88: 27-44.
- Oppo, D.W., McManus, J.F. and Cullen, J.L., 2003. Palaeo-oceanography: Deepwater variability in the Holocene epoch. *Nature*, , 422: 277-278.
- Prinsenberg, S.J., 1986. The circulation pattern and current structure of Hudson Bay. *Canadian Inland Seas*. Elsevier, New York.
- Reimer, P.J., Baillie, M.G.L., Bard, E., Bayliss, A., Beck, J.W., Blackwell, P.G., Bronk Ramsey, C., Buck, C.E., Burr, G.S., Edwards, R.L., Friedrich, M., Grootes, P.M., Guilderson, T.P., Hajdas, I., Heaton, T.J., Hogg, A.G., Hughen, K.A., Kaiser, K.F., Kromer, B., McCormac, F.G., Manning, S.W., Reimer, R.W., Richards, D.A., Southon, J.R., Talamo, S., Turney, C.S.M., van der Plicht, J. and Weyhenmeyer, C.E., 2009. IntCal09 and Marine09 radiocarbon age calibration curves, 0–50,000 years cal BP. *Radiocarbon*, 51 (4): 1111-1150.
- Saucier, F., Larouche, P., D'Astous, A. and Dionne, J., 1994. Moored physical oceanographic data from northeastern Hudson Bay between august 1992 and September 1993, Institut Maurice-Lamontagne.

- Saucier, F.J., Senneville, S., Prinsenberg, S., Roy, F., Smith, G., Gachon, P., Caya, D. and Laprise, R., 2004. Modelling the sea ice-ocean seasonal cycle in Hudson Bay, Foxe Basin and Hudson Strait, Canada. *Canadian Climate Dynamics*, 23: 303-326.
- Shilts, W.W., 1986. Glaciation of the Hudson Bay Region. *Canadian Inland Seas*, 44. Elsevier Oceanography Series, New York, 55-78 pp.
- St-Onge, G. and Hillaire-Marcel, C., 2001. Isotopic constraints of sedimentary inputs and organic carbon burial rates in the Saguenay Fjord, Quebec. *Marine Geology*, 176: 1-22.
- Stocker, T.F. and Mysak, L.A., 1992. Climate fluctuations on the century time scale: a review of high-resolution proxy data and possible mechanisms. *Climate Change*, 20: 227-250.
- Stuiver, M. and Braziunas, T.F., 1993. Sun, ocean climate and atmospheric $^{14}\text{CO}_2$: an evaluation of causal relationships. *The Holocene*, 3: 289-305.
- Stuiver, M. and Braziunas, T.F., 1995. Evidence of solar activity variations. In: R.S. Bradley and P.D. Jones (Editors), *Climate since AD 1500*. Routledge, London, pp. 593-605.
- Stuiver, M., Grootes, P.M. and Braziunas, T.F., 1995. The GISP2 $\delta^{18}\text{O}$ climate record of the past 16,500 years and the role of sun, ocean and volcanoes. *Quaternary Research*, 44: 341-354.
- Suess, H.E., 1986. Secular variations of cosmogenic ^{14}C on earth: their discovery and interpretation. *Radiocarbon* 28 (2A): 259-265.
- Syvitski, J.P.M. and Milliman, J.D., 2007. Geology, Geography, and Humans Battle for Dominance over the Delivery of Fluvial Sediment to the Coastal Ocean. *The Journal of Geology*, 115: 1-19.
- White, J.W.C., Gorodetzky, D., Cook, E.R. and Barlow, L.K., 1996. Frequency analysis of an annually resolved, 700 year paleoclimate record from the GISP2 ice core. In: P.D. Jones, R. Bradley and J. Jouzel (Editors), *Climatic Variations and Forcing Mechanisms of the last 2000 years*. NATO ASI Series Vol. 1 (41). Springer, Berlin,, pp. 193-212.

Chapter 4

A sedimentary record of climatically controlled Holocene river discharge in NE-

Canada: Saglek and Nachvak Fjords

Abstract

The postglacial sediment and river discharge evolution of northern Labrador is reconstructed from physical and organic geochemical analysis of two piston cores taken from the central basins of Nachvak and Saglek Fjords. Sediment mass accumulation rates were lowest during the Temperate Period in the early Holocene, possibly as a result of sediment trapping in glacial lakes and rerouting of meltwater during the deglaciation. Sedimentary textures suggest that the fjords were deglaciated since at least 9,800 cal yr BC. Year-round sea-ice cover prevailed until ~8,800 cal yr BC. After ~8,800 cal yr BC sea-ice rafting appears to have increased during the Temperate Period and year round open water conditions may have existed during the Holocene Thermal Maximum (HTM) in northern Labrador. After 2,000 yr BC sea-ice rafting increased again, most likely as a result of global cooling during the Neoglacial. The magnetic susceptibility trends reveal long-term cyclicities in terrestrial minerogenic input. Most likely these are related to orbitally-forced Milankovitch-scale variations in insolation, masked by a high delivery of glacial rock flour during the Temperate Period due to melting of the prevailing ice sheets of the Labrador Sector of the Laurentide Ice Sheet. Superimposed on this long-term trend is a higher frequency variability, which may be related to a ~1,000 yr solar forced

cyclicity in global climate. Since ~1,000 yr BC, solar forcing appears to have increased the input of terrestrial minerogenic matter during warm climatic intervals indicating increased river discharge during climatically warmer periods. This might be related to solar forcing. This ~1,000 yr fluctuation is weaker during the HTM, suggesting generally more stable climatic conditions during this period. Variation in sedimentary TOC, TN, C/N, and $\delta^{13}\text{C}$ suggest increase in primary productivity during the Temperate Period and HTM. This trend appears to have stagnated since the onset of the Neoglacial cooling ~2,000 yr BC, suggesting a gradual shift in paleoenvironmental conditions compared to the HTM. Except for a slight increase in productivity during the Medieval Warm Period in Nachvak Fjord, no response to historical climatic changes was observed during the past 2,000 years.

Introduction:

It is crucial to understand how the hydrologic cycle reacts to climate change, because rivers discharge minerals, nutrients, organic matter and other trace species, such as pollutants, into the marine system (Anderson et al., 2004), and also exert control on both marine salinity and sea-ice formation (Saucier et al., 2004). Understanding the past response of freshwater and sediment discharge in response to climatic changes will help to improve the understanding, detection and projection of ongoing climate change (Johannessen et al., 2004; Déry et al., 2005; Gagnon and Gough, 2005; Lawrence and Slater, 2005).

Recent studies on climatically controlled variations in the hydrologic cycle of northern Canada, including Labrador, suggest that freshwater runoff became increasingly

variable during the period 1964 to 2007, which has been related to atmospheric oscillations, such as the Arctic Oscillation (Déry et al., 2009). The influence of large-scale atmospheric oscillations on river discharge in Canada suggests that global climatic variations could have an impact on river discharge in these areas.

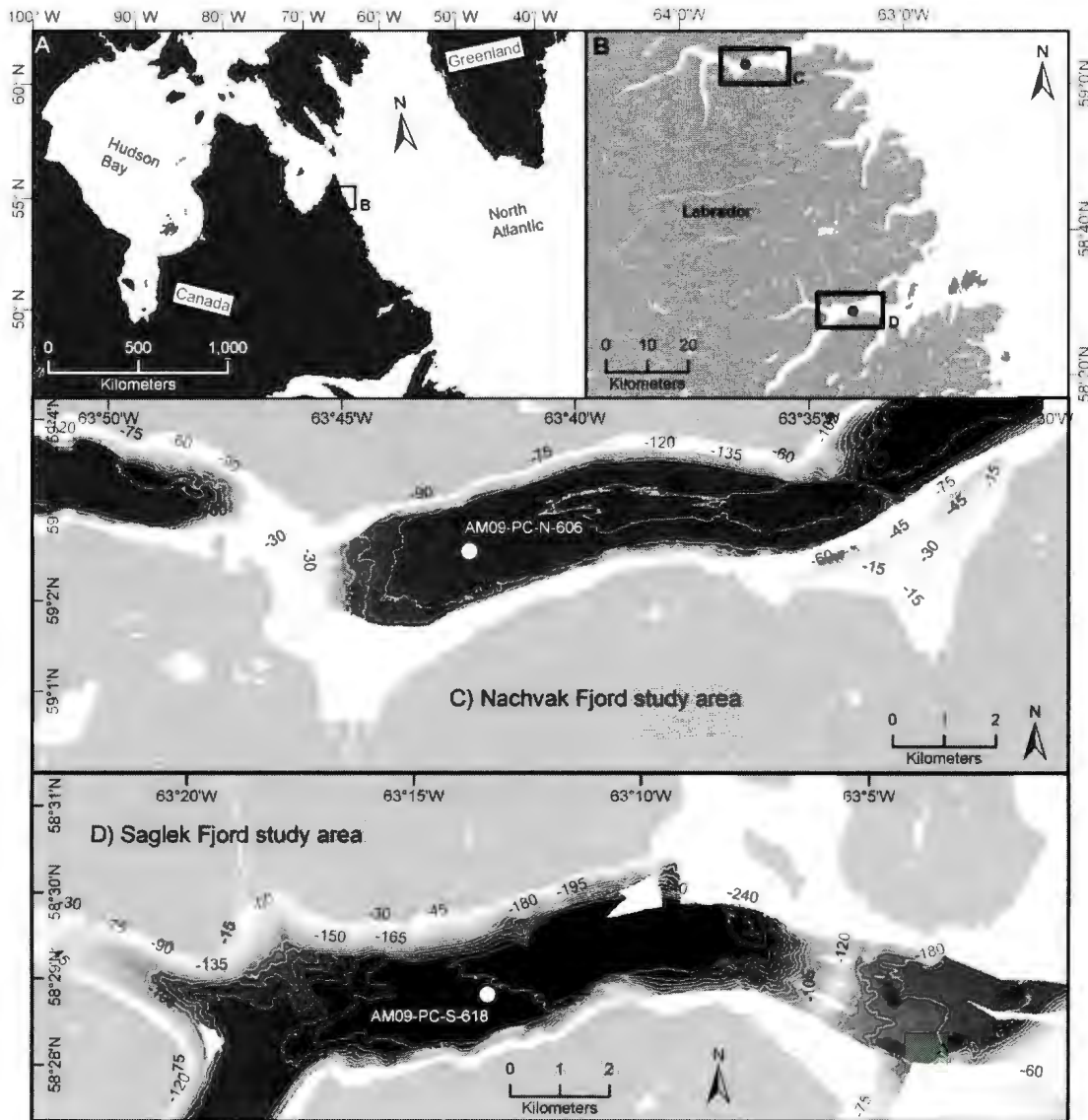


Figure 1: Map A) displays the location of the study areas shown in map B). Maps C) and D) show the bathymetry of the main basins in Nachvak and Saglek Fjords. Contour intervals are 20 m. Coring locations are marked with white dots.

Studies of climatically controlled variations in freshwater discharge in northern Labrador are few. Most published studies concentrate on larger scale climatic variations, such as the Late Wisconsinan-Holocene deglaciation (e.g., Evans and Rogerson, 1986; Bell et al., 1988; Jansson, 2003; Carlson et al., 2007). High-resolution studies of freshwater discharge variations as recorded in the marine sedimentary record on sub-millennial timescales are completely lacking.

This study addresses the response of river discharge to past climatic variations as recorded in the sedimentary records of Nachvak and Saglek Fjords. We present continuous high-resolution records from marine sediment cores from the central basins of Nachvak and Saglek Fjords in northern Labrador. Two piston cores covering up to 10,000 yr of sedimentation elucidate centennial-scale variations in river discharge of northern Labrador since the deglaciation.

In order to place the modern hydrology of northern Labrador in the context of global climate change, the stratigraphic development of postglacial river discharge, and its paleoenvironmental significance, were reconstructed by assessing postglacial: 1) sediment mass fluxes; 2) marine depositional environments; 3) short term variability in terrestrial minerogenic input as a proxy for weathering and climate change in the drainage basins; and 4) variations in sedimentary TOC, TN, C/N, and $\delta^{13}\text{C}$ as indicators for paleoenvironmental variability since ~10,000 yr BP.

2. Study area

The locations for this study are the central basins of Nachvak and Saglek Fjords on the northern Labrador Coast. These basins are fed by the largest rivers entering each

fjord: McCormick River in Nachvak Fjord and Nachvak Brook in Saglek Fjord. These basins are excellent natural sediment traps, for which modern sediment budgets have been recently established (Bentley and Kahlmeyer, 2012), against which paleoenvironmental and river discharge records during the past few thousand years will be compared.

2.1 Deglacial and postglacial history

The modern landscape of northern Labrador was shaped by the Laurentide Ice Sheet (LIS), which carved deep fjords into the Proterozoic Torngat Mountains (Wardle, 1983) during the Wisconsinan glaciation. After the opening of Hudson Bay ~6,400 cal yr BC (Barber et al., 1999; Dyke, 2004), three fragments of the LIS remained (Labrador, Keewatin and Baffin Island/Foxe Basin sectors), of which the Labrador Sector of the Laurentide Ice Sheet (LS-LIS) was the largest (Carlson et al., 2007). The deglaciation of the Labrador continental shelf occurred ~10,800 yr BC (Hall et al. 1999). The fjord mouth deglaciation in the Nachvak and Saglek Fjord area occurred ~8,800yr BC (Dyke, 2004; Ochietti et al., 2011). Approximately 8,000 yr BC, ice retreated from the inner moraines of Nachvak and Saglek Fjords main basins and ~6,200 yr BC from the innermost fjord heads (Dyke, 2004; Ochietti et al., 2011). During glacial retreat, the fjords were progressively invaded by Labrador Sea waters and the thick glacial tills were overlain by glaciomarine and marine sediments (Syvitski, 1993). Strandlines indicate marine limits of ~60 m in the Nachvak and Saglek Fjord area (Løken, 1962; Andrews, 1963), but ongoing isostatic rebound has exposed these sediments along the fjord coasts (Syvitski, 1993). Lack of shell material precludes exact dating. In Nain, however, the marine limit was likely reached ~6,500 cal yr BC (Clark and Fitzhugh, 1990).

Numerous small ephemeral lakes are inferred to have formed in tributary valleys due to damming by ice tongues (Ives, 1958; Ochietti et al., 2011). After westward ice-margin retreat from the drainage divide (~6,200 cal yr BC), longer-lived glacial lakes formed, some of which (e.g. in the Koroc River basin, northwest of Nachvak Brook) drained into Saglek Bay (Ives, 1958), and subsequently also through Palmer River into Nachvak Fjord (Ives, 1958; Ochietti et al., 2011). Lacustrine strandlines and sediments in the McCormick River valley indicate that glacial lakes existed in the tributaries of Nachvak Fjord (Evans and Rogerson, 1986). The LS-LIS finally disappeared ~4,800-4,000 cal yr BC (Clark and Fitzhugh, 1990; Wilton, 1996; Clark et al., 2003; Dyke, 2004; Ochietti et al., 2011). Whether smaller cirque glaciers persisted throughout the Holocene Thermal Maximum is uncertain, but McCoy (1983) has proposed several moraine abandonment phases in the Torngat Mountains since ~1,000 cal yr BC, indicating the existence of glaciers throughout Neoglacial times.

2.2 Climate and oceanography

Holocene climate in Labrador can be subdivided into three major periods.

- 1) The early Holocene or Temperate Period, from 9.7 to 5 cal kyr BC, is characterized by high insolation in the northern Hemisphere leading to melting ice sheets in North America and Eurasia (e.g. Wanner et al., 2011).
- 2) The Holocene Thermal Maximum (HTM) from 5 to 2.2 cal kyr BC (e.g., Wanner et al., 2011), was delayed by the cooling influence of the remnant LS-LIS compared to maximum insolation by up to 4 kyr compared to the global average (Carlson et al., 2007; Renssen et al., 2009). The onset of the Holocene Thermal Maximum (HTM) in northern Labrador is indicated by glacial

retreat from Saglek Moraine and Square Lake in the headwaters of Nakvak Brook in Saglek Fjord, where the HTM peaked ~4.5 cal kyr BC (Clark and Fitzhugh 1990; Dyke et al., 2004 Carlson et al. 2007). 3) The Neoglacial period started ~2 cal kyr BC, and is characterized by decreasing summer temperatures in the Northern Hemisphere due an orbitally forced decrease in insolation (Porter and Denton, 1967; Denton and Karlén, 1973; Wanner et al., 2011). The Neoglacial is inferred to be terminated by anthropogenic forced global warming (IPCC, 2007).

The prolonged existence of the LS-LIS during the Temperate caused a freshening and stratification of the Labrador Sea induced by glacial meltwater runoff (Solignac et al., 2004). This runoff in turn influenced the regional oceanography by preventing the formation of Labrador Sea Deep Water (LSDW) (Cottet-Puiné et al. 2004) before 57 cal kyr BC (Hillaire-Marcel et al. 2001).

The modern climate of northern Labrador is of sub-Arctic character, with land-fast sea ice covering the inner shelf for several month each year, while drifting pack ice may cover the shelf for up to 11 months each year (Hall et al., 1999). The cold Labrador Current has a cooling influence on the region compared to similar latitudes in Europe and transports icebergs from Greenland and the Canadian High Arctic along the Labrador shelf (Hall et al., 1999).

2.3 Basin Properties Saglek Fjord

The mouth of Saglek Fjord is located at approximately 58.58° N, 62.78° W, 230 km north of Nain, Labrador. The fjord stretches 60 km land inward and the maximum water depth in Saglek Fjord is ~300 m (Bentley and Kahlmeyer, 2012). Saglek Fjord is

protected from oceanic influences by a relatively shallow sill of -95 m (this study). A major source of sediment to Saglek Fjord is Nachvak Brook, an un-glaciated catchment of 809 km² size. River discharge was estimated to be 0.0624 km³/yr from eight drainage basins (905 km²) draining into the central basin of the fjord (Bentley and Kahlmeyer, 2012). The maximum relief is 1307 m. Under present conditions sediment deposition in the basin is ~43,000 t/yr (Bentley and Kahlmeyer, 2012). Stream flow measurements in Nachvak Brook suggest a melting/discharge season from early June to early November, peaking in June and during late summer storms (Bentley and Kahlmeyer, 2012).

2.4 Basin Properties Nachvak Fjord

The mouth of Nachvak Fjord is located at approximately 59.10° N, 63.40° W, 300 km north of Nain, Labrador. The fjord stretches 45 km land inward. The maximum water depth in Nachvak Fjord is 180 m (Bentley and Kahlmeyer, 2012). In total 14 drainage basins (148 km²) deliver water and sediment to Nachvak Fjord. Maximum relief is 1408 m. The main basin of Nachvak Fjord is fed from the glacierized McCormick River, with a catchment area of 77 km². The presence of glacio-marine sediments, particularly near the mouth of McCormick River, suggests that erosion of riverterraces may supply a significant amount of sand and mud to the marine basin of Nachvak Fjord. In comparison to the marine basin of Saglek Fjord, the marine basin of Nachvak Fjord lacks a distinct separation from the basin seaward of the basin studied due to a relatively deep sill of 175 m (this study). This allows for the possibility of sediment transport from the ocean, especially during storm events, and due to tidal exchange. However, relatively high measured sediment yield to Nachvak Fjord, with respect to measured sediment

deposition, suggests that the major part of the sediments should come from adjacent areas. Stream flow measurements from the McCornick River suggest melting/discharge season from late March to mid November, peaking in late July/early August (Bentley and Kahlmeyer, 2012). Today ~39,000 t/yr of sediment are deposited in the Nachvak Fjord main basin (32.4 km^2) (Bentley and Kahlmeyer, 2012).

3. Materials and Methods

3.1 Core sampling

Sites for piston core collection in the main basins of Nachvak and Saglek Fjords were chosen from bathymetry and 3.5 kHz subbottom profiles (Kahlmeyer, 2011) collected with a Kongsberg-Simrad EM-300 multibeam echosounder and a hull-mounted Knudsen Chirp 3200 (processed by the Ocean Mapping Group of the University of New Brunswick, Fredericton, Canada) during previous ArcticNet cruises on the CCGS Amundsen. These locations are also characterized by locally high sedimentation rates (Bentley and Kahlmeyer, 2012). During the 2009 ArcticNet cruise on the Canadian Coastguard icebreaker CCGS Amundsen, core AM09-PC-S-618 was recovered from Saglek Fjord at 58.48° N , 63.22° W (water depth 241 m), and core AM09-PC-N-606 was recovered from the main basin of Nachvak Fjord at 59.43° N , 63.70° W (water depth 158 m). For transport and storage, the cores were cut in 1 m sections shipboard and kept at 4°C .

3.2 Laboratory methods

3.2.1 Radiocarbon analyses

Radiocarbon dates were measured on bulk organic carbon, due to insufficient particulate carbonate/carbonaceous material, and to maintain consistency with parallel measurements in Hudson Bay (Hülse and Bentley, 2012). After core splitting, 1 cm thick slices of sediment were taken from the work half of the cores, homogenized, dried at 40° C and ground to fine powder. From each core six samples (Table 1) were sent to the Radiochronology Laboratory at Laval University, Quebec City, Canada, for sample preparation, and inorganic carbon was removed by HCl treatment. Organic carbon was combusted to CO₂ and sent to the Keck Carbon Cycle AMS Facility, University of California, Irvine, CA, USA, to produce graphite targets and AMS measurements. Radiocarbon dates were reported in Years BP and calibrated to median calendar ages ¹⁴C_{cal} (years BC/AD) using the online OxCal 4.1 calibration program (Bronk Ramsey, 2009) and the Marine09 correction curve (Reimer et al., 2009). Ages were corrected for a marine reservoir effect of 510 +/- 40 yr in Nachvak and 540 +/- 40 yr in Saglek Fjord and using known ΔR values of 150 +/- 40 yr and 180 +/- 40 yr, respectively (McNeely et al., 2006). To create a geochronological framework the radiocarbon dates were used to convert depth into time. Sediment accumulation rates (SAR, cm/yr) then were calculated after Equation 1, where Δ¹⁴C_{cal} [yr] is the time elapsed between two radiocarbon dates and ΔD [cm] is the depth difference between the two dates.

$$SAR = \Delta D / \Delta^{14}C_{cal} \quad \text{Eq. 1}$$

To investigate sediment mass fluxes through time, mass accumulation rates (MARs, g/cm²/yr) were calculated after Equation 2, where σ is porosity averaged for the time intervals between radiocarbon dates, and ρ_S is the assumed sediment grain density of 2.65 g/cm³. Porosity was taken from Geotek Multi-Sensor-Core-Logger (MSCL) measurements.

$$MAR = SAR * (1 - \sigma) * \rho_S \quad \text{Eq. 2}$$

3.2.2 Granulometry

Grain diameter distributions were measured in 5 cm intervals with a Horiba Partica LA-950 laser diffraction particle analyzer. Prior to measurement small amounts of wet samples were placed in 0.5 % NaPO₃ solution to disintegrate clay particles, sonicated for half an hour, left in solution over night, and then sonicated again before analyses.

3.2.3 X-radiography

To display physical and biological sedimentary structures, the sediment cores were imaged x-radiographically using a Thales Flashscan 35 x-ray detector, illuminated with a Lorad LPX160 X-ray generator. An aluminum compensator plate was designed specifically for the core diameter to counterbalance decreasing core thickness towards the sides of the core. Images were stored as 16-bit TIFFs and studied using ImageJ visualization software.

3.2.4 Magnetic susceptibility and bulk density

Magnetic susceptibility (MS) was measured using the Bartington Meter Model MS2 with the loop sensor MS2C and the point sensor MS2E/1 on a Geotek Multi-Sensor-Core-Logger (MSCL). The loop sensor was used for whole core measurements and records average values for an approximately 20 mm thick slice of sediment, while the point sensor was used in 1 cm intervals on split cores delivering a vertical resolution of 3.8 mm with a horizontal sensor width of 10.5 mm. Results are reported in volume specific MS κ , which then was corrected for density, generating mass specific MS X [m^3/kg] using the Geotek MSCL processing panel. Magnetic susceptibility is an indicator of the total iron-containing matter in sediments (Nagata, 1961) and in nearshore marine environments MS therefore is primarily a function of mineralogy and climate in the terrestrial drainage basin. Sources for terrigenous magnetic detritus are ferromagnetic minerals, clays, iron sulfides and ferromagnesian silicates. Calcite, quartz and organic matter as diamagnetic materials may have a diluting effect, but due to the high susceptibility of even small amounts of detrital components, this effect generally is relatively small (Ellwood et al., 2000).

Bulk density was measured using the Geotek gamma densitometer, which contains a ^{137}Cs source that emits a narrow beam of gamma rays. The gamma rays pass through the centre of the core and are recorded on the other side by a detector. Bulk density is reported in g/cm^3 .

3.2.5 Sedimentary organic matter

Samples were analyzed in 5 cm intervals to determine weight % (wt. %) of total organic carbon (TOC) and total organic nitrogen (TN), C/N ratios (ratios of TOC and TN), and $^{13}\text{C}/^{12}\text{C}$ ratios ($\delta^{13}\text{C}$) of TOC. To remove inorganic carbon (calcium carbonate), wet sediment samples were acidified in 10 % HCl overnight and then centrifuged and rinsed with distilled water three times, dried overnight at 50° C and powdered for analysis. TOC and TN were measured using a Carlo Erba NA 1500 Series 2 elemental analyzer (EA) and $\delta^{13}\text{C}$ was measured in the CREATIT Network TERRA Facility Stable Isotope Laboratory at the Memorial University of Newfoundland using a ThermoElectron Delta V Plus mass spectrometer ($\delta^{13}\text{C}$) interfaced with the EA via a Conflo II interface. Regressions were added to trends for determination of r^2 using the SigmaPlot Regression Wizard.

4. Results

4.1 Geochronology and sediment accumulation rates

Six radiocarbon dates per core were used to establish a geochronological framework for Saglek and Nachvak Fjord sediments. Radiocarbon dates represent maximum ages of bulk sedimentary organic matter, due to the likely presence of older reworked organic matter from sediments in the drainage basins. The time-depth plots (Figure 2) of the calibrated ^{14}C -dates show large age offsets beyond marine reservoir corrections. The age offset was calculated by fitting regressions to the calibrated $^{14}\text{C}_{\text{cal}}$ dates and extrapolating to the sediment surface (Figure 2). The difference between the intersection of the regressions with the sediment surface and the year of core collection

Table 1: Table a) shows ^{14}C sample depth in sediment, calibrated $^{14}\text{C}_{\text{OxCal}}$, dating errors, age offset and calibrated and offset corrected $^{14}\text{C}_{\text{cal}}$ ages. Table b) displays results for sediment and mass accumulation rates (SAR, MAR) and density and porosity values used for SAR and MAR calculations for time intervals between $^{14}\text{C}_{\text{cal}}$ dates.

a) ^{14}C age calibration

	Depth [cm]	$^{14}\text{C}_{\text{uncal}}(\text{yr BP})$	Error (+/-)	$^{14}\text{C}_{\text{OxCal}}(\text{yr BC/AD})$	Range	Offset	$^{14}\text{C}_{\text{cal}}(\text{yr BC/AD})$
AM09-PC-N-606	30	2635	20	721	90	1000	1721
	110	1830	15	-203	139	"	798
	210	3705	15	-1501	108	"	-501
	300	4470	15	-2496	132	"	-1496
	500	6325	20	-4659	123	"	-3659
	800	11420	35	-10806	146	"	-9806
AM09-PC-S-618	30	1305	15	716	54	1050	1766
	110	1780	20	236	98	"	1286
	210	2455	15	-582	168	"	488
	300	3050	15	-1328	81	"	-278
	500	4075	20	-2668	171	"	-1618
	750	5685	20	-4504	46	"	-3454

b) Sediment and mass accumulation rates

	Time Interval	Porosity	Density [g/cm ³]	SAR [cm/yr]	MAR [g/cm ²]
AM09-PC-N-606	2009 to 1721	0.76	2.65	0.10	0.07
	1721 to 798	0.75	"	0.09	0.06
	798 to -501	0.74	"	0.08	0.05
	-501 to -1496	0.73	"	0.09	0.07
	-1496 to -3659	0.73	"	0.09	0.07
	-3659 to -9806	0.65	"	0.05	0.05
AM09-PC-S-618	2009 to 1765	0.85	"	0.12	0.05
	1765 to 1288	0.80	"	0.17	0.09
	1288 to 468	0.82	"	0.12	0.06
	468 to -278	0.80	"	0.12	0.06
	-278 to -1618	0.79	"	0.15	0.08
	-1618 to -3454	0.78	"	0.14	0.08

then was added to the calibrated ^{14}C ages, giving calibrated and “offset-corrected” $^{14}\text{C}_{\text{cal}}$ ages (Table 1). This correction is supported by the nearly linear age-depth relationships of ^{14}C ages. In addition, Bentley and Kahlmeyer (2012) have documented active and relatively constant recent sediment accumulation in Nachvak and Saglek fjords. In core AM09-PC-N-606 only the upper four radiocarbon dates were used to calculate the age offset because in the deeper part of the core sediment accumulation rates are inferred to have been significantly different (see Discussion section). The calculated offsets are

1,050 yr and 1,000 yr for cores AM09-PC-S-618 and AM09-PC-N-606, respectively. Depth then was converted into time by linearly interpolating between $^{14}\text{C}_{\text{cal}}$ dates.

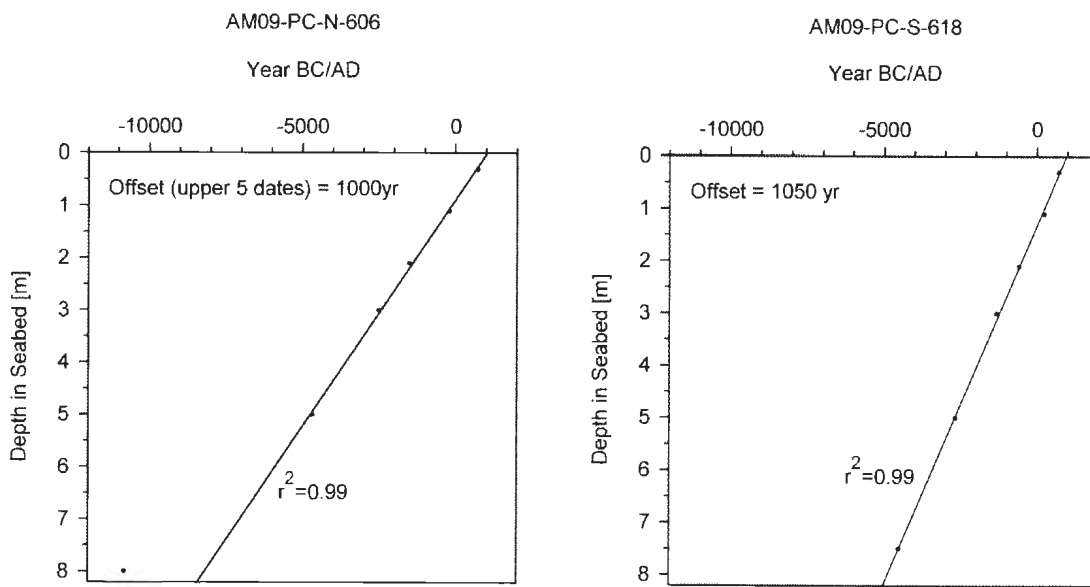


Figure 2: The graphs display ^{14}C age-depth relationships of cores AM09-PC-N-606 and AM09-PC-S-618. In core AM09-PC-N-606 only the upper five dates were used to fit the regression (see text for explanation). Years are reported in BC/AD (before Christ / anno domini).

Core AM09-PC-N-606 dates back to ~9,800 yr BC (Table 1, Fig.3). Overall, SARs increase from core bottom to top but can be subdivided in five time intervals. Between ~9,800 yr BC and ~3,700 yr BC SAR is 0.05 cm/yr. This is followed by an interval of 0.09 cm/yr between ~3,700 yr BC and ~500 yr BC. From ~500 yr BC to ~800 yr AD SAR is 0.08 cm/yr and increases to 0.10 cm/yr at the sediment surface.

MARs in Nachvak Fjord follow the same pattern (Fig. 3). Between ~9,800 yr BC and ~3,700 yr BC MAR is 0.05 g/cm²/yr. This is followed by an interval of slightly increased

MAR of $0.07 \text{ g/cm}^2/\text{yr}$ until ~ 500 yr BC. From ~ 500 yr BC to ~ 800 yr AD MAR is $0.05 \text{ g/cm}^2/\text{yr}$. After 800 yr AD, MARs increase to $0.07 \text{ g/cm}^2 \text{ yr}$ at the sediment surface.

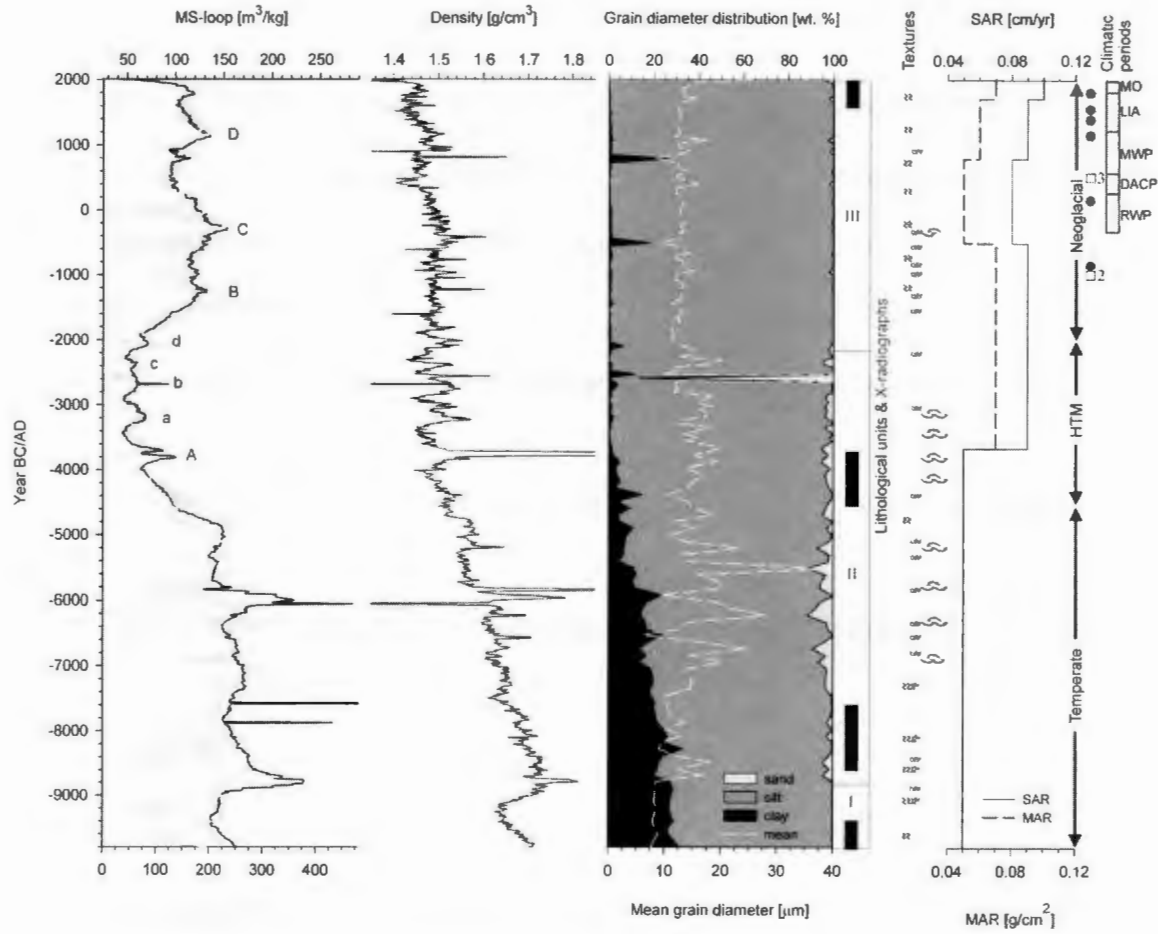


Figure 3: The graphs display results for magnetic susceptibility from the loop and point sensors (MS-loop, MS-point), density, grain diameter distribution, mean grain diameter, sediment and mass accumulation rates (SAR, MAR) for core AM09-PC-N-606, Nachvak Fjord plotted versus calibrated Years BC/AD. Further, the extent of the lithostratigraphic Units I-III is displayed as hollow bars. Vertical black bars show positions of X-radiographs in Figure 5. At the right side, Holocene and historical climatic periods are marked. Black dots represent moraine abandonment phases and squares with roman numbers refer to glacial episodes in the Nachvak Fjord area (McCoy, 1983). The most prominent periods of global cooling during the Holocene are shown as grey bars in Figures 3 and 4 (Wanner et al., 2011).

Core AM09-PC-S-618 dates to ~3400 yr BC (Table 1, Fig. 4). Between ~3,400 yr BC and ~1,600 yr BC SAR is 0.14 cm/yr, followed by an interval of 0.15 cm/yr between ~1,600 yr BC and ~300 yr BC. From ~300 yr BC to ~1,300 yr AD SAR is lower with 0.12 cm/yr, followed by higher SARs of 0.17 cm/yr between ~1,300 yr AD and ~1,800 yr AD. Since ~1,800 yr AD SAR is 0.12 cm/yr.

MARs in Saglek Fjord (Fig. 4) are ~0.08 g/cm²/yr between ~3,400 yr BC and 300 yr BC. From ~300 yr BC to ~1,200 yr AD MAR is 0.06 g/cm²/yr at. Between ~1,200 yr AD and ~1,800 yr AD MAR is 0.09 g/cm²/yr. After ~1,800 yr AD, MAR drops to 0.05 g/cm²/yr.

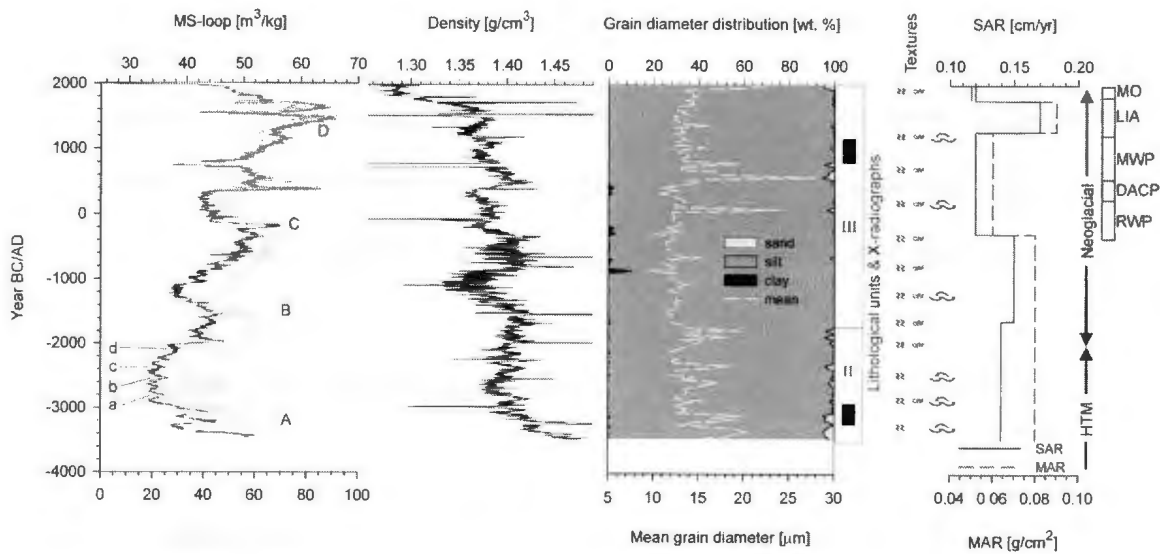


Figure 4: The graphs display results for magnetic susceptibility from the loop and point sensors (MS-loop, MS-point), density, grain diameter distribution, mean grain diameter, sediment and mass accumulation rates (SAR, MAR) plotted versus calibrated Years BC/AD for core AM09-PC-S-618, Saglek Fjord. Further, the extent of the lithostratigraphic Units I-III is displayed as hollow bars. Vertical black bars show positions of X-radiographs in Figure 5. At the right side, Holocene and historical climatic periods are marked. Black dots represent moraine abandonment phases and squares with roman numbers refer to glacial episodes in the Nachvak Fjord area (McCoy, 1983). The most prominent periods of global cooling during the Holocene are shown as grey bars in Figures 3 and 4 (Wanner et al., 2011).

4.2 Core Lithology

Based on sedimentary textures in X-radiographs (Fig. 5), the sedimentary record in Nachvak and Saglek Fjord can be subdivided into three different lithostratigraphic units. In general, both cores consist of relatively homogeneous muds of mottled, bioturbated texture. Primary sedimentary structures have been partially to wholly disrupted by bioturbation.

Unit I (Fig. 5a) is only recorded in core AM09-PC-N-606. It extends from the core bottom (~9800 yr BC) to ~8800 yr BC (Fig. 3). Unit I is characterized by massive, bioturbated muds. Shells and clasts are absent. Primary structures are not present and burrows are not evident.

Unit II (Fig. 5b,c,e) is recorded in both cores. In core AM09-PC-N-606, Unit II dates from ~8800 yr BC to ~2000 yr BC (Fig. 3). In core AM09-PC-S-618, Unit II is only recovered from ~3400 yr BC (core bottom) and ends at ~1600 yr BC (Fig. 4). Unit II is characterized by higher numbers of preserved burrows, clasts, and shell debris (Fig. 3,4,5). Clast content in AM09-PC-N-606 is highest between 6500 yr BC and 4500 yr BC and then is lower between ~4500 yr BC and ~2000 yr BC, where shell content is highest (Fig. 3,5). Due to the shorter coverage in AM09-PC-S-618, no such trends were observed (Fig. 4,5). The texture of Unit II is mottled, compared to the uniform, massive muds in Unit I. Physical sedimentary structures are not preserved.

Unit III (Fig. 5d,f) dates from ~2000 yr BC to present and from ~1600 yr BC to present in Nachvak and Saglek Fjords, respectively (Fig. 3,4). This unit is characterized by a lower shell content compared to the underlying Unit II. In AM09-PC-N-606, clast content appears greater, compared to the underlying Unit II, while no trend in clast

content was observed in AM09-PC-S-618. In both cores, the sediment is of mottled, bioturbated texture and no primary sedimentary structures are preserved. Open burrows are present in AM09-PC-S-618.

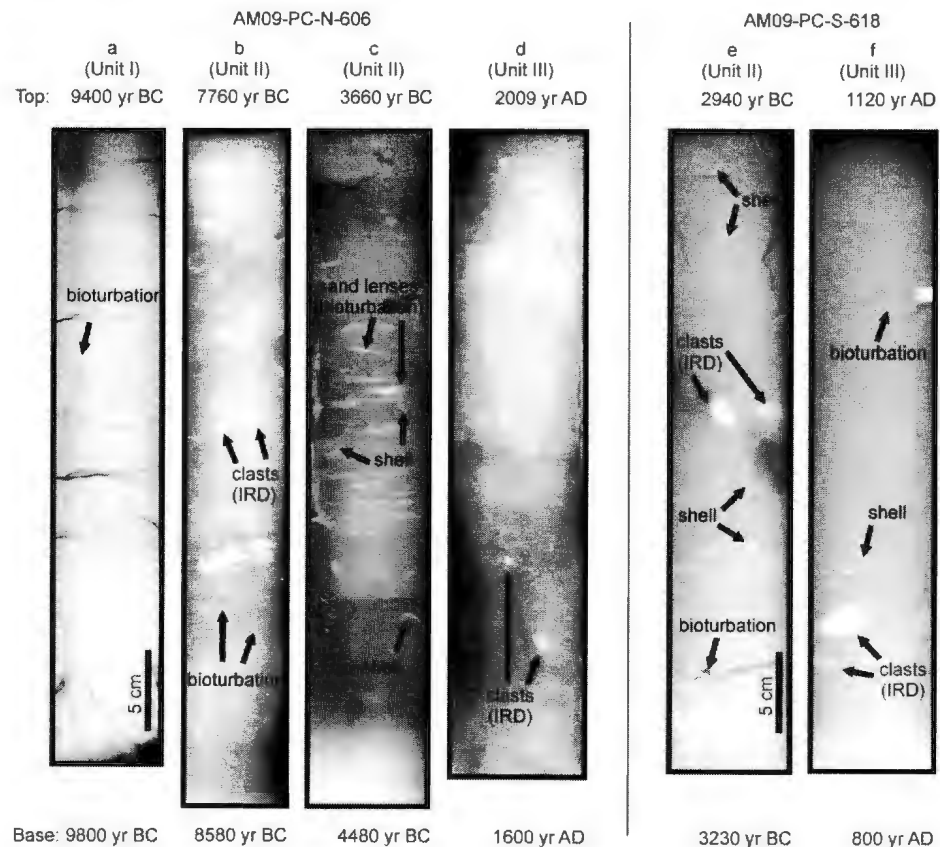


Figure 5: X-radiographs display textures in cores AM09-PC-N-606 (left) and AM09-PC-S-618 (right). Lighter areas display higher densities, darker areas lower densities. Depth and age are given and the top of each image. Cracks (a) are probably from gas expulsion.

4.3 Granulometry

In core AM09-PC-N-606 (Fig. 3) distribution of mean grain size outlines three broader units, which are in temporal accordance with the three lithostratigraphic Units I-III. Mean grain diameter in the oldest unit from 9800 yr BC to 8800 yr BC is very

uniform around 8 μm . Above, mean grain diameter increases and becomes highly variable between 8800 yr BC and 2000 yr BC with largest fluctuations up to 30 μm between ~7000 yr BC and ~5000 yr BC. The overall mean grain diameter between 8800 yr BC and 2000 yr BC is 15 μm and ~20 μm during the period of greatest variability. After ~2000 yr BC mean grain diameter remains uniform at ~13 μm . The variations in mean grain diameter before ~2000 yr BC are paralleled by significant variations in clay and sand content. The lowermost unit is characterized by a relatively high clay content of 25-30 wt. % and a lack of sand. After 8800 yr BC clay content decreases more or less continuously until ~3500 yr BC. In the same interval, sand content increases and peaks with up to ~10 wt. % between ~7000 yr BC and 5000 yr BC, the period of highest and most variable mean grain diameter. Since ~2000 yr BC sand is generally below 5 wt. % or absent and clay is ~5 wt. % with two peaks up to ~25 wt. % at 400 yr BC and 800 yr AD.

In core AM09-PC-S-618 (Fig. 4) mean grain diameter can be subdivided into two time intervals. Between ~3500 yr BC and ~1500 yr BC mean grain diameter is ~15 μm and very variable with fluctuations of 8 μm . After 1500 yr BC until present, mean grain diameter is slightly lower (~12 μm from ~1500 to 0 yr BC/AD; ~14 μm from ~0 yr BC/AD to present) and more uniform. Only between ~0 yr BC/AD and ~900 yr AD, mean grain diameter is highly variable with peaks up to 28 μm . The sediment of core AM09-PC-S-618 mainly consists of silt and is very low in clay and sand. The observed shifts in mean grain diameter are primarily controlled by variations in sand content.

4.4 Magnetic susceptibility and bulk density

In core AM09-PC-N-606 (Fig. 3) the magnetic susceptibility loop sensor signal broadly can be subdivided into three units of relatively higher and lower MS values. Highest MS values $>180 \text{ m}^3/\text{kg}$ occur between 9800 yr BC and ~ 4500 yr BC. Between 4500 yr BC and 2000 yr BC MS values drop to $\sim 50 \text{ m}^3/\text{kg}$. After 2000 yr BC MS values rise again to $\sim 125 \text{ m}^3/\text{kg}$ and stay relatively high until present. Superimposed on this pattern are higher frequency fluctuations over periods of $973 +/ - 361$ yr ($n=10$ over 11,800 yr), with shortest periods ($567 +/ - 153$ yr; $n=4$ over 1700 yr) during the time span with overall lower MS values. During the phases of relative higher MS values from 9800 yr BC to 4500 yr BC and 2000 yr BC to present, the superimposed fluctuations are $1225 +/ - 287$ yr ($n=5$ over 4100 yr) and $1025 +/ - 287$ yr ($n=5$ over 4100 yr), respectively. The MS-point signal follows the MS-loop signal very well.

Density of core AM09-PC-N-606 (Figure 4) can be broadly subdivided into two units. The lower unit from 9800 yr BC to ~ 4000 yr BC is characterized by continuously decreasing density from $>1.75 \text{ g/cm}^3$ to $\sim 1.47 \text{ g/cm}^3$. An exception is a relative low of $\sim 1.62 \text{ g/cm}^3$ at ~ 9200 yr BC. After ~ 4000 yr BC, density is more stable at $\sim 1.5 \text{ g/cm}^3$ and at ~ 500 yr BC it starts to decrease to $\sim 1.4 \text{ g/cm}^3$ at the sediment surface.

The magnetic susceptibility signal of the loop sensor in core AM09-PC-S-618 (Fig. 4) follows an overall increasing trend from core bottom to top with lowest MS values of $34 \text{ m}^3/\text{kg}$ between ~ 3 kyr BC and 2.3 kyr BC and highest MS values of $66 \text{ m}^3/\text{kg}$ between ~ 1300 yr AD and ~ 1750 yr AD. Superimposed on this trend are fluctuations with periods of $1200 +/ - 316$ yr ($n=5$ over 5400 yr). The MS point sensor generally follows the same trend as the MS-loop sensor.

Density in core AM09-PC-S-618 (Figure 5) follows an overall decreasing trend. The density is highest with ~ 1.49 g/cm 3 at the base of the core at 3500 yr BC, decreases until ~ 2600 yr BC to ~ 1.38 g/cm 3 and remains relatively constant until ~ 1500 yr BC. After ~ 1500 yr BC density drops to a low of <1.35 g/cm 3 at ~ 1000 yr BC and rises again to 1.44 g/cm 3 at ~ 600 yr BC. After ~ 600 yr BC density is variable but overall decreases to 1.35 g/cm 3 at ~ 1750 yr AD and drops to <1.28 g/cm 3 at the sediment surface.

4.5 Sedimentary Organic Matter

In core AM09-PC-N-606 (Fig. 6) TOC is lowest between 9400 yr BC and 6700 yr BC with values around 0.65 wt.%. From 6700 yr BC to 2600 yr BC TOC increases ($r^2=0.82$) to ~ 1.3 wt.%. After 2600 yr BC TOC stays constant around 1.2 % until ~ 200 yr AD. Then, TOC increases to 1.5 wt.% at ~ 500 yr AD, followed by a decrease to 1.1 wt.% at ~ 1300 yr AD. After 1300 yr AD, TOC increases to >1.5 wt.% at the sediment surface. These trends are paralleled by TN values. TN is lowest between 9400 yr BC and 6700 yr BC with values around 0.07 wt.%. From 6700 yr BC to 2600 yr BC TN increases ($r^2=0.86$) to ~ 0.18 wt.%. After 2600 yr BC TN decreases to 0.12 wt.% at ~ 200 yr AD. Then, TN increase to 0.16 wt.% at ~ 500 yr AD, followed by a decrease to 0.13 wt.% at ~ 1300 yr AD. After 1300 yr AD, TN increases to 0.2 wt.% at the sediment surface. C/N values (from wt. % of TOC and TN) decrease ($r^2=0.95$) from ~ 10.8 to ~ 7.4 between ~ 9400 yr BC and ~ 1500 yr BC. At ~ 1500 yr AD a sudden shift to a C/N of 9.4 occurs. Above, C/N values slowly decrease to 8.6 just below the sediment surface and jump to 11.2 at the sediment surface. The $\delta^{13}\text{C}$ increases ($r^2=0.92$) from -24 ‰ to -22.1 ‰ between ~ 9400 yr BC and ~ 1500 yr BC. After ~ 1.5 kyr BC the increasing trend ceases

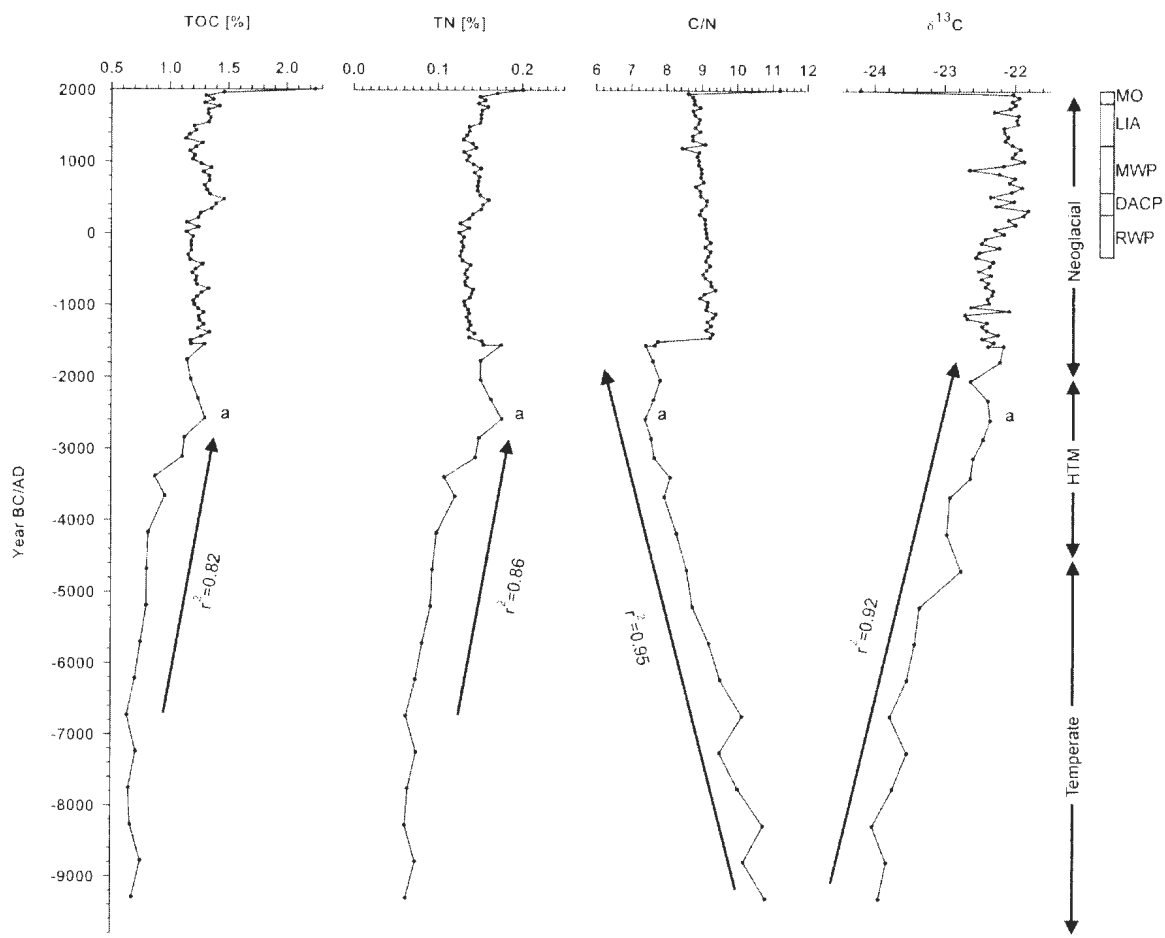


Figure 6: The graphs display results for total organic carbon (TOC), total nitrogen (TN), C/N ratios (TOC/TN), and $\delta^{13}\text{C}$ of TOC plotted versus calibrated Years BC/AD for core AM09-PC-N-606 (Nachvak Fjord). At the right side, Holocene and historical climatic periods are marked. The most prominent periods of global cooling during the Holocene are shown as grey bars in Figures 3 and 4 (Wanner et al., 2011).

and $\delta^{13}\text{C}$ varies around -22.3 ‰ , before it rises to -21.8 ‰ at ~ 200 yr AD. Above, $\delta^{13}\text{C}$ values vary around -22 ‰ with a low of -22.7 at ~ 1000 yr AD and a rapid drop to -24.2 ‰ at the sediment surface.

In core AM09-PC-S-618 (Figure 7) TOC increases ($r^2=0.78$) from ~ 1.8 wt.% to ~ 2.4 wt.% between ~ 3400 yr BC and ~ 2200 yr BC. From 2200 yr BC to 0 yr BC/AD

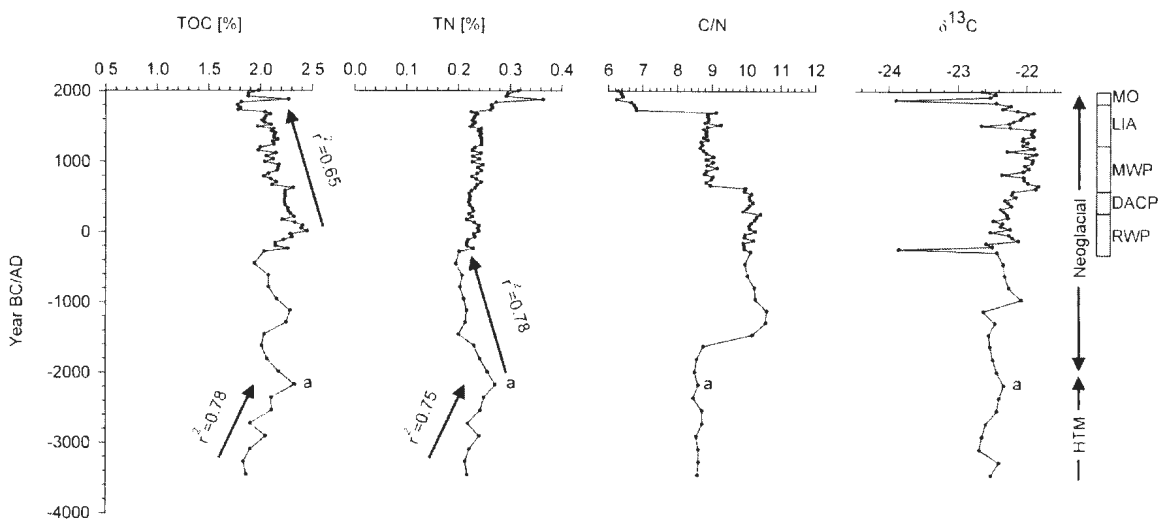


Figure 7: The graphs display results for total organic carbon (TOC), total nitrogen (TN), C/N ratios (TOC/TN), and $\delta^{13}\text{C}$ of TOC plotted versus calibrated Years BC/AD for core AM09-PC-S-618, Saglek Fjord. At the right side, Holocene and historical climatic periods are marked. The most prominent periods of global cooling during the Holocene are shown as grey bars in Figures 3 and 4 (Wanner et al., 2011).

TOC varies between 1.9 and 2.5 wt.%. After 0 yr BC/AD TOC decreases ($r^2=0.65$) from 2.5 wt.% to 2 wt.% at the sediment surface. TN increases ($r^2=0.75$) from ~0.21 wt.% at ~3400 yr BC to ~0.27 wt.% at ~2200 yr BC. After ~2200 yr BC, TN decreases ($r^2=0.78$) to ~0.19 wt.% at ~400 yr BC. Between ~400 yr BC and ~1700 yr AD, TN varies around 0.22 wt%, then rapidly increases to ~0.37 wt.% at ~1900 yr AD and drops to ~0.32 wt.% at the sediment surface. C/N values are around 8.6 between ~3400 yr BC and ~1600 yr BC, then values rapidly increase to ~10.6 and vary around 10.2 until ~700 yr AD, where C/N values suddenly drop to ~8.9. Until ~1700 yr AD, C/N values vary around 8.9, then drop to 6.8 and decrease to ~6.3 at the sediment surface. Values of $\delta^{13}\text{C}$ do not follow any strong trends but are weakly increasing from -22.6 ‰ to -21.8 ‰ between ~3400 yr BC to 700 yr AD and vary around -22 ‰ until ~1700 yr AD. Above, $\delta^{13}\text{C}$ values drop to ~-

22.7 ‰ at the sediment surface. Two negative peaks of ~-23.9 ‰ were observed at ~200 yr BC and ~1900 yr AD.

5. Discussion

5.1 Geochronology - Holocene sediment mass fluxes

Results from this study suggest that MARs in Nachvak and Saglek Fjord generally increase during periods of global cooling and decrease during periods of global warming. In Nachvak Fjord, results from this study suggest a lower sediment delivery to Nachvak Fjord during the Temperate Period, compared to most of the Holocene Thermal Maximum (HTM) and the beginning of the Neoglacial (Fig. 3). This is not wholly consistent with previous findings that during the Temperate Period the LS-LIS rapidly retreated (Clark and Fitzhugh, 1990; Carlson et al., 2007) and discharged great amounts of meltwater into the Labrador Sea. This discharge is thought to have lead to intense water column stratification that prevented Labrador Sea Water (LSW) formation before ~4,000 yr BC (Licciardi et al., 1999; de Vernal and Hillaire-Marcel, 2000; Cottet-Puinel et al., 2004). One potential explanation for the relatively low MARs during the Temperate Period is the existence of glacial lakes in the Nachvak Fjord catchments, which formed during the deglaciation and disappeared latest ~4000 yr BC (Ives, 1958; Evans et al., 1985; Occhietti et al., 2011). These glacial lakes may have acted as sediment traps, leading to low MARs in the fjord basin. Further, in the earlier stages of glacial lake formation, freshwater was routed through Koroc River and Nachvak Brook into Saglek Fjord and only later through Palmer River into Nachvak Fjord (Ives, 1958; Occhietti et al.,

2011). This could have lead to increased sediment discharge into Saglek Fjord during this period, compared to decreased sediment discharge into Nachvak Fjord.

A different explanation for low MARs during the Temperate Period may be a cooling effect of the remaining ice sheet, which led to a drier local climate with less precipitation (Carlson et al., 2007). This is coherent with a Holocene average precipitation curve for Labrador and N-Québec (Viau and Gajewski, 2008). However, it is likely that high discharge from the melting LS-LIS should have outpaced a decrease in precipitation.

In the HTM, the increase in MAR (Nachvak Fjord) at ~3,600 yr BC roughly correlates with a decrease in meltwater runoff from the LIS ~ 3,000 yr BC (Licciardi et al., 1999; de Vernal and Hillaire-Marcel, 2000; Cottet-Puinel et al., 2004) and the final disappearance of the LS-LIS (Wilton, 1996; Dyke, 2004; Ochietti et al., 2011). The rerouting of freshwater through Palmer River into Nachvak Fjord, as well as the disappearance of glacial lakes trapping sediment, may have led to a local increase in freshwater and sediment discharge. The increase in MAR correlates well with an overall increase in precipitation in Labrador and N-Quebec during the HTM and the Neoglacial (Viau and Gajewski, 2008).

In Saglek Fjord, only ~5.4 kyr of sedimentation are encompassed by our core (compared to 11.8 kyr in Nachvak Fjord), due to the much higher average SAR of ~0.14 cm/yr in core AM09-PC-S-618 (Fig. 4). Thus, paleoenvironmental changes in Saglek Fjord are recorded only since the HTM. The much higher SAR and MAR in Saglek Fjord relative to Nachvak Fjord may be explained by the much larger drainage basin of Nakvak Brook, which drains into Saglek Fjord (Bentley and Kahlmeyer, 2012). Further,

morphological evidence of high sediment discharge over time includes the presence of a subaqueous delta at Nakvak Brook in Saglek Fjord (Fig. 1), with a well developed channel in the Nakvak Brook delta front suggesting high sediment discharge to the Saglek Fjord main basin.

During the Neoglacial, in both Nachvak and Saglek Fjords, MARs indicate a decreased sediment delivery to the fjords' main basins, roughly covering the historical climatic periods Roman Warm Period (RWP), Dark Ages Cold Period (DACP), and Medieval Warm Period (MWP) (Wanner et al., 2011). Because the spacing of ¹⁴C dates precludes reference to historical climatic changes during the past ~2000 yr, it is difficult to relate the observed drops in MAR to climatic cooling or warming. Increased offshore sediment dispersal due to increased wave resuspension, possibly caused by less sea-ice coverage, seems unlikely in a fjord environment. Also precipitation curves of these time periods for the study area are inconclusive (Viau and Gajewski, 2008), suggesting that the observed decrease in MARs may be related to processes in the catchments.

The moderately (Nachvak Fjord) to very high (Saglek Fjord) MARs during the Little Ice Age (LIA) in Nachvak and Saglek Fjords may be explained by increased glacial action (McCoy, 1983). At least in Nachvak Fjord, glaciers are still present in the catchment today and glaciers may have grown during the LIA providing easily erodible material to the marine basins. Glacial activity during the entire Neoglacial is evident in the Nachvak Fjord catchment by several moraine abandonment phases (Fig. 3, 4) in the Torngat Mountains at ~800 BC, ~150 AD, and 1050-1850 AD (McCoy, 1983). These moraines most likely relate to the cold phases Superguksoak 2 (~1000 yr BC) and Superguksoak 3 (~500 yr AD) (Fig. 3, 4; unofficial terms) (Miller, 1973; McCoy, 1983;

Evans et al., 1985). The youngest set of moraine abandonment phases between 1050 and 1850 yr AD appears to correlate with the LIA, whereas the glacial episodes Superguksoak 2 and 3 may relate to the cold interval at ~800 yr BC and the DACP, respectively (Fig. 3).

5.2 Sedimentary textures - Holocene depositional environments and sea-ice variability

Sedimentary textures and grain diameter patterns in Nachvak and Saglek Fjords suggest, that sea-ice coverage responded to orbitally forced climatic changes since the deglaciation. Especially during the earlier Temperate Period, increased sea-ice coverage may have led to more proximal deposition, leading to decreased sediment accumulation in the basins centers. Similar effects have been observed during the Little Ice Age at the Great Whale River in Hudson Bay (Hülse and Bentley, 2012).

In Nachvak Fjord, the homogeneous, fine sediments, and lack of ice rafted clasts of the basal Unit I indicates that perennial landfast sea-ice may have existed from 9,800 to 8,800 yr BC, preventing sea-ice rafting and wave resuspension of sediment (Forwick and Vorren, 2009). This is most likely related to cool climate conditions in northern Labrador due to the persistence of the LS-LIS (Carlson et al., 2007). Unit 1 is interpreted to reflect under-ice sedimentation, mainly from suspension settling, and with high glacial flour content (Syvitski and Shaw, 1995), provided by glacial activity of the retreating LS-LIS.

A similar explanation for very fine grained sediments in fjords on Svalbard was suggested by Forwick and Vorren (2009), who proposed that multiannual and/or shore-fast sea-ice suppressed iceberg rafting during the Younger Dryas. Homogeneous intervals of fine clay have been used to infer glacial meltwater as the major sediment supplier (Stevens, 1990; Howe et al., 2010). Lack of laminates and rhythmites indicate a more

glacial distal deposition with greater influence of marine processes and/or intense bioturbation, which would indicate oxic bottom water conditions (as occur today). This further suggests that the Nachvak Fjord main basin must have been deglaciated at least since 9,800 yr BC, which is ~1,000 years earlier than the previously suggested fjord mouth deglaciation of ~8,800 yr BC (Dyke, 2004; Ochiatti et al., 2011) of Nachvak and Saglek Fjord.

Decreasing clay content in Unit II, is interpreted to reflect decreasing delivery of glacial flour (Syvitski and Shaw, 1995). Textures in Unit II suggest at least a temporary break-up of the sea-ice during most of the Temperate and the HTM. The parallel increase in sand deposition, peaking between 7,000 and 5,000 yr BC may suggest a higher current energy and/or increased sea-ice rafting. In both cases, this would be indicative of a temporary break-up of the sea-ice (Forwick and Vorren, 2009). Further, the proposed glacial retreat from the basins inner moraines (8,000 yr BC) and the fjord heads (6200 yr BC) (Dyke, 2004; Ochiatti et al., 2011), may have provided increased amounts of easily erodible sediments. After the marine limit was reached ~6,500 yr BC in Nain and probably not much later in the Saglek and Nachvak Fjord area, exposure of glacial and marine sediment then lead to extensive reworking by fluvial processes in the catchments (Evans and Rogerson, 1986), providing coarse sediments to the fjords. Mass-wasting from the steep fjord flanks may have increased with the warming during the Temperate Period (e.g., Holtedahl, 1975) supplying additional coarser material. On the modern sea-floor, however, there is not much evidence for mass-wasting from adjacent slopes (Fig. 1). The upward-increasing amount of shell debris in Unit II from 8,800 yr BC to ~2,000 yr BC, peaking during the HTM are regarded to reflect the Holocene climatic and

oceanographic conditions more conducive to marine productivity. Low content of large mineral clasts during the HTM (Fig. 3, 4, 5bce) suggests that periods of year-round open water conditions in Nachvak and Saglek Fjord may have existed during the HTM. Similar sedimentary textures indicating favorable climatic and oceanographic conditions, have been observed in Isfjorden on Svalbard during the HTM (Forwick and Vorren, 2009).

After ~2,000 yr BC, the beginning of the Neoglacial cooling (Wanner et al., 2011), a decrease in shell debris and an increase in ice rafted debris (Fig., 3, 4, 5df), suggest less favorable climatic and oceanographic conditions and an increase in sea-ice rafting (Forwick and Vorren, 2009). The overall slightly finer and relatively stable mean grain diameter, as well as very low sand content, during this period indicates reduced wave activity, possibly due to increased sea-ice dampening. A response to historical climatic changes during the past ~2000 yr (RWP, DACP, MWP and LIA) is not recorded in the grain diameter signal and sedimentary textures.

5.3 Magnetic susceptibility – Holocene climate and discharge variability

Magnetic susceptibility results suggest variations in weathering and discharge in Nachvak and Saglek Fjords during the Holocene. The timescales of these shifts seem to be consistent with timescales of orbital and solar forcings. While orbital forcing on a multi-millennial time scale seems to increase (decrease) sediment discharge during colder (warmer) periods as a result of increased (decreased) glacial activity, the solar forcing on a millennial time scale seems to decrease (increase) sediment discharge during colder (warmer) periods as a result of decreased (increased) precipitation.

A multi-millennial fluctuation in MS of approximately 9,000 yr appears to be present in core AM09-PC-N-606 (Fig. 3). We interpret the relative high MS-values during the Temperate Period to reflect freshly produced glacial flour from the retreating LS-LIS (Syvitski and Shaw, 1995). Minerals such as magnetite can be enriched in fine grained glacial flour, making MS an excellent indicator for past glacial activities (Reynolds et al., 2004; Rosenbaum and Reynolds, 2004). This is supported by the relatively high clay content (Fig. 3), which decreases towards ~3,500 yr BC. The rapid decrease in MS ~4,500 yr BC compares favorably in time with the proposed rapid deglaciation of the LS-LIS between 5,000 and 4,000 yr BC (Dyke, 2004; Ochietti et al., 2011). The relatively low MS-values during HTM are interpreted to reflect a period of decreased weathering and/or terrestrial input, possibly caused by a drier climate during this period (2,000 to 5,000 yr BC), and a lack of glacial flour production (Syvitski and Shaw, 1995; Forwick and Vorren, 2009).

We interpret this multi-millennial variability in sediment delivery to reflect climate shifts, which in turn are consistent in time with orbitally-forced changes in solar insolation. Solar insolation peaked ~10,000 yr BC due to changes in Earth's axis leading to the global HTM and the collapse of the LIS (Wanner et al., 2011). The prolonged existence of the LS-LIS during the Temperate, however, overprinted the orbitally-forced rise in global temperature and delayed the HTM in Labrador by ~4,000 yr compared to global temperatures (e.g., Wanner et al., 2011). Towards the Neoglacial solar insolation decreased as a result of changes in Earth's axis, leading to globally cooler temperatures (Wanner et al., 2011). The presence of modern glaciers in the Nachvak Fjord catchment suggests that more glacial flour may have been produced during the Neoglacial.

Furthermore, a recorded increase in precipitation (Viau and Gajewski, 2008) may have increased weathering, runoff, and terrestrial minerogenic input to the fjord basins.

Superimposed on this long-term trend are MS fluctuations with average periods of 973 +/- 361 yr and 1200 +/- 316 yr in Nachvak and Saglek Fjord, respectively. Although, the peaks are slightly offset between the cores, their patterns match reasonably well considering the resolution of our age models (Figs. 3 & 4), suggesting that similar forcing have been operative in both fjords. Fluctuations with similar periodicities were observed in Greenlandic ice-cores (Stuiver et al., 1995; Stuiver and Braziunas, 1993; Stuiver et al., 1995; Grootes and Stuiver, 1997), from the sedimentary record of lakes in northern Canada (Campbell et al., 1998) and the North Atlantic (Chapman and Shackleton, 2000). Further, variations in sea surface summer temperatures (SSST) from the Vøring Plateau of multi-centennial scale variability are documented during the HTM, whereas a submillennial-scale mode of variability is evident during the Neoglacial and directly associated with varying solar forcing (Berner et al., 2011). This was related to the generally warmer climate of the HTM, which lowers the likelihood of drastic changes in the oceanic circulation in response to solar irradiation anomalies (Berner et al., 2011). Similar processes may be responsible in Nachvak and Saglek Fjords for the higher frequency variability during the HTM compared to the lower frequency variability during the Neoglacial. We thus propose that the in Nachvak and Saglek Fjords observed periodicities in MS record solar-forced changes in precipitation, weathering and terrestrial minerogenic input to the basins.

Magnetic susceptibility results from Nachvak Fjord suggest that at least during the past 3,000 years river discharge reacted to centennial scale climatic fluctuations with

decreasing discharge during colder periods and vice versa. Highs and lows in MS since ~1000 yr BC correlate with known periods of past global warming and cooling, respectively (Figs. 3 & 4). Neoglacial moraine abandonment phases since 1,000 yr BC (McCoy, 1983; Evans and Rogerson, 1986) roughly correlate with lows in MS and historical cold periods (Fig. 3, 4). The historical cold periods LIA and DACP, appear to correlate with low MS-values suggesting decreased weathering and/or terrestrial runoff during these periods. This trend compares favorably with the palaeo-precipitation record in Labrador during these periods (Viau and Gajewski, 2008). Because an increase in precipitation should lead to an increase in weathering (e.g., White and Blum, 1995), runoff, and river discharge, we suggest that the MS signal can be used as a relative proxy for river discharge variations in Nachvak Fjord, although the temporal resolution of our age models do not allow for climate-related mass accumulation and discharge reconstructions.

Although the MS patterns in Nachvak and Saglek fjords are similar, direct correlation between both fjords is difficult. We suggest that this offset is caused by dating uncertainties. Especially, the signal of relative low MS during the HTM seems to be temporally compressed in Saglek Fjord relative to the signal in Nachvak Fjord (lower case letters in Figs. 3 and 4). If the dated MS record of core AM09 PC N 606 is interpreted as a proxy for river-sediment discharge magnitude, then the environmental chronology compares well with other regional paleoclimatic studies (McCoy, 1983; Evans and Rogerson, 1986; Viau and Gajewski, 2008; Wanner et al., 2011).

5.4 Sedimentary organic matter - Holocene environmental change

Results for sedimentary organic matter suggest that primary productivity increased during the Temperate Period and the HTM. Increasing TOC and TN during these periods suggest increasing input of labile organic matter. Decreasing C/N-ratios indicate decreasing input of terrestrial plant matter, supported by increasing $\delta^{13}\text{C}$, which is indicative of increased marine organic input. Further, a weak increase in $\delta^{13}\text{C}$ towards the MWP, possibly suggests an increase in primary productivity during this period.

Because core AM09-PC-S-618 (Fig. 7) only covers the period after ~3,500 yr BC, this trend is difficult to observe in Saglek Fjord, but AM09-PC-S-618 appears to correlate, also slightly offset, with the signal of core AM09-PC-N-606 in Nachvak Fjord. In both cores, the positive productivity trend in TOC and TN seems to stagnate after ~2,500 yr BC in Nachvak Fjord and ~2,200 yr BC in Saglek Fjord (marked “a” in Figs. 6 and 7). After ~ 2,500 yr BC TOC and TN values are relatively stable. The slightly elevated TOC and TN values in Nachvak Fjord between 400 yr AD and 1,000 yr AD correlate with the MWP, possibly suggesting an increase in productivity during this period. An increase in $\delta^{13}\text{C}$ is recorded towards the MWP in both cores, which stays high afterwards, suggesting a slightly less terrestrial/more marine influenced organic matter supply after ~1,000 yr AD compared to the period before.

The increasing trend during the Temperate Period correlates with our results from the sedimentary textures, both suggesting more favorable climatic and oceanographic conditions for marine primary productivity towards the HTM.

The dramatic shifts in the C/N record suggest rapid environmental change. Potential explanations include variations in water column stratification or changes in

marine current directions, which may lead to sill overflow suddenly preventing/allowing inflow of marine waters. This explanation remains speculative because of insufficient data. Also, once the Labrador Sea Water (LSW) formed at ~3 kyr BC (Licciardi et al., 1999; de Vernal and Hillaire-Marcel, 2000; Cottet-Puinel et al., 2004), no major changes in water column properties are known. These shifts could also be controlled in part by changes in benthic metabolism of organic material, perhaps due to evolving fjord circulation patterns, in turn producing relatively large changes in C/N ratios, because small changes in TOC or TN remineralization can cause relatively large changes in C/N (Sampei and Matsumoto, 2001). Sediment reworking can promote efficient remineralization of labile organic compounds, and leave only refractory organic matter. Therefore, it is possible that organic carbon was removed from the burial record by oxidation (Febo et al., 2008; Goni et al., 2008).

6. Conclusions:

The major findings of our proxy study on river discharge and environmental changes of Nachvak and Saglek Fjords are:

- 1) The sediment cores analyzed in this study cover 11,800 yr of climate and river discharge history of northern Labrador.
- 2) Mass accumulation rates in Nachvak and Saglek Fjord seem to generally increase during periods of global cooling and to decrease during periods of global warming. Dating strategy and, especially during the Temperate Period, local catchment processes, such as glacial activity, preclude exact reference to historic climatic periods on sediment discharge at a higher resolution and exact correlation between Nachvak and

Saglek Fjords. Low mass accumulation rates during the Temperate Period are most likely related to sediment trapping in glacial lakes in the catchments.

3) Sedimentary textures and grain diameter patterns in Nachvak and Saglek Fjords indicate, that sea-ice coverage responded to orbitally-forced climatic changes since the deglaciation. Year-round sea-ice cover prevailed until ~8800 yr BC. After 8800 yr BC sea-ice rafting appears to have increased during the Temperate, and year round open water conditions may have existed during the Holocene Thermal Maximum. After 2000 yr BC sea-ice rafting appears to have increased again, most likely as a result of global cooling during the Neoglacial cooling. Especially during the earlier Temperate Period, increased sea-ice coverage may have led to more proximal sediment deposition, leading to decreased sediment accumulation in the basins centers.

4) Magnetic susceptibility results suggest, that during the past 11.8 kyr weathering and discharge were primarily controlled by orbitally-forced multi-millennial climatic variations on which solar-forced millennial to centennial scale climatic variations are superimposed. These forcings lead to variations in glacial activity and precipitation. At least during the past 2000 yr, this leads to increased input of terrestrial minerogenic matter during warmer intervals and the opposite effect during colder periods. Further, this higher frequency signal is weaker during the HTM, which is most likely related to generally more stable climatic conditions during this interval.

5) Results for sedimentary organic matter suggest that primary productivity increased during the Temperate Period and the HTM. With onset of the Neoglacial, this increasing trend ceases, except for a weak increase in $\delta^{13}\text{C}$ towards the MWP, and possibly suggests an increase in primary productivity during this period.

Acknowledgements:

This project was funded by an ArcticNet grant to Samuel J. Bentley, with additional support from the Canada Research Chair Secretariat, the Canada Foundation for Innovation, Memorial University of Newfoundland, and the Harrison Chair for Sedimentary Geology, Louisiana State University. Special thanks go to Thomas Richerol and Lina Stolze, as well as the captains and crews of the CCGS Amundsen, who were of indispensable help during the field season in 2009. We would like to thank Duncan McIlroy and Susan Ziegler for their helpful discussions and reviews.

References:

- Anderson, L.G., Jutterström, S., Kaltin, S., Jones, E.P. and Björk, G., 2004. Variability in river runoff distribution in the Eurasian Basin of the Arctic Ocean. *Journal of Geophysical Research*, 109.
- Andrews, J.T., 1963. End moraines and late glacial chronology in the northern Nain-Okak section of the Labrador coast. *Geografiska annaler*, 45A: 158 - 171.
- Barber, D.C., Dyke, A., Hillaire-Marcel, C., Jennings, A.E., Andrews, J.T., Kerwin, M.W., Bilodeau, G., McNeely, R., Southon, J., Morehead, M.D. and Gagnon, J.-M., 1999. Forcing of the cold event of 8200 years ago by catastrophic drainage of Laurentide lakes. *Nature*, 400: 344-348.
- Bell, T., Rogerson, R.J. and Mengel, F., 1988. Reconstructed ice-flow patterns and ice limits using drift pebble lithology, outer Nachvak Fiord, northern Labrador. *Canadian Journal of Earth Sciences*, 26: 577-590.
- Bentley, S.J. and Kahlmeyer, E., 2012. Patterns and mechanisms of fluvial sediment flux and accumulation in two sub-arctic fjords: Nachvak and Saglek Fjords, Nunatsiavut, Canada. *Canadian Journal of Earth Sciences*, submitted.
- Berner, K.S., Koç, N., Godtliebsen, F. and Divine, D., 2011. Holocene climate variability of the Norwegian Atlantic Current during high and low solar insolation forcing. *Paleoceanography*, 26(PA2220).

- Bronk Ramsey, C., 2009. Bayesian analysis of radiocarbon dates. *Radiocarbon*, 51 (1): 337-360.
- Carlson, A.E., Clark, P.U., Raisbeck, G.M. and Brook, E.J., 2007. Rapid Holocene Deglaciation of the Labrador Sector of the Laurentide Ice Sheet. *Journal of Climate*, 20: 5126-5133.
- Chapman, M.R. and Shackleton, N.J., 2000. Evidence of 550-year and 1000-year cyclicities in North Atlantic circulation patterns during the Holocene. *Holocene*, 10(3): 287-291.
- Clark, P.U. and Fitzhugh, W.W., 1990. Late Deglaciation of the Central Labrador Coast and Its Implications for the Age of Glacial Lakes Naskaupi and McLean and for Prehistory. *Quaternary Research*, 34: 296-305.
- Clark, P.U., Brook, E.J., Raisbeck, G.M., Yiou, F. and Clark, J., 2003. Cosmogenic ^{10}Be ages of the Saglek Moraines, Torngat Mountains, Labrador. *Geology*, 31: 617-620.
- Cottet-Puinel, M., Weaver, A.J., Hillaire-Marcel, C., de Vernal, A., Clark, P.U. and Eby, M., 2004. Variation of Labrador Sea Water formation over the Last Glacial cycle in a climate model of intermediate complexity. *Quaternary Science Reviews*, 23: 449-465.
- de Vernal, A. and Hillaire-Marcel, C., 2000. Sea-ice, sea-surface salinity and the halo/thermocline structure in the northern North Atlantic: Modern versus full glacial conditions. *Quaternary Science Reviews*, 19: 65-85.
- Déry, S.J., Stieglitz, M., McKenna, E.C. and Wood, E.F., 2005. Characteristics and Trends of River Discharge into Hudson, James, and Ungava Bays, 1964-2000. *Journal of Climate*, 18: 2540-2557.
- Déry, S.J., Hernandez-Henriquez, M.A., Burford, J., E. and Wood, E.F., 2009. Observational evidence of an intensifying hydrological cycle in northern Canada. *Geophysical Research Letters*, 36(LI3402).
- Dyke, A.S., 2004. An outline of North American Deglaciation with emphasis on central and northern Canada. *Developments in Quaternary Science*, 2 (B): 373-424.
- Ellwood, B.B., Crick, R.E., Hassani, A., Benoist, S.L. and Young, R.H., 2000. Magnetosusceptibility event and cyclostratigraphy method applied to marine rocks: Dterital input versus carbonate productivity. *Geology*, 28(12): 1135-1138.

- Evans, D.J.A. and Rogerson, R.J., 1986. Glacial geomorphology and chronology in the Selamiut Range - Nachvak Fiord area, Torngat Mountains, Labrador. Canadian Journal of Earth Sciences, 23: 66-76.
- Febo, L.A., Bentley, S.J., Wrenn, J.H., Droxler, A.W., Dickens, G.R., Petterson, L.C. and Opdyke, B.N., 2008. Late Pleistocene and Holocene sedimentation, organic-carbon delivery, and paleoclimatic inferences on the continental slope of the northern Pandora Trough, Gulf of Papua. Journal of Geophysical Research, 113(F01S618).
- Forwick, M. and Vorren, T.O., 2009. Late Weichselian and Holocene sedimentary environments and ice rafting in Isfjorden, Spitsbergen. Palaeogeography, Palaeoclimatology, Palaeoecology, 280: 258-274.
- Gagnon, A.S. and Gough, W.A., 2005. Climate Change Scenarios for the Hudson Bay region: an intermodel comparison. Climate Change, 69: 269-297.
- Goni, M.A., Monacci, N., Gisewhite, R., Crockett, J., Nittrouer, C., Ogston, A., Alin, S.R. and Aalto, R., 2008. Terrigenous organic matter in sediments from the Fly River delta-clinoform system (Papua New Guinea). Journal of Geophysical Research, 113(F01S10).
- Hall, F.R., Andrews, J.T., Jennings, A.E., Vilks, G. and Moran, K., 1999. Late Quaternary sediments and chronology of the northeast Labrador Shelf (Karlsefni Trough, Saglek Bank): Links to glacial history. GSA Bulletin, 111(11): 1700-1713.
- Holtedahl, H., 1975. The geology of the Hardangerfjord, West Norway. Norges Geologiske Undersøkelse, 323: 1-87.
- Howe, J.A., Austin, W.E.N., Forwick, M., Paetzel, M., Harland, R. and Cage, A.G., 2010. Fjord systems and archives: a review. In: J.A. Howe, W.E.N. Austin, M. Forwick and M. Paetzel (Editors), Fjord Systems and Archives. The Geological Society of London Special Publications, London, pp. 5-15.
- Hülse, P. and Bentley, S.J.S., 2012. Climatically controlled sediment and water discharge during the past two millennia: the subarctic Great Whale River, Hudson Bay, Canada. Memorial University of Newfoundland.
- Ives, J.D., 1958. Glacial geomorphology of the Torngat Mountains, northern Labrador. Geographical Bulletin, 12: 47 -75.
- Jansson, K.N., 2003. Early Holocene glacial lakes and ice marginal retreat pattern in Labrador/Ungava, Canada. Palaeogeography, Palaeoclimatology, Palaeoecology, 193: 473-501.

- Johannessen, O.M., Bengtsson, L., Miles, M.W., Kuzmina, S.I., Semenov, V.A., Alekseev, G.V., Nagurny, A.P., Zakharov, V.F., Bobylev, L.P., Pettersson, L.H., Hasselmann, K. and Cattle, H.P., 2004. Arctic climate change: observed and modelled temperature and sea-ice variability. *Tellus*, 56 (A): 328-341.
- Kahlmeyer, E., 2011. Marine Records of Riverine Water and Sediment Discharge in Fjords of Nunatsiavut, Memorial University of Newfoundland, St. John's, 158 pp.
- Lawrence, D.M. and Slater, A.G., 2005. A projection of near surface permafrost degradation during the 21st century. *Geophysical Research Letters*, 32 (L24401 doi: 10.1029/2005GL025080).
- Licciardi, J.M., Teller, J.T. and Clark, P.U., 1999. Freshwater routing by the Laurentide Ice Sheet during the last deglaciation. In: P.U. Clark, R.S. Webb and L.D. Keigwin (Editors), *Mechanisms of Global Climate Change at Millennial Timescales*. American Geophysical Union, Washington, DC, pp. 177-202.
- Løken, H., 1962. The late glacial and postglacial emergence and the deglaciation of northeastemmost Labrador. *Geographical Bulletin*, 17: 23-56.
- McCoy, W.D., 1983. Holocene glacier fluctuations in the Torngat Mountains, northern Labrador. *Géographie physique et Quaternaire*, 37: 211-216.
- McNeely, R., Dyke, A.S. and Southon, J.R., 2006. Canadian marine reservoir ages, preliminary data assessment. Geological Survey of Canada, Open File 5049, 3.
- Nagata, T., 1961. Rock Magnetism. Maruzen, Tokyo.
- Ochietti, S., Parent, M., Lajeunesse, P., Robert, F. and Govare, E., 2011. Late Pleistocene-Early Holocene Decay of the Laurentide Ice Sheet in Québec-Labrador. In: J. Ehlers, P.L. Gibbard and H. P.D (Editors), *Quaternary Glaciations – Extent and Chronology. A Closer Look. Developments in Quaternary Science*. Elsevier.
- Reimer, P.J., Baillie, M.G.L., Bard, E., Bayliss, A., Beck, J.W., Blackwell, P.G., Bronk Ramsey, C., Buck, C.E., Burr, G.S., Edwards, R.L., Friedrich, M., Grootes, P.M., Guilderson, T.P., Hajdas, I., Heaton, T.J., Hogg, A.G., Hughen, K.A., Kaiser, K.F., Kromer, B., McCormac, F.G., Manning, S.W., Reimer, R.W., Richards, D.A., Southon, J.R., Talamo, S., Turney, C.S.M., van der Plicht, J. and Weyhenmeyer, C.E., 2009. IntCal09 and Marine09 radiocarbon age calibration curves, 0–50,000 years cal BP. *Radiocarbon*, 51 (4): 1111-1150.
- Reynolds, R.L., Rosenbaum, J.G., Rapp, J., Kerwin, M.W., Platt-Bradbury, J., Colman, S. and Adam, D., 2004. Record of late Pleistocene glaciation and deglaciation in

- the southern Cascade Range. I. Petrological evidence from lacustrine sediment in Upper Klamath Lake, southern Oregon. *Journal of Paleolimnology*, 31: 217–233.
- Rosenbaum, J.G. and Reynolds, R.L., 2004. Basis for paleoenvironmental interpretation of magnetic properties of sediment from Upper Klamath Lake (Oregon): effects of weathering and mineralogical sorting. *Journal of Paleolimnology*, 31: 253-265.
- Sampei, Y. and Matsumoto, E., 2001. C/N ratios in a sediment core from Nakaumi Lagoon, southwest Japan - usefulness as an organic indicator. *Geochemical Journal*, 35: 189– 205.
- Saucier, F.J., Senneville, S., Prinsenberg, S., Roy, F., Smith, G., Gachon, P., Caya, D. and Laprise, R., 2004. Modelling the sea ice-ocean seasonal cycle in Hudson Bay, Foxe Basin and Hudson Strait, Canada. *Canadian Climate Dynamics*, 23: 303-326.
- Stevens, R.L., 1990. Proximal and distal glacimarine deposits in southwestern Sweden: contrasts in sedimentation. In: J.A. Dowdeswell and J.D. Scourse (Editors), *Glacimarine Environments: Processes and Sediments*. Geological Society of London Special Publication, London, pp. 307-316.
- Syvitski, J.P.M., 1993. Glacimarine environments in Canada: an overview. *Canadian Journal of Earth Sciences*, 30(354–371).
- Syvitski, J.P.M. and Shaw, J., 1995. *Sedimentology and Geomorphology of Fjords. Geomorphology and Sedimentology of Esutaries. Developments in Sedimentology*, 53: 113-178.
- Viau, A.E. and Gajewski, K., 2008. Reconstructing Millennial-Scale, Regional Paleoclimates of Boreal Canada during the Holocene. *Journal of Climate*, 22: 316-350.
- Wanner, H., Solomina, O., Grosjean, M., Ritz, S.P. and Jetel, M., 2011. Structure and origin of Holocene cold events. *Quaternary Science Reviews*, 30: 3109-3123.
- Wardle, R.J., 1983. Nain-Churchill province cross section, Nachvak Fjord, northern Labrador..
- White, A.F. and Blum, A.E., 1995. Effects of climate on chemical weathering in watersheds. *Geochim Cosmochim Acta*, 59: 1729–1747.
- Wilton, D.H.C., 1996. Metallogenic overview of the Nain Province, northern Labrador. *CIM Bulletin*, 89: 43-52.

Chapter 5

Summary

In order to evaluate possible effects of climate change on freshwater discharge in northeastern Canada, and to place recently observed changes in freshwater discharge in an appropriate temporal and global framework of change, the sedimentary record offshore the Great Whale River in eastern Hudson Bay and in Nachvak and Saglek Fjords, northern Labrador, were analyzed in terms of climatic and river discharge proxies.

Further, there is a knowledge gap in the sediment dispersal patterns of high latitude sediment dispersal systems relative to much better understood marine dispersal systems from lower latitudes. This study aims to fill this gap. It was hypothesized, that cold periods result in decreased sediment and water discharge, with deposition close to the river mouth. In warm periods increased sediment and water discharge are expected, but it is inferred that greater wave mixing results in effective dispersal of sediment over a wide area.

1. Review of objectives

The following objectives were identified to address the above aims:

- 1) To investigate sediment dispersal patterns at the Great Whale River as an example of higher latitude sediment dispersal systems, a modern sediment budget was calculated for the Great Whale River study area. This will be used as a baseline for

comparison of modern dispersal patterns to models of sedimentation in the past and in the future.

- 2) Possible consequences of modern climate change trends on freshwater discharge were investigated by studying past responses of river discharge to historical periods of climatic change. The Medieval Warm Period (MWP) was chosen as an analogue to modern conditions, to evaluate possible effects of future climatic warming. By studying the Holocene discharge evolution since the last deglaciation ~10,000 yr BC, we have placed modern conditions in a large scale context including orbitally- and solar-forced climatic controls. Comparison between the two study sites (Great Whale River in eastern Hudson Bay, and Nachvak and Saglek Fjords in northern Labrador) allowed us to evaluate patterns in climate change over a broader area of Arctic Canada in contrasting depositional and oceanographic settings.

2. Summary of methods

To achieve the above objectives, the following methods were used:

- 1) ^{210}Pb geochronology to calculate sediment accumulation rates on time scales <200 yr
- 2) the granulometric proxy record and physical sedimentary structures (X-radiographic imaging) to assess sedimentary processes and oceanographic conditions
- 3) subbottom sonar data to estimate total Holocene fluvio-deltaic sediment thickness and to choose coring locations
- 4) Accelerated Mass Spectrometry ^{14}C (AMS ^{14}C) dating to create a geochronological framework and calculate ancient sedimentation rates

- 5) magnetic susceptibility as proxy for terrestrial minerogenic input and evaluate on changes in weathering, precipitation and runoff
- 6) sediment geochemistry (TOC, TN, TOC/TN, $\delta^{13}\text{C}_{\text{org}}$) to assess paleoenvironmental changes

3. Summary of conclusions

3.1 Modern (<150 yr) sediment and river discharge at the Great Whale River, Hudson Bay

Sediment accumulation at the Great Whale River study site appears to be a relatively steady process over time scales of 50-150 yr. Average SAR over this time scale is 0.16 cm/yr. Biological activity largely overprinted the primary depositional fabric. An offshore shift in the locus of fine-grained sediment deposition during the past 50-150 yr is suggested by subtle differences between ^{137}Cs and ^{210}Pb SARs. This increased offshore transport of fine-grained sediment is attributed to decreased sea-ice coverage and concomitantly to increased wave resuspension and offshore sediment transport during the past 50-150 yr. Under present day conditions 23 % (40,000 t/yr) of the discharged sediment accumulates within 25 km² of the river mouth, while 77 % (136,000 t/yr) of the discharged sediment bypass the study area. Variability in colloidal/clay and silt peaks in the grain diameter frequency record suggest that variations in environmental processes on decadal timescales control sediment transport and deposition. These grain diameter frequency variabilities may reflect variations in: 1) sediment plume intensity, 2) sediment winnowing by wave resuspension; and 3) bioturbation. Controls behind this variability

may be variations in river discharge and/or variations in wave climate, possibly due to windier conditions or less sea-ice dampening, or a combination of both.

3.2 Ancient sediment and river discharge at the Great Whale River, Hudson Bay

Between 3,500 and 2,000 yr BP (1,500 BC and 0 yr BC/AD), average sedimentation offshore the GWR was substantially higher than in the last 2000 yr and modern values. The exact mass accumulated has not been determined, because cores did not reach beyond 2000 yr BP (0 yr BC/AD). During the past 2000 years, cooler climatic periods, such as the LIA, are characterized by decreased sediment mass accumulation rates. During colder climatic periods, the locus of sediment mass accumulation appears to move to more river proximal areas. This is possibly related to both, wave dampening, caused by increased sea-ice coverage, and the lower freshwater discharge expected during periods of global cooling. River discharge calculations herein suggest that during the MWP river discharge appears to have been similar to modern values. The magnetic susceptibility record shows that a persistent higher frequency signal of terrestrial minerogenic input with a period of 195-263 yr is superimposed on these climatic variations during the past 2000 yr. Other comparable studies document similar frequencies and relate them to variability in the hydrologic cycle due to sea surface temperature variations in the North Atlantic (e.g., Stocker and Mysak, 1992; White et al., 1996; O'Sullivan et al., 2002; Berner et al., 2011). During the LIA, low magnitude MS variations and a consistent mean grain diameter in the river-distal areas of the GWR suggest more stable hydrodynamic conditions during the LIA relative to the MWP. This supports the above inference of increased sea-ice coverage during the LIA. The

approximately 60 years of instrumental records at the GWR and the similarity between the average half-period of MS fluctuations and the time scale of variability in the instrumental record of GWR, suggests that with such short instrumental records, it is not possible to separate anthropogenic influence from natural cycles. The overall consistent TOC, TN, C/N, and $\delta^{13}\text{C}$ values imply that no major changes in paleoenvironmental processes controlling carbon and nitrogen burial conditions occurred during the past ~2000 yr.

3.3 Ancient sediment and river discharge in Nachvak and Saglek Fjords, NE-Labrador

The sediment cores from Labrador reach further back in time than at the Great Whale River and record river discharge and oceanographic variability since ~9,800 cal yr BC. Ice-rafted debris contents imply that year-round sea-ice cover prevailed until ~ 8,800 cal yr BC. After 8,800 cal yr BC sea-ice rafting appears to have increased during the Temperate Period (9,800-4,000 cal yr BC) and year round open water conditions may have existed during the Holocene Thermal Maximum (4,000-2,000 yr cal BC). After 2000 cal yr BC, sea-ice rafting appears to have increased again, most likely as a result of global cooling during the Neoglacial. These multi-millennial trends in sea-ice coverage are also paralleled by trends in the magnetic susceptibility (MS) record, which imply long-term cyclicities of terrestrial minerogenic input. It is considered that this cyclicity in MS is likely related to orbitally forced Milankovitch-scale variations in insolation controlling climate and glacial activity, and therefore the amount of glacial flour transported to the fjords basin. Superimposed on this long-term trend in MS is a higher frequency variability, which may be related to solar forced ~1000 yr cyclicity. At least in

Nachvak Fjord during the past 2000 yr, there are cyclical changes in rates of input of terrestrial mineralogenic matter during warmer intervals relative to colder periods. Further, this higher frequency climatic signal is weaker during the HTM, which is most likely related to the generally more stable climatic conditions documented during this interval (e.g., Berner et al., 2011).

During the past ~11,000 yr sediment mass accumulation rates were lowest during the Temperate Period. This relatively low sedimentation during a period of supposedly high meltwater discharge (e.g., Licciardi et al., 1999; de Vernal and Hillaire-Marcel, 2000; Cottet-Puiné et al., 2004) is most likely related to the presence of local ice sheets and glacial lakes (Ives, 1958; Evans and Rogerson, 1986; Ochietti et al., 2011), which have the potential to trap sediment and reroute freshwater discharge. Historical climatic changes during the past 2000 yr could not be resolved within sediment accumulation rates in great detail due to AMS ^{14}C sample positions. There is, however, evidence for increased sediment discharge during the LIA in Saglek Fjord.

In Nachvak Fjord, an increasing productivity trend is observed in TOC, TN, TOC, and $\delta^{13}\text{C}$ during the Temperate Period and the HTM. Productivity rates decrease at the onset of the Neoglacial cooling ~2000 yr BC. Except for a slight increase in productivity during the MWP in Nachvak Fjord, no response to historical climatic changes was recorded in the organic paleoproductivity proxies during the past 2000 yr.

In summary, palaeo-discharge studies at the Great Whale River study site suggest that a warming climate may lead to increasing water and sediment discharge from the Great Whale River. Simultaneously the locus of fine-grained sediment deposition is likely

to shift further offshore as a result of decreased sea-ice coverage and concomitant increase in wave-current resuspension. The offshore shift in sediment deposition during the past ~50 yr compared to the past ~150 yr (determined from sediment radiochemistry) may already be an early signal of global warming. A temporal shift due to dating uncertainties unfortunately complicates the exact correlation with Nachvak and Saglek Fjords. Therefore, also correlation from the Great Whale River across the Labrador Peninsula to Nachvak and Saglek Fjords is complicated because the AMS ^{14}C dates did not sufficiently cover historical climatic periods to confirm any sediment discharge relationships relative to global climatic change during the past ~2000 yr. In Saglek Fjord an increase in SAR was recorded during the LIA (the opposite trend to that of the Great Whale River). The magnetic susceptibility record of Nachvak Fjord suggests a relationship between historical climatic change and variability in terrestrial minerogenic input (increase during warmer periods relative to periods of cooling). This is interpreted as a sign of increased precipitation in NE-Labrador and increased river discharge during warm periods (the same trend as at the Great Whale River).

4. Significance of research:

This thesis provides information and data relating to sediment properties, sedimentation rates, and sediment dispersal patterns. These are used to relate sedimentary proxies to climatic controls on sediment and river discharge in northeastern Canada.

This information is important because freshwater and sediment discharge influence both salinity and sediment supply, and thereby directly influence marine

ecosystems. This study can be used as baseline against which ongoing climatic change can be measured. Such a reference dataset can be used to “hindcast” changes in sediment and freshwater discharge with climatic warming.

River and sediment discharge is also important for location of potential hydro-power development, because increasing/decreasing freshwater and sediment discharge will influence the efficiency of hydro-power plants.

5. Open questions and future directions:

All cores recovered from the Great Whale River study area were retrieved from sites of active sedimentation. A systematic program of coring along longshore and offshore transects close to the Great Whale River would help to further improve the understanding of fluvial sediment dispersal in this region.

Sampling intervals for AMS ^{14}C dating did not allow for precise discharge reconstructions related to historic climatic periods in Nachvak and Saglek Fjords, complicating correlations across the Labrador Peninsula. More detailed dating would improve the understanding of the ancient climate-river discharge interactions of NE Canada.

References:

- Berner, K.S., Koç, N., Godtliebsen, F. and Divine, D., 2011. Holocene climate variability of the Norwegian Atlantic Current during high and low solar insolation forcing. *Paleoceanography*, 26(PA2220): 15.
- Cottet-Puiné, M., Weaver, A.J., Hillaire-Marcel, C., de Vernal, A., Clark, P.U. and Eby, M., 2004. Variation of Labrador Sea Water formation over the Last Glacial

- cycle in a climate model of intermediate complexity. *Quaternary Science Reviews*, 23: 449–465.
- de Vernal, A. and Hillaire-Marcel, C., 2000. Sea-ice, sea-surface salinity and the halo/thermocline structure in the northern North Atlantic: Modern versus full glacial conditions. *Quaternary Science Reviews*, 19: 65–85.
- Evans, D.J.A. and Rogerson, R.J., 1986. Glacial geomorphology and chronology in the Selamiut Range - Nachvak Fiord area, Torngat Mountains, Labrador. *Canadian Journal of Earth Sciences*, 23: 66-76.
- Ives, J.D., 1958. Glacial geomorphology of the Torngat Mountains, northern Labrador. *Geographical Bulletin*, 12: 47 -75.
- Licciardi, J.M., Teller, J.T. and Clark, P.U., 1999. Freshwater routing by the Laurentide Ice Sheet during the last deglaciation. In: P.U. Clark, R.S. Webb and L.D. Keigwin (Editors), *Mechanisms of Global Climate Change at Millennial Timescales*. American Geophysical Union, Washington, DC, pp. 177-202.
- O'Sullivan, P.E., Moyeed, R., Cooper, M.C. and Nicholson, M.J., 2002. Comparison between instrumental, observational and high resolution proxy sedimentary records of Late Holocene climatic change - a discussion of possibilities. *Quaternary International* 88: 27-44.
- Ochietti, S., Parent, M., Lajeunesse, P., Robert, F. and Govare, E., 2011. Late Pleistocene-Early Holocene Decay of the Laurentide Ice Sheet in Québec-Labrador. In: J. Ehlers, P.L. Gibbard and H. P.D (Editors), *Quaternary Glaciations – Extent and Chronology. A Closer Look. Developments in Quaternary Science*. Elsevier.
- Stocker, T.F. and Mysak, L.A., 1992. Climate fluctuations on the century time scale: a review of high-resolution proxy data and possible mechanisms. *Climate Change*, 20: 227-250.
- White, J.W.C., Gorodetzky, D., Cook, E.R. and Barlow, L.K., 1996. Frequency analysis of an annually resolved, 700 year paleoclimate record from the GISP2 ice core.. In: P.D. Jones, R. Bradley and J. Jouzel (Editors), *Climatic Variations and Forcing Mechanisms of the last 2000 years*. NATO ASI Series Vol. 1 (41). Springer, Berlin,, pp. 193-212.

Appendix A

Radiochemistry data for boxcores 2007 and gravity cores 2009, Hudson Bay

Appendix A contains result for ^{210}Pb and ^{137}Cs analyses performed on boxcores and gravity cores collected from the Great Whale River study site in Hudson Bay.

The tables list total and excess activities for ^{210}Pb ($^{210}\text{Pb}_{\text{total}}$ and $^{210}\text{Pb}_{\text{XS}}$) and for ^{137}Cs . Units are in decays per minute per gram [dpm/g]. ^{210}Pb was determined by measurement of the 46.5 keV gamma peak. $^{210}\text{Pb}_{\text{XS}}$ was determined by measurement of the supported ^{210}Pb originating from the decay of ^{226}Ra within the seabed. Supported ^{210}Pb was determined by measurement of the granddaughter of ^{226}Ra : ^{214}Pb (295 and 352 keV) and ^{214}Bi (609 keV). $^{210}\text{Pb}_{\text{XS}}$ then was determined by subtracting the supported ^{210}Pb from the $^{210}\text{Pb}_{\text{total}}$. ^{137}Cs activities were determined by measuring the 662 keV peak directly.

Core-ID: AM07-702-BC

Depth [cm]	$^{210}\text{Pb}_{\text{total}}$ [dpm/g]	$^{210}\text{Pb}_{\text{XS}}$ [dpm/g]	$^{210}\text{Pb}_{\text{XS}}$ Error [dpm/g]	^{137}Cs [dpm/g]	^{137}Cs Error [dpm/g]
0.5	10.51	8.89	0.35	0.59	0.08
1.5	10.56	8.71	0.32	0.54	0.06
2.5	9.51	8.23	0.31	0.59	0.06
3.5	9.79	8.30	0.30	0.84	0.07
4.5	8.41	7.06	0.28	0.81	0.07
5.5	7.88	6.49	0.29	0.82	0.07
6.5	3.67	2.59	0.18	0.25	0.05
7.5	5.13	3.75	0.23	0.69	0.07
8.5	3.37	1.89	0.17	0.52	0.07
9.5	2.80	1.40	0.16	0.35	0.06
10.5	2.06	0.64	0.09	0.28	0.06
11.5	1.90	0.45	0.07	0.00	0.00
12.5	1.95	0.77	0.11	0.00	0.00
13.5	1.35	-0.20	-0.05	0.00	0.00
14.5	2.09	0.80	0.10	0.00	0.00
15.5	1.61	0.05	0.01	0.00	0.00
16.5	1.43	-0.15	-0.03	0.00	0.00
17.5	2.02	0.75	0.10	0.00	0.00
18.5	1.85	0.42	0.07	0.00	0.00
19.5	1.32	0.03	0.01	0.00	0.00
20.5	1.36	-0.14	-0.03	0.00	0.00
21.5	1.29	-0.20	-0.04	0.00	0.00
22.5	0.95	-0.59	-0.18	0.00	0.00
23.5	1.28	-0.14	-0.03	0.00	0.00
24.5	1.30	-0.04	-0.01	0.00	0.00
25.5	1.04	-0.18	-0.05	0.00	0.00
26.5	1.05	-0.31	-0.08	0.00	0.00
27.5	1.68	0.05	0.01	0.00	0.00
28.5	1.74	0.39	0.06	0.00	0.00
29.5	1.19	-0.20	-0.05	0.00	0.00
30.5	1.15	0.03	0.01	0.00	0.00
31.5	0.91	-0.31	-0.10	0.00	0.00
32.5	1.14	-0.13	-0.03	0.00	0.00
33.5	1.16	-0.19	-0.05	0.00	0.00
34.5	1.88	0.62	0.09	0.00	0.00
35.5	0.24	-0.79	-1.00	0.00	0.00

Core-ID: AM07-702-1-BC

Depth [cm]	$^{210}\text{Pb}_{\text{total}}$ [dpm/g]	$^{210}\text{Pb}_{\text{XS}}$ [dpm/g]	$^{210}\text{Pb}_{\text{XS}}$ Error [dpm/g]	^{137}Cs [dpm/g]	^{137}Cs Error [dpm/g]
0.5	12.08	10.67	0.39	0.89	0.09
1.5	11.95	10.33	0.35	0.99	0.08
2.5	11.62	10.23	0.33	1.03	0.08
3.5	10.72	9.48	0.32	1.08	0.08
4.5	8.50	7.27	0.26	0.90	0.06
5.5	9.51	8.16	0.31	1.18	0.08
6.5	8.50	7.09	0.30	1.15	0.08
7.5	9.29	7.92	0.29	1.30	0.08
8.5	7.90	6.65	0.29	1.42	0.08
9.5	6.94	5.65	0.27	1.49	0.08
10.5	5.57	4.66	0.24	1.57	0.08
11.5	6.28	5.03	0.27	1.50	0.09
12.5	4.90	3.58	0.25	1.32	0.09
13.5	3.75	2.94	0.20	0.77	0.06
14.5	3.31	2.12	0.21	0.49	0.07
15.5	2.97	1.99	0.18	0.29	0.06
16.5	3.23	2.03	0.19	0.43	0.06
17.5	2.89	1.86	0.20	0.38	0.07
18.5	2.39	1.09	0.13	0.00	0.00
19.5	1.83	0.65	0.11	0.00	0.00
20.5	1.64	0.68	0.10	0.00	0.00
21.5	1.72	0.63	0.09	0.00	0.00
22.5	1.51	0.24	0.05	0.00	0.00
23.5	1.36	0.08	0.01	0.00	0.00
24.5	1.48	0.45	0.07	0.00	0.00
25.5	1.40	0.42	0.07	0.00	0.00
26.5	1.58	0.28	0.05	0.00	0.00
27.5	1.17	-0.06	-0.01	0.00	0.00
28.5	0.98	-0.23	-0.07	0.00	0.00
29.5	1.08	-0.12	-0.03	0.00	0.00
30.5	1.01	-0.21	-0.05	0.00	0.00
31.5	1.14	-0.14	-0.03	0.00	0.00
32.5	1.34	0.32	0.06	0.00	0.00
33.5	1.15	0.17	0.03	0.00	0.00
34.5	1.05	-0.35	-0.10	0.00	0.00
35.5	0.94	-0.43	-0.13	0.00	0.00
36.5	1.30	0.01	0.00	0.00	0.00
37.5	1.22	-0.01	0.00	0.00	0.00
38.5	0.78	-0.35	-0.10	0.00	0.00
39.5	1.41	0.39	0.07	0.00	0.00

Core-ID: AM07-702-2-BC

Depth [cm]	$^{210}\text{Pb}_{\text{total}}$ [dpm/g]	$^{210}\text{Pb}_{\text{XS}}$ [dpm/g]	$^{210}\text{Pb}_{\text{XS}}$ Error [dpm/g]	^{137}Cs [dpm/g]	^{137}Cs Error [dpm/g]
0.5	10.09	9.24	0.31	0.76	0.07
1.5	10.04	8.77	0.31	1.00	0.08
2.5	6.89	6.24	0.25	0.85	0.05
3.5	8.46	7.29	0.30	1.10	0.08
4.5	7.81	6.96	0.26	0.96	0.06
5.5	9.33	8.07	0.33	0.89	0.08
6.5	8.21	7.04	0.30	1.16	0.08
7.5	7.44	6.56	0.26	1.07	0.07
8.5	7.37	6.43	0.27	1.21	0.07
9.5	6.90	5.97	0.25	1.44	0.07
10.5	6.24	5.08	0.27	1.88	0.09
11.5	5.09	4.03	0.23	1.74	0.08
12.5	5.05	4.07	0.27	0.04	0.00
13.5	4.20	3.11	0.26	0.02	0.00
14.5	4.96	3.94	0.25	0.01	0.00
15.5	3.48	2.51	0.22	0.01	0.00
16.5	2.96	2.18	0.19	0.00	0.00
17.5	3.05	2.17	0.18	0.00	0.00
18.5	2.51	1.30	0.15	0.00	0.00
19.5	1.95	0.76	0.12	0.00	0.00
20.5	1.86	1.08	0.13	0.00	0.00
21.5	2.24	1.06	0.13	0.00	0.00
22.5	1.41	0.19	0.04	0.00	0.00
23.5	1.60	0.61	0.09	0.00	0.00

Core-ID: RA09-GW-4-P3

Depth [cm]	$^{210}\text{Pb}_{\text{total}}$ [dpm/g]	$^{210}\text{Pb}_{\text{XS}}$ [dpm/g]	$^{210}\text{Pb}_{\text{XS}}$ Error [dpm/g]	^{137}Cs [dpm/g]	^{137}Cs Error [dpm/g]
0.5	9.84	8.72	0.34	1.10	0.09
1.5	8.66	7.60	0.30	1.41	0.09
2.5	6.36	5.25	0.28	1.50	0.09
3.5	5.37	4.13	0.26	1.36	0.10
4.5	4.83	3.63	0.25	1.33	0.09
5.5	3.84	2.77	0.21	0.74	0.08
6.5	3.06	1.88	0.18	0.39	0.07
7.5	3.36	2.15	0.20	0.18	0.07
8.5	2.66	1.41	0.16	0.17	0.07
9.5	2.68	1.61	0.18	0.00	0.00
10.5	2.24	0.86	0.12	0.00	0.00
11.5	2.61	1.55	0.17	0.26	0.07
12.5	2.55	1.24	0.15	0.29	0.07
13.5	1.65	0.74	0.13	0.00	0.00
14.5	1.50	0.41	0.07	0.00	0.00
15.5	1.59	0.28	0.04	0.00	0.00
16.5	1.54	0.25	0.05	0.00	0.00
18.5	1.88	0.71	0.11	0.00	0.00
20.5	1.04	-0.15	-0.04	0.00	0.00
22.5	1.77	0.64	0.10	0.00	0.00
24.5	1.00	-0.28	-0.07	0.00	0.00
26.5	1.11	-0.33	-0.09	0.00	0.00
28.5	2.08	0.80	0.10	0.00	0.00
30.5	1.11	-0.19	-0.04	0.00	0.00
32.5	1.35	0.12	0.02	0.00	0.00
34.5	0.48	-0.63	-0.37	0.00	0.00
36.5	1.29	0.11	0.02	0.00	0.00
38.5	0.90	-0.39	-0.11	0.00	0.00
40.5	0.86	-0.26	-0.08	0.00	0.00

Core-ID: RA09-GW-5-P2

Depth [cm]	$^{210}\text{Pb}_{\text{total}}$ [dpm/g]	$^{210}\text{Pb}_{\text{XS}}$ [dpm/g]	$^{210}\text{Pb}_{\text{XS}}$ Error [dpm/g]	^{137}Cs [dpm/g]	^{137}Cs Error [dpm/g]
0.5	11.54	10.67	0.36	1.06	0.08
1.5	9.86	9.11	0.33	1.15	0.08
2.5	7.21	6.40	0.30	1.08	0.08
3.5	4.15	3.11	0.22	0.67	0.07
4.5	3.50	2.50	0.20	0.53	0.07
5.5	3.33	2.28	0.19	0.24	0.06
6.5	2.06	1.20	0.16	0.00	0.00
7.5	1.92	0.98	0.14	0.00	0.00
8.5	2.28	1.05	0.12	0.00	0.00
9.5	1.80	0.58	0.09	0.00	0.00
10.5	1.50	0.37	0.07	0.00	0.00
11.5	1.21	-0.02	-0.01	0.00	0.00
12.5	1.16	-0.01	0.00	0.00	0.00
13.5	0.91	-0.23	-0.06	0.00	0.00
14.5	1.14	-0.12	-0.03	0.00	0.00
16.5	0.86	-0.16	-0.05	0.00	0.00
18.5	1.04	-0.04	-0.01	0.00	0.00
20.5	1.39	0.45	0.07	0.00	0.00
22.5	1.00	-0.20	-0.05	0.00	0.00
24.5	0.97	-0.23	-0.05	0.00	0.00
26.5	1.09	-0.05	-0.01	0.00	0.00
28.5	1.32	0.25	0.05	0.00	0.00
30.5	0.79	-0.51	-0.16	0.00	0.00
32.5	1.46	0.15	0.03	0.00	0.00
34.5	0.87	-0.39	-0.11	0.00	0.00
36.5	1.41	0.24	0.04	0.00	0.00
38.5	1.20	-0.12	-0.03	0.00	0.00

Core-ID: RA09-GW-6-P4

Depth [cm]	$^{210}\text{Pb}_{\text{total}}$ [dpm/g]	$^{210}\text{Pb}_{\text{XS}}$ [dpm/g]	$^{210}\text{Pb}_{\text{XS}}$ Error [dpm/g]	^{137}Cs [dpm/g]	^{137}Cs Error [dpm/g]
0.5	9.88	9.15	0.35	0.83	0.07
1.5	7.88	7.08	0.33	1.01	0.07
2.5	6.58	5.73	0.30	1.28	0.08
3.5	6.41	5.45	0.28	1.15	0.08
4.5	4.92	3.81	0.25	1.19	0.08
5.5	4.78	3.77	0.25	0.82	0.07
6.5	3.85	2.83	0.24	0.52	0.06
7.5	3.17	2.12	0.20	0.28	0.05
8.5	3.02	1.79	0.19	0.22	0.06
9.5	2.97	1.82	0.18	0.00	0.00
10.5	2.32	1.14	0.15	0.00	0.00
11.5	2.14	1.01	0.15	0.14	0.06
12.5	1.44	0.19	0.04	0.00	0.00
13.5	1.52	0.28	0.05	0.00	0.00
14.5	1.75	0.60	0.09	0.00	0.00
16.5	2.04	1.06	0.15	0.00	0.00
18.5	1.41	0.35	0.07	0.00	0.00
20.5	1.91	0.67	0.10	0.00	0.00
22.5	0.93	-0.27	-0.07	0.00	0.00
24.5	1.30	0.07	0.01	0.00	0.00
26.5	1.04	-0.20	-0.05	0.00	0.00
28.5	1.05	-0.13	-0.03	0.00	0.00
30.5	1.26	0.02	0.01	0.00	0.00
32.5	0.85	-0.44	-0.15	0.00	0.00
34.5	0.82	-0.45	-0.15	0.00	0.00
36.5	0.64	-0.62	-0.28	0.00	0.00
38.5	1.30	0.01	0.00	0.00	0.00

Core-ID: RA09-GW-7-P10

Depth [cm]	$^{210}\text{Pb}_{\text{total}}$ [dpm/g]	$^{210}\text{Pb}_{\text{XS}}$ [dpm/g]	$^{210}\text{Pb}_{\text{XS}}$ Error [dpm/g]	^{137}Cs [dpm/g]	^{137}Cs Error [dpm/g]
0.5	8.44	7.37	0.33	0.54	0.07
1.5	7.80	6.74	0.33	0.69	0.08
2.5	8.06	7.21	0.31	0.86	0.07
3.5	8.00	7.08	0.33	0.93	0.08
4.5	6.25	5.20	0.29	1.18	0.08
5.5	5.15	4.00	0.28	1.25	0.08
6.5	4.52	3.49	0.25	1.38	0.08
7.5	3.93	2.74	0.23	1.19	0.08
8.5	3.97	2.87	0.23	0.64	0.07
9.5	3.48	2.45	0.19	0.36	0.06
10.5	2.69	1.66	0.18	0.36	0.06
11.5	2.58	1.45	0.16	0.00	0.00
12.5	2.46	1.24	0.14	0.17	0.05
13.5	1.54	0.35	0.06	0.00	0.00
14.5	1.93	0.78	0.11	0.00	0.00
15.5	2.19	1.01	0.13	0.00	0.00
17.5	1.10	-0.13	-0.03	0.00	0.00
19.5	1.67	0.49	0.08	0.00	0.00
21.5	1.62	0.22	0.03	0.00	0.00
23.5	1.35	0.18	0.03	0.00	0.00
25.5	1.58	0.43	0.07	0.00	0.00
27.5	1.53	0.38	0.07	0.00	0.00
29.5	1.30	0.05	0.01	0.00	0.00
31.5	1.55	0.46	0.07	0.00	0.00
33.5	0.41	-0.83	-0.52	0.00	0.00
35.5	1.24	0.03	0.01	0.00	0.00
37.5	1.14	0.08	0.02	0.00	0.00
39.5	1.18	-0.09	-0.02	0.00	0.00

Core-ID: RA09-GW-8-P5

Depth [cm]	$^{210}\text{Pb}_{\text{total}}$ [dpm/g]	$^{210}\text{Pb}_{\text{XS}}$ [dpm/g]	$^{210}\text{Pb}_{\text{XS}}$ Error [dpm/g]	^{137}Cs [dpm/g]	^{137}Cs Error [dpm/g]
0.5	10.95	9.65	0.35	0.92	0.09
1.5	10.13	8.91	0.32	1.24	0.09
2.5	7.98	6.94	0.33	1.37	0.09
3.5	7.51	6.30	0.31	1.53	0.10
4.5	5.87	4.77	0.26	1.48	0.09
5.5	5.03	3.83	0.24	1.53	0.10
6.5	4.52	3.59	0.23	0.95	0.08
7.5	3.19	2.13	0.18	0.57	0.07
8.5	2.64	1.63	0.15	0.36	0.05
9.5	2.69	1.71	0.17	0.00	0.00
10.5	2.16	0.85	0.10	0.00	0.00
11.5	1.88	0.61	0.08	0.00	0.00
12.5	1.81	0.34	0.03	0.00	0.00
13.5	1.74	0.36	0.06	0.00	0.00
14.5	1.88	0.73	0.10	0.00	0.00
16.5	1.52	0.25	0.04	0.00	0.00
18.5	1.23	-0.02	0.00	0.00	0.00
20.5	1.56	0.20	0.03	0.00	0.00
22.5	1.08	-0.31	-0.07	0.00	0.00
24.5	1.26	-0.11	-0.02	0.00	0.00
26.5	0.93	-0.28	-0.08	0.00	0.00
28.5	1.35	0.14	0.03	0.00	0.00
30.5	1.04	-0.40	-0.10	0.00	0.00
32.5	1.23	-0.15	-0.03	0.00	0.00
34.5	1.21	-0.28	-0.06	0.00	0.00
36.5	0.58	-0.77	-0.35	0.00	0.00
38.5	0.94	-0.34	-0.08	0.00	0.00

Appendix B

Granulometric data for boxcores 2007 and gravity cores 2009, Hudson Bay

Appendix B contains results of granulometric analyses performed on box cores (2007) and gravity cores (2009) collected at the Great Whale River study site in Hudson Bay.

The tables list mean grain diameter [μm] (Appendix 11 to 18) and grain diameter frequencies [%] (Appendix 19 to 58). Grain diameter frequencies in gravity cores were measured for the top ~40 cm only. Grain diameter frequencies are plotted versus Year AD. Years AD were calculated after sediment accumulation rates and spacing equals to cm intervals. Grain diameter frequencies for individual grain diameters are plotted in columns. Year AD is plotted in rows. Due to the file sizes, some tables continue on the next pages. Granulometric measurements were performed using a HORIBA Partica LA-950 laser diffraction particle size analysis system, with a particle size range of 0.1-3000 μm .

Core-ID: AM07-702-BC	
Depth [cm]	Mean grain diameter [μm]
0.5	10.44
1.5	17.13
2.5	14.96
3.5	12.51
4.5	15.76
5.5	14.91
6.5	10.85
7.5	12.48
8.5	10.46
9.5	11.82
10.5	18.09
11.5	7.64
12.5	12.06
13.5	12.31
14.5	9.61
15.5	11.11
16.5	13.66
17.5	12.60
18.5	15.46
19.5	10.13
20.5	27.54
21.5	15.28
22.5	13.17
23.5	11.82
24.5	10.47
25.5	18.97
26.5	11.18
27.5	267.88
28.5	16.45
29.5	15.99
30.5	9.74
31.5	13.81
32.5	10.33
33.5	13.49
34.5	8.26
35.5	13.19

Core-ID: AM07-702-1-BC

Depth [cm]	Mean grain diameter [μm]
0.5	22.38
1.5	25.43
2.5	7.97
3.5	25.07
4.5	27.34
5.5	20.25
6.5	20.98
7.5	27.45
8.5	23.19
9.5	22.12
10.5	15.67
11.5	13.30
12.5	16.31
13.5	19.97
14.5	28.97
15.5	18.95
16.5	23.13
17.5	19.14
18.5	24.63
19.5	21.22
20.5	23.53
21.5	19.05
22.5	13.70
23.5	17.25
24.5	10.37
25.5	16.15
26.5	16.85
27.5	15.35
28.5	22.78
29.5	20.37
30.5	16.05
31.5	16.38
32.5	23.25
33.5	13.73
34.5	12.61
35.5	21.45
36.5	14.18
37.5	15.79
38.5	20.28
39.5	13.03

Core-ID: AM07-702-2-BC

Depth [cm]	Mean grain diameter [μm]
0.5	29.45
1.5	27.72
2.5	31.85
3.5	30.80
4.5	28.76
5.5	27.92
6.5	29.42
7.5	22.37
8.5	30.59
9.5	24.94
10.5	25.60
11.5	19.27
12.5	24.95
13.5	22.87
14.5	27.02
15.5	28.21
16.5	27.78
17.5	24.97
18.5	24.37
19.5	30.78
20.5	25.49
21.5	27.23
22.5	26.36
23.5	25.29

Core-ID: RA09-GW-4-P3

Depth [cm]	Mean grain diameter [μm]	Depth [cm]	Mean grain diameter [μm]
0.5	10.939	36.5	18.9933
1.5	12.962	37.5	10.8554
2.5	15.0381	38.5	12.8526
3.5	14.6539	39.5	12.0249
4.5	14.6824	40.5	14.3964
5.5	10.5573	45.5	15.0286
6.5	18.1313	50.5	15.01
7.5	13.791	55.5	14.6114
8.5	12.6363	60.5	13.349
9.5	12.3612	65.5	14.2695
10.5	16.0066	70.5	15.5177
11.5	13.6319	75.5	16.1434
12.5	15.1622	80.5	18.0538
13.5	18.7742	85.5	15.4883
14.5	17.0346	90.5	15.7602
15.5	16.4153	95.5	11.5689
16.5	14.5892	100.5	16.7283
17.5	13.1937	105.5	11.101
18.5	15.2215	110.5	11.1402
19.5	16.4796	115.5	15.972
20.5	13.2667	120.5	13.0793
21.5	17.1374	125.5	14.2519
22.5	22.1484	130.5	13.08
23.5	14.4824	135.5	11.0641
24.5	12.2778	140.5	13.4289
25.5	8.7548	145.5	15.3463
26.5	13.0731	150.5	17.6145
27.5	14.0984	155.5	12.0574
28.5	15.476	160.5	13.4714
29.5	12.3959	165.5	13.7332
30.5	11.9798	170.5	12.7302
31.5	17.6515	175.5	10.1775
32.5	12.9213	180.5	11.4713
33.5	11.5602	185.5	12.4417
34.5	15.8261	190.5	11.6812
35.5	12.6387	195.5	9.8881

Core-ID: RA09-GW-5-P2

Depth [cm]	Mean grain diameter [μm]
0.5	13.1445
1.5	10.0089
2.5	10.6466
3.5	9.1434
4.5	10.8774
5.5	8.7775
6.5	11.2388
7.5	10.786
8.5	10.4123
9.5	10.4702
10.5	10.9725
11.5	12.6065
12.5	10.667
13.5	11.4475
14.5	11.9336
15.5	11.1819
16.5	13.4317
17.5	11.4081
18.5	10.4854
19.5	10.8258
20.5	10.4651
21.5	11.7449
22.5	10.6969
23.5	11.2419
24.5	10.1529
25.5	10.5314
26.5	11.8152
27.5	12.0998
28.5	11.605
29.5	15.2501
30.5	8.7868
31.5	13.5821
32.5	12.5813
33.5	12.5766
34.5	10.8667
35.5	11.0936
36.5	10.866
37.5	12.6685
38.5	13.719
39.5	9.7346

Core-ID: RA09-GW-6-P4

Depth [cm]	Mean grain diameter [μm]
0.5	17.0925
1.5	13.3392
2.5	13.6942
3.5	11.5287
4.5	9.8696
5.5	12.5725
6.5	12.9706
7.5	14.6633
8.5	11.1016
9.5	11.8136
10.5	12.6602
11.5	17.5945
12.5	12.4743
13.5	14.5733
14.5	10.8353
15.5	11.7171
16.5	13.79
17.5	9.4964
18.5	13.0918
19.5	11.3222
20.5	10.9327
21.5	12.4526
22.5	14.0911
23.5	12.8363
24.5	11.7628
25.5	11.7613
26.5	11.5351
27.5	15.5642
28.5	10.938
29.5	10.6074
30.5	10.2205
31.5	10.9819
32.5	10.4329
33.5	10.7114
34.5	10.965
35.5	10.5721
36.5	10.1619
37.5	12.6071
38.5	10.4549
39.5	12.9424

Core-ID: RA09-GW-7-P10			
Depth [cm]	Mean grain diameter [μm]	Depth [cm]	Mean grain diameter [μm]
0.5	15.7332	37.5	17.8991
1.5	26.0984	38.5	19.9235
2.5	20.7309	39.5	9.592
3.5	20.9076	45.5	16.31912
4.5	16.0877	50.5	19.5254
5.5	21.1985	55.5	19.49093
6.5	21.3193	60.5	15.37467
7.5	19.8313	65.5	31.13179
8.5	21.4324	70.5	16.04836
9.5	20.0276	75.5	17.77324
10.5	23.1129	80.5	20.75096
11.5	16.0072	85.5	18.24287
12.5	20.5835	90.5	18.0513
13.5	20.2306	95.5	20.9857
14.5	21.7803	100.5	20.51526
15.5	23.3148	105.5	18.33442
16.5	20.7385	110.5	21.16172
17.5	21.96	115.5	19.09116
18.5	20.9627	120.5	19.12866
19.5	22.7895	125.5	24.40664
20.5	23.166	130.5	20.54218
21.5	22.7898	135.5	17.80523
22.5	21.5014	140.5	15.36686
23.5	24.5541	145.5	21.30856
24.5	21.9354	150.5	20.85986
25.5	16.1295	155.5	21.95817
26.5	24.6623	160.5	16.49687
27.5	18.9934	165.5	16.46599
28.5	19.0719	170.5	16.52945
29.5	19.7825	175.5	26.53346
30.5	20.7195	180.5	15.91419
31.5	20.0616	185.5	16.38775
32.5	22.363	190.5	7.73832
33.5	19.4712	195.5	20.49244
34.5	22.5212	200.5	19.28066
35.5	18.8706	205.5	15.36353
36.5	24.3041	210.5	9.85538

Core-ID: RA09-GW-8-P5			
Depth [cm]	Mean grain diameter [μm]	Depth [cm]	Mean grain diameter [μm]
0.5	12.7321	45.5	15.85711
1.5	8.7989	50.5	12.68426
2.5	9.3949	55.5	17.51801
3.5	10.6542	60.5	11.60061
4.5	8.9705	65.5	11.23787
5.5	8.5572	70.5	13.89606
6.5	9.5885	75.5	16.04276
7.5	15.4915	80.5	11.59784
8.5	11.9617	85.5	14.25184
9.5	11.6413	90.5	11.90383
10.5	12.0315	95.5	14.43912
11.5	11.6527	100.5	12.94726
12.5	10.0047	105.5	13.66284
13.5	8.9565	110.5	13.90076
14.5	10.0777	115.5	10.9804
15.5	11.6416	120.5	10.23917
16.5	10.9335	125.5	12.10251
17.5	16.7194	130.5	8.78499
18.5	7.7535	135.5	15.2971
19.5	12.6719	140.5	10.55625
20.5	12.2325	145.5	9.01297
21.5	12.9328	150.5	7.48073
22.5	11.6146	155.5	10.26005
23.5	15.66	160.5	12.32867
24.5	10.3452	165.5	12.0383
25.5	11.0636	170.5	6.15478
26.5	10.2512	175.5	10.94823
27.5	14.8182	180.5	16.02964
28.5	10.4254	185.5	12.54096
29.5	10.9228	190.5	11.13774
30.5	9.9149	195.5	16.7849
31.5	12.6712	200.5	12.62181
32.5	11.5298	205.5	9.31952
33.5	12.8688	210.5	10.70036
34.5	11.3282	215.5	9.64331
35.5	9.1173	220.5	17.17411
36.5	10.6163	225.5	14.81348
37.5	11.1276	230.5	10.91338
38.5	13.809	235.5	10.85109
39.5	15.344	240.5	10.52275
40.5	12.8891	245.5	10.23001

Core-ID AM07-702-BC

Year	Micrometer [%]									
	297.3	250	210.22	176.78	148.65	125	105.11	88.388	74.325	62.5
2007	0.239	0.300	0.000	0.000	0.068	0.172	0.239	0.300	0.361	0.451
1997	0.768	0.771	0.000	0.148	0.598	0.720	0.768	0.771	0.786	0.873
1987	0.375	0.489	0.000	0.043	0.189	0.273	0.375	0.489	0.626	0.825
1977	0.237	0.326	0.000	0.000	0.000	0.122	0.237	0.326	0.427	0.576
1967	0.314	0.315	0.000	0.093	0.333	0.324	0.314	0.315	0.334	0.384
1957	0.285	0.404	0.000	0.000	0.065	0.179	0.285	0.404	0.529	0.693
1947	0.224	0.288	0.000	0.000	0.000	0.123	0.224	0.288	0.361	0.477
1937	0.586	0.528	0.067	0.323	0.511	0.610	0.586	0.528	0.514	0.522
1927	0.023	0.178	0.000	0.000	0.000	0.000	0.023	0.178	0.269	0.415
1917	0.347	0.377	0.000	0.053	0.226	0.300	0.347	0.377	0.412	0.484
1907	0.790	0.632	0.036	0.702	1.041	0.975	0.790	0.632	0.540	0.520
1897	0.000	0.000	0.000	0.000	0.000	0.000	0.000	0.000	0.000	0.105
1887	0.254	0.363	0.000	0.000	0.000	0.125	0.254	0.363	0.483	0.645
1877	0.278	0.350	0.000	0.000	0.077	0.198	0.278	0.350	0.417	0.503
1867	0.189	0.191	0.000	0.000	0.079	0.174	0.189	0.191	0.194	0.216
1857	0.202	0.243	0.000	0.000	0.000	0.117	0.202	0.243	0.284	0.349
1847	0.537	0.602	0.000	0.066	0.294	0.427	0.537	0.602	0.650	0.735
1837	0.653	0.619	0.000	0.078	0.365	0.555	0.653	0.619	0.545	0.508
1827	0.375	0.439	0.000	0.053	0.223	0.299	0.375	0.439	0.505	0.606
1817	0.141	0.196	0.000	0.000	0.000	0.000	0.141	0.196	0.243	0.312
1807	0.888	1.261	0.000	0.061	0.304	0.546	0.888	1.261	1.676	2.271
1797	0.645	0.614	0.000	0.107	0.454	0.593	0.645	0.614	0.560	0.538
1787	0.450	0.472	0.000	0.073	0.305	0.395	0.450	0.472	0.490	0.541
1777	0.433	0.345	0.000	0.112	0.460	0.513	0.433	0.345	0.299	0.304
1767	0.169	0.217	0.000	0.000	0.000	0.092	0.169	0.217	0.264	0.330
1757	0.426	0.824	0.000	0.000	0.000	0.145	0.426	0.824	1.309	1.905
1747	0.403	0.418	0.000	0.060	0.261	0.352	0.403	0.418	0.432	0.476
1737	0.375	0.394	0.655	0.482	0.419	0.384	0.375	0.394	0.436	0.506
1727	0.460	0.473	0.000	0.113	0.424	0.450	0.460	0.473	0.503	0.577
1717	0.727	0.722	0.000	0.159	0.633	0.724	0.727	0.722	0.746	0.838
1707	0.166	0.210	0.000	0.000	0.000	0.094	0.166	0.210	0.255	0.316
1697	0.581	0.509	0.000	0.120	0.496	0.598	0.581	0.509	0.448	0.435
1687	0.248	0.273	0.000	0.036	0.154	0.208	0.248	0.273	0.299	0.351
1677	0.474	0.524	0.000	0.065	0.284	0.394	0.474	0.524	0.576	0.674
1667	0.020	0.142	0.000	0.000	0.000	0.000	0.020	0.142	0.171	0.219
1657	0.462	0.560	0.000	0.049	0.221	0.338	0.462	0.560	0.644	0.757

continued

Micrometer [%]

52.556	44.194	37.163	31.25	26.278	22.097	18.581	15.625	13.139	11.049	9.291
0.552	0.617	0.665	0.712	0.788	0.930	1.212	1.792	2.616	3.664	4.818
0.979	1.036	1.064	1.085	1.143	1.282	1.578	2.177	2.995	3.986	5.021
1.036	1.144	1.207	1.246	1.310	1.464	1.797	2.479	3.420	4.575	5.789
0.759	0.888	0.994	1.096	1.227	1.434	1.810	2.532	3.489	4.623	5.767
0.460	0.532	0.606	0.707	0.876	1.161	1.694	2.847	4.642	7.159	10.154
0.875	0.994	1.089	1.185	1.329	1.579	2.048	2.976	4.252	5.816	7.444
0.625	0.730	0.814	0.892	0.990	1.153	1.459	2.061	2.875	3.860	4.886
0.535	0.548	0.575	0.646	0.789	1.063	1.622	2.413	3.423	4.544	5.486
0.610	0.754	0.874	0.978	1.086	1.249	1.556	2.169	3.011	4.049	5.154
0.566	0.616	0.652	0.691	0.767	0.920	1.222	1.841	2.713	3.813	5.012
0.523	0.528	0.534	0.557	0.632	0.793	1.115	1.798	2.803	4.119	5.605
0.197	0.273	0.358	0.464	0.604	0.799	1.124	1.761	2.654	3.785	5.027
0.815	0.905	0.961	1.002	1.067	1.212	1.516	2.141	3.012	4.088	5.236
0.587	0.635	0.672	0.717	0.811	1.000	1.377	2.171	3.329	4.829	6.491
0.252	0.288	0.328	0.386	0.489	0.667	1.000	1.710	2.775	4.202	5.849
0.433	0.504	0.574	0.662	0.803	1.035	1.454	2.292	3.470	4.944	6.522
0.805	0.822	0.819	0.818	0.862	0.995	1.281	1.868	2.680	3.682	4.747
0.488	0.481	0.478	0.491	0.548	0.676	0.935	1.487	2.297	3.362	4.576
0.725	0.810	0.883	0.970	1.114	1.368	1.843	2.808	4.182	5.934	7.847
0.400	0.474	0.546	0.632	0.761	0.966	1.330	2.056	3.073	4.357	5.762
2.934	3.261	3.405	3.407	3.366	3.443	3.739	4.310	4.961	5.561	5.935
0.525	0.521	0.521	0.541	0.619	0.793	1.149	1.939	3.161	4.851	6.871
0.596	0.629	0.653	0.686	0.766	0.928	1.251	1.924	2.894	4.144	5.539
0.341	0.384	0.429	0.490	0.593	0.762	1.061	1.661	2.506	3.580	4.771
0.408	0.466	0.519	0.584	0.690	0.875	1.226	1.967	3.072	4.546	6.247
2.403	2.495	2.407	2.179	1.921	1.795	1.870	2.231	2.819	3.576	4.400
0.521	0.542	0.554	0.572	0.628	0.754	1.013	1.560	2.357	3.395	4.564
0.573	0.600	0.608	0.612	0.636	0.712	0.887	1.270	1.833	2.579	3.454
0.671	0.738	0.794	0.862	0.984	1.208	1.643	2.565	3.950	5.828	8.029
0.924	0.944	0.934	0.912	0.922	1.013	1.249	1.761	2.491	3.408	4.408
0.380	0.419	0.450	0.486	0.555	0.693	0.975	1.601	2.576	3.939	5.601
0.441	0.450	0.460	0.484	0.555	0.701	0.991	1.621	2.584	3.914	5.530
0.421	0.480	0.535	0.606	0.719	0.901	1.224	1.849	2.697	3.731	4.823
0.779	0.831	0.858	0.881	0.939	1.078	1.370	1.968	2.796	3.817	4.901
0.285	0.344	0.404	0.476	0.583	0.752	1.054	1.669	2.553	3.695	4.979
0.851	0.877	0.874	0.865	0.894	1.014	1.293	1.880	2.702	3.723	4.811

continued

Micrometer [%]

7.813	6.57	5.524	4.645	3.906	3.285	2.762	2.323	1.953	1.642	1.381
5.774	6.111	6.108	5.820	5.331	4.831	4.367	3.850	3.358	2.777	2.097
5.813	6.041	5.967	5.647	5.182	4.733	4.323	3.856	3.388	2.813	2.128
6.712	6.939	6.785	6.318	5.665	5.033	4.451	3.810	3.227	2.578	1.867
6.579	6.725	6.524	6.044	5.419	4.835	4.311	3.737	3.205	2.596	1.911
12.534	12.739	11.646	9.578	7.126	5.053	3.444	2.138	1.380	0.832	0.435
8.595	8.704	8.242	7.320	6.164	5.089	4.135	3.178	2.448	1.773	1.155
5.678	5.922	5.882	5.613	5.208	4.820	4.472	4.072	3.641	3.076	2.367
5.841	5.872	5.632	5.197	4.753	4.347	3.898	3.457	2.906	2.228	1.556
6.034	6.321	6.291	6.003	5.548	5.098	4.685	4.209	3.717	3.096	2.342
5.998	6.355	6.373	6.110	5.647	5.172	4.727	4.210	3.689	3.049	2.291
6.842	7.237	7.149	6.645	5.854	5.060	4.329	3.564	2.934	2.290	1.626
6.047	6.395	6.378	6.058	5.525	4.988	4.499	3.966	3.465	2.870	2.165
6.137	6.407	6.336	5.984	5.453	4.926	4.437	3.882	3.346	2.720	2.005
7.829	8.199	8.022	7.381	6.425	5.467	4.576	3.632	2.870	2.133	1.432
7.260	7.744	7.697	7.189	6.337	5.463	4.651	3.797	3.099	2.394	1.678
7.725	7.994	7.756	7.094	6.169	5.268	4.439	3.562	2.845	2.139	1.455
5.595	5.882	5.875	5.627	5.221	4.820	4.452	4.024	3.574	2.999	2.294
5.630	6.051	6.117	5.881	5.410	4.913	4.447	3.931	3.439	2.853	2.157
9.317	9.587	9.168	8.175	6.844	5.571	4.430	3.294	2.459	1.725	1.086
6.918	7.320	7.313	6.960	6.351	5.721	5.120	4.436	3.793	3.065	2.257
5.866	5.428	4.835	4.134	3.497	2.999	2.599	2.209	1.887	1.543	1.168
8.664	9.290	9.204	8.485	7.280	6.030	4.861	3.655	2.744	1.930	1.215
6.708	7.121	7.110	6.736	6.095	5.427	4.788	4.066	3.411	2.696	1.930
5.783	6.190	6.274	6.087	5.694	5.279	4.888	4.426	3.934	3.299	2.518
7.694	8.156	8.039	7.421	6.442	5.450	4.533	3.585	2.840	2.126	1.440
5.076	5.326	5.338	5.160	4.866	4.576	4.315	4.002	3.638	3.131	2.465
5.548	5.903	5.915	5.640	5.160	4.669	4.207	3.665	3.115	2.452	1.696
4.257	4.603	4.649	4.407	3.929	3.392	2.860	2.280	1.815	1.373	0.953
9.906	10.424	10.108	9.073	7.563	6.084	4.763	3.477	2.561	1.773	1.097
5.241	5.565	5.615	5.440	5.109	4.772	4.463	4.094	3.681	3.125	2.416
7.153	7.815	7.930	7.552	6.749	5.861	5.002	4.072	3.301	2.525	1.744
7.064	7.785	8.011	7.784	7.135	6.364	5.577	4.659	3.836	2.968	2.077
5.683	5.970	5.964	5.720	5.323	4.934	4.586	4.185	3.750	3.175	2.451
5.759	6.040	6.014	5.737	5.300	4.867	4.469	4.010	3.539	2.949	2.238
6.067	6.471	6.497	6.202	5.667	5.114	4.600	4.035	3.508	2.891	2.170
5.660	5.907	5.831	5.491	4.990	4.508	4.080	3.623	3.192	2.672	2.043

continued

Micrometer [%]

1.161	0.977	0.821	0.691	0.581	0.488	0.411	0.345	0.29	0.244	0.205
1.450	1.016	0.738	0.592	0.593	0.728	1.073	1.894	3.090	4.463	5.198
1.477	1.044	0.772	0.639	0.662	0.832	1.226	2.048	3.006	3.728	3.524
1.232	0.830	0.583	0.459	0.459	0.570	0.846	1.461	2.243	2.931	2.943
1.285	0.882	0.633	0.511	0.523	0.662	1.000	1.757	2.730	3.596	3.624
0.158	0.000	0.000	0.000	0.000	0.000	0.000	0.000	0.000	0.000	0.000
0.680	0.416	0.266	0.193	0.186	0.232	0.363	0.697	1.211	1.806	2.099
1.667	1.190	0.886	0.737	0.765	0.965	1.428	2.409	3.576	4.483	4.280
1.091	0.786	0.619	0.606	0.727	1.055	1.853	3.048	4.477	5.345	4.579
1.613	1.126	0.817	0.660	0.669	0.829	1.217	2.051	3.064	3.885	3.769
1.573	1.099	0.803	0.656	0.675	0.850	1.265	2.159	3.251	4.142	4.025
1.051	0.693	0.473	0.356	0.341	0.410	0.610	1.130	1.975	3.105	4.012
1.486	1.027	0.730	0.568	0.554	0.667	0.978	1.755	2.952	4.441	5.437
1.349	0.927	0.666	0.540	0.557	0.713	1.094	1.961	3.096	4.131	4.197
0.878	0.560	0.378	0.293	0.299	0.389	0.623	1.202	2.051	2.962	3.278
1.070	0.696	0.470	0.351	0.336	0.407	0.612	1.156	2.062	3.303	4.343
0.905	0.585	0.401	0.315	0.326	0.430	0.696	1.355	2.323	3.363	3.719
1.609	1.148	0.856	0.716	0.747	0.947	1.407	2.377	3.529	4.422	4.218
1.487	1.034	0.741	0.582	0.570	0.687	1.005	1.784	2.964	4.397	5.305
0.621	0.372	0.236	0.171	0.165	0.205	0.311	0.555	0.874	1.160	1.177
1.530	1.066	0.783	0.650	0.679	0.854	1.240	1.967	2.676	3.012	2.534
0.826	0.603	0.466	0.408	0.441	0.566	0.825	1.304	1.762	1.974	1.661
0.692	0.412	0.259	0.186	0.179	0.225	0.356	0.695	1.222	1.841	2.156
1.261	0.846	0.596	0.474	0.484	0.614	0.936	1.669	2.627	3.501	3.569
1.756	1.243	0.917	0.754	0.774	0.965	1.411	2.343	3.432	4.253	4.020
0.885	0.558	0.365	0.265	0.250	0.303	0.462	0.899	1.661	2.766	3.804
1.784	1.307	0.996	0.841	0.863	1.041	1.412	2.038	2.541	2.636	2.054
1.025	0.615	0.373	0.244	0.209	0.234	0.343	0.688	1.410	2.783	4.968
0.614	0.410	0.287	0.224	0.220	0.267	0.394	0.708	1.195	1.817	2.287
0.609	0.350	0.208	0.117	0.000	0.077	0.157	0.225	0.293	0.327	0.286
1.708	1.223	0.912	0.759	0.784	0.982	1.440	2.396	3.512	4.353	4.109
1.091	0.695	0.458	0.332	0.310	0.368	0.545	1.018	1.812	2.913	3.869
1.328	0.878	0.612	0.484	0.491	0.613	0.900	1.476	2.093	2.466	2.181
1.731	1.240	0.927	0.774	0.806	1.017	1.506	2.537	3.757	4.698	4.470
1.556	1.101	0.815	0.676	0.702	0.889	1.324	2.250	3.364	4.247	4.083
1.483	1.022	0.726	0.565	0.550	0.661	0.965	1.718	2.867	4.277	5.196
1.426	1.001	0.724	0.573	0.563	0.680	0.992	1.754	2.902	4.287	5.149

continued

Micrometer [%]

0.173	0.145	0.122	0.103	0.086
4.341	2.663	1.285	0.406	0.089
2.354	1.193	0.479	0.117	0.000
2.083	1.106	0.465	0.119	0.000
2.559	1.347	0.558	0.140	0.000
0.000	0.000	0.000	0.000	0.000
1.700	1.005	0.466	0.131	0.000
2.874	1.454	0.579	0.139	0.000
2.866	1.408	0.451	0.099	0.000
2.578	1.327	0.539	0.133	0.000
2.749	1.411	0.570	0.140	0.000
3.715	2.490	1.311	0.453	0.104
4.761	3.030	1.510	0.490	0.108
2.966	1.553	0.635	0.156	0.000
2.507	1.401	0.611	0.160	0.000
4.075	2.751	1.455	0.503	0.115
2.831	1.569	0.676	0.174	0.000
2.830	1.431	0.570	0.138	0.000
4.588	2.894	1.432	0.462	0.102
0.845	0.461	0.202	0.003	0.000
1.519	0.713	0.270	0.004	0.000
1.004	0.478	0.185	0.003	0.000
1.755	1.040	0.483	0.136	0.000
2.544	1.350	0.563	0.142	0.000
2.684	1.357	0.542	0.132	0.000
3.724	2.606	1.427	0.510	0.118
1.162	0.527	0.195	0.003	0.000
6.567	6.105	4.504	2.229	0.751
2.091	1.401	0.744	0.242	0.000
0.189	0.061	0.000	0.000	0.000
2.734	1.375	0.546	0.131	0.000
3.683	2.528	1.363	0.483	0.112
1.369	0.667	0.261	0.004	0.000
2.990	1.507	0.598	0.144	0.000
2.760	1.404	0.563	0.137	0.000
4.525	2.874	1.432	0.466	0.103
4.434	2.787	1.375	0.442	0.097

Core-ID: AM07-702-1-BC

Micrometer [%]

Year	297.3	250	210.22	176.78	148.65	125	105.11	88.388	74.325	62.5
2007	0.000	0.127	0.500	0.602	0.701	0.798	0.911	1.093	1.302	1.438
2001	0.000	0.120	0.479	0.597	0.741	0.908	1.117	1.441	1.843	2.117
1996	0.000	0.000	0.000	0.000	0.000	0.000	0.000	0.000	0.000	0.000
1990	0.000	0.112	0.471	0.639	0.822	1.008	1.231	1.584	2.001	2.250
1985	0.025	0.498	0.758	0.819	0.909	1.047	1.252	1.591	1.980	2.186
1979	0.000	0.054	0.233	0.338	0.478	0.644	0.854	1.172	1.561	1.811
1974	0.000	0.000	0.000	0.148	0.392	0.714	1.142	1.754	2.442	2.790
1968	0.000	0.120	0.484	0.633	0.855	1.146	1.526	2.100	2.748	3.077
1963	0.000	0.090	0.384	0.544	0.740	0.953	1.207	1.599	2.061	2.325
1957	0.000	0.126	0.488	0.566	0.643	0.736	0.870	1.103	1.398	1.601
1951	0.000	0.000	0.000	0.105	0.226	0.339	0.468	0.650	0.887	1.078
1946	0.000	0.000	0.000	0.113	0.225	0.327	0.456	0.647	0.883	1.047
1940	0.000	0.000	0.000	0.102	0.228	0.372	0.576	0.906	1.372	1.730
1935	0.000	0.056	0.241	0.339	0.449	0.563	0.704	0.933	1.249	1.501
1929	0.652	0.597	0.565	0.557	0.599	0.710	0.902	1.245	1.728	2.098
1924	0.000	0.049	0.212	0.307	0.422	0.548	0.704	0.964	1.331	1.631
1918	0.000	0.128	0.502	0.592	0.681	0.785	0.933	1.195	1.540	1.788
1912	0.000	0.040	0.177	0.266	0.390	0.540	0.731	1.021	1.390	1.649
1907	0.000	0.115	0.490	0.680	0.900	1.125	1.374	1.737	2.102	2.256
1901	0.000	0.113	0.440	0.524	0.620	0.731	0.882	1.131	1.429	1.613
1896	0.000	0.089	0.362	0.470	0.604	0.762	0.968	1.306	1.758	2.089
1890	0.000	0.044	0.193	0.287	0.407	0.542	0.710	0.979	1.350	1.641
1885	0.000	0.000	0.000	0.000	0.142	0.212	0.304	0.467	0.733	0.994
1879	0.000	0.040	0.174	0.249	0.340	0.434	0.543	0.717	0.965	1.179
1874	0.000	0.000	0.000	0.000	0.000	0.000	0.000	0.000	0.000	0.000
1868	0.000	0.092	0.363	0.423	0.463	0.508	0.582	0.736	0.956	1.123
1862	0.000	0.036	0.159	0.238	0.351	0.495	0.686	0.977	1.337	1.578
1857	0.000	0.000	0.065	0.170	0.253	0.345	0.456	0.635	0.893	1.115
1851	0.000	0.138	0.536	0.627	0.710	0.799	0.923	1.152	1.458	1.684
1846	0.000	0.096	0.407	0.558	0.703	0.831	0.972	1.214	1.514	1.716
1840	0.000	0.039	0.172	0.259	0.367	0.482	0.612	0.808	1.050	1.225
1835	0.000	0.037	0.167	0.263	0.386	0.517	0.664	0.881	1.147	1.335
1829	0.000	0.082	0.359	0.528	0.733	0.934	1.144	1.449	1.794	1.994
1824	0.000	0.072	0.296	0.368	0.406	0.425	0.455	0.547	0.695	0.824
1818	0.000	0.000	0.000	0.000	0.161	0.245	0.340	0.487	0.694	0.874
1812	0.026	0.518	0.772	0.760	0.712	0.695	0.732	0.861	1.045	1.182

continued
Micrometer [%]

52.556	44.194	37.163	31.25	26.278	22.097	18.581	15.625	13.139	11.049
1.540	1.645	1.817	2.129	2.726	3.933	5.641	7.792	10.032	11.385
2.324	2.496	2.691	2.996	3.560	4.659	6.141	7.908	9.608	10.404
0.000	0.000	0.000	0.108	0.493	1.578	3.365	5.631	7.888	9.322
2.410	2.509	2.608	2.806	3.231	4.079	5.207	6.522	7.785	8.490
2.292	2.330	2.370	2.521	2.917	3.799	5.096	6.766	8.563	9.756
1.985	2.104	2.216	2.416	2.833	3.680	4.832	6.215	7.601	8.479
2.953	2.942	2.828	2.795	2.968	3.458	4.140	4.898	5.553	5.825
3.229	3.227	3.144	3.145	3.366	3.944	4.750	5.668	6.496	6.885
2.482	2.554	2.599	2.724	3.049	3.723	4.599	5.568	6.417	6.786
1.757	1.895	2.067	2.343	2.859	3.879	5.284	7.011	8.788	9.924
1.257	1.448	1.691	2.038	2.620	3.691	5.075	6.670	8.200	9.102
1.181	1.303	1.447	1.672	2.081	2.855	3.855	4.996	6.081	6.733
2.032	2.273	2.459	2.667	3.020	3.641	4.364	5.082	5.627	5.768
1.721	1.938	2.186	2.526	3.093	4.140	5.501	7.087	8.621	9.503
2.400	2.648	2.859	3.114	3.561	4.410	5.521	6.800	8.000	8.612
1.899	2.157	2.426	2.751	3.254	4.104	5.097	6.114	6.932	7.201
1.983	2.153	2.344	2.627	3.138	4.119	5.431	6.996	8.549	9.467
1.853	2.023	2.197	2.453	2.925	3.832	5.026	6.412	7.746	8.515
2.308	2.297	2.304	2.437	2.804	3.574	4.607	5.803	6.948	7.617
1.736	1.823	1.927	2.133	2.568	3.471	4.744	6.339	8.036	9.247
2.351	2.562	2.757	3.018	3.493	4.407	5.618	7.030	8.381	9.098
1.890	2.117	2.344	2.631	3.107	3.959	5.014	6.169	7.198	7.704
1.269	1.578	1.921	2.314	2.870	3.767	4.791	5.828	6.663	6.969
1.383	1.606	1.886	2.270	2.890	4.000	5.392	6.938	8.326	8.969
0.000	0.000	0.000	0.000	0.326	1.495	3.857	7.482	11.737	14.768
1.261	1.390	1.540	1.765	2.164	2.915	3.890	5.012	6.093	6.762
1.761	1.903	2.040	2.244	2.624	3.329	4.205	5.154	5.983	6.373
1.326	1.548	1.806	2.143	2.680	3.636	4.831	6.160	7.366	7.976
1.868	2.039	2.243	2.544	3.071	4.058	5.344	6.838	8.278	9.103
1.870	2.007	2.176	2.440	2.895	3.670	4.545	5.394	6.018	6.156
1.372	1.516	1.699	1.975	2.451	3.317	4.397	5.585	6.650	7.189
1.488	1.627	1.792	2.043	2.487	3.295	4.288	5.355	6.283	6.731
2.119	2.199	2.299	2.510	2.957	3.861	5.085	6.545	7.996	8.885
0.943	1.076	1.258	1.524	1.966	2.749	3.705	4.730	5.620	6.050
1.049	1.244	1.484	1.812	2.335	3.248	4.347	5.512	6.506	6.950
1.293	1.405	1.564	1.827	2.308	3.242	4.497	6.000	7.522	8.542

continued

Micrometer [%]

9.291	7.813	6.57	5.524	4.645	3.906	3.285	2.762	2.323	1.953	1.642
10.954	9.575	7.574	5.503	3.858	2.618	1.628	1.058	0.646	0.345	0.129
9.725	8.310	6.449	4.640	3.245	2.209	1.387	0.910	0.560	0.300	0.112
9.374	8.826	7.807	6.569	5.491	4.592	3.728	3.052	2.375	1.682	1.088
8.261	7.534	6.433	5.238	4.210	3.348	2.536	1.949	1.417	0.928	0.547
9.570	8.598	7.061	5.384	3.987	2.885	1.949	1.361	0.893	0.512	0.249
8.388	7.762	6.720	5.521	4.448	3.521	2.618	1.959	1.376	0.864	0.487
5.605	5.144	4.505	3.861	3.329	2.893	2.468	2.117	1.732	1.298	0.889
6.649	6.084	5.271	4.415	3.679	3.049	2.424	1.936	1.465	1.006	0.632
6.504	5.898	5.053	4.184	3.456	2.850	2.270	1.831	1.407	0.986	0.631
9.752	8.863	7.442	5.863	4.513	3.411	2.426	1.768	1.216	0.745	0.401
8.949	8.253	7.141	5.886	4.778	3.826	2.900	2.216	1.599	1.043	0.621
6.687	6.292	5.629	4.878	4.223	3.668	3.117	2.657	2.157	1.601	1.085
5.503	5.064	4.501	3.973	3.567	3.256	2.955	2.666	2.290	1.806	1.310
9.261	8.425	7.145	5.743	4.535	3.526	2.587	1.930	1.362	0.864	0.495
8.290	7.477	6.305	5.076	4.044	3.197	2.418	1.866	1.368	0.903	0.533
6.839	6.187	5.324	4.466	3.758	3.169	2.588	2.121	1.648	1.166	0.756
9.223	8.354	7.027	5.585	4.360	3.357	2.449	1.827	1.289	0.814	0.455
8.332	7.647	6.579	5.395	4.357	3.470	2.611	1.979	1.412	0.904	0.522
7.491	6.943	6.064	5.077	4.200	3.436	2.674	2.091	1.545	1.036	0.635
9.311	8.714	7.589	6.222	4.977	3.903	2.877	2.147	1.510	0.952	0.539
8.767	7.885	6.605	5.254	4.119	3.191	2.348	1.765	1.258	0.804	0.458
7.475	6.878	6.002	5.068	4.261	3.570	2.877	2.325	1.780	1.241	0.794
6.677	6.122	5.375	4.631	4.023	3.525	3.028	2.599	2.119	1.581	1.083
8.546	7.607	6.304	4.960	3.846	2.940	2.123	1.569	1.102	0.702	0.407
14.685	13.079	10.437	7.528	5.251	3.591	2.305	1.563	1.001	0.558	0.260
6.731	6.339	5.665	4.892	4.209	3.623	3.035	2.551	2.040	1.489	0.992
6.177	5.700	5.012	4.297	3.698	3.201	2.714	2.312	1.879	1.399	0.955
7.716	7.027	6.022	4.953	4.044	3.286	2.564	2.029	1.528	1.048	0.655
8.876	8.091	6.887	5.568	4.430	3.476	2.584	1.952	1.396	0.900	0.524
5.819	5.282	4.605	3.964	3.459	3.056	2.661	2.317	1.924	1.469	1.038
6.987	6.427	5.602	4.724	3.981	3.362	2.763	2.292	1.814	1.314	0.870
6.552	6.079	5.388	4.660	4.045	3.528	3.001	2.549	2.056	1.516	1.028
8.736	8.022	6.876	5.589	4.462	3.509	2.610	1.971	1.407	0.905	0.526
5.894	5.480	4.881	4.266	3.765	3.360	2.945	2.548	2.060	1.479	0.936
6.705	6.150	5.371	4.570	3.909	3.370	2.854	2.435	1.987	1.491	1.027
8.565	8.046	7.095	5.952	4.909	3.995	3.086	2.396	1.756	1.163	0.700

continued
Micrometer [%]

1.381	1.161	0.977	0.821	0.691	0.581	0.488	0.411	0.345	0.29	0.244
0.000	0.000	0.000	0.000	0.000	0.000	0.000	0.000	0.000	0.000	0.000
0.000	0.000	0.000	0.000	0.000	0.000	0.000	0.000	0.000	0.000	0.000
0.721	0.499	0.387	0.387	0.485	0.738	1.334	2.149	2.951	3.121	2.308
0.328	0.202	0.115	0.000	0.000	0.124	0.201	0.250	0.270	0.229	0.113
0.076	0.000	0.000	0.000	0.000	0.000	0.000	0.000	0.000	0.000	0.000
0.285	0.174	0.008	0.000	0.088	0.207	0.405	0.726	1.131	1.391	1.195
0.613	0.435	0.336	0.326	0.390	0.572	1.035	1.771	2.726	3.452	3.144
0.409	0.278	0.212	0.209	0.256	0.374	0.628	0.927	1.154	1.098	0.746
0.412	0.278	0.206	0.195	0.235	0.352	0.671	1.219	2.009	2.756	2.714
0.218	0.044	0.000	0.000	0.000	0.000	0.000	0.000	0.000	0.000	0.000
0.385	0.253	0.189	0.186	0.233	0.352	0.622	0.964	1.256	1.248	0.878
0.743	0.523	0.404	0.391	0.470	0.692	1.256	2.148	3.299	4.155	3.756
0.959	0.730	0.617	0.644	0.809	1.186	1.973	2.896	3.600	3.422	2.300
0.292	0.179	0.008	0.000	0.000	0.122	0.207	0.269	0.301	0.264	0.132
0.316	0.189	0.009	0.000	0.000	0.000	0.000	0.000	0.000	0.000	0.000
0.504	0.352	0.279	0.284	0.363	0.565	1.047	1.726	2.424	2.625	1.985
0.256	0.053	0.000	0.000	0.000	0.000	0.000	0.000	0.000	0.000	0.000
0.312	0.195	0.116	0.051	0.156	0.240	0.463	0.814	1.243	1.496	1.261
0.405	0.273	0.208	0.207	0.258	0.386	0.664	0.999	1.262	1.214	0.830
0.314	0.188	0.009	0.000	0.000	0.119	0.200	0.257	0.286	0.250	0.126
0.264	0.153	0.007	0.000	0.000	0.000	0.000	0.000	0.000	0.000	0.000
0.525	0.366	0.289	0.292	0.366	0.543	0.911	1.330	1.624	1.502	0.988
0.757	0.554	0.454	0.470	0.598	0.904	1.584	2.454	3.226	3.252	2.304
0.245	0.154	0.007	0.000	0.079	0.188	0.389	0.779	1.426	2.210	2.445
0.077	0.000	0.000	0.000	0.000	0.000	0.000	0.000	0.000	0.000	0.000
0.670	0.467	0.357	0.344	0.414	0.612	1.120	1.937	3.011	3.847	3.528
0.660	0.471	0.369	0.363	0.441	0.656	1.199	2.061	3.176	4.012	3.636
0.420	0.279	0.204	0.194	0.234	0.354	0.688	1.274	2.141	2.997	3.005
0.314	0.194	0.112	0.000	0.000	0.129	0.214	0.271	0.295	0.252	0.125
0.749	0.567	0.483	0.513	0.661	1.001	1.736	2.643	3.401	3.344	2.312
0.585	0.406	0.310	0.299	0.360	0.535	0.987	1.726	2.718	3.532	3.300
0.715	0.522	0.430	0.450	0.579	0.891	1.593	2.509	3.343	3.405	2.425
0.314	0.193	0.112	0.000	0.000	0.129	0.214	0.273	0.298	0.256	0.127
0.587	0.372	0.253	0.222	0.250	0.363	0.705	1.392	2.641	4.520	5.771
0.717	0.517	0.410	0.406	0.495	0.735	1.335	2.272	3.461	4.313	3.858
0.436	0.285	0.210	0.202	0.244	0.356	0.602	0.900	1.139	1.105	0.766

continued
 Micrometer [%]

	0.205	0.173	0.145	0.122
	0.000	0.000	0.000	0.000
	0.000	0.000	0.000	0.000
	1.266	0.546	0.142	0.000
	0.000	0.000	0.000	0.000
	0.000	0.000	0.000	0.000
	0.746	0.366	0.109	0.000
	2.081	1.083	0.369	0.084
	0.391	0.165	0.002	0.000
	1.922	1.071	0.392	0.093
	0.000	0.000	0.000	0.000
	0.471	0.203	0.003	0.000
	2.466	1.272	0.430	0.097
	1.170	0.470	0.115	0.000
	0.000	0.000	0.000	0.000
	0.000	0.000	0.000	0.000
	1.107	0.485	0.128	0.000
	0.000	0.000	0.000	0.000
	0.775	0.375	0.110	0.000
	0.436	0.184	0.003	0.000
	0.000	0.000	0.000	0.000
	0.000	0.000	0.000	0.000
	0.502	0.206	0.003	0.000
	1.221	0.509	0.129	0.000
	1.910	1.172	0.474	0.118
	0.000	0.000	0.000	0.000
	2.347	1.227	0.421	0.096
	2.392	1.235	0.417	0.094
	2.159	1.219	0.452	0.108
	0.000	0.000	0.000	0.000
	1.200	0.491	0.121	0.000
	2.234	1.190	0.417	0.096
	1.285	0.535	0.134	0.000
	0.000	0.000	0.000	0.000
	5.237	3.788	1.850	0.625
	2.512	1.285	0.430	0.097
	0.409	0.176	0.003	0.000

Core-ID: AM07-702-2-BC

Year	Micrometer [%]										
	297.3	250	210.22	176.78	148.65	125	105.11	88.388	74.325	62.5	
2007	0.000	0.119	0.515	0.747	1.038	1.347	1.692	2.166	2.646	2.853	
2003	0.000	0.179	0.699	0.826	0.970	1.148	1.395	1.805	2.286	2.548	
1999	0.000	0.187	0.743	0.927	1.172	1.488	1.909	2.557	3.242	3.508	
1995	0.028	0.545	0.857	0.987	1.153	1.375	1.681	2.171	2.695	2.913	
1991	0.000	0.150	0.610	0.795	1.030	1.306	1.643	2.135	2.642	2.846	
1987	0.000	0.106	0.467	0.701	0.994	1.297	1.632	2.113	2.610	2.818	
1983	0.000	0.172	0.688	0.865	1.080	1.331	1.646	2.132	2.654	2.888	
1979	0.000	0.117	0.446	0.510	0.596	0.726	0.927	1.287	1.796	2.178	
1975	0.036	0.718	1.075	1.109	1.154	1.255	1.438	1.782	2.190	2.403	
1971	0.000	0.121	0.500	0.656	0.814	0.961	1.136	1.440	1.839	2.117	
1967	0.000	0.113	0.468	0.622	0.807	1.008	1.250	1.624	2.071	2.343	
1963	0.000	0.000	0.000	0.137	0.319	0.506	0.726	1.046	1.473	1.802	
1959	0.000	0.096	0.396	0.519	0.669	0.849	1.091	1.492	2.028	2.409	
1955	0.000	0.000	0.094	0.256	0.416	0.626	0.906	1.354	1.987	2.480	
1951	0.000	0.162	0.634	0.755	0.885	1.037	1.246	1.605	2.073	2.386	
1947	0.000	0.180	0.690	0.789	0.906	1.064	1.305	1.730	2.302	2.693	
1943	0.000	0.099	0.427	0.617	0.854	1.116	1.434	1.920	2.507	2.855	
1939	0.000	0.091	0.375	0.499	0.652	0.835	1.080	1.485	2.034	2.433	
1935	0.000	0.082	0.341	0.460	0.606	0.781	1.016	1.396	1.906	2.273	
1931	0.000	0.155	0.623	0.783	0.977	1.224	1.578	2.181	2.977	3.479	
1927	0.000	0.113	0.450	0.563	0.703	0.872	1.098	1.466	1.957	2.311	
1923	0.000	0.130	0.515	0.636	0.796	1.007	1.305	1.798	2.437	2.850	
1919	0.000	0.128	0.520	0.669	0.848	1.052	1.310	1.714	2.190	2.459	

continued

Micrometer [%]

52.556	44.194	37.163	31.25	26.278	22.097	18.581	15.625	13.139	11.049	9.291
2.924	2.901	2.884	3.014	3.435	4.391	5.761	7.443	9.096	9.903	9.269
2.686	2.727	2.740	2.852	3.200	3.991	5.117	6.495	7.886	8.728	8.525
3.547	3.402	3.184	3.094	3.257	3.816	4.682	5.759	6.846	7.505	7.357
2.969	2.901	2.802	2.819	3.070	3.707	4.624	5.731	6.830	7.503	7.392
2.892	2.819	2.720	2.750	3.034	3.775	4.899	6.349	7.894	8.908	8.744
2.874	2.815	2.735	2.779	3.073	3.809	4.896	6.263	7.683	8.597	8.458
2.971	2.938	2.880	2.940	3.245	3.976	5.025	6.304	7.582	8.336	8.121
2.484	2.721	2.903	3.111	3.479	4.152	4.961	5.788	6.424	6.558	6.149
2.501	2.516	2.517	2.619	2.954	3.742	4.914	6.425	8.045	9.124	8.973
2.324	2.484	2.642	2.877	3.328	4.221	5.422	6.842	8.224	8.996	8.715
2.509	2.593	2.651	2.794	3.168	4.008	5.231	6.774	8.382	9.382	9.136
2.083	2.331	2.572	2.877	3.386	4.313	5.481	6.780	7.950	8.495	8.144
2.693	2.893	3.035	3.224	3.614	4.409	5.482	6.733	7.917	8.524	8.210
2.893	3.225	3.477	3.733	4.148	4.880	5.758	6.659	7.360	7.507	7.038
2.602	2.743	2.850	3.024	3.415	4.268	5.502	7.055	8.657	9.591	9.217
2.963	3.124	3.207	3.328	3.646	4.373	5.420	6.705	7.978	8.661	8.304
3.060	3.141	3.157	3.246	3.563	4.327	5.453	6.864	8.295	9.086	8.691
2.743	2.973	3.145	3.348	3.733	4.505	5.540	6.744	7.873	8.429	8.090
2.552	2.755	2.914	3.132	3.573	4.486	5.759	7.308	8.842	9.655	9.204
3.783	3.886	3.819	3.759	3.881	4.360	5.141	6.118	7.074	7.554	7.243
2.581	2.788	2.964	3.205	3.665	4.590	5.857	7.376	8.849	9.577	9.064
3.120	3.250	3.277	3.343	3.609	4.254	5.177	6.278	7.335	7.896	7.640
2.610	2.671	2.705	2.833	3.196	4.017	5.208	6.705	8.259	9.217	8.973

continued

Micrometer [%]

7.813	6.57	5.524	4.645	3.906	3.285	2.762	2.323	1.953	1.642	1.381
7.900	6.089	4.324	2.967	1.967	1.188	0.753	0.447	0.222	0.000	0.000
7.744	6.530	5.201	4.060	3.118	2.261	1.675	1.174	0.738	0.412	0.234
6.755	5.806	4.760	3.851	3.088	2.369	1.847	1.367	0.910	0.541	0.322
6.841	5.946	4.940	4.051	3.288	2.548	1.996	1.482	0.995	0.604	0.375
7.909	6.585	5.132	3.905	2.920	2.060	1.496	1.023	0.614	0.315	0.100
7.724	6.542	5.221	4.081	3.138	2.279	1.691	1.185	0.740	0.407	0.225
7.372	6.227	4.984	3.924	3.050	2.251	1.697	1.211	0.774	0.438	0.249
5.491	4.659	3.860	3.219	2.700	2.212	1.835	1.457	1.061	0.707	0.478
8.116	6.742	5.229	3.954	2.936	2.053	1.479	1.004	0.597	0.303	0.095
7.869	6.606	5.246	4.086	3.125	2.239	1.631	1.116	0.679	0.366	0.203
8.202	6.782	5.259	3.995	2.992	2.123	1.553	1.071	0.648	0.334	0.105
7.342	6.211	5.030	4.029	3.190	2.391	1.811	1.293	0.829	0.480	0.287
7.411	6.261	5.055	4.041	3.209	2.443	1.896	1.397	0.927	0.548	0.326
6.282	5.326	4.405	3.663	3.061	2.493	2.056	1.620	1.167	0.768	0.514
8.128	6.556	4.927	3.610	2.591	1.740	1.212	0.793	0.452	0.218	0.066
7.391	6.093	4.755	3.660	2.795	2.041	1.534	1.090	0.682	0.364	0.187
7.659	6.198	4.701	3.493	2.555	1.762	1.258	0.845	0.496	0.245	0.075
7.284	6.143	4.962	3.978	3.178	2.445	1.919	1.430	0.957	0.566	0.332
8.090	6.537	4.956	3.685	2.699	1.866	1.336	0.902	0.534	0.269	0.084
6.503	5.459	4.386	3.501	2.790	2.151	1.696	1.269	0.844	0.485	0.268
7.914	6.350	4.786	3.543	2.586	1.785	1.277	0.863	0.511	0.257	0.080
6.947	5.932	4.861	3.957	3.213	2.520	2.011	1.524	1.039	0.627	0.376
8.063	6.679	5.194	3.958	2.974	2.118	1.554	1.075	0.653	0.339	0.108

continued

Micrometer [%]

1.161	0.977	0.821	0.691	0.581	0.488	0.411	0.345	0.29	0.244	0.205
0.000	0.000	0.000	0.000	0.000	0.000	0.000	0.000	0.000	0.000	0.000
0.048	0.000	0.000	0.000	0.000	0.000	0.000	0.000	0.000	0.000	0.000
0.192	0.009	0.000	0.000	0.000	0.000	0.000	0.000	0.000	0.000	0.000
0.239	0.166	0.145	0.154	0.190	0.256	0.312	0.326	0.266	0.127	0.000
0.000	0.000	0.000	0.000	0.000	0.000	0.000	0.000	0.000	0.000	0.000
0.046	0.000	0.000	0.000	0.000	0.000	0.000	0.000	0.000	0.000	0.000
0.052	0.000	0.000	0.000	0.000	0.000	0.000	0.000	0.000	0.000	0.000
0.333	0.254	0.244	0.292	0.431	0.794	1.390	2.206	2.905	2.762	1.904
0.000	0.000	0.000	0.000	0.000	0.000	0.000	0.000	0.000	0.000	0.000
0.042	0.000	0.000	0.000	0.000	0.042	0.200	0.271	0.297	0.239	0.086
0.000	0.000	0.000	0.000	0.000	0.000	0.000	0.000	0.000	0.000	0.000
0.179	0.008	0.000	0.093	0.220	0.425	0.754	1.162	1.414	1.206	0.749
0.194	0.009	0.000	0.000	0.000	0.000	0.000	0.000	0.000	0.000	0.000
0.355	0.267	0.248	0.275	0.347	0.468	0.558	0.562	0.436	0.255	0.077
0.000	0.000	0.000	0.000	0.000	0.000	0.000	0.000	0.000	0.000	0.000
0.036	0.000	0.000	0.000	0.000	0.000	0.000	0.000	0.000	0.000	0.000
0.000	0.000	0.000	0.000	0.000	0.000	0.000	0.000	0.000	0.000	0.000
0.193	0.009	0.000	0.000	0.000	0.000	0.000	0.000	0.000	0.000	0.000
0.000	0.000	0.000	0.000	0.000	0.000	0.000	0.000	0.000	0.000	0.000
0.054	0.000	0.000	0.000	0.000	0.000	0.000	0.000	0.000	0.000	0.000
0.000	0.000	0.000	0.000	0.000	0.000	0.000	0.000	0.000	0.000	0.000
0.222	0.117	0.000	0.000	0.000	0.000	0.000	0.000	0.000	0.000	0.000
0.000	0.000	0.000	0.000	0.000	0.000	0.000	0.000	0.000	0.000	0.000

continued

Micrometer [%]		
0.173	0.145	0.122
0.000	0.000	0.000
0.000	0.000	0.000
0.000	0.000	0.000
0.000	0.000	0.000
0.000	0.000	0.000
0.000	0.000	0.000
0.000	0.000	0.000
0.000	0.000	0.000
1.035	0.371	0.087
0.000	0.000	0.000
0.000	0.000	0.000
0.000	0.000	0.000
0.366	0.109	0.000
0.000	0.000	0.000
0.000	0.000	0.000
0.000	0.000	0.000
0.000	0.000	0.000
0.000	0.000	0.000
0.000	0.000	0.000
0.000	0.000	0.000
0.000	0.000	0.000
0.000	0.000	0.000
0.000	0.000	0.000
0.000	0.000	0.000
0.000	0.000	0.000
0.000	0.000	0.000
0.000	0.000	0.000
0.000	0.000	0.000
0.000	0.000	0.000
0.000	0.000	0.000

Core-ID: RA09-GW-4-P3

Year	Micrometer [%]										
	297.3	250	210.22	176.78	148.65	125	105.11	88.388	74.325	62.5	
2009	0.000	0.000	0.000	0.000	0.000	0.000	0.000	0.103	0.211	0.333	
2002	0.000	0.000	0.000	0.000	0.019	0.149	0.230	0.358	0.543	0.708	
1995	0.000	0.000	0.000	0.117	0.223	0.302	0.384	0.490	0.612	0.701	
1988	0.000	0.039	0.148	0.161	0.181	0.213	0.266	0.360	0.506	0.647	
1980	0.000	0.000	0.000	0.105	0.206	0.292	0.397	0.552	0.760	0.927	
1973	0.000	0.000	0.000	0.000	0.000	0.000	0.000	0.002	0.186	0.338	
1966	0.000	0.085	0.335	0.402	0.466	0.527	0.599	0.725	0.886	1.004	
1959	0.000	0.000	0.073	0.172	0.218	0.263	0.310	0.387	0.494	0.593	
1952	0.000	0.000	0.000	0.000	0.019	0.146	0.201	0.282	0.399	0.509	
1945	0.000	0.000	0.000	0.000	0.000	0.053	0.187	0.305	0.502	0.705	
1938	0.000	0.000	0.000	0.094	0.203	0.324	0.488	0.725	1.014	1.204	
1930	0.000	0.000	0.000	0.000	0.158	0.228	0.301	0.411	0.561	0.693	
1923	0.000	0.053	0.201	0.223	0.252	0.296	0.362	0.476	0.640	0.780	
1916	0.000	0.053	0.241	0.371	0.526	0.664	0.788	0.950	1.114	1.205	
1909	0.000	0.065	0.273	0.361	0.444	0.508	0.569	0.670	0.795	0.890	
1902	0.000	0.077	0.296	0.337	0.376	0.417	0.470	0.562	0.677	0.764	
1895	0.000	0.000	0.082	0.214	0.312	0.410	0.517	0.678	0.893	1.072	
1888	0.000	0.000	0.000	0.000	0.146	0.202	0.252	0.323	0.422	0.511	
1880	0.000	0.000	0.081	0.206	0.289	0.370	0.455	0.580	0.738	0.860	
1873	0.000	0.076	0.288	0.326	0.372	0.425	0.488	0.588	0.707	0.791	
1866	0.000	0.000	0.000	0.000	0.000	0.070	0.246	0.385	0.573	0.734	
1859	0.000	0.088	0.353	0.432	0.498	0.541	0.580	0.651	0.733	0.789	
1852	0.000	0.125	0.522	0.702	0.886	1.041	1.185	1.396	1.591	1.665	
1845	0.000	0.000	0.000	0.000	0.025	0.199	0.295	0.427	0.607	0.760	
1838	0.000	0.000	0.000	0.000	0.000	0.000	0.000	0.155	0.336	0.510	
1831	0.000	0.000	0.000	0.000	0.000	0.000	0.000	0.000	0.000	0.000	
1823	0.000	0.000	0.000	0.000	0.000	0.050	0.185	0.324	0.560	0.805	
1816	0.000	0.000	0.000	0.111	0.199	0.257	0.327	0.433	0.582	0.715	
1809	0.000	0.056	0.229	0.291	0.342	0.378	0.419	0.501	0.621	0.727	
1802	0.000	0.000	0.000	0.000	0.000	0.000	0.088	0.210	0.339	0.471	
1795	0.000	0.000	0.000	0.000	0.000	0.000	0.095	0.225	0.358	0.492	
1788	0.000	0.097	0.377	0.443	0.508	0.570	0.643	0.767	0.911	1.003	
1781	0.000	0.000	0.000	0.000	0.020	0.161	0.246	0.379	0.572	0.748	
1773	0.000	0.000	0.000	0.000	0.000	0.000	0.078	0.178	0.272	0.373	
1766	0.000	0.000	0.082	0.210	0.297	0.380	0.468	0.599	0.768	0.900	
1759	0.000	0.000	0.000	0.000	0.124	0.162	0.215	0.320	0.509	0.714	
1752	0.028	0.546	0.820	0.796	0.679	0.572	0.516	0.536	0.606	0.685	
1745	0.000	0.000	0.000	0.000	0.000	0.000	0.093	0.225	0.373	0.534	
1738	0.000	0.000	0.000	0.093	0.175	0.240	0.325	0.462	0.655	0.819	
1731	0.000	0.000	0.000	0.000	0.000	0.000	0.093	0.229	0.380	0.534	
1723	0.000	0.000	0.064	0.167	0.246	0.330	0.427	0.572	0.761	0.912	

continued

Micrometer [%]

52.556	44.194	37.163	31.25	26.278	22.097	18.581	15.625	13.139	11.049	9.291
0.500	0.748	1.104	1.565	2.231	3.364	4.752	6.290	7.714	8.538	8.438
0.872	1.053	1.272	1.576	2.093	3.100	4.498	6.246	8.113	9.490	9.673
0.781	0.875	1.027	1.296	1.818	2.969	4.787	7.364	10.456	12.900	13.031
0.795	0.974	1.215	1.560	2.141	3.283	4.895	6.946	9.162	10.771	10.875
1.081	1.242	1.447	1.749	2.278	3.305	4.711	6.432	8.211	9.424	9.445
0.561	0.897	1.347	1.871	2.554	3.603	4.771	5.949	6.912	7.313	7.060
1.101	1.205	1.362	1.631	2.139	3.195	4.746	6.796	9.104	10.865	11.027
0.694	0.823	1.017	1.323	1.862	2.951	4.513	6.527	8.734	10.383	10.568
0.625	0.767	0.966	1.264	1.783	2.844	4.401	6.470	8.836	10.748	11.139
0.929	1.195	1.514	1.907	2.493	3.500	4.727	6.063	7.265	7.910	7.764
1.350	1.469	1.605	1.844	2.327	3.337	4.788	6.633	8.614	10.027	10.075
0.825	0.980	1.194	1.516	2.072	3.159	4.665	6.537	8.518	9.944	10.080
0.913	1.064	1.266	1.565	2.084	3.104	4.531	6.332	8.280	9.742	9.953
1.264	1.321	1.433	1.669	2.148	3.159	4.640	6.586	8.764	10.427	10.607
0.973	1.072	1.236	1.518	2.040	3.096	4.604	6.538	8.654	10.241	10.428
0.839	0.927	1.072	1.327	1.817	2.862	4.442	6.590	9.091	11.112	11.449
1.240	1.421	1.649	1.961	2.456	3.305	4.319	5.387	6.296	6.704	6.480
0.602	0.718	0.895	1.177	1.687	2.765	4.405	6.661	9.323	11.517	11.927
0.970	1.095	1.274	1.562	2.078	3.100	4.531	6.332	8.265	9.698	9.884
0.864	0.947	1.085	1.333	1.811	2.838	4.402	6.547	9.069	11.131	11.493
0.893	1.071	1.296	1.621	2.182	3.282	4.808	6.703	8.690	10.067	10.100
0.835	0.896	1.017	1.252	1.717	2.723	4.257	6.360	8.831	10.872	11.282
1.683	1.678	1.719	1.883	2.268	3.073	4.188	5.552	6.965	7.966	8.067
0.906	1.065	1.268	1.571	2.118	3.264	4.986	7.315	9.983	11.994	12.062
0.718	0.974	1.285	1.679	2.293	3.437	4.972	6.826	8.711	9.955	9.919
0.000	0.160	0.489	1.051	1.901	3.274	4.769	6.189	7.249	7.583	7.210
1.082	1.414	1.805	2.271	2.933	3.998	5.197	6.389	7.321	7.631	7.272
0.847	1.003	1.219	1.542	2.096	3.178	4.676	6.545	8.531	9.971	10.117
0.830	0.958	1.149	1.448	1.974	3.013	4.477	6.335	8.354	9.877	10.103
0.621	0.810	1.060	1.410	1.990	3.122	4.720	6.765	9.001	10.686	10.904
0.642	0.827	1.069	1.404	1.954	3.015	4.486	6.328	8.305	9.783	10.014
1.072	1.143	1.266	1.497	1.949	2.884	4.232	5.978	7.923	9.460	9.772
0.927	1.130	1.379	1.718	2.268	3.290	4.633	6.217	7.788	8.802	8.785
0.490	0.646	0.866	1.187	1.728	2.807	4.352	6.351	8.565	10.297	10.634
1.020	1.152	1.341	1.638	2.173	3.238	4.745	6.667	8.759	10.315	10.477
0.945	1.230	1.573	1.984	2.571	3.545	4.695	5.907	6.955	7.469	7.290
0.766	0.877	1.060	1.350	1.847	2.796	4.075	5.624	7.227	8.376	8.538
0.723	0.962	1.263	1.641	2.200	3.163	4.346	5.648	6.833	7.478	7.336
0.974	1.140	1.341	1.617	2.074	2.918	4.025	5.333	6.649	7.559	7.666
0.705	0.911	1.165	1.503	2.054	3.115	4.579	6.398	8.317	9.689	9.805
1.049	1.193	1.378	1.653	2.130	3.045	4.274	5.755	7.276	8.350	8.479

continued

Micrometer [%]

7.813	6.57	5.524	4.645	3.906	3.285	2.762	2.323	1.953	1.642	1.381
7.890	6.995	5.976	5.076	4.295	3.503	2.861	2.217	1.569	1.023	0.692
9.182	8.137	6.786	5.510	4.373	3.246	2.420	1.696	1.069	0.613	0.369
11.774	9.504	6.881	4.713	3.073	1.794	1.095	0.622	0.305	0.105	0.000
10.127	8.701	6.951	5.369	4.023	2.779	1.948	1.280	0.748	0.392	0.215
8.810	7.656	6.264	4.997	3.896	2.834	2.078	1.430	0.883	0.493	0.289
6.525	5.784	5.033	4.421	3.923	3.427	2.987	2.475	1.877	1.305	0.922
10.247	8.727	6.865	5.207	3.834	2.614	1.825	1.199	0.698	0.359	0.188
9.916	8.588	6.908	5.363	4.033	2.789	1.952	1.278	0.745	0.391	0.217
10.624	9.355	7.638	6.015	4.602	3.268	2.352	1.592	0.962	0.522	0.294
7.239	6.425	5.528	4.746	4.072	3.383	2.810	2.218	1.603	1.072	0.743
9.346	8.002	6.374	4.905	3.652	2.493	1.724	1.114	0.640	0.331	0.181
9.504	8.354	6.911	5.581	4.423	3.303	2.496	1.785	1.155	0.682	0.419
9.449	8.360	6.954	5.637	4.480	3.354	2.536	1.811	1.166	0.681	0.412
9.916	8.533	6.814	5.262	3.957	2.770	1.981	1.334	0.800	0.426	0.232
9.812	8.546	6.944	5.472	4.204	3.012	2.190	1.501	0.923	0.512	0.296
10.771	9.274	7.343	5.588	4.119	2.804	1.954	1.280	0.743	0.381	0.200
5.966	5.240	4.495	3.881	3.380	2.897	2.498	2.058	1.557	1.080	0.757
11.257	9.711	7.686	5.839	4.296	2.921	2.033	1.329	0.767	0.388	0.199
9.366	8.275	6.878	5.576	4.435	3.326	2.520	1.805	1.168	0.687	0.419
10.821	9.310	7.355	5.578	4.094	2.774	1.924	1.253	0.722	0.364	0.187
9.394	8.104	6.545	5.134	3.922	2.777	1.988	1.335	0.801	0.434	0.247
10.699	9.299	7.439	5.720	4.262	2.939	2.070	1.371	0.806	0.420	0.224
7.661	6.842	5.813	4.849	3.985	3.103	2.420	1.781	1.185	0.720	0.455
11.000	9.102	6.887	5.006	3.522	2.283	1.534	0.965	0.530	0.248	0.075
9.201	7.950	6.471	5.142	3.999	2.906	2.133	1.471	0.909	0.507	0.296
6.579	5.768	4.981	4.368	3.891	3.439	3.040	2.564	1.990	1.424	1.035
6.630	5.785	4.950	4.273	3.720	3.176	2.719	2.221	1.671	1.167	0.837
9.542	8.384	6.927	5.581	4.409	3.278	2.466	1.754	1.128	0.660	0.402
9.590	8.473	7.026	5.674	4.491	3.346	2.520	1.793	1.150	0.668	0.402
10.288	8.997	7.347	5.826	4.514	3.275	2.410	1.673	1.041	0.582	0.336
9.550	8.517	7.164	5.890	4.765	3.654	2.826	2.068	1.370	0.826	0.514
9.362	8.346	6.971	5.656	4.485	3.337	2.505	1.774	1.133	0.657	0.395
8.227	7.245	6.080	5.025	4.102	3.180	2.475	1.816	1.203	0.724	0.452
10.173	9.050	7.531	6.088	4.814	3.576	2.684	1.902	1.216	0.706	0.426
9.840	8.560	6.957	5.489	4.228	3.043	2.223	1.529	0.942	0.521	0.297
6.789	6.047	5.258	4.589	4.024	3.447	2.948	2.400	1.794	1.243	0.886
8.163	7.346	6.291	5.297	4.404	3.487	2.763	2.069	1.406	0.876	0.568
6.818	6.018	5.145	4.398	3.774	3.163	2.669	2.149	1.584	1.068	0.730
7.349	6.691	5.863	5.092	4.402	3.671	3.045	2.384	1.691	1.091	0.720
9.228	8.092	6.669	5.353	4.199	3.075	2.267	1.570	0.973	0.546	0.321
8.097	7.298	6.280	5.324	4.463	3.573	2.858	2.159	1.480	0.927	0.602

continued

Micrometer [%]

1.161	0.977	0.821	0.691	0.581	0.488	0.411	0.345	0.29	0.244	0.205
0.496	0.404	0.420	0.534	0.793	1.310	1.861	2.193	1.941	1.222	0.599
0.236	0.173	0.169	0.211	0.322	0.578	0.913	1.211	1.227	0.877	0.477
0.000	0.000	0.000	0.000	0.000	0.000	0.000	0.000	0.000	0.000	0.000
0.044	0.000	0.000	0.000	0.006	0.209	0.339	0.478	0.530	0.422	0.255
0.179	0.008	0.049	0.152	0.242	0.483	0.872	1.357	1.654	1.403	0.864
0.679	0.556	0.568	0.705	1.031	1.722	2.550	3.211	3.108	2.136	1.113
0.037	0.000	0.000	0.000	0.000	0.000	0.000	0.000	0.000	0.000	0.000
0.045	0.000	0.000	0.000	0.137	0.325	0.615	1.011	1.314	1.186	0.769
0.172	0.008	0.000	0.000	0.108	0.185	0.245	0.280	0.251	0.129	0.000
0.545	0.455	0.480	0.614	0.908	1.480	2.065	2.388	2.069	1.278	0.616
0.037	0.000	0.000	0.000	0.110	0.264	0.508	0.851	1.133	1.047	0.693
0.271	0.195	0.182	0.209	0.280	0.413	0.534	0.582	0.485	0.300	0.093
0.260	0.182	0.164	0.183	0.240	0.347	0.445	0.483	0.406	0.254	0.080
0.047	0.000	0.000	0.000	0.000	0.000	0.000	0.000	0.000	0.000	0.000
0.178	0.008	0.000	0.000	0.122	0.209	0.274	0.309	0.272	0.181	0.059
0.040	0.000	0.000	0.000	0.000	0.000	0.000	0.000	0.000	0.000	0.000
0.546	0.431	0.422	0.508	0.738	1.305	2.170	3.240	3.973	3.520	2.286
0.039	0.000	0.000	0.000	0.000	0.000	0.000	0.000	0.000	0.000	0.000
0.266	0.188	0.171	0.192	0.252	0.365	0.468	0.507	0.423	0.264	0.082
0.037	0.000	0.000	0.000	0.000	0.000	0.000	0.000	0.000	0.000	0.000
0.148	0.007	0.000	0.078	0.187	0.380	0.701	1.123	1.418	1.248	0.793
0.045	0.000	0.000	0.000	0.000	0.000	0.000	0.000	0.000	0.000	0.000
0.303	0.228	0.224	0.276	0.406	0.686	1.016	1.266	1.202	0.815	0.426
0.000	0.000	0.000	0.000	0.000	0.000	0.000	0.000	0.000	0.000	0.000
0.182	0.008	0.000	0.097	0.232	0.455	0.815	1.263	1.541	1.315	0.817
0.784	0.663	0.692	0.869	1.272	2.102	3.061	3.779	3.573	2.401	1.227
0.632	0.538	0.567	0.714	1.027	1.604	2.149	2.391	1.999	1.201	0.570
0.256	0.182	0.166	0.188	0.247	0.360	0.461	0.500	0.418	0.261	0.081
0.251	0.174	0.155	0.170	0.220	0.314	0.400	0.434	0.365	0.231	0.073
0.200	0.112	0.000	0.000	0.120	0.197	0.251	0.276	0.239	0.120	0.000
0.334	0.240	0.220	0.247	0.321	0.455	0.569	0.601	0.487	0.296	0.091
0.249	0.174	0.156	0.174	0.227	0.328	0.420	0.455	0.382	0.240	0.075
0.296	0.219	0.213	0.265	0.407	0.758	1.270	1.828	2.049	1.613	0.937
0.268	0.187	0.168	0.186	0.241	0.344	0.436	0.469	0.391	0.244	0.077
0.175	0.008	0.000	0.000	0.005	0.170	0.218	0.243	0.214	0.109	0.000
0.665	0.564	0.595	0.751	1.083	1.696	2.276	2.532	2.112	1.264	0.596
0.389	0.302	0.303	0.377	0.556	0.926	1.343	1.629	1.497	0.982	0.499
0.514	0.396	0.383	0.457	0.665	1.183	1.989	3.012	3.757	3.393	2.243
0.496	0.382	0.378	0.464	0.689	1.199	1.866	2.484	2.555	1.858	1.013
0.199	0.140	0.133	0.165	0.260	0.510	0.909	1.396	1.684	1.418	0.869
0.411	0.317	0.315	0.386	0.561	0.920	1.318	1.583	1.445	0.944	0.480

continued

Micrometer [%]

0.173	0.145	0.122
0.237	0.003	0.000
0.208	0.003	0.000
0.000	0.000	0.000
0.046	0.000	0.000
0.418	0.123	0.000
0.461	0.117	0.000
0.000	0.000	0.000
0.392	0.121	0.000
0.000	0.000	0.000
0.240	0.003	0.000
0.360	0.113	0.000
0.000	0.000	0.000
0.000	0.000	0.000
0.000	0.000	0.000
0.000	0.000	0.000
0.000	0.000	0.000
1.172	0.396	0.090
0.000	0.000	0.000
0.000	0.000	0.000
0.000	0.000	0.000
0.396	0.120	0.000
0.000	0.000	0.000
0.180	0.003	0.000
0.000	0.000	0.000
0.400	0.119	0.000
0.498	0.124	0.000
0.219	0.003	0.000
0.000	0.000	0.000
0.000	0.000	0.000
0.000	0.000	0.000
0.000	0.000	0.000
0.000	0.000	0.000
0.430	0.120	0.000
0.000	0.000	0.000
0.000	0.000	0.000
0.228	0.003	0.000
0.205	0.003	0.000
1.173	0.406	0.094
0.438	0.116	0.000
0.420	0.123	0.000
0.198	0.003	0.000

Core-ID: RA09-GW-5-P2

Micrometer [%]

Year	297.3	250	210.22	176.78	148.65	125	105.11	88.388	74.325	62.5
2009	0.000	0.040	0.170	0.226	0.263	0.282	0.301	0.346	0.418	0.488
1998	0.000	0.000	0.000	0.000	0.000	0.000	0.000	0.002	0.152	0.230
1987	0.000	0.000	0.000	0.000	0.000	0.000	0.000	0.000	0.000	0.091
1976	0.000	0.000	0.000	0.000	0.000	0.000	0.000	0.000	0.000	0.079
1965	0.000	0.000	0.000	0.000	0.000	0.000	0.000	0.000	0.000	0.082
1954	0.000	0.000	0.000	0.000	0.000	0.000	0.000	0.000	0.031	0.167
1942	0.000	0.000	0.000	0.000	0.000	0.000	0.000	0.000	0.000	0.088
1931	0.000	0.000	0.000	0.000	0.000	0.000	0.000	0.000	0.041	0.213
1920	0.000	0.000	0.000	0.000	0.000	0.000	0.000	0.002	0.204	0.311
1909	0.000	0.000	0.000	0.000	0.000	0.000	0.000	0.000	0.032	0.169
1898	0.000	0.000	0.000	0.000	0.000	0.000	0.000	0.002	0.151	0.232
1887	0.000	0.000	0.000	0.000	0.000	0.053	0.178	0.269	0.407	0.544
1876	0.000	0.000	0.000	0.000	0.000	0.000	0.000	0.000	0.000	0.000
1865	0.000	0.000	0.000	0.000	0.000	0.000	0.000	0.000	0.038	0.216
1854	0.000	0.000	0.000	0.000	0.000	0.000	0.000	0.104	0.229	0.362
1843	0.000	0.000	0.000	0.000	0.000	0.000	0.000	0.000	0.033	0.177
1831	0.000	0.000	0.079	0.185	0.221	0.244	0.267	0.316	0.396	0.481
1820	0.000	0.000	0.000	0.000	0.000	0.000	0.000	0.002	0.175	0.247
1809	0.000	0.000	0.000	0.000	0.000	0.000	0.000	0.000	0.000	0.082
1798	0.000	0.000	0.000	0.000	0.000	0.000	0.000	0.000	0.000	0.000
1787	0.000	0.000	0.000	0.000	0.000	0.000	0.000	0.000	0.035	0.185
1776	0.000	0.000	0.000	0.000	0.000	0.000	0.000	0.129	0.228	0.310
1765	0.000	0.000	0.000	0.000	0.000	0.000	0.000	0.000	0.044	0.232
1754	0.000	0.000	0.000	0.000	0.000	0.000	0.000	0.000	0.035	0.184
1743	0.000	0.000	0.000	0.000	0.000	0.000	0.000	0.000	0.030	0.162
1732	0.000	0.000	0.000	0.000	0.000	0.000	0.000	0.000	0.030	0.162
1720	0.000	0.000	0.000	0.000	0.000	0.000	0.000	0.141	0.318	0.494
1709	0.000	0.000	0.000	0.000	0.021	0.154	0.195	0.264	0.371	0.479
1698	0.000	0.000	0.000	0.000	0.000	0.048	0.153	0.215	0.315	0.419
1687	0.000	0.039	0.162	0.218	0.275	0.325	0.376	0.458	0.569	0.665
1676	0.000	0.000	0.000	0.000	0.000	0.000	0.000	0.000	0.035	0.189
1665	0.000	0.059	0.216	0.220	0.217	0.219	0.232	0.271	0.336	0.405
1654	0.000	0.000	0.000	0.000	0.022	0.171	0.236	0.336	0.482	0.616
1643	0.000	0.053	0.193	0.193	0.184	0.181	0.194	0.237	0.317	0.407
1632	0.000	0.000	0.000	0.000	0.000	0.000	0.079	0.167	0.236	0.314
1621	0.000	0.000	0.000	0.000	0.000	0.000	0.000	0.002	0.196	0.288
1609	0.000	0.000	0.000	0.000	0.000	0.000	0.000	0.000	0.047	0.252
1598	0.000	0.000	0.000	0.000	0.000	0.000	0.076	0.187	0.310	0.440
1587	0.000	0.000	0.000	0.000	0.000	0.065	0.235	0.397	0.646	0.874

continued

Micrometer [%]

52.556	44.194	37.163	31.25	26.278	22.097	18.581	15.625	13.139	11.049	9.291
0.562	0.664	0.831	1.104	1.593	2.587	4.019	5.864	7.890	9.450	9.738
0.334	0.492	0.736	1.090	1.666	2.768	4.275	6.117	8.012	9.302	9.344
0.279	0.474	0.773	1.188	1.839	3.066	4.725	6.738	8.800	10.202	10.258
0.222	0.337	0.522	0.806	1.292	2.284	3.725	5.596	7.659	9.250	9.544
0.256	0.445	0.738	1.155	1.814	3.064	4.771	6.868	9.054	10.588	10.700
0.277	0.459	0.743	1.136	1.724	2.737	3.967	5.300	6.501	7.180	7.123
0.269	0.462	0.770	1.214	1.918	3.251	5.060	7.263	9.520	11.031	11.025
0.322	0.483	0.715	1.048	1.600	2.705	4.301	6.383	8.711	10.552	10.930
0.446	0.634	0.896	1.255	1.823	2.883	4.291	5.973	7.672	8.842	8.957
0.271	0.432	0.681	1.041	1.631	2.790	4.427	6.502	8.729	10.358	10.540
0.338	0.495	0.730	1.075	1.649	2.793	4.425	6.520	8.812	10.558	10.844
0.694	0.881	1.131	1.483	2.063	3.178	4.715	6.626	8.651	10.117	10.267
0.127	0.305	0.547	0.925	1.559	2.829	4.637	6.935	9.400	11.189	11.366
0.382	0.651	1.045	1.566	2.336	3.692	5.404	7.344	9.158	10.154	9.877
0.532	0.764	1.071	1.474	2.098	3.267	4.856	6.820	8.887	10.363	10.482
0.277	0.426	0.646	0.967	1.511	2.647	4.375	6.748	9.538	11.830	12.271
0.578	0.715	0.935	1.279	1.873	3.048	4.693	6.748	8.911	10.417	10.467
0.335	0.462	0.656	0.956	1.485	2.612	4.349	6.757	9.611	11.966	12.414
0.249	0.422	0.691	1.080	1.709	2.926	4.611	6.698	8.879	10.395	10.475
0.113	0.258	0.445	0.750	1.297	2.488	4.344	6.919	9.948	12.393	12.795
0.295	0.471	0.747	1.148	1.790	3.001	4.618	6.546	8.475	9.749	9.781
0.406	0.539	0.741	1.051	1.597	2.742	4.473	6.824	9.551	11.739	12.107
0.355	0.538	0.808	1.188	1.799	2.972	4.585	6.572	8.640	10.077	10.160
0.287	0.440	0.665	0.991	1.539	2.677	4.403	6.773	9.567	11.864	12.298
0.273	0.447	0.703	1.059	1.625	2.710	4.209	6.081	8.077	9.573	9.838
0.266	0.429	0.675	1.025	1.591	2.700	4.271	6.286	8.502	10.228	10.578
0.704	0.961	1.266	1.643	2.223	3.284	4.686	6.357	8.047	9.193	9.252
0.599	0.753	0.972	1.291	1.830	2.881	4.347	6.192	8.178	9.676	9.936
0.538	0.698	0.929	1.269	1.839	2.946	4.471	6.353	8.321	9.723	9.868
0.757	0.873	1.053	1.347	1.885	2.999	4.650	6.853	9.361	11.314	11.556
0.306	0.501	0.809	1.241	1.878	2.936	4.151	5.383	6.386	6.822	6.619
0.481	0.588	0.762	1.044	1.553	2.614	4.201	6.333	8.793	10.807	11.254
0.756	0.924	1.152	1.483	2.041	3.111	4.559	6.312	8.106	9.339	9.419
0.511	0.659	0.886	1.227	1.800	2.903	4.409	6.238	8.099	9.325	9.305
0.408	0.541	0.746	1.059	1.594	2.661	4.175	6.100	8.188	9.776	10.069
0.403	0.562	0.788	1.111	1.650	2.728	4.287	6.330	8.630	10.470	10.866
0.401	0.621	0.928	1.336	1.963	3.123	4.667	6.519	8.401	9.682	9.753
0.591	0.787	1.051	1.423	2.037	3.243	4.960	7.176	9.607	11.398	11.524
1.107	1.355	1.629	1.972	2.522	3.551	4.923	6.568	8.228	9.310	9.264

continued

Micrometer [%]

7.813	6.57	5.524	4.645	3.906	3.285	2.762	2.323	1.953	1.642	1.381
9.304	8.268	6.875	5.545	4.358	3.190	2.347	1.621	1.005	0.567	0.337
8.729	7.597	6.227	4.994	3.939	2.937	2.223	1.596	1.040	0.618	0.381
9.604	8.383	6.885	5.514	4.320	3.164	2.337	1.628	1.025	0.593	0.363
9.115	8.088	6.707	5.404	4.262	3.160	2.371	1.685	1.084	0.636	0.388
10.052	8.798	7.237	5.810	4.577	3.394	2.551	1.815	1.172	0.693	0.428
6.733	6.093	5.373	4.756	4.237	3.703	3.219	2.657	2.007	1.395	0.990
10.224	8.805	7.113	5.605	4.328	3.136	2.311	1.613	1.019	0.588	0.355
10.467	9.302	7.705	6.181	4.835	3.533	2.610	1.820	1.145	0.657	0.395
8.525	7.649	6.541	5.504	4.577	3.625	2.873	2.156	1.473	0.929	0.613
9.930	8.678	7.080	5.603	4.317	3.089	2.230	1.512	0.919	0.507	0.294
10.316	9.119	7.539	6.060	4.768	3.525	2.639	1.868	1.195	0.696	0.422
9.688	8.523	7.054	5.697	4.516	3.375	2.552	1.825	1.180	0.695	0.425
10.671	9.282	7.538	5.954	4.604	3.341	2.466	1.723	1.086	0.622	0.370
8.981	7.627	6.141	4.861	3.787	2.776	2.061	1.444	0.912	0.525	0.316
9.858	8.639	7.123	5.735	4.534	3.383	2.555	1.826	1.177	0.688	0.416
11.612	10.057	7.996	6.107	4.522	3.100	2.175	1.435	0.840	0.434	0.228
9.725	8.359	6.703	5.211	3.938	2.751	1.946	1.292	0.768	0.414	0.236
11.720	10.099	7.965	6.022	4.405	2.972	2.056	1.336	0.769	0.389	0.201
9.792	8.502	6.915	5.471	4.226	3.041	2.212	1.512	0.928	0.518	0.303
12.005	10.263	8.020	6.011	4.360	2.919	2.009	1.302	0.747	0.378	0.196
9.179	8.075	6.733	5.511	4.444	3.391	2.606	1.893	1.249	0.758	0.483
11.404	9.838	7.808	5.963	4.419	3.037	2.136	1.415	0.833	0.434	0.231
9.521	8.306	6.807	5.438	4.250	3.106	2.290	1.589	0.991	0.562	0.335
11.620	10.040	7.959	6.061	4.476	3.063	2.146	1.412	0.821	0.418	0.216
9.432	8.468	7.167	5.922	4.800	3.666	2.807	2.026	1.322	0.790	0.494
10.155	9.090	7.632	6.242	5.010	3.799	2.906	2.103	1.375	0.817	0.502
8.735	7.754	6.545	5.428	4.438	3.440	2.675	1.964	1.306	0.794	0.503
9.508	8.513	7.194	5.947	4.843	3.748	2.924	2.161	1.448	0.884	0.557
9.334	8.248	6.870	5.585	4.450	3.330	2.507	1.780	1.143	0.673	0.417
10.794	9.236	7.283	5.530	4.073	2.775	1.937	1.272	0.742	0.382	0.202
6.158	5.514	4.862	4.344	3.939	3.546	3.178	2.716	2.135	1.550	1.142
10.770	9.506	7.765	6.112	4.672	3.315	2.385	1.615	0.979	0.534	0.304
8.882	7.849	6.570	5.388	4.344	3.305	2.528	1.825	1.193	0.715	0.449
8.633	7.456	6.069	4.838	3.797	2.819	2.130	1.529	0.996	0.591	0.363
9.642	8.618	7.236	5.918	4.740	3.568	2.698	1.923	1.237	0.726	0.446
10.427	9.289	7.721	6.223	4.902	3.623	2.707	1.907	1.209	0.692	0.409
9.189	8.117	6.791	5.570	4.494	3.426	2.627	1.901	1.245	0.747	0.468
10.711	9.167	7.286	5.613	4.221	2.966	2.132	1.446	0.874	0.468	0.255
8.607	7.470	6.130	4.919	3.867	2.845	2.108	1.468	0.918	0.521	0.309

continued

Micrometer [%]

1.161	0.977	0.821	0.691	0.581	0.488	0.411	0.345	0.29	0.244	0.205
0.213	0.154	0.151	0.194	0.312	0.621	1.110	1.698	2.019	1.667	1.001
0.246	0.177	0.167	0.204	0.316	0.632	1.203	2.074	2.980	3.060	2.242
0.238	0.181	0.184	0.238	0.375	0.689	1.096	1.456	1.464	1.035	0.554
0.248	0.177	0.168	0.205	0.320	0.646	1.240	2.152	3.108	3.198	2.343
0.279	0.205	0.195	0.228	0.311	0.465	0.605	0.659	0.548	0.337	0.104
0.735	0.614	0.641	0.814	1.215	2.068	3.097	3.920	3.792	2.587	1.332
0.226	0.161	0.149	0.171	0.231	0.345	0.454	0.504	0.431	0.273	0.086
0.250	0.178	0.165	0.189	0.256	0.384	0.504	0.557	0.472	0.296	0.093
0.431	0.347	0.361	0.464	0.702	1.191	1.737	2.102	1.912	1.233	0.615
0.181	0.008	0.050	0.155	0.250	0.502	0.914	1.430	1.753	1.494	0.923
0.268	0.189	0.172	0.194	0.255	0.370	0.475	0.516	0.432	0.270	0.085
0.271	0.192	0.175	0.197	0.258	0.371	0.472	0.509	0.423	0.263	0.082
0.229	0.157	0.139	0.152	0.196	0.281	0.359	0.393	0.335	0.215	0.068
0.201	0.146	0.142	0.180	0.285	0.558	0.986	1.498	1.780	1.479	0.897
0.261	0.180	0.159	0.174	0.221	0.311	0.391	0.420	0.350	0.221	0.070
0.046	0.000	0.000	0.000	0.000	0.000	0.000	0.000	0.000	0.000	0.000
0.050	0.000	0.000	0.079	0.194	0.398	0.739	1.184	1.492	1.306	0.826
0.040	0.000	0.000	0.000	0.000	0.000	0.000	0.000	0.000	0.000	0.000
0.188	0.113	0.052	0.162	0.258	0.515	0.927	1.438	1.747	1.479	0.911
0.039	0.000	0.000	0.000	0.000	0.000	0.000	0.000	0.000	0.000	0.000
0.327	0.255	0.259	0.329	0.500	0.867	1.303	1.634	1.551	1.044	0.541
0.046	0.000	0.000	0.000	0.000	0.000	0.000	0.000	0.000	0.000	0.000
0.210	0.151	0.146	0.183	0.290	0.566	1.000	1.519	1.805	1.498	0.908
0.042	0.000	0.000	0.000	0.000	0.000	0.000	0.000	0.000	0.000	0.000
0.328	0.249	0.248	0.311	0.467	0.805	1.210	1.522	1.455	0.988	0.516
0.322	0.228	0.207	0.230	0.297	0.422	0.529	0.562	0.460	0.282	0.087
0.336	0.255	0.252	0.312	0.459	0.774	1.142	1.415	1.335	0.900	0.469
0.365	0.265	0.244	0.273	0.352	0.493	0.608	0.633	0.506	0.303	0.093
0.274	0.208	0.208	0.262	0.400	0.705	1.083	1.394	1.364	0.945	0.501
0.040	0.000	0.000	0.000	0.000	0.000	0.000	0.000	0.000	0.000	0.000
0.877	0.753	0.795	1.005	1.474	2.425	3.501	4.270	3.972	2.620	1.316
0.179	0.008	0.000	0.000	0.116	0.197	0.258	0.291	0.257	0.131	0.000
0.299	0.229	0.229	0.288	0.435	0.756	1.143	1.448	1.394	0.952	0.500
0.232	0.165	0.153	0.183	0.279	0.550	1.040	1.792	2.595	2.702	2.012
0.290	0.215	0.210	0.259	0.386	0.667	1.012	1.292	1.260	0.875	0.467
0.251	0.169	0.147	0.159	0.202	0.285	0.361	0.392	0.333	0.213	0.068
0.311	0.236	0.234	0.291	0.435	0.746	1.118	1.405	1.346	0.918	0.482
0.052	0.000	0.000	0.000	0.000	0.000	0.000	0.000	0.000	0.000	0.000
0.194	0.138	0.133	0.167	0.263	0.516	0.916	1.401	1.678	1.403	0.855

continued

Micrometer [%]

0.173	0.145	0.122
0.471	0.134	0.000
1.291	0.490	0.118
0.238	0.003	0.000
1.347	0.509	0.122
0.000	0.000	0.000
0.542	0.134	0.000
0.000	0.000	0.000
0.000	0.000	0.000
0.247	0.003	0.000
0.448	0.132	0.000
0.000	0.000	0.000
0.000	0.000	0.000
0.000	0.000	0.000
0.429	0.125	0.000
0.000	0.000	0.000
0.000	0.000	0.000
0.410	0.124	0.000
0.000	0.000	0.000
0.441	0.130	0.000
0.000	0.000	0.000
0.226	0.003	0.000
0.000	0.000	0.000
0.433	0.126	0.000
0.000	0.000	0.000
0.217	0.003	0.000
0.000	0.000	0.000
0.198	0.003	0.000
0.000	0.000	0.000
0.214	0.003	0.000
0.000	0.000	0.000
0.524	0.127	0.000
0.000	0.000	0.000
0.211	0.003	0.000
1.182	0.460	0.113
0.201	0.003	0.000
0.000	0.000	0.000
0.205	0.003	0.000
0.000	0.000	0.000
0.410	0.120	0.000

Core-ID: RA09-GW-6-P²

Year	Micrometer [%]									
	297.3	250	210.22	176.78	148.65	125	105.11	88.388	74.325	62.5
2009	0.000	0.125	0.458	0.464	0.446	0.431	0.432	0.467	0.527	0.583
2003	0.000	0.000	0.000	0.000	0.023	0.176	0.239	0.332	0.466	0.592
1997	0.000	0.054	0.216	0.260	0.296	0.331	0.377	0.464	0.579	0.669
1990	0.000	0.000	0.000	0.000	0.000	0.000	0.081	0.173	0.249	0.336
1984	0.000	0.000	0.000	0.000	0.000	0.000	0.000	0.121	0.235	0.340
1978	0.000	0.000	0.000	0.101	0.163	0.191	0.231	0.300	0.404	0.503
1972	0.000	0.000	0.000	0.092	0.178	0.243	0.311	0.406	0.528	0.633
1965	0.000	0.083	0.298	0.296	0.291	0.295	0.317	0.375	0.466	0.555
1959	0.000	0.000	0.000	0.000	0.000	0.000	0.000	0.002	0.183	0.283
1953	0.000	0.000	0.000	0.000	0.000	0.054	0.171	0.240	0.347	0.456
1947	0.000	0.000	0.000	0.000	0.133	0.174	0.215	0.283	0.387	0.488
1940	0.037	0.596	0.548	0.469	0.395	0.358	0.357	0.404	0.493	0.586
1934	0.000	0.000	0.000	0.000	0.000	0.058	0.191	0.274	0.394	0.509
1928	0.000	0.039	0.166	0.230	0.295	0.349	0.403	0.489	0.602	0.697
1922	0.000	0.000	0.000	0.000	0.000	0.000	0.000	0.000	0.000	0.066
1915	0.000	0.000	0.000	0.000	0.000	0.000	0.000	0.107	0.202	0.287
1909	0.000	0.042	0.161	0.182	0.201	0.223	0.254	0.313	0.401	0.488
1903	0.000	0.000	0.000	0.000	0.000	0.000	0.000	0.002	0.164	0.276
1897	0.000	0.000	0.000	0.000	0.023	0.177	0.259	0.372	0.521	0.652
1890	0.000	0.000	0.000	0.000	0.000	0.000	0.000	0.002	0.181	0.263
1884	0.000	0.000	0.000	0.000	0.000	0.000	0.000	0.118	0.239	0.354
1878	0.000	0.000	0.000	0.000	0.000	0.000	0.081	0.180	0.267	0.360
1872	0.000	0.000	0.000	0.000	0.020	0.163	0.257	0.390	0.565	0.714
1865	0.000	0.000	0.000	0.000	0.000	0.050	0.165	0.240	0.347	0.450
1859	0.000	0.000	0.000	0.000	0.000	0.000	0.000	0.122	0.249	0.371
1853	0.000	0.000	0.000	0.000	0.000	0.000	0.000	0.124	0.244	0.354
1847	0.000	0.000	0.000	0.000	0.021	0.152	0.192	0.258	0.361	0.467
1840	0.000	0.054	0.222	0.287	0.355	0.412	0.466	0.548	0.646	0.721
1834	0.000	0.000	0.000	0.000	0.000	0.052	0.162	0.219	0.309	0.403
1828	0.000	0.000	0.000	0.000	0.000	0.000	0.000	0.002	0.154	0.237
1822	0.000	0.000	0.000	0.000	0.000	0.000	0.000	0.000	0.042	0.219
1815	0.000	0.000	0.000	0.000	0.000	0.000	0.000	0.002	0.156	0.230
1809	0.000	0.000	0.000	0.000	0.000	0.000	0.000	0.002	0.210	0.327
1803	0.000	0.000	0.000	0.000	0.000	0.000	0.000	0.000	0.043	0.224
1797	0.000	0.000	0.000	0.000	0.000	0.000	0.000	0.125	0.229	0.318
1790	0.000	0.000	0.000	0.000	0.000	0.000	0.000	0.000	0.000	0.000
1784	0.000	0.000	0.000	0.000	0.129	0.181	0.231	0.303	0.400	0.489
1778	0.000	0.000	0.000	0.000	0.000	0.000	0.000	0.002	0.210	0.327
1772	0.000	0.000	0.000	0.000	0.000	0.000	0.000	0.002	0.151	0.236
1765	0.000	0.000	0.000	0.102	0.172	0.211	0.264	0.360	0.516	0.677

continued

Micrometer [%]

52.556	44.194	37.163	31.25	26.278	22.097	18.581	15.625	13.139	11.049
0.642	0.728	0.890	1.181	1.733	2.923	4.757	7.289	10.241	12.501
0.724	0.888	1.117	1.453	2.028	3.172	4.802	6.892	9.172	10.863
0.749	0.840	0.980	1.214	1.647	2.536	3.820	5.480	7.318	8.748
0.440	0.587	0.807	1.134	1.688	2.796	4.392	6.465	8.774	10.578
0.464	0.625	0.834	1.111	1.559	2.438	3.687	5.296	7.078	8.489
0.608	0.741	0.939	1.244	1.775	2.836	4.345	6.273	8.370	9.944
0.737	0.865	1.055	1.353	1.876	2.917	4.386	6.238	8.209	9.608
0.647	0.768	0.952	1.243	1.757	2.795	4.290	6.228	8.381	10.065
0.412	0.589	0.836	1.180	1.742	2.844	4.402	6.395	8.581	10.266
0.579	0.743	0.979	1.328	1.912	3.044	4.598	6.506	8.477	9.829
0.599	0.742	0.951	1.270	1.819	2.915	4.477	6.480	8.674	10.344
0.686	0.821	1.031	1.357	1.916	3.009	4.527	6.422	8.433	9.893
0.634	0.794	1.024	1.367	1.956	3.122	4.765	6.837	9.043	10.606
0.789	0.905	1.085	1.378	1.900	2.941	4.401	6.237	8.195	9.616
0.197	0.328	0.547	0.887	1.475	2.693	4.495	6.873	9.531	11.571
0.391	0.533	0.741	1.049	1.582	2.703	4.417	6.789	9.604	11.931
0.582	0.709	0.907	1.220	1.772	2.888	4.498	6.582	8.882	10.638
0.430	0.654	0.957	1.339	1.890	2.845	4.045	5.409	6.714	7.522
0.788	0.951	1.178	1.513	2.080	3.174	4.676	6.530	8.472	9.846
0.364	0.505	0.708	1.008	1.525	2.606	4.253	6.524	9.218	11.478
0.496	0.689	0.954	1.317	1.892	2.969	4.420	6.188	8.018	9.307
0.467	0.612	0.826	1.150	1.719	2.923	4.766	7.309	10.282	12.597
0.864	1.035	1.262	1.601	2.193	3.375	5.059	7.215	9.553	11.229
0.560	0.700	0.900	1.209	1.762	2.931	4.718	7.180	10.061	12.325
0.521	0.723	0.998	1.374	1.975	3.123	4.705	6.676	8.771	10.294
0.487	0.666	0.917	1.279	1.883	3.083	4.787	6.957	9.293	10.970
0.586	0.742	0.966	1.296	1.845	2.903	4.354	6.136	7.983	9.251
0.788	0.872	1.018	1.276	1.763	2.782	4.289	6.293	8.579	10.419
0.510	0.655	0.868	1.183	1.712	2.732	4.123	5.818	7.574	8.837
0.348	0.517	0.775	1.147	1.750	2.905	4.486	6.429	8.445	9.852
0.324	0.484	0.728	1.084	1.667	2.803	4.383	6.353	8.423	9.868
0.325	0.463	0.674	0.989	1.528	2.632	4.262	6.431	8.903	10.900
0.478	0.688	0.976	1.359	1.947	3.008	4.382	5.984	7.558	8.582
0.334	0.490	0.711	1.025	1.549	2.606	4.153	6.197	8.525	10.426
0.425	0.572	0.787	1.103	1.633	2.682	4.173	6.090	8.209	9.881
0.123	0.284	0.493	0.823	1.392	2.566	4.289	6.540	9.027	10.914
0.582	0.699	0.873	1.149	1.642	2.666	4.188	6.235	8.609	10.578
0.478	0.688	0.976	1.359	1.947	3.008	4.382	5.984	7.558	8.582
0.350	0.522	0.781	1.149	1.739	2.853	4.359	6.190	8.082	9.424
0.855	1.078	1.378	1.776	2.382	3.422	4.680	6.037	7.246	7.887

continued

Micrometer [%]

9.291	7.813	6.57	5.524	4.645	3.906	3.285	2.762	2.323	1.953	1.642
12.597	11.430	9.335	6.908	4.877	3.310	2.045	1.316	0.793	0.417	0.153
11.027	10.325	8.929	7.185	5.596	4.242	2.986	2.138	1.442	0.872	0.476
9.013	8.603	7.633	6.338	5.111	4.028	2.978	2.226	1.572	1.001	0.579
10.910	10.398	9.188	7.572	6.050	4.721	3.448	2.549	1.779	1.116	0.634
8.806	8.494	7.654	6.485	5.354	4.337	3.322	2.560	1.865	1.227	0.734
10.161	9.610	8.430	6.903	5.475	4.223	3.019	2.175	1.468	0.886	0.484
9.678	9.011	7.761	6.239	4.866	3.700	2.620	1.889	1.288	0.792	0.443
10.388	9.922	8.802	7.299	5.875	4.621	3.407	2.540	1.787	1.134	0.654
10.573	10.103	8.989	7.495	6.081	4.832	3.615	2.731	1.950	1.257	0.737
9.878	9.231	8.033	6.572	5.244	4.092	2.983	2.194	1.517	0.943	0.533
10.606	10.068	8.876	7.317	5.861	4.589	3.369	2.504	1.758	1.113	0.641
10.051	9.483	8.327	6.869	5.525	4.355	3.228	2.422	1.721	1.107	0.651
10.677	9.923	8.519	6.807	5.261	3.945	2.724	1.906	1.249	0.730	0.385
9.762	9.199	8.062	6.626	5.297	4.134	3.008	2.206	1.520	0.939	0.525
11.865	11.179	9.702	7.796	6.052	4.573	3.213	2.300	1.553	0.941	0.514
12.366	11.659	10.026	7.885	5.939	4.322	2.894	1.987	1.279	0.727	0.362
10.899	10.307	9.021	7.353	5.808	4.472	3.213	2.342	1.611	0.996	0.559
7.501	7.072	6.326	5.460	4.697	4.047	3.401	2.870	2.306	1.692	1.131
9.954	9.370	8.233	6.819	5.519	4.385	3.280	2.473	1.756	1.121	0.647
11.986	11.435	10.007	8.057	6.240	4.695	3.285	2.345	1.575	0.938	0.492
9.427	8.920	7.907	6.631	5.445	4.396	3.350	2.562	1.844	1.195	0.703
12.777	11.713	9.716	7.338	5.312	3.719	2.397	1.603	1.005	0.550	0.256
11.280	10.421	8.863	7.001	5.359	3.998	2.778	1.977	1.327	0.796	0.425
12.541	11.555	9.652	7.354	5.372	3.797	2.473	1.667	1.054	0.582	0.275
10.461	9.880	8.700	7.206	5.829	4.634	3.482	2.647	1.904	1.236	0.727
11.063	10.277	8.797	6.986	5.355	3.974	2.707	1.871	1.211	0.697	0.362
9.294	8.677	7.542	6.169	4.932	3.873	2.870	2.159	1.540	0.995	0.585
10.792	10.294	9.071	7.420	5.862	4.504	3.220	2.333	1.592	0.972	0.534
9.027	8.645	7.796	6.681	5.622	4.667	3.683	2.908	2.170	1.473	0.922
9.956	9.366	8.222	6.800	5.495	4.356	3.246	2.436	1.722	1.095	0.633
9.934	9.258	7.999	6.466	5.088	3.918	2.829	2.079	1.447	0.911	0.521
11.330	10.848	9.604	7.894	6.272	4.856	3.508	2.569	1.772	1.097	0.612
8.608	8.130	7.253	6.195	5.233	4.387	3.526	2.836	2.156	1.486	0.934
10.883	10.502	9.412	7.866	6.374	5.048	3.757	2.823	2.001	1.275	0.733
10.254	9.891	8.912	7.547	6.231	5.055	3.885	3.007	2.202	1.459	0.879
11.184	10.556	9.193	7.421	5.781	4.366	3.039	2.141	1.414	0.835	0.446
11.054	10.634	9.460	7.809	6.226	4.834	3.504	2.570	1.773	1.093	0.602
8.608	8.130	7.253	6.195	5.233	4.387	3.526	2.836	2.156	1.486	0.934
9.586	9.124	8.157	6.913	5.751	4.717	3.674	2.870	2.119	1.416	0.866
7.739	7.220	6.420	5.547	4.795	4.155	3.505	2.958	2.374	1.746	1.186

continued

Micrometer [%]

1.381	1.161	0.977	0.821	0.691	0.581	0.488	0.411	0.345	0.29	0.244
0.000	0.000	0.000	0.000	0.000	0.000	0.000	0.000	0.000	0.000	0.000
0.271	0.161	0.007	0.000	0.000	0.113	0.198	0.265	0.305	0.275	0.185
0.348	0.218	0.153	0.142	0.171	0.266	0.539	1.048	1.849	2.729	2.872
0.375	0.231	0.158	0.141	0.157	0.207	0.305	0.400	0.447	0.386	0.249
0.452	0.290	0.208	0.195	0.236	0.362	0.715	1.347	2.293	3.240	3.265
0.279	0.170	0.008	0.000	0.095	0.232	0.472	0.870	1.380	1.714	1.477
0.259	0.158	0.007	0.000	0.079	0.191	0.400	0.806	1.483	2.304	2.552
0.393	0.247	0.173	0.157	0.178	0.236	0.348	0.455	0.502	0.427	0.270
0.449	0.286	0.203	0.185	0.209	0.276	0.401	0.514	0.557	0.464	0.288
0.317	0.199	0.144	0.140	0.178	0.286	0.572	1.028	1.585	1.908	1.595
0.384	0.241	0.168	0.152	0.171	0.227	0.334	0.436	0.481	0.410	0.260
0.400	0.259	0.188	0.177	0.205	0.277	0.412	0.536	0.585	0.488	0.302
0.215	0.045	0.000	0.000	0.000	0.141	0.335	0.635	1.043	1.353	1.219
0.308	0.190	0.113	0.051	0.157	0.247	0.484	0.860	1.321	1.592	1.341
0.292	0.172	0.008	0.000	0.000	0.109	0.185	0.242	0.273	0.244	0.125
0.184	0.036	0.000	0.000	0.000	0.000	0.000	0.000	0.000	0.000	0.000
0.327	0.199	0.116	0.000	0.084	0.174	0.256	0.336	0.376	0.327	0.213
0.765	0.533	0.406	0.389	0.462	0.673	1.206	2.046	3.126	3.934	3.574
0.387	0.242	0.170	0.157	0.184	0.263	0.442	0.665	0.855	0.853	0.613
0.262	0.052	0.000	0.000	0.000	0.000	0.000	0.000	0.000	0.000	0.000
0.430	0.277	0.202	0.195	0.243	0.377	0.715	1.220	1.788	2.043	1.635
0.077	0.000	0.000	0.000	0.000	0.000	0.000	0.000	0.000	0.000	0.000
0.233	0.048	0.000	0.000	0.000	0.000	0.000	0.000	0.000	0.000	0.000
0.083	0.000	0.000	0.000	0.000	0.000	0.000	0.000	0.000	0.000	0.000
0.442	0.278	0.193	0.171	0.186	0.238	0.334	0.420	0.449	0.374	0.234
0.198	0.041	0.000	0.000	0.000	0.121	0.287	0.549	0.912	1.206	1.109
0.356	0.226	0.159	0.148	0.178	0.272	0.541	1.032	1.793	2.612	2.728
0.304	0.179	0.008	0.000	0.000	0.108	0.181	0.233	0.259	0.228	0.115
0.603	0.420	0.335	0.346	0.441	0.661	1.115	1.621	1.957	1.781	1.152
0.381	0.242	0.175	0.168	0.209	0.325	0.621	1.073	1.596	1.859	1.517
0.310	0.193	0.114	0.049	0.149	0.231	0.471	0.924	1.653	2.491	2.684
0.354	0.212	0.119	0.000	0.079	0.158	0.223	0.284	0.312	0.269	0.134
0.606	0.412	0.316	0.314	0.391	0.593	1.065	1.710	2.349	2.498	1.872
0.434	0.266	0.179	0.154	0.165	0.207	0.288	0.361	0.388	0.326	0.208
0.547	0.354	0.254	0.231	0.257	0.330	0.461	0.570	0.594	0.477	0.288
0.252	0.151	0.007	0.000	0.081	0.196	0.400	0.739	1.182	1.490	1.307
0.342	0.199	0.009	0.000	0.000	0.005	0.172	0.215	0.236	0.205	0.104
0.606	0.412	0.316	0.314	0.391	0.593	1.065	1.710	2.349	2.498	1.872
0.551	0.370	0.281	0.278	0.342	0.502	0.840	1.230	1.513	1.417	0.948
0.829	0.609	0.504	0.521	0.648	0.925	1.444	1.943	2.178	1.840	1.119

continued

Micrometer [%]

0.205	0.173	0.145	0.122
0.000	0.000	0.000	0.000
0.061	0.000	0.000	0.000
2.145	1.258	0.485	0.118
0.079	0.000	0.000	0.000
2.349	1.325	0.491	0.117
0.919	0.448	0.132	0.000
1.993	1.223	0.495	0.124
0.085	0.000	0.000	0.000
0.090	0.000	0.000	0.000
0.969	0.462	0.133	0.000
0.082	0.000	0.000	0.000
0.094	0.000	0.000	0.000
0.789	0.401	0.124	0.000
0.824	0.399	0.118	0.000
0.000	0.000	0.000	0.000
0.000	0.000	0.000	0.000
0.068	0.000	0.000	0.000
2.369	1.240	0.428	0.099
0.340	0.058	0.000	0.000
0.000	0.000	0.000	0.000
0.962	0.446	0.126	0.000
0.000	0.000	0.000	0.000
0.000	0.000	0.000	0.000
0.000	0.000	0.000	0.000
0.073	0.000	0.000	0.000
0.732	0.380	0.120	0.000
2.034	1.195	0.464	0.114
0.000	0.000	0.000	0.000
0.577	0.234	0.003	0.000
0.909	0.430	0.124	0.000
2.053	1.236	0.491	0.122
0.000	0.000	0.000	0.000
1.045	0.461	0.124	0.000
0.066	0.000	0.000	0.000
0.088	0.000	0.000	0.000
0.829	0.414	0.126	0.000
0.000	0.000	0.000	0.000
1.045	0.461	0.124	0.000
0.491	0.206	0.003	0.000
0.537	0.210	0.003	0.000

Core-ID: RA09-GW-7-P10

Year	Micrometer [%]										
	297.3	250	210.22	176.78	148.65	125	105.11	88.388	74.325	62.5	
2009	0.000	0.000	0.000	0.000	0.130	0.230	0.370	0.595	0.919	1.188	
2003	0.000	0.143	0.593	0.795	1.030	1.266	1.521	1.884	2.219	2.322	
1998	0.000	0.059	0.250	0.353	0.496	0.672	0.887	1.196	1.539	1.729	
1992	0.000	0.104	0.430	0.567	0.707	0.833	0.967	1.176	1.402	1.519	
1987	0.000	0.000	0.000	0.113	0.246	0.391	0.583	0.872	1.245	1.509	
1981	0.000	0.105	0.425	0.534	0.643	0.746	0.866	1.068	1.319	1.490	
1976	0.000	0.090	0.357	0.442	0.550	0.676	0.831	1.064	1.340	1.522	
1970	0.000	0.070	0.284	0.364	0.457	0.562	0.695	0.908	1.180	1.381	
1965	0.000	0.121	0.459	0.514	0.580	0.673	0.812	1.061	1.400	1.653	
1959	0.000	0.000	0.096	0.262	0.435	0.662	0.943	1.334	1.763	1.990	
1953	0.000	0.047	0.217	0.360	0.593	0.897	1.277	1.815	2.383	2.648	
1948	0.000	0.000	0.000	0.000	0.021	0.183	0.345	0.596	0.939	1.212	
1942	0.000	0.079	0.312	0.384	0.486	0.622	0.811	1.111	1.492	1.749	
1937	0.000	0.000	0.098	0.273	0.446	0.648	0.878	1.201	1.584	1.829	
1931	0.000	0.070	0.302	0.439	0.619	0.821	1.056	1.401	1.793	2.020	
1926	0.000	0.084	0.363	0.525	0.724	0.930	1.161	1.502	1.884	2.094	
1920	0.000	0.000	0.071	0.195	0.331	0.524	0.784	1.173	1.669	2.013	
1914	0.000	0.047	0.199	0.292	0.445	0.666	0.976	1.460	2.079	2.482	
1909	0.000	0.072	0.292	0.381	0.503	0.655	0.852	1.162	1.556	1.826	
1903	0.000	0.052	0.235	0.373	0.579	0.826	1.115	1.516	1.959	2.197	
1898	0.000	0.077	0.316	0.424	0.577	0.765	1.002	1.362	1.808	2.101	
1892	0.000	0.083	0.335	0.441	0.597	0.800	1.061	1.452	1.907	2.173	
1887	0.000	0.051	0.232	0.366	0.555	0.766	0.999	1.324	1.683	1.886	
1881	0.000	0.145	0.555	0.643	0.754	0.901	1.109	1.459	1.903	2.193	
1876	0.000	0.000	0.101	0.285	0.472	0.703	1.001	1.475	2.111	2.561	
1870	0.000	0.000	0.000	0.000	0.162	0.264	0.392	0.593	0.888	1.151	
1864	0.000	0.108	0.461	0.644	0.859	1.090	1.356	1.736	2.101	2.227	
1859	0.000	0.000	0.000	0.000	0.201	0.363	0.586	0.944	1.468	1.900	
1853	0.000	0.044	0.193	0.286	0.408	0.542	0.697	0.920	1.189	1.375	
1848	0.000	0.050	0.215	0.306	0.423	0.552	0.709	0.960	1.312	1.605	
1842	0.000	0.049	0.211	0.309	0.456	0.636	0.854	1.169	1.537	1.770	
1837	0.000	0.039	0.170	0.259	0.389	0.552	0.759	1.079	1.511	1.849	
1831	0.000	0.073	0.303	0.410	0.551	0.716	0.916	1.211	1.576	1.832	
1826	0.000	0.000	0.089	0.235	0.363	0.519	0.708	0.990	1.358	1.639	
1820	0.000	0.095	0.405	0.561	0.734	0.900	1.080	1.353	1.658	1.832	
1814	0.000	0.000	0.065	0.179	0.290	0.421	0.582	0.829	1.174	1.461	
1809	0.000	0.130	0.522	0.658	0.804	0.955	1.135	1.424	1.764	1.971	
1803	0.000	0.000	0.000	0.000	0.020	0.175	0.331	0.629	1.169	1.735	
1798	0.000	0.000	0.085	0.223	0.345	0.500	0.697	0.990	1.375	1.664	
1792	0.000	0.000	0.000	0.000	0.000	0.000	0.000	0.000	0.000	0.000	
1787	0.000	0.000	0.000	0.000	0.000	0.000	0.000	0.000	0.000	0.000	

continued

Micrometer [%]

52.556	44.194	37.163	31.25	26.278	22.097	18.581	15.625	13.139	11.049	9.291
1.435	1.666	1.895	2.186	2.689	3.675	5.032	6.700	8.433	9.612	9.603
2.318	2.248	2.201	2.288	2.615	3.366	4.441	5.779	7.182	8.166	8.207
1.843	1.908	1.984	2.170	2.599	3.527	4.881	6.630	8.545	9.936	9.980
1.582	1.623	1.704	1.903	2.330	3.218	4.467	6.032	7.702	8.924	9.054
1.718	1.886	2.040	2.259	2.664	3.442	4.454	5.609	6.694	7.299	7.144
1.621	1.742	1.904	2.179	2.695	3.716	5.110	6.806	8.536	9.658	9.555
1.658	1.779	1.943	2.229	2.783	3.915	5.527	7.570	9.724	11.082	10.760
1.547	1.708	1.912	2.228	2.799	3.916	5.444	7.308	9.208	10.397	10.189
1.861	2.050	2.259	2.555	3.070	4.024	5.242	6.624	7.917	8.620	8.393
2.117	2.171	2.218	2.379	2.787	3.659	4.859	6.286	7.674	8.464	8.225
2.762	2.752	2.696	2.740	3.006	3.632	4.482	5.445	6.321	6.762	6.574
1.465	1.707	1.963	2.310	2.903	4.024	5.504	7.245	8.952	9.967	9.758
1.940	2.086	2.230	2.459	2.907	3.794	4.979	6.376	7.749	8.598	8.494
2.004	2.133	2.269	2.502	2.967	3.889	5.127	6.595	8.044	8.929	8.786
2.162	2.246	2.332	2.515	2.918	3.724	4.780	5.985	7.114	7.742	7.580
2.216	2.279	2.352	2.535	2.957	3.823	4.988	6.357	7.686	8.469	8.307
2.275	2.464	2.615	2.839	3.297	4.231	5.505	7.025	8.518	9.384	9.132
2.767	2.936	3.026	3.162	3.486	4.135	4.941	5.776	6.434	6.612	6.256
2.032	2.196	2.363	2.624	3.116	4.053	5.252	6.591	7.806	8.410	8.120
2.332	2.392	2.447	2.611	3.017	3.880	5.071	6.508	7.949	8.846	8.709
2.312	2.466	2.612	2.847	3.316	4.247	5.495	6.963	8.385	9.175	8.889
2.343	2.442	2.527	2.708	3.118	3.954	5.069	6.364	7.594	8.267	8.031
2.012	2.092	2.187	2.396	2.850	3.779	5.052	6.591	8.144	9.133	9.025
2.396	2.536	2.661	2.865	3.281	4.098	5.159	6.359	7.467	8.037	7.791
2.906	3.147	3.303	3.474	3.792	4.366	5.027	5.654	6.060	6.001	5.532
1.410	1.687	2.000	2.396	3.021	4.147	5.591	7.247	8.811	9.653	9.334
2.243	2.189	2.156	2.263	2.623	3.445	4.628	6.106	7.657	8.730	8.740
2.286	2.622	2.896	3.181	3.638	4.469	5.516	6.673	7.707	8.188	7.886
1.525	1.666	1.847	2.142	2.688	3.766	5.252	7.078	8.960	10.188	10.071
1.875	2.150	2.458	2.846	3.442	4.448	5.637	6.881	7.909	8.269	7.813
1.940	2.074	2.227	2.491	3.003	4.005	5.338	6.902	8.422	9.303	9.081
2.146	2.420	2.695	3.027	3.545	4.423	5.452	6.505	7.343	7.588	7.157
2.033	2.210	2.413	2.722	3.282	4.357	5.787	7.472	9.094	9.936	9.490
1.880	2.106	2.355	2.694	3.260	4.283	5.574	7.025	8.361	9.042	8.728
1.941	2.019	2.130	2.362	2.837	3.773	5.008	6.439	7.810	8.602	8.429
1.728	2.000	2.304	2.696	3.322	4.449	5.890	7.537	9.083	9.877	9.487
2.107	2.204	2.321	2.546	3.011	3.952	5.235	6.773	8.304	9.226	9.025
2.356	3.014	3.604	4.097	4.640	5.363	6.053	6.598	6.821	6.518	5.875
1.904	2.112	2.322	2.619	3.162	4.239	5.723	7.536	9.362	10.418	10.047
0.000	0.185	0.402	0.742	1.338	2.566	4.321	6.505	8.752	10.234	10.205
0.000	0.000	0.000	0.000	0.194	1.126	3.321	6.866	11.011	13.862	13.777

continued

Micrometer [%]

7.813	6.57	5.524	4.645	3.906	3.285	2.762	2.323	1.953	1.642	1.381
8.931	7.736	6.311	5.021	3.906	2.838	2.081	1.433	0.883	0.490	0.283
7.702	6.754	5.603	4.545	3.616	2.709	2.049	1.464	0.946	0.557	0.342
9.237	7.882	6.265	4.829	3.630	2.544	1.821	1.227	0.736	0.390	0.211
8.555	7.545	6.274	5.094	4.057	3.044	2.306	1.651	1.067	0.627	0.382
6.598	5.753	4.825	4.018	3.331	2.659	2.141	1.639	1.143	0.727	0.472
8.776	7.475	5.981	4.661	3.548	2.518	1.817	1.238	0.760	0.424	0.248
9.524	7.662	5.683	4.074	2.835	1.820	1.215	0.762	0.420	0.162	0.000
9.227	7.707	6.023	4.584	3.410	2.367	1.686	1.135	0.685	0.370	0.206
7.681	6.602	5.426	4.405	3.539	2.707	2.096	1.543	1.034	0.637	0.408
7.441	6.252	4.958	3.847	2.925	2.082	1.514	1.043	0.650	0.369	0.219
6.064	5.307	4.497	3.796	3.191	2.579	2.088	1.600	1.114	0.710	0.466
8.904	7.566	6.074	4.776	3.686	2.671	1.968	1.372	0.863	0.494	0.295
7.873	6.849	5.680	4.638	3.740	2.865	2.217	1.626	1.084	0.661	0.418
8.088	6.964	5.694	4.575	3.621	2.711	2.057	1.477	0.960	0.567	0.347
7.004	6.108	5.116	4.240	3.478	2.717	2.131	1.582	1.067	0.662	0.428
7.638	6.578	5.394	4.353	3.464	2.612	1.995	1.445	0.952	0.574	0.361
8.283	6.992	5.585	4.379	3.380	2.464	1.833	1.293	0.822	0.471	0.277
5.652	4.865	4.095	3.462	2.934	2.410	1.986	1.555	1.113	0.732	0.497
7.377	6.293	5.133	4.131	3.277	2.453	1.854	1.326	0.862	0.516	0.326
8.003	6.861	5.570	4.433	3.469	2.559	1.915	1.355	0.864	0.499	0.297
8.030	6.754	5.385	4.224	3.268	2.396	1.795	1.276	0.817	0.470	0.275
7.313	6.231	5.054	4.033	3.165	2.336	1.741	1.222	0.770	0.439	0.261
8.315	7.142	5.801	4.617	3.613	2.666	1.997	1.415	0.904	0.522	0.311
7.116	6.116	5.045	4.120	3.337	2.581	2.021	1.504	1.021	0.636	0.411
4.892	4.136	3.452	2.924	2.510	2.126	1.822	1.497	1.132	0.786	0.551
8.421	7.070	5.613	4.366	3.325	2.361	1.700	1.152	0.699	0.384	0.221
8.143	7.063	5.774	4.606	3.599	2.639	1.961	1.377	0.873	0.502	0.300
7.185	6.189	5.146	4.257	3.509	2.784	2.231	1.701	1.182	0.751	0.490
9.216	7.807	6.202	4.807	3.651	2.602	1.897	1.308	0.811	0.450	0.257
6.977	5.870	4.761	3.844	3.085	2.364	1.832	1.344	0.893	0.541	0.339
8.274	7.030	5.660	4.475	3.481	2.555	1.908	1.351	0.864	0.502	0.303
6.414	5.451	4.502	3.724	3.079	2.456	1.975	1.506	1.044	0.661	0.430
8.390	6.852	5.276	3.999	2.999	2.139	1.576	1.102	0.684	0.368	0.193
7.910	6.724	5.463	4.392	3.501	2.664	2.059	1.512	1.007	0.608	0.377
7.750	6.683	5.497	4.459	3.575	2.726	2.107	1.548	1.037	0.639	0.409
8.499	7.091	5.618	4.392	3.400	2.508	1.895	1.360	0.879	0.507	0.295
8.217	6.957	5.567	4.373	3.384	2.478	1.854	1.316	0.842	0.484	0.284
5.120	4.299	3.602	3.091	2.704	2.350	2.056	1.720	1.324	0.937	0.671
8.925	7.288	5.569	4.161	3.057	2.115	1.513	1.024	0.612	0.316	0.101
9.411	8.034	6.411	4.989	3.805	2.722	1.990	1.381	0.870	0.501	0.302
12.343	9.955	7.271	5.122	3.509	2.214	1.457	0.904	0.498	0.245	0.078

continued

Micrometer [%]

1.161	0.977	0.821	0.691	0.581	0.488	0.411	0.345	0.29	0.244	0.205
0.171	0.008	0.000	0.082	0.185	0.328	0.524	0.714	0.757	0.573	0.329
0.220	0.159	0.149	0.173	0.237	0.359	0.476	0.530	0.452	0.283	0.088
0.043	0.000	0.000	0.000	0.000	0.000	0.000	0.000	0.000	0.000	0.000
0.244	0.173	0.159	0.181	0.243	0.360	0.471	0.520	0.441	0.277	0.086
0.318	0.237	0.227	0.275	0.418	0.802	1.460	2.399	3.261	3.169	2.212
0.152	0.007	0.000	0.000	0.128	0.232	0.318	0.370	0.333	0.222	0.072
0.000	0.000	0.000	0.000	0.000	0.000	0.000	0.000	0.000	0.000	0.000
0.043	0.000	0.000	0.000	0.000	0.000	0.000	0.000	0.000	0.000	0.000
0.275	0.208	0.201	0.238	0.326	0.486	0.628	0.678	0.555	0.335	0.102
0.047	0.000	0.000	0.000	0.146	0.351	0.711	1.316	2.056	2.289	1.795
0.322	0.250	0.252	0.317	0.487	0.887	1.444	2.007	2.159	1.631	0.913
0.185	0.111	0.000	0.086	0.181	0.271	0.358	0.402	0.348	0.225	0.072
0.277	0.206	0.195	0.225	0.302	0.441	0.563	0.602	0.491	0.298	0.091
0.222	0.157	0.143	0.161	0.213	0.312	0.403	0.442	0.374	0.236	0.074
0.294	0.230	0.234	0.297	0.449	0.774	1.158	1.447	1.370	0.919	0.474
0.239	0.177	0.169	0.197	0.269	0.401	0.522	0.569	0.474	0.291	0.090
0.166	0.008	0.000	0.000	0.000	0.000	0.000	0.000	0.000	0.000	0.000
0.354	0.285	0.294	0.376	0.577	1.042	1.668	2.272	2.388	1.763	0.969
0.220	0.171	0.175	0.225	0.348	0.618	0.952	1.226	1.199	0.830	0.440
0.184	0.009	0.000	0.000	0.130	0.222	0.287	0.318	0.275	0.137	0.000
0.163	0.007	0.000	0.000	0.000	0.000	0.000	0.000	0.000	0.000	0.000
0.162	0.008	0.000	0.086	0.205	0.398	0.708	1.092	1.328	1.132	0.703
0.192	0.111	0.000	0.000	0.128	0.212	0.268	0.292	0.250	0.124	0.000
0.278	0.210	0.201	0.234	0.314	0.458	0.580	0.616	0.499	0.299	0.091
0.397	0.312	0.304	0.365	0.532	0.951	1.608	2.456	3.103	2.839	1.899
0.047	0.000	0.000	0.000	0.150	0.349	0.646	1.037	1.316	1.164	0.744
0.186	0.110	0.000	0.079	0.161	0.231	0.296	0.325	0.278	0.137	0.000
0.333	0.250	0.236	0.269	0.351	0.493	0.608	0.629	0.498	0.294	0.089
0.149	0.007	0.000	0.000	0.000	0.000	0.000	0.000	0.000	0.000	0.000
0.222	0.165	0.160	0.199	0.306	0.575	0.977	1.434	1.648	1.332	0.792
0.189	0.112	0.000	0.080	0.163	0.233	0.298	0.327	0.279	0.138	0.000
0.293	0.223	0.220	0.274	0.415	0.753	1.232	1.733	1.901	1.471	0.844
0.038	0.000	0.000	0.000	0.000	0.000	0.000	0.000	0.000	0.000	0.000
0.242	0.169	0.151	0.164	0.208	0.291	0.365	0.390	0.324	0.204	0.064
0.275	0.206	0.197	0.227	0.303	0.436	0.549	0.578	0.466	0.280	0.085
0.173	0.008	0.000	0.000	0.000	0.000	0.000	0.000	0.000	0.000	0.000
0.168	0.008	0.000	0.000	0.000	0.000	0.000	0.000	0.000	0.000	0.000
0.498	0.408	0.415	0.510	0.739	1.230	1.827	2.328	2.300	1.624	0.870
0.000	0.000	0.000	0.000	0.000	0.000	0.000	0.000	0.000	0.000	0.000
0.191	0.116	0.052	0.161	0.257	0.533	1.053	1.885	2.820	3.003	2.267
0.000	0.000	0.000	0.000	0.005	0.182	0.417	0.839	1.362	1.490	1.109

continued

Micrometer [%]		
0.173	0.145	0.122
0.057	0.000	0.000
0.000	0.000	0.000
0.000	0.000	0.000
0.000	0.000	0.000
1.212	0.435	0.102
0.000	0.000	0.000
0.000	0.000	0.000
0.000	0.000	0.000
0.000	0.000	0.000
1.105	0.448	0.112
0.403	0.108	0.000
0.000	0.000	0.000
0.000	0.000	0.000
0.000	0.000	0.000
0.197	0.003	0.000
0.000	0.000	0.000
0.000	0.000	0.000
0.420	0.111	0.000
0.188	0.003	0.000
0.000	0.000	0.000
0.000	0.000	0.000
0.344	0.005	0.000
0.000	0.000	0.000
0.000	0.000	0.000
1.004	0.351	0.081
0.374	0.114	0.000
0.000	0.000	0.000
0.000	0.000	0.000
0.372	0.107	0.000
0.000	0.000	0.000
0.383	0.106	0.000
0.000	0.000	0.000
0.000	0.000	0.000
0.000	0.000	0.000
0.000	0.000	0.000
0.372	0.005	0.000
0.000	0.000	0.000
1.343	0.524	0.128
0.632	0.211	0.000

Core-ID: RA09-GW-8-P^c

Year	Micrometer [%]									
	297.3	250	210.22	176.78	148.65	125	105.11	88.388	74.325	62.5
2009	0.000	0.125	0.458	0.464	0.446	0.431	0.432	0.467	0.527	0.583
2002	0.000	0.000	0.000	0.000	0.023	0.176	0.239	0.332	0.466	0.592
1996	0.000	0.054	0.216	0.260	0.296	0.331	0.377	0.464	0.579	0.669
1989	0.000	0.000	0.000	0.000	0.000	0.000	0.081	0.173	0.249	0.336
1982	0.000	0.000	0.000	0.000	0.000	0.000	0.000	0.121	0.235	0.340
1976	0.000	0.000	0.000	0.101	0.163	0.191	0.231	0.300	0.404	0.503
1969	0.000	0.000	0.000	0.092	0.178	0.243	0.311	0.406	0.528	0.633
1962	0.000	0.083	0.298	0.296	0.291	0.295	0.317	0.375	0.466	0.555
1956	0.000	0.000	0.000	0.000	0.000	0.000	0.000	0.002	0.183	0.283
1949	0.000	0.000	0.000	0.000	0.000	0.054	0.171	0.240	0.347	0.456
1942	0.000	0.000	0.000	0.000	0.133	0.174	0.215	0.283	0.387	0.488
1936	0.037	0.596	0.548	0.469	0.395	0.358	0.357	0.404	0.493	0.586
1929	0.000	0.000	0.000	0.000	0.000	0.058	0.191	0.274	0.394	0.509
1922	0.000	0.039	0.166	0.230	0.295	0.349	0.403	0.489	0.602	0.697
1916	0.000	0.000	0.000	0.000	0.000	0.000	0.000	0.000	0.000	0.066
1909	0.000	0.042	0.161	0.182	0.201	0.223	0.254	0.313	0.401	0.488
1902	0.000	0.000	0.000	0.000	0.023	0.177	0.259	0.372	0.521	0.652
1896	0.000	0.000	0.000	0.000	0.000	0.000	0.000	0.118	0.239	0.354
1889	0.000	0.000	0.000	0.000	0.020	0.163	0.257	0.390	0.565	0.714
1882	0.000	0.000	0.000	0.000	0.000	0.000	0.000	0.122	0.249	0.371
1876	0.000	0.000	0.000	0.000	0.021	0.152	0.192	0.258	0.361	0.467
1869	0.000	0.000	0.000	0.000	0.000	0.052	0.162	0.219	0.309	0.403
1862	0.000	0.000	0.000	0.000	0.000	0.000	0.000	0.000	0.042	0.219
1856	0.000	0.000	0.000	0.000	0.000	0.000	0.000	0.002	0.210	0.327
1849	0.000	0.000	0.000	0.000	0.000	0.000	0.000	0.125	0.229	0.318
1842	0.000	0.000	0.000	0.000	0.000	0.000	0.000	0.000	0.000	0.000
1836	0.000	0.000	0.000	0.000	0.000	0.000	0.000	0.002	0.151	0.236
1829	0.000	0.054	0.207	0.233	0.255	0.277	0.308	0.372	0.471	0.569
1822	0.000	0.000	0.000	0.000	0.000	0.000	0.000	0.000	0.000	0.000
1816	0.000	0.000	0.000	0.000	0.000	0.000	0.000	0.000	0.040	0.220
1809	0.000	0.000	0.000	0.000	0.000	0.000	0.000	0.000	0.000	0.000
1802	0.000	0.000	0.000	0.000	0.000	0.054	0.185	0.287	0.436	0.575
1796	0.000	0.000	0.000	0.000	0.000	0.000	0.000	0.127	0.255	0.372
1789	0.000	0.000	0.000	0.000	0.130	0.182	0.233	0.309	0.413	0.510
1782	0.000	0.000	0.000	0.000	0.000	0.000	0.000	0.002	0.203	0.311
1776	0.000	0.000	0.000	0.000	0.000	0.000	0.000	0.163	0.429	0.749
1769	0.000	0.000	0.000	0.000	0.000	0.000	0.000	0.000	0.047	0.259
1762	0.000	0.000	0.000	0.000	0.000	0.000	0.000	0.000	0.041	0.220
1756	0.000	0.037	0.140	0.154	0.170	0.193	0.231	0.304	0.425	0.550
1749	0.000	0.037	0.140	0.154	0.170	0.193	0.231	0.304	0.425	0.550
1742	0.000	0.000	0.000	0.000	0.000	0.067	0.228	0.348	0.522	0.685

continued

Micrometer [%]

52.556	44.194	37.163	31.25	26.278	22.097	18.581	15.625	13.139	11.049
0.642	0.728	0.890	1.181	1.733	2.923	4.757	7.289	10.241	12.501
0.724	0.888	1.117	1.453	2.028	3.172	4.802	6.892	9.172	10.863
0.749	0.840	0.980	1.214	1.647	2.536	3.820	5.480	7.318	8.748
0.440	0.587	0.807	1.134	1.688	2.796	4.392	6.465	8.774	10.578
0.464	0.625	0.834	1.111	1.559	2.438	3.687	5.296	7.078	8.489
0.608	0.741	0.939	1.244	1.775	2.836	4.345	6.273	8.370	9.944
0.737	0.865	1.055	1.353	1.876	2.917	4.386	6.238	8.209	9.608
0.647	0.768	0.952	1.243	1.757	2.795	4.290	6.228	8.381	10.065
0.412	0.589	0.836	1.180	1.742	2.844	4.402	6.395	8.581	10.266
0.579	0.743	0.979	1.328	1.912	3.044	4.598	6.506	8.477	9.829
0.599	0.742	0.951	1.270	1.819	2.915	4.477	6.480	8.674	10.344
0.686	0.821	1.031	1.357	1.916	3.009	4.527	6.422	8.433	9.893
0.634	0.794	1.024	1.367	1.956	3.122	4.765	6.837	9.043	10.606
0.789	0.905	1.085	1.378	1.900	2.941	4.401	6.237	8.195	9.616
0.197	0.328	0.547	0.887	1.475	2.693	4.495	6.873	9.531	11.571
0.582	0.709	0.907	1.220	1.772	2.888	4.498	6.582	8.882	10.638
0.788	0.951	1.178	1.513	2.080	3.174	4.676	6.530	8.472	9.846
0.496	0.689	0.954	1.317	1.892	2.969	4.420	6.188	8.018	9.307
0.864	1.035	1.262	1.601	2.193	3.375	5.059	7.215	9.553	11.229
0.521	0.723	0.998	1.374	1.975	3.123	4.705	6.676	8.771	10.294
0.586	0.742	0.966	1.296	1.845	2.903	4.354	6.136	7.983	9.251
0.510	0.655	0.868	1.183	1.712	2.732	4.123	5.818	7.574	8.837
0.324	0.484	0.728	1.084	1.667	2.803	4.383	6.353	8.423	9.868
0.478	0.688	0.976	1.359	1.947	3.008	4.382	5.984	7.558	8.582
0.425	0.572	0.787	1.103	1.633	2.682	4.173	6.090	8.209	9.881
0.123	0.284	0.493	0.823	1.392	2.566	4.289	6.540	9.027	10.914
0.350	0.522	0.781	1.149	1.739	2.853	4.359	6.190	8.082	9.424
0.674	0.814	1.031	1.369	1.958	3.131	4.790	6.893	9.151	10.780
0.110	0.323	0.675	1.189	1.952	3.291	4.982	6.916	8.771	9.904
0.363	0.584	0.908	1.349	2.029	3.276	4.914	6.841	8.737	9.923
0.101	0.285	0.577	1.015	1.696	2.943	4.570	6.477	8.362	9.594
0.721	0.895	1.122	1.448	2.002	3.093	4.624	6.559	8.645	10.193
0.510	0.690	0.930	1.264	1.814	2.896	4.431	6.400	8.568	10.245
0.610	0.738	0.927	1.223	1.747	2.823	4.401	6.489	8.856	10.743
0.447	0.636	0.901	1.267	1.855	2.983	4.551	6.529	8.668	10.275
1.167	1.692	2.253	2.814	3.530	4.682	6.052	7.530	8.828	9.413
0.439	0.721	1.119	1.621	2.328	3.498	4.886	6.366	7.670	8.342
0.356	0.559	0.845	1.233	1.848	3.023	4.651	6.690	8.869	10.469
0.688	0.866	1.116	1.473	2.061	3.185	4.719	6.611	8.594	10.001
0.688	0.866	1.116	1.473	2.061	3.185	4.719	6.611	8.594	10.001
0.858	1.062	1.327	1.699	2.307	3.430	4.896	6.611	8.288	9.324

continued

Micrometer [%]

9.291	7.813	6.57	5.524	4.645	3.906	3.285	2.762	2.323	1.953	1.642
12.597	11.430	9.335	6.908	4.877	3.310	2.045	1.316	0.793	0.417	0.153
11.027	10.325	8.929	7.185	5.596	4.242	2.986	2.138	1.442	0.872	0.476
9.013	8.603	7.633	6.338	5.111	4.028	2.978	2.226	1.572	1.001	0.579
10.910	10.398	9.188	7.572	6.050	4.721	3.448	2.549	1.779	1.116	0.634
8.806	8.494	7.654	6.485	5.354	4.337	3.322	2.560	1.865	1.227	0.734
10.161	9.610	8.430	6.903	5.475	4.223	3.019	2.175	1.468	0.886	0.484
9.678	9.011	7.761	6.239	4.866	3.700	2.620	1.889	1.288	0.792	0.443
10.388	9.922	8.802	7.299	5.875	4.621	3.407	2.540	1.787	1.134	0.654
10.573	10.103	8.989	7.495	6.081	4.832	3.615	2.731	1.950	1.257	0.737
9.878	9.231	8.033	6.572	5.244	4.092	2.983	2.194	1.517	0.943	0.533
10.606	10.068	8.876	7.317	5.861	4.589	3.369	2.504	1.758	1.113	0.641
10.051	9.483	8.327	6.869	5.525	4.355	3.228	2.422	1.721	1.107	0.651
10.677	9.923	8.519	6.807	5.261	3.945	2.724	1.906	1.249	0.730	0.385
9.762	9.199	8.062	6.626	5.297	4.134	3.008	2.206	1.520	0.939	0.525
11.865	11.179	9.702	7.796	6.052	4.573	3.213	2.300	1.553	0.941	0.514
10.899	10.307	9.021	7.353	5.808	4.472	3.213	2.342	1.611	0.996	0.559
9.954	9.370	8.233	6.819	5.519	4.385	3.280	2.473	1.756	1.121	0.647
9.427	8.920	7.907	6.631	5.445	4.396	3.350	2.562	1.844	1.195	0.703
11.280	10.421	8.863	7.001	5.359	3.998	2.778	1.977	1.327	0.796	0.425
10.461	9.880	8.700	7.206	5.829	4.634	3.482	2.647	1.904	1.236	0.727
9.294	8.677	7.542	6.169	4.932	3.873	2.870	2.159	1.540	0.995	0.585
9.027	8.645	7.796	6.681	5.622	4.667	3.683	2.908	2.170	1.473	0.922
9.934	9.258	7.999	6.466	5.088	3.918	2.829	2.079	1.447	0.911	0.521
8.608	8.130	7.253	6.195	5.233	4.387	3.526	2.836	2.156	1.486	0.934
10.254	9.891	8.912	7.547	6.231	5.055	3.885	3.007	2.202	1.459	0.879
11.184	10.556	9.193	7.421	5.781	4.366	3.039	2.141	1.414	0.835	0.446
9.586	9.124	8.157	6.913	5.751	4.717	3.674	2.870	2.119	1.416	0.866
10.897	10.176	8.789	7.084	5.545	4.237	3.024	2.196	1.507	0.930	0.519
9.818	9.132	7.984	6.647	5.459	4.439	3.439	2.685	1.984	1.328	0.812
9.837	9.109	7.885	6.461	5.195	4.109	3.064	2.306	1.637	1.048	0.611
9.629	9.064	8.026	6.762	5.614	4.613	3.614	2.847	2.122	1.435	0.889
10.391	9.834	8.665	7.167	5.777	4.567	3.400	2.562	1.825	1.173	0.683
10.549	10.074	8.954	7.457	6.042	4.795	3.583	2.705	1.928	1.239	0.721
11.107	10.576	9.305	7.598	5.992	4.595	3.277	2.369	1.613	0.984	0.541
10.519	10.001	8.860	7.372	5.981	4.764	3.583	2.723	1.955	1.266	0.742
9.013	8.136	6.914	5.642	4.571	3.680	2.837	2.218	1.650	1.116	0.690
8.154	7.572	6.693	5.738	4.917	4.220	3.519	2.938	2.332	1.694	1.135
10.665	10.091	8.894	7.362	5.944	4.711	3.522	2.665	1.908	1.234	0.725
10.116	9.523	8.364	6.925	5.606	4.463	3.360	2.560	1.846	1.205	0.715
10.116	9.523	8.364	6.925	5.606	4.463	3.360	2.560	1.846	1.205	0.715
9.228	8.552	7.431	6.141	4.997	4.015	3.061	2.351	1.704	1.112	0.656

continued

Micrometer [%]

1.381	1.161	0.977	0.821	0.691	0.581	0.488	0.411	0.345	0.29	0.244
0.000	0.000	0.000	0.000	0.000	0.000	0.000	0.000	0.000	0.000	0.000
0.271	0.161	0.007	0.000	0.000	0.113	0.198	0.265	0.305	0.275	0.185
0.348	0.218	0.153	0.142	0.171	0.266	0.539	1.048	1.849	2.729	2.872
0.375	0.231	0.158	0.141	0.157	0.207	0.305	0.400	0.447	0.386	0.249
0.452	0.290	0.208	0.195	0.236	0.362	0.715	1.347	2.293	3.240	3.265
0.279	0.170	0.008	0.000	0.095	0.232	0.472	0.870	1.380	1.714	1.477
0.259	0.158	0.007	0.000	0.079	0.191	0.400	0.806	1.483	2.304	2.552
0.393	0.247	0.173	0.157	0.178	0.236	0.348	0.455	0.502	0.427	0.270
0.449	0.286	0.203	0.185	0.209	0.276	0.401	0.514	0.557	0.464	0.288
0.317	0.199	0.144	0.140	0.178	0.286	0.572	1.028	1.585	1.908	1.595
0.384	0.241	0.168	0.152	0.171	0.227	0.334	0.436	0.481	0.410	0.260
0.400	0.259	0.188	0.177	0.205	0.277	0.412	0.536	0.585	0.488	0.302
0.215	0.045	0.000	0.000	0.000	0.141	0.335	0.635	1.043	1.353	1.219
0.308	0.190	0.113	0.051	0.157	0.247	0.484	0.860	1.321	1.592	1.341
0.292	0.172	0.008	0.000	0.000	0.109	0.185	0.242	0.273	0.244	0.125
0.327	0.199	0.116	0.000	0.084	0.174	0.256	0.336	0.376	0.327	0.213
0.387	0.242	0.170	0.157	0.184	0.263	0.442	0.665	0.855	0.853	0.613
0.430	0.277	0.202	0.195	0.243	0.377	0.715	1.220	1.788	2.043	1.635
0.233	0.048	0.000	0.000	0.000	0.000	0.000	0.000	0.000	0.000	0.000
0.442	0.278	0.193	0.171	0.186	0.238	0.334	0.420	0.449	0.374	0.234
0.356	0.226	0.159	0.148	0.178	0.272	0.541	1.032	1.793	2.612	2.728
0.603	0.420	0.335	0.346	0.441	0.661	1.115	1.621	1.957	1.781	1.152
0.310	0.193	0.114	0.049	0.149	0.231	0.471	0.924	1.653	2.491	2.684
0.606	0.412	0.316	0.314	0.391	0.593	1.065	1.710	2.349	2.498	1.872
0.547	0.354	0.254	0.231	0.257	0.330	0.461	0.570	0.594	0.477	0.288
0.252	0.151	0.007	0.000	0.081	0.196	0.400	0.739	1.182	1.490	1.307
0.551	0.370	0.281	0.278	0.342	0.502	0.840	1.230	1.513	1.417	0.948
0.301	0.182	0.008	0.000	0.000	0.122	0.205	0.264	0.293	0.255	0.128
0.514	0.343	0.257	0.251	0.306	0.446	0.746	1.098	1.363	1.295	0.880
0.372	0.238	0.174	0.168	0.210	0.327	0.623	1.072	1.589	1.841	1.498
0.572	0.388	0.299	0.299	0.371	0.548	0.923	1.355	1.666	1.555	1.034
0.412	0.258	0.178	0.157	0.171	0.217	0.305	0.383	0.410	0.342	0.215
0.434	0.272	0.188	0.168	0.185	0.239	0.341	0.434	0.470	0.394	0.248
0.309	0.184	0.008	0.000	0.000	0.116	0.195	0.251	0.278	0.244	0.123
0.449	0.282	0.195	0.174	0.192	0.249	0.356	0.455	0.494	0.415	0.261
0.440	0.293	0.217	0.204	0.233	0.310	0.450	0.572	0.611	0.501	0.305
0.784	0.570	0.469	0.487	0.613	0.896	1.449	2.018	2.338	2.038	1.268
0.441	0.279	0.195	0.174	0.192	0.246	0.347	0.436	0.465	0.385	0.240
0.440	0.282	0.201	0.183	0.205	0.269	0.388	0.495	0.533	0.443	0.275
0.440	0.282	0.201	0.183	0.205	0.269	0.388	0.495	0.533	0.443	0.275
0.400	0.255	0.182	0.172	0.210	0.319	0.596	1.012	1.489	1.719	1.398

continued

Micrometer [%]

0.205	0.173	0.145	0.122
0.000	0.000	0.000	0.000
0.061	0.000	0.000	0.000
2.145	1.258	0.485	0.118
0.079	0.000	0.000	0.000
2.349	1.325	0.491	0.117
0.919	0.448	0.132	0.000
1.993	1.223	0.495	0.124
0.085	0.000	0.000	0.000
0.090	0.000	0.000	0.000
0.969	0.462	0.133	0.000
0.082	0.000	0.000	0.000
0.094	0.000	0.000	0.000
0.789	0.401	0.124	0.000
0.824	0.399	0.118	0.000
0.000	0.000	0.000	0.000
0.068	0.000	0.000	0.000
0.340	0.058	0.000	0.000
0.962	0.446	0.126	0.000
0.000	0.000	0.000	0.000
0.073	0.000	0.000	0.000
2.034	1.195	0.464	0.114
0.577	0.234	0.003	0.000
2.053	1.236	0.491	0.122
1.045	0.461	0.124	0.000
0.088	0.000	0.000	0.000
0.829	0.414	0.126	0.000
0.491	0.206	0.003	0.000
0.000	0.000	0.000	0.000
0.463	0.197	0.003	0.000
0.895	0.423	0.122	0.000
0.532	0.221	0.003	0.000
0.068	0.000	0.000	0.000
0.078	0.000	0.000	0.000
0.000	0.000	0.000	0.000
0.082	0.000	0.000	0.000
0.094	0.000	0.000	0.000
0.616	0.242	0.003	0.000
0.075	0.000	0.000	0.000
0.085	0.000	0.000	0.000
0.085	0.000	0.000	0.000
0.836	0.396	0.114	0.000

Appendix C

Physical sediment properties for gravity cores 2009, Hudson Bay

Appendix C contains data for magnetic susceptibility loop and point sensors (MS-loop, MS-point; m^3/kg), sediment density [g/cm^3], and fractional porosity for each depth interval [cm] for the Great Whale River study site. Each depth interval was converted to Year BC/AD using $^{14}\text{C}_{\text{cal}}$ -ages and interpolating between dates. Sediment cores were scanned using a Geotek Multi-Sensor-Core-Logger. Magnetic susceptibility was measured using the Bartington Meter Model MS2 with the loop sensor MS2C and the point sensor MS2E1. Bulk desndity was measured using the Geotek gamma densitometer, which contains a ^{137}Cs source, that emits a narrow beam of gamma rays. The gamma rays pass through the centre of the core and are recorded on the other side by a detector. Porosity is calculated by the Geotek calibration software directly from gamma density.

Core-ID: RA09-GW-4-P'

Depth [cm]	Year BC/AD	MS-loop [m ³ /kg]	MS-point [m ³ /kg]	Density [g/cm ³]	Porosity
0.5	2009		223	1.47	0.74
1	2006		215	1.47	0.74
1.5	2004		218	1.47	0.74
2	2001		217	1.47	0.74
2.5	1999		209	1.48	0.74
3	1996		224	1.50	0.72
3.5	1994		223	1.51	0.72
4	1991	95	220	1.50	0.72
4.5	1988	102	227	1.49	0.73
5	1986	104	225	1.49	0.73
5.5	1983	105	220	1.49	0.73
6	1981	105	215	1.48	0.74
6.5	1978	105	227	1.47	0.74
7	1976	108	215	1.47	0.74
7.5	1973	107	209	1.48	0.74
8	1970	107	188	1.49	0.73
8.5	1968	109	234	1.49	0.73
9	1965	109	232	1.50	0.73
9.5	1963	110	213	1.49	0.73
10	1960	113	210	1.48	0.74
10.5	1958	113	207	1.44	0.76
11	1955	112	217	1.46	0.75
11.5	1952	110	217	1.46	0.75
12	1950	110	217	1.49	0.73
12.5	1947	109	217	1.49	0.73
13	1945	110	237	1.52	0.71
13.5	1942	109	231	1.50	0.72
14	1940	112	227	1.52	0.71
14.5	1937	112	221	1.51	0.72
15	1934	111	221	1.51	0.72
15.5	1932	112	221	1.52	0.71
16	1929	112	206	1.51	0.72
16.5	1927	112	201	1.51	0.72
17	1924	112	203	1.51	0.72
17.5	1922	113	212	1.51	0.72
18	1919		212	1.51	0.72
18.5	1916	112	206	1.52	0.71
19	1914	112	201	1.53	0.71
19.5	1911	110	207	1.55	0.70
20	1909	112	224	1.57	0.68
20.5	1906	113	218	1.55	0.70
21	1904	114	221	1.56	0.69
21.5	1901	114	207	1.57	0.68
22	1898	115	230	1.57	0.68
22.5	1896	115	233	1.58	0.68

continued

Depth [cm]	Year BC/AD	MS-loop [m ³ /kg]	MS-point [m ³ /kg]	Density [g/cm ³]	Porosity
23	1893	117	225	1.58	0.68
23.5	1891	115	225	1.56	0.69
24	1888	115	224	1.58	0.68
24.5	1886	116	211	1.60	0.67
25	1883	116	218	1.59	0.67
25.5	1881	116	226	1.60	0.67
26	1878	118	228	1.60	0.67
26.5	1875	119	214	1.58	0.68
27	1873	118	225	1.57	0.68
27.5	1870	119	228	1.59	0.67
28	1868	118	233	1.58	0.68
28.5	1865	118	221	1.59	0.67
29	1863	117	215	1.60	0.67
29.5	1860	118	215	1.60	0.67
30	1857	118	217	1.59	0.67
30.5	1855	119	234	1.60	0.67
31	1852	119	223	1.60	0.67
31.5	1850	118	239	1.60	0.67
32	1847	120	239	1.61	0.66
32.5	1845	120	239	1.59	0.67
33	1842	120	239	1.59	0.68
33.5	1839	120	222	1.59	0.68
34	1837	119	232	1.59	0.67
34.5	1834		230	1.60	0.67
35	1832		235	1.58	0.68
35.5	1829	120	235	1.59	0.68
36	1827	122	241	1.58	0.68
36.5	1824	120	233	1.58	0.68
37	1821	120	218	1.60	0.67
37.5	1819	119	206	1.59	0.67
38	1816	121	203	1.61	0.66
38.5	1814	121	226	1.59	0.67
39	1811	120	241	1.60	0.67
39.5	1809	120	240	1.62	0.65
40	1806	119	252	1.63	0.65
40.5	1803	119	253	1.64	0.64
41	1801	120	254	1.64	0.64
41.5	1798	120	251	1.63	0.65
42	1796	122	257	1.64	0.65
42.5	1793	121	260	1.60	0.66
43	1791	121	227	1.62	0.65
43.5	1788	119	220	1.62	0.65
44	1785	121	245	1.63	0.65
44.5	1783	123	240	1.61	0.66
45	1780	123	229	1.58	0.68

continued

Depth [cm]	Year BC/AD	MS-loop [m ³ /kg]	MS-point [m ³ /kg]	Density [g/cm ³]	Porosity
45.5	1778	122	235	1.58	0.68
46	1775	123	243	1.59	0.67
46.5	1773	119	240	1.58	0.68
47	1770	119	243	1.59	0.67
47.5	1767	120	226	1.59	0.67
48	1765	121	226	1.58	0.68
48.5	1762	119	224	1.57	0.68
49	1760	119	222	1.58	0.68
49.5	1757	117	217	1.59	0.67
50	1755	117	220	1.60	0.67
50.5	1752	118	227	1.60	0.67
51	1746	116	240	1.61	0.66
51.5	1741	116	258	1.63	0.65
52	1735	117	262	1.64	0.64
52.5	1730	117	265	1.64	0.65
53	1724	117	255	1.64	0.64
53.5	1719	121	234	1.64	0.64
54	1713	121	232	1.62	0.65
54.5	1708	123	246	1.62	0.66
55	1702	122	254	1.60	0.66
55.5	1697	123	252	1.62	0.65
56	1691	123	251	1.62	0.65
56.5	1686	124	248	1.62	0.66
57	1680	123	244	1.61	0.66
57.5	1675	122	256	1.62	0.66
58	1669	124	247	1.63	0.65
58.5	1664	124	216	1.60	0.66
59	1658	123	239	1.60	0.67
59.5	1652	123	242	1.60	0.67
60	1647	121	247	1.61	0.66
60.5	1641	122	244	1.62	0.66
61	1636	121	239	1.60	0.67
61.5	1630	120	243	1.60	0.67
62	1625	120	238	1.61	0.66
62.5	1619	119	231	1.61	0.66
63	1614	120	235	1.60	0.67
63.5	1608	121	221	1.59	0.67
64	1603	120	219	1.58	0.68
64.5	1597	120	219	1.58	0.68
65	1592	119	235	1.58	0.68
65.5	1586	119	230	1.60	0.66
66	1581	119	226	1.60	0.67
66.5	1575	119	235	1.61	0.66
67	1570	119	236	1.60	0.67
67.5	1564	120	216	1.60	0.66

continued

Depth [cm]	Year BC/AD	MS-loop [m ³ /kg]	MS-point [m ³ /kg]	Density [g/cm ³]	Porosity
68	1558	119	230	1.59	0.67
68.5	1553	120	231	1.60	0.67
69	1547	119	232	1.58	0.68
69.5	1542	119	225	1.58	0.68
70	1536	118	217	1.58	0.68
70.5	1531	117	212	1.59	0.67
71	1525	118	212	1.60	0.66
71.5	1520	118	220	1.60	0.67
72	1514	119	231	1.60	0.67
72.5	1509	117	232	1.59	0.68
73	1503	118	226	1.60	0.67
73.5	1498	118	229	1.59	0.68
74	1492	118	244	1.60	0.67
74.5	1487	119	243	1.59	0.67
75	1481	118	221	1.59	0.67
75.5	1476	119	224	1.59	0.67
76	1470	118	236	1.60	0.67
76.5	1464	118	237	1.61	0.66
77	1459	119	237	1.62	0.66
77.5	1453	120	236	1.61	0.66
78	1448	121	231	1.60	0.67
78.5	1442	121	232	1.59	0.67
79	1437	123	231	1.59	0.67
79.5	1431	121	248	1.59	0.67
80	1426	121	248	1.61	0.66
80.5	1420	120	267	1.63	0.65
81	1415	122	267	1.64	0.64
81.5	1409	122	267	1.62	0.65
82	1404	121	263	1.64	0.65
82.5	1398	123	261	1.64	0.64
83	1393	124	246	1.62	0.66
83.5	1387	125	228	1.61	0.66
84	1382	125	225	1.60	0.67
84.5	1376	125	231	1.60	0.67
85	1370	122	231	1.60	0.67
85.5	1365	121	215	1.60	0.67
86	1363	122	223	1.61	0.66
86.5	1360	121	231	1.59	0.67
87	1358	119	238	1.59	0.67
87.5	1355	119	239	1.60	0.67
88	1353	120	217	1.60	0.67
88.5	1350	121	225	1.58	0.68
89	1348	119	252	1.57	0.68
89.5	1345	119	248	1.59	0.67
90	1343	119	246	1.60	0.67

continued

Depth [cm]	Year BC/AD	MS-loop [m ³ /kg]	MS-point [m ³ /kg]	Density [g/cm ³]	Porosity
90.5	1340	119	234	1.59	0.67
91	1338	118	234	1.59	0.68
91.5	1336	120	221	1.60	0.67
92	1333	119	225	1.58	0.68
92.5	1331	119	231	1.57	0.68
93	1328	118	241	1.57	0.69
93.5	1326	117	236	1.58	0.68
94	1323	118	227	1.60	0.67
94.5	1321	117	239	1.58	0.68
95	1318	116	233	1.59	0.67
95.5	1316	116	234	1.60	0.67
96	1314	117	226	1.62	0.66
96.5	1311	116	164	1.59	0.67
97	1309	117	164	1.60	0.67
97.5	1306	118	242	1.60	0.67
98	1304	118	242	1.60	0.67
98.5	1301	119	239	1.62	0.66
99	1299	119	247	1.60	0.66
99.5	1296	118	239	1.60	0.67
100	1294	119	248	1.62	0.66
100.5	1291	120	245	1.60	0.67
101	1289	119	250	1.60	0.67
101.5	1287	120	242	1.62	0.66
102	1284	120	239	1.60	0.67
102.5	1282	121	243	1.61	0.66
103	1279	119	242	1.60	0.67
103.5	1277	120	245	1.62	0.66
104	1274	120	238	1.60	0.66
104.5	1272	120	233	1.61	0.66
105	1269	120	229	1.59	0.67
105.5	1267	121	245	1.60	0.66
106	1265	120	237	1.59	0.67
106.5	1262	120	229	1.58	0.68
107	1260	121	226	1.58	0.68
107.5	1257	120	228	1.58	0.68
108	1255	119	228	1.58	0.68
108.5	1252	118	227	1.58	0.68
109	1250	119	229	1.60	0.67
109.5	1247	119	235	1.59	0.67
110	1245	119	231	1.59	0.67
110.5	1242	119	227	1.59	0.67
111	1240	119	222	1.60	0.67
111.5	1238	118	238	1.59	0.67
112	1235	119	250	1.60	0.67
112.5	1233	117	251	1.59	0.67

continued

Depth [cm]	Year BC/AD	MS-loop [m ³ /kg]	MS-point [m ³ /kg]	Density [g/cm ³]	Porosity
113	1230	117	232	1.61	0.66
113.5	1228	117	224	1.61	0.66
114	1225	118	235	1.59	0.67
114.5	1223	118	242	1.58	0.68
115	1220	118	239	1.58	0.68
115.5	1218	118	216	1.58	0.68
116	1216	116	218	1.57	0.68
116.5	1213	114	208	1.58	0.68
117	1211	116	211	1.60	0.67
117.5	1208	116	211	1.58	0.68
118	1206	116	225	1.57	0.68
118.5	1203	115	221	1.57	0.68
119	1201	113	209	1.58	0.68
119.5	1198	114	227	1.60	0.67
120	1196	114	225	1.58	0.68
120.5	1193	114	214	1.59	0.67
121	1191	114	205	1.58	0.68
121.5	1189	115	207	1.59	0.68
122	1186	114	206	1.59	0.67
122.5	1184	114	216	1.60	0.67
123	1181	114	223	1.59	0.67
123.5	1179	114	231	1.59	0.67
124	1176	113	224	1.60	0.66
124.5	1174	114	220	1.61	0.66
125	1171	114	218	1.60	0.67
125.5	1169	114	221	1.59	0.67
126	1167	114	213	1.60	0.67
126.5	1164	114	219	1.59	0.67
127	1162	115	226	1.60	0.67
127.5	1159	118	230	1.58	0.68
128	1157	117	213	1.57	0.69
128.5	1154	117	221	1.57	0.68
129	1152	117	223	1.58	0.68
129.5	1149	116	225	1.60	0.67
130	1147	117	218	1.61	0.66
130.5	1144	119	188	1.61	0.66
131	1142	117	200	1.58	0.68
131.5	1140	118	216	1.61	0.66
132	1137	120	225	1.60	0.67
132.5	1135	119	236	1.60	0.67
133	1132	120	230	1.61	0.66
133.5	1130	120	230	1.62	0.65
134	1127	121	242	1.63	0.65
134.5	1125	122	246	1.63	0.65
135	1122	122	246	1.62	0.66

continued

Depth [cm]	Year BC/AD	MS-loop [m ³ /kg]	MS-point [m ³ /kg]	Density [g/cm ³]	Porosity
135.5	1120	123	247	1.61	0.66
136	1118	124	252	1.62	0.65
136.5	1115	125	248	1.61	0.66
137	1113	126	241	1.60	0.67
137.5	1110	126	242	1.61	0.66
138	1108	126	244	1.60	0.66
138.5	1105	126	241	1.61	0.66
139	1103	126		1.61	0.66
139.5	1100	126	252	1.60	0.66
140	1098	126	250	1.61	0.66
140.5	1095	126	249	1.61	0.66
141	1093	125	248	1.61	0.66
141.5	1091	126	233	1.62	0.65
142	1088	126	233	1.61	0.66
142.5	1086	125	240	1.61	0.66
143	1083	124	242	1.62	0.65
143.5	1081	125	254	1.64	0.64
144	1078	126	268	1.63	0.65
144.5	1076	126	274	1.62	0.65
145	1073	124	274	1.63	0.65
145.5	1071	125	242	1.63	0.65
146	1069	126	242	1.61	0.66
146.5	1066	125	242	1.59	0.67
147	1064	123	198	1.60	0.67
147.5	1061	121	221	1.63	0.65
148	1059	122	240	1.63	0.65
148.5	1056	122	241	1.62	0.66
149	1054	121	241	1.62	0.66
149.5	1051	122	235	1.61	0.66
150	1049	121	231	1.59	0.67
150.5	1046	121	229	1.59	0.67
151	1044	120	231	1.60	0.67
151.5	1042	120	240	1.59	0.67
152	1039	119	232	1.59	0.68
152.5	1037	119	231	1.59	0.68
153	1034	120	222	1.59	0.67
153.5	1032	118	222	1.57	0.68
154	1029	119	211	1.58	0.68
154.5	1027	118	217	1.57	0.69
155	1024	117	220	1.59	0.67
155.5	1022	116	210	1.60	0.67
156	1020	115	218	1.61	0.66
156.5	1017	115	219	1.62	0.66
157	1015	115	223	1.62	0.66
157.5	1012	117		1.62	0.66

continued

Depth [cm]	Year BC/AD	MS-loop [m ³ /kg]	MS-point [m ³ /kg]	Density [g/cm ³]	Porosity
158	1010	115		1.60	0.67
158.5	1007	116	225	1.63	0.65
159	1005	116	240	1.63	0.65
159.5	1002	116	242	1.64	0.64
160	1000	117	243	1.63	0.65
160.5	998	118	255	1.65	0.64
161	995	120	252	1.65	0.64
161.5	993	120	252	1.63	0.65
162	990	121	238	1.64	0.64
162.5	988	121	232	1.64	0.65
163	985	124	230	1.63	0.65
163.5	983	124	230	1.60	0.67
164	981	124	235	1.60	0.67
164.5	978	123	243	1.62	0.66
165	976	124	248	1.63	0.65
165.5	973	125	251	1.61	0.66
166	971	126	245	1.61	0.66
166.5	968	126	230	1.61	0.66
167	966	127	237	1.62	0.66
167.5	963	127	253	1.61	0.66
168	961	126	264	1.60	0.66
168.5	959	126	267	1.62	0.66
169	956	126	259	1.62	0.65
169.5	954	126	251	1.63	0.65
170	951	125	258	1.63	0.65
170.5	949	127	276	1.64	0.64
171	946	127	275	1.62	0.66
171.5	944	128	256	1.62	0.65
172	942	128	256	1.60	0.67
172.5	939	128	248	1.61	0.66
173	937	128	249	1.61	0.66
173.5	934	127	241	1.60	0.67
174	932	128	225	1.61	0.66
174.5	929	126	221	1.60	0.67
175	927	127	234	1.61	0.66
175.5	924	127	235	1.61	0.66
176	922	127		1.61	0.66
176.5	920	126	242	1.62	0.66
177	917	127	243	1.62	0.66
177.5	915	126	237	1.62	0.66
178	912	128	239	1.62	0.66
178.5	910	126	237	1.59	0.67
179	907	127	236	1.61	0.66
179.5	905	126	234	1.61	0.66
180	903	126	230	1.62	0.66

continued

Depth [cm]	Year BC/AD	MS-loop [m ³ /kg]	MS-point [m ³ /kg]	Density [g/cm ³]	Porosity
180.5	900	126	248	1.62	0.65
181	898	125	247	1.63	0.65
181.5	895	125	242	1.64	0.64
182	893		227	1.63	0.65
182.5	890		226	1.64	0.64
183	888		182	1.64	0.65
183.5	885		190	1.64	0.65
184	883		233	1.63	0.65
184.5	881		233	1.62	0.65
185	878	124	236	1.62	0.66
185.5	876	124	244	1.61	0.66
186	873	124	253	1.61	0.66
186.5	871	122	241	1.61	0.66
187	868	122	239	1.60	0.66
187.5	866	122	232	1.60	0.67
188	864	123	235	1.60	0.67
188.5	861	123	224	1.59	0.68
189	859	121	208	1.59	0.67
189.5	856	119	204	1.61	0.66
190	854	119	218	1.60	0.67
190.5	851	120	211	1.60	0.67
191	849	118	196	1.60	0.67
191.5	846	119		1.60	0.67
192	844	118	233	1.59	0.67
192.5	842	116	227	1.59	0.67
193	839	115	224	1.60	0.67
193.5	837	114	222	1.62	0.66
194	834	114	214	1.61	0.66
194.5	832	113	217	1.61	0.66
195	829	113	226	1.61	0.66
195.5	827	111	226	1.62	0.66

Core-ID: RA09-GW-7-P10

Depth [cm]	Year BC/AD	MS-loop [m ³ /kg]	MS-point [m ³ /kg]	Density [g/cm ³]	Porosity
0.5	2009			1.49	0.73
1	2005			1.50	0.72
1.5	2001			1.50	0.73
2	1997	129		1.50	0.72
2.5	1993	135		1.51	0.72
3	1989	138		1.51	0.72
3.5	1984	142		1.49	0.73
4	1980	140	307	1.51	0.72
4.5	1976	140	280	1.50	0.72
5	1972	150	291	1.53	0.71
5.5	1968	150	299	1.52	0.71
6	1964	155	279	1.53	0.71
6.5	1960	157	291	1.53	0.71
7	1956	158	300	1.53	0.71
7.5	1952	154	278	1.51	0.72
8	1948	159	295	1.55	0.69
8.5	1944	161	290	1.59	0.67
9	1939	165	238	1.60	0.67
9.5	1935	170	211	1.60	0.67
10	1931	168	211	1.58	0.68
10.5	1927	167	294	1.56	0.69
11	1923	168	303	1.59	0.67
11.5	1919	166	323	1.61	0.66
12	1915	166	342	1.60	0.67
12.5	1911	176	336	1.62	0.65
13	1907	178	335	1.62	0.66
13.5	1903		324	1.62	0.66
14	1899	181	328	1.62	0.66
14.5	1894	182	354	1.61	0.66
15	1890	183	363	1.62	0.66
15.5	1886	183	376	1.63	0.65
16	1882	183	364	1.62	0.66
16.5	1878	182	354	1.63	0.65
17	1874	184	351	1.64	0.64
17.5	1870	184	353	1.64	0.64
18	1866	186	361	1.65	0.64
18.5	1862	187	326	1.65	0.64
19	1858	189	327	1.63	0.65
19.5	1854	188	319	1.62	0.65
20	1849	188	343	1.60	0.67
20.5	1845	187	360	1.60	0.67
21	1841	188	345	1.59	0.68
21.5	1837	186	346	1.59	0.67
22	1833	183	300	1.59	0.67
22.5	1829	184	349	1.60	0.67

continued

Depth [cm]	Year BC/AD	MS-loop [m ³ /kg]	MS-point [m ³ /kg]	Density [g/cm ³]	Porosity
23	1825	180	321	1.59	0.67
23.5	1821	178	330	1.58	0.68
24	1817	178	333	1.60	0.66
24.5	1813	178	333	1.62	0.66
25	1809	177	360	1.61	0.66
25.5	1804	176	360	1.61	0.66
26	1800	178	323	1.61	0.66
26.5	1796	177	309	1.62	0.66
27	1792	176	294	1.60	0.66
27.5	1788	177	260	1.61	0.66
28	1784	175	273	1.62	0.66
28.5	1780	175	297	1.61	0.66
29	1776	177	264	1.63	0.65
29.5	1772	177	281	1.64	0.64
30	1768	179	259	1.63	0.65
30.5	1764	177	272	1.63	0.65
31	1759	179	258	1.61	0.66
31.5	1755	179	277	1.63	0.65
32	1751	179		1.62	0.66
32.5	1747	179		1.61	0.66
33	1743	178	237	1.61	0.66
33.5	1739	179	237	1.61	0.66
34	1735	179	237	1.63	0.65
34.5	1731	178	220	1.61	0.66
35	1727		312	1.61	0.66
35.5	1723		323	1.62	0.65
36	1719	180	346	1.62	0.65
36.5	1714	179	350	1.61	0.66
37	1710	179	321	1.62	0.66
37.5	1706	180	319	1.64	0.65
38	1702	180	303	1.64	0.64
38.5	1698	182	247	1.64	0.64
39	1694	182	307	1.64	0.64
39.5	1690	183	328	1.63	0.65
40	1686	183	338	1.62	0.65
40.5	1682	183	345	1.62	0.66
41	1678	184	350	1.62	0.66
41.5	1674	181	301	1.62	0.65
42	1669	184	316	1.61	0.66
42.5	1665	181	352	1.62	0.65
43	1661	182	349	1.60	0.67
43.5	1657	181	316	1.61	0.66
44	1653	179	360	1.60	0.66
44.5	1649	179	337	1.61	0.66
45	1645	173	356	1.62	0.66

continued

Depth [cm]	Year BC/AD	MS-loop [m ³ /kg]	MS-point [m ³ /kg]	Density [g/cm ³]	Porosity
45.5	1641	176	359	1.61	0.66
46	1637	176	346	1.67	0.63
46.5	1633	177	344	1.64	0.64
47	1629	176	335	1.62	0.65
47.5	1624	176	295	1.62	0.65
48	1620	173	305	1.63	0.65
48.5	1616	175	276	1.63	0.65
49	1612	175	276	1.66	0.63
49.5	1608	177	276	1.65	0.64
50	1604	178	387	1.65	0.64
50.5	1600	178	387	1.64	0.64
51	1596	179	387	1.65	0.64
51.5	1592	181	250	1.65	0.64
52	1588	185	250	1.64	0.64
52.5	1584	184	334	1.64	0.64
53	1579	185	352	1.61	0.66
53.5	1575		345	1.62	0.66
54	1571	185	345	1.63	0.65
54.5	1567	186	354	1.64	0.64
55	1563	185	359	1.62	0.65
55.5	1559	185	370	1.62	0.66
56	1554	183	369	1.62	0.65
56.5	1548	183	324	1.62	0.65
57	1543	183	347	1.65	0.64
57.5	1538	185	359	1.63	0.65
58	1533	186	357	1.64	0.65
58.5	1527	181	327	1.62	0.66
59	1522	181	320	1.61	0.66
59.5	1517	180	320	1.61	0.66
60	1511	179	302	1.60	0.66
60.5	1506	179	249	1.62	0.66
61	1501	176	245	1.62	0.65
61.5	1496	178	245	1.63	0.65
62	1490	177	245	1.63	0.65
62.5	1485		245	1.61	0.66
63	1480		339	1.62	0.66
63.5	1474	179	319	1.62	0.66
64	1469	180	315	1.61	0.66
64.5	1464	180	307	1.61	0.66
65	1459	180	303	1.60	0.67
65.5	1453	178	292	1.61	0.66
66	1448		302	1.60	0.67
66.5	1443		261	1.62	0.65
67	1437		330	1.62	0.66
67.5	1432	183	352	1.63	0.65

continued

Depth [cm]	Year BC/AD	MS-loop [m ³ /kg]	MS-point [m ³ /kg]	Density [g/cm ³]	Porosity
68	1427	184	298	1.63	0.65
68.5	1422	184	304	1.61	0.66
69	1416	184	269	1.61	0.66
69.5	1411	184	386	1.61	0.66
70	1406	183	381	1.62	0.66
70.5	1401	183	363	1.61	0.66
71	1395	183	366	1.62	0.66
71.5	1390	183	341	1.63	0.65
72	1385	181	315	1.63	0.65
72.5	1379	182	224	1.63	0.65
73	1374	185	224	1.65	0.64
73.5	1369	186	362	1.64	0.65
74	1364	188	391	1.62	0.66
74.5	1358	189	380	1.61	0.66
75	1353	187	365	1.60	0.67
75.5	1348	188	346	1.59	0.67
76	1342	188	337	1.61	0.66
76.5	1337	187	361	1.60	0.67
77	1332	187	369	1.61	0.66
77.5	1327	187	358	1.61	0.66
78	1321	185	326	1.61	0.66
78.5	1316	186	318	1.61	0.66
79	1311	183	321	1.63	0.65
79.5	1305	182	343	1.62	0.66
80	1300	182	347	1.64	0.64
80.5	1295	183	322	1.64	0.64
81	1290	180	297	1.64	0.65
81.5	1284	178	284	1.63	0.65
82	1279	179	284	1.63	0.65
82.5	1274	177	333	1.65	0.64
83	1268	176	353	1.64	0.65
83.5	1263	174	359	1.64	0.65
84	1258	172	375	1.64	0.65
84.5	1253		319	1.65	0.64
85	1247	173	254	1.66	0.63
85.5	1242		254	1.65	0.64
86	1237		326	1.64	0.65
86.5	1231	167	331	1.62	0.66
87	1226	168	327	1.63	0.65
87.5	1221	168	327	1.65	0.64
88	1216	169	304	1.65	0.64
88.5	1210	169	297	1.64	0.64
89	1205	171		1.64	0.65
89.5	1200	171	245	1.63	0.65
90	1194	173	242	1.61	0.66

continued

Depth [cm]	Year BC/AD	MS-loop [m ³ /kg]	MS-point [m ³ /kg]	Density [g/cm ³]	Porosity
90.5	1189	172	240	1.61	0.66
91	1184	172	240	1.60	0.67
91.5	1179	171	229	1.62	0.65
92	1173	171	229	1.62	0.65
92.5	1168	170	229	1.64	0.64
93	1163	172	325	1.66	0.63
93.5	1158	173	314	1.67	0.63
94	1152	172	308	1.67	0.63
94.5	1147	175	307	1.66	0.63
95	1142	175	275	1.67	0.62
95.5	1136	179	255	1.66	0.63
96	1131	184	289	1.65	0.64
96.5	1126	181	263	1.62	0.66
97	1121	182	233	1.58	0.68
97.5	1115	179	233	1.61	0.66
98	1110	176	294	1.61	0.66
98.5	1105	178	357	1.64	0.64
99	1099	176	387	1.68	0.62
99.5	1094	180	323	1.66	0.63
100	1089	182	245	1.68	0.62
100.5	1084	183	205	1.64	0.64
101	1079	186	205	1.64	0.64
101.5	1075	184	303	1.64	0.65
102	1071	182	301	1.63	0.65
102.5	1067	183	420	1.65	0.64
103	1063	187	413	1.68	0.62
103.5	1059	187	385	1.66	0.63
104	1055	188	367	1.67	0.62
104.5	1051		341	1.68	0.62
105	1047		324	1.68	0.62
105.5	1043		321	1.68	0.62
106	1039	190	352	1.68	0.62
106.5	1035	189	354	1.68	0.62
107	1031	187	312	1.68	0.62
107.5	1026	186	371	1.68	0.62
108	1022	187	382	1.70	0.61
108.5	1018	187	416	1.70	0.61
109	1014	189	394	1.69	0.61
109.5	1010	189	369	1.69	0.62
110	1006	190	316	1.67	0.62
110.5	1002	189	316	1.65	0.64
111	998	189	384	1.64	0.64
111.5	994	188	398	1.64	0.64
112	990	186	423	1.63	0.65
112.5	986	186	361	1.64	0.64

continued

Depth [cm]	Year BC/AD	MS-loop [m ³ /kg]	MS-point [m ³ /kg]	Density [g/cm ³]	Porosity
113	982	186	309	1.66	0.63
113.5	978	186	432	1.66	0.63
114	973	184	417	1.66	0.63
114.5	969	184	408	1.66	0.64
115	965	183	389	1.65	0.64
115.5	961	182	306	1.65	0.64
116	957	182	276	1.65	0.64
116.5	953	182	243	1.65	0.64
117	949	183	243	1.65	0.64
117.5	945	184	366	1.65	0.64
118	941	183	359	1.64	0.64
118.5	937	183	332	1.64	0.64
119	933	181	362	1.65	0.64
119.5	929	183	354	1.65	0.64
120	925	180	335	1.67	0.63
120.5	920	181	359	1.65	0.64
121	916	181	339	1.67	0.62
121.5	912	180	323	1.67	0.63
122	908	182	282	1.66	0.63
122.5	904	181	248	1.68	0.62
123	900	180	231	1.66	0.63
123.5	896	182	213	1.65	0.64
124	892	183	213	1.65	0.64
124.5	888	184	342	1.63	0.65
125	884		340	1.63	0.65
125.5	880		330	1.62	0.66
126	876	178	277	1.61	0.66
126.5	872	177	210	1.61	0.66
127	867	175	382	1.64	0.65
127.5	863	177	351	1.64	0.64
128	859	173	393	1.66	0.63
128.5	855	173	363	1.64	0.65
129	851	172	337	1.64	0.64
129.5	847	172	277	1.64	0.64
130	843	171	256	1.64	0.64
130.5	839	171	221	1.64	0.64
131	835	171	221	1.64	0.65
131.5	831	171	314	1.64	0.64
132	827	173	312	1.62	0.65
132.5	823	170	324	1.62	0.66
133	819	171	319	1.60	0.67
133.5	814	171	315	1.61	0.66
134	810	171	309	1.60	0.66
134.5	806	170	315	1.61	0.66
135	802	167	282	1.60	0.67

continued

Depth [cm]	Year BC/AD	MS-loop [m ³ /kg]	MS-point [m ³ /kg]	Density [g/cm ³]	Porosity
135.5	798	168	247	1.62	0.66
136	794	168	220	1.62	0.65
136.5	790	170	192	1.63	0.65
137	786	168	182	1.62	0.65
137.5	782	166	176	1.61	0.66
138	778	165	343	1.62	0.66
138.5	774		319	1.64	0.65
139	770	167	290	1.64	0.64
139.5	766	169	281	1.64	0.65
140	761	167	299	1.63	0.65
140.5	757	166	213	1.61	0.66
141	753	166	306	1.63	0.65
141.5	749	169	287	1.64	0.65
142	745	170	267	1.64	0.65
142.5	741	167	304	1.61	0.66
143	737	170	310	1.60	0.67
143.5	733	168	270	1.63	0.65
144	729	170	239	1.62	0.66
144.5	725	170	234	1.63	0.65
145	721	169	242	1.64	0.64
145.5	717	171	221	1.64	0.64
146	713	170	201	1.67	0.63
146.5	708	171	201	1.66	0.63
147	704	175	325	1.67	0.62
147.5	700	176	333	1.67	0.63
148	696	174	339	1.65	0.64
148.5	692		337	1.63	0.65
149	688	176	340	1.65	0.64
149.5	684	177	348	1.63	0.65
150	680	179	317	1.64	0.64
150.5	676	180	278	1.63	0.65
151	672	180	201	1.63	0.65
151.5	668	180	376	1.62	0.65
152	664	177	358	1.62	0.66
152.5	660	177	336	1.62	0.65
153	655	175	299	1.65	0.64
153.5	651	180	255	1.65	0.64
154	647	184	203	1.67	0.63
154.5	643	182	311	1.68	0.62
155	639	183	359	1.66	0.63
155.5	635	183	366	1.67	0.63
156	631	186	361	1.66	0.63
156.5	627	185	345	1.66	0.63
157	623	179	323	1.63	0.65
157.5	619	180	314	1.64	0.65

continued

Depth [cm]	Year BC/AD	MS-loop [m ³ /kg]	MS-point [m ³ /kg]	Density [g/cm ³]	Porosity
158	615	181	304	1.67	0.63
158.5	611	180	263	1.65	0.64
159	606	181	203	1.63	0.65
159.5	602	182	360	1.64	0.64
160	598	178	372	1.63	0.65
160.5	594	181		1.63	0.65
161	590	180		1.63	0.65
161.5	586	177		1.60	0.67
162	582	176	346	1.60	0.67
162.5	578	176	353	1.62	0.66
163	574	175	296	1.63	0.65
163.5	570	176	373	1.62	0.66
164	566	175	375	1.62	0.65
164.5	562	177	353	1.62	0.66
165	557	179	345	1.63	0.65
165.5	553	177	306	1.62	0.65
166	549	176	332	1.61	0.66
166.5	545	179	304	1.63	0.65
167	541	180	269	1.64	0.65
167.5	537	181	269	1.64	0.65
168	533	179	338	1.64	0.64
168.5	529	179	338	1.65	0.64
169	525	179	337	1.66	0.63
169.5	521	182	336	1.66	0.63
170	517	182	316	1.65	0.64
170.5	512	183	342	1.67	0.63
171	508		270	1.66	0.63
171.5	504		270	1.66	0.63
172	500			1.66	0.63
172.5	496	184		1.67	0.62
173	492	182	378	1.64	0.64
173.5	488	184	370	1.63	0.65
174	484	180	275	1.64	0.64
174.5	480	181	355	1.62	0.65
175	476	182	362	1.65	0.64
175.5	472	180	379	1.63	0.65
176	468	179	366	1.63	0.65
176.5	463	181	329	1.63	0.65
177	459	179	392	1.63	0.65
177.5	455	179	356	1.61	0.66
178	451	178	301	1.62	0.66
178.5	447	178	310	1.61	0.66
179	443	179	394	1.62	0.65
179.5	439	178	339	1.61	0.66
180	435	178	316	1.61	0.66

continued

Depth [cm]	Year BC/AD	MS-loop [m ³ /kg]	MS-point [m ³ /kg]	Density [g/cm ³]	Porosity
180.5	431	177	276	1.61	0.66
181	427	178	400	1.62	0.66
181.5	423	173	392	1.63	0.65
182	419	171	349	1.62	0.66
182.5	414	171	339	1.62	0.66
183	410	170	326	1.64	0.65
183.5	406	170	323	1.62	0.66
184	402	169	297	1.62	0.65
184.5	398	167	229	1.61	0.66
185	394	167	333	1.62	0.66
185.5	390	167	315	1.61	0.66
186	386	161	311	1.61	0.66
186.5	382	159	307	1.61	0.66
187	378	159	243	1.61	0.66
187.5	374	154	347	1.59	0.67
188	369	152	333	1.59	0.67
188.5	365	150	337	1.59	0.68
189	361	150	304	1.58	0.68
189.5	357	150	228	1.57	0.69
190	353	149	341	1.55	0.70
190.5	349	148	332	1.53	0.71
191	345	148	333	1.53	0.71
191.5	341	147	315	1.53	0.71
192	337	147	279	1.53	0.71
192.5	333	147	204	1.55	0.70
193	329	150	241	1.55	0.70
193.5	325	150	225	1.55	0.70
194	320	151	217	1.54	0.70
194.5	316	151	193	1.54	0.70
195	312	153	192	1.53	0.71
195.5	308	152	173	1.53	0.71
196	304	152	199	1.51	0.72
196.5	300	152	199	1.53	0.71
197	296	150	298	1.52	0.71
197.5	292	152	279	1.52	0.71
198	288	151	275	1.54	0.70
198.5	284	155	307	1.53	0.71
199	280	154	270	1.54	0.70
199.5	275	154	270	1.54	0.70
200	271	157	248	1.55	0.70
200.5	267	158	232	1.55	0.70
201	263	159	244	1.54	0.70
201.5	259	158	212	1.54	0.70
202	255	158	296	1.55	0.70
202.5	251	157	294	1.56	0.69

continued

Depth [cm]	Year BC/AD	MS-loop [m ³ /kg]	MS-point [m ³ /kg]	Density [g/cm ³]	Porosity
203	247	157	296	1.57	0.68
203.5	243	157	284	1.59	0.67
204	239	158	239	1.58	0.68
204.5	235	160	259	1.58	0.68
205	231	160	318	1.57	0.68
205.5	226	161	308	1.60	0.67
206	222	160	316	1.59	0.67
206.5	218	157	306	1.58	0.68
207	214	159	324	1.58	0.68
207.5	210	154	329	1.60	0.67
208	206	153	266	1.58	0.68
208.5	202	146	266	1.59	0.67
209	198	142	363	1.61	0.66
209.5	194	141	350	1.61	0.66
210	190	140	333	1.61	0.66
210.5	186	139	335	1.62	0.65

Core-ID: RA09-GW-8-P:

Depth [cm]	Year BC/AD	MS-loop [m ³ /kg]	MS-point [m ³ /kg]	Density [g/cm ³]	Porosity
0.5	2009	23	194	1.53	0.71
1	2004	25	200	1.54	0.70
1.5	1999	27	255	1.54	0.70
2	1993	29	194	1.56	0.69
2.5	1988	31	188	1.57	0.69
3	1983	32	191	1.57	0.68
3.5	1978	33	196	1.59	0.67
4	1973	34	203	1.60	0.67
4.5	1967	34	210	1.61	0.66
5	1962	35	218	1.61	0.66
5.5	1957	36	223	1.61	0.66
6	1952	37	206	1.61	0.66
6.5	1947	37	160	1.61	0.66
7	1941	38	173	1.62	0.66
7.5	1936	38	175	1.63	0.65
8	1931	38	151	1.66	0.63
8.5	1926	38	151	1.68	0.62
9	1921	38	245	1.66	0.63
9.5	1915	40	262	1.63	0.65
10	1910	40	274	1.62	0.66
10.5	1905	40	237	1.63	0.65
11	1900	40	228	1.62	0.66
11.5	1895	39	249	1.65	0.64
12	1890	40	245	1.63	0.65
12.5	1884	40	210	1.63	0.65
13	1879	40	198	1.62	0.65
13.5	1874	40	168	1.62	0.65
14	1869	40	172	1.63	0.65
14.5	1864	39	177	1.65	0.64
15	1858	39	172	1.65	0.64
15.5	1853	40	167	1.63	0.65
16	1848	40	172	1.62	0.66
16.5	1843	39	152	1.63	0.65
17	1838	40	145	1.62	0.65
17.5	1832	39	145	1.64	0.64
18	1827	39	206	1.64	0.64
18.5	1822	39	203	1.63	0.65
19	1817	39	187	1.64	0.64
19.5	1812	38	184	1.65	0.64
20	1806	39	188	1.64	0.65
20.5	1801	38	209	1.63	0.65
21	1796	39	193	1.62	0.65
21.5	1791	39	174	1.62	0.66
22	1786	39	161	1.64	0.65
22.5	1780	38	161	1.64	0.64

continued

Depth [cm]	Year BC/AD	MS-loop [m ³ /kg]	MS-point [m ³ /kg]	Density [g/cm ³]	Porosity
23	1775	38	205	1.65	0.64
23.5	1770	38	208	1.67	0.63
24	1765	38	203	1.65	0.64
24.5	1760	38	192	1.66	0.63
25	1754	38	202	1.66	0.63
25.5	1749	39	189	1.65	0.64
26	1744	39	193	1.66	0.63
26.5	1739	39	204	1.66	0.63
27	1734	39	208	1.66	0.63
27.5	1728	39	216	1.66	0.63
28	1723	39	217	1.66	0.63
28.5	1718	39	213	1.67	0.63
29	1713	39	216	1.67	0.63
29.5	1708	40	215	1.64	0.65
30	1702	40	209	1.64	0.65
30.5	1697	40	207	1.64	0.64
31	1692	40	204	1.65	0.64
31.5	1687	39	208	1.66	0.63
32	1682	40	202	1.63	0.65
32.5	1676	40	182	1.65	0.64
33	1671	40	147	1.63	0.65
33.5	1666	41	199	1.63	0.65
34	1661	41	190	1.64	0.65
34.5	1656	40	200	1.66	0.63
35	1651	41	203	1.66	0.63
35.5	1645	40	194	1.68	0.62
36	1640	40	207	1.69	0.61
36.5	1635	41	179	1.69	0.62
37	1630	41	176	1.67	0.62
37.5	1625	41	176	1.69	0.61
38	1619	41	236	1.68	0.62
38.5	1614	41	244	1.68	0.62
39	1609	41	239	1.70	0.61
39.5	1604	41	229	1.68	0.62
40	1599	42	227	1.67	0.62
40.5	1593	40	225	1.68	0.62
41	1588	41	223	1.68	0.62
41.5	1583	41	225	1.67	0.63
42	1578	41	226	1.66	0.63
42.5	1573	41	224	1.66	0.64
43	1567	41	224	1.65	0.64
43.5	1562	40	224	1.67	0.63
44	1557	40	224	1.67	0.63
44.5	1552	40	224	1.66	0.63
45	1547	40	224	1.63	0.65

continued

Depth [cm]	Year BC/AD	MS-loop [m ³ /kg]	MS-point [m ³ /kg]	Density [g/cm ³]	Porosity
45.5	1541	41	224	1.61	0.66
46	1536	41	224	1.61	0.66
46.5	1531	41	224	1.60	0.67
47	1526	41	224	1.61	0.66
47.5	1521	39	224	1.65	0.64
48	1515	39	224	1.66	0.63
48.5	1510	39	208	1.69	0.62
49	1505	39	210	1.70	0.61
49.5	1500	39	213	1.70	0.61
50	1495	40	215	1.68	0.62
50.5	1489	39	215	1.69	0.62
51	1484	40	204	1.68	0.62
51.5	1479	40	188	1.69	0.61
52	1474	40	152	1.70	0.61
52.5	1469	40	219	1.69	0.62
53	1463	41	230	1.71	0.60
53.5	1458	41	225	1.70	0.61
54	1453	41	229	1.69	0.61
54.5	1448	41	228	1.69	0.62
55	1443	41	198	1.69	0.61
55.5	1438	42	153	1.68	0.62
56	1433	42	159	1.67	0.63
56.5	1428	42	160	1.67	0.63
57	1423	42	160	1.68	0.62
57.5	1418	42	152	1.68	0.62
58	1413	42	160	1.68	0.62
58.5	1409		164	1.68	0.62
59	1404		168	1.69	0.61
59.5	1399		164	1.68	0.62
60	1394	42	163	1.67	0.62
60.5	1389	41	144	1.68	0.62
61	1384	41	219	1.69	0.62
61.5	1380	42	215	1.68	0.62
62	1375	41	223	1.70	0.61
62.5	1370	41	212	1.69	0.62
63	1365	41	211	1.70	0.61
63.5	1360	40	219	1.70	0.61
64	1355	40	212	1.69	0.61
64.5	1351	41	195	1.68	0.62
65	1346	41	183	1.67	0.62
65.5	1341	41	171	1.68	0.62
66	1336	41	159	1.69	0.62
66.5	1331	41	226	1.68	0.62
67	1326	41	224	1.67	0.63
67.5	1322	41	219	1.66	0.63

continued

Depth [cm]	Year BC/AD	MS-loop [m ³ /kg]	MS-point [m ³ /kg]	Density [g/cm ³]	Porosity
68	1317	40	210	1.67	0.63
68.5	1312	40	210	1.66	0.63
69	1307	40	200	1.67	0.63
69.5	1302	40	171	1.67	0.63
70	1297	40	177	1.66	0.63
70.5	1293	40	207	1.66	0.63
71	1288	39	202	1.69	0.62
71.5	1283	40	204	1.67	0.63
72	1278	40	195	1.67	0.63
72.5	1273	40	191	1.66	0.63
73	1269	40	190	1.66	0.64
73.5	1264	40	172	1.66	0.63
74	1259	40	175	1.65	0.64
74.5	1254	40	150	1.66	0.63
75	1249	39	130	1.67	0.63
75.5	1244	39	216	1.68	0.62
76	1240	39	214	1.67	0.63
76.5	1235	39	211	1.68	0.62
77	1230		210	1.67	0.63
77.5	1225		207	1.68	0.62
78	1220		199	1.66	0.63
78.5	1215	40	172	1.66	0.63
79	1211	40	123	1.66	0.63
79.5	1206	40	204	1.66	0.63
80	1201	41	228	1.65	0.64
80.5	1196	40	222	1.67	0.63
81	1191	40	220	1.67	0.63
81.5	1186	40	204	1.66	0.63
82	1182	40	208	1.67	0.63
82.5	1177	40	194	1.67	0.62
83	1172	41	173	1.66	0.63
83.5	1167	41	142	1.66	0.63
84	1162	41	142	1.65	0.64
84.5	1157	41	231	1.65	0.64
85	1153	41	223	1.65	0.64
85.5	1148	41	221	1.66	0.63
86	1143	41	213	1.65	0.64
86.5	1138	41	195	1.68	0.62
87	1133		211	1.68	0.62
87.5	1128	41	220	1.69	0.62
88	1124	41	248	1.69	0.62
88.5	1119	42	238	1.67	0.62
89	1114	42	224	1.68	0.62
89.5	1109	42	245	1.70	0.61
90	1104	42	242	1.70	0.61

continued

Depth [cm]	Year BC/AD	MS-loop [m ³ /kg]	MS-point [m ³ /kg]	Density [g/cm ³]	Porosity
90.5	1100	41	246	1.70	0.61
91	1095	42	241	1.69	0.62
91.5	1090	42	199	1.69	0.62
92	1085	42	170	1.68	0.62
92.5	1080	42	218	1.67	0.62
93	1075	42	224	1.67	0.62
93.5	1071	42	215	1.69	0.62
94	1066	41	214	1.68	0.62
94.5	1061	41	224	1.68	0.62
95	1056	41	210	1.67	0.63
95.5	1051	40	194	1.67	0.63
96	1046	40	77	1.68	0.62
96.5	1042	40	117	1.68	0.62
97	1037	41	191	1.62	0.66
97.5	1032	40	197	1.65	0.64
98	1027	39	184	1.66	0.63
98.5	1022	40	196	1.66	0.63
99	1017	40	196	1.68	0.62
99.5	1013	40	196	1.66	0.63
100	1008	40	196	1.69	0.61
100.5	1003	40	217	1.68	0.62
101	998	40	229	1.68	0.62
101.5	993	40	238	1.70	0.61
102	988	40	244	1.70	0.61
102.5	984	40	240	1.69	0.61
103	979	40	233	1.69	0.61
103.5	974	40	239	1.70	0.61
104	969	40	217	1.70	0.61
104.5	964	41	88	1.68	0.62
105	959	41	48	1.68	0.62
105.5	955	41	57	1.67	0.62
106	950	40	111	1.69	0.61
106.5	945	40	111	1.69	0.61
107	940	40	54	1.68	0.62
107.5	935	40	126	1.68	0.62
108	931	40	201	1.65	0.64
108.5	926	40	219	1.66	0.63
109	921	39	220	1.67	0.62
109.5	916	39	220	1.67	0.63
110	911	39	203	1.65	0.64
110.5	906	39	196	1.66	0.63
111	902	39	200	1.66	0.63
111.5	897	39	204	1.65	0.64
112	892	38	205	1.68	0.62
112.5	887	38	179	1.66	0.63

continued

Depth [cm]	Year BC/AD	MS-loop [m ³ /kg]	MS-point [m ³ /kg]	Density [g/cm ³]	Porosity
113	882	38	157	1.65	0.64
113.5	877	38	136	1.66	0.63
114	873		155	1.66	0.63
114.5	868		200	1.65	0.64
115	863		180	1.65	0.64
115.5	858		180	1.66	0.63
116	853	38	200	1.67	0.63
116.5	848	39	202	1.66	0.63
117	844	39	205	1.67	0.63
117.5	839	38	210	1.68	0.62
118	834	38	207	1.68	0.62
118.5	829	39	208	1.67	0.63
119	824	39	188	1.66	0.63
119.5	819	39	188	1.67	0.63
120	815	40	196	1.64	0.64
120.5	810	40	193	1.63	0.65
121	805	39	210	1.66	0.63
121.5	800	39	205	1.66	0.63
122	795	40	195	1.65	0.64
122.5	790	40	206	1.66	0.63
123	786	39	201	1.67	0.63
123.5	781	39	205	1.66	0.63
124	776	39	192	1.67	0.63
124.5	771	39	193	1.69	0.61
125	766	39	181	1.69	0.61
125.5	762	40	172	1.68	0.62
126	756	40	172	1.68	0.62
126.5	751	40	224	1.68	0.62
127	746	40	238	1.69	0.61
127.5	741	41	246	1.69	0.62
128	736	41	234	1.69	0.62
128.5	731	41	213	1.68	0.62
129	725	41	216	1.68	0.62
129.5	720	41	196	1.69	0.62
130	715	41	198	1.68	0.62
130.5	710	41	182	1.69	0.62
131	705	41	220	1.68	0.62
131.5	700	42	211	1.66	0.63
132	695	41	190	1.67	0.62
132.5	689	41	196	1.67	0.63
133	684	41	187	1.67	0.63
133.5	679	42	165	1.66	0.63
134	674	41	206	1.67	0.63
134.5	669	41	202	1.65	0.64
135	664	41	189	1.67	0.63

continued

Depth [cm]	Year BC/AD	MS-loop [m ³ /kg]	MS-point [m ³ /kg]	Density [g/cm ³]	Porosity
135.5	658	41	183	1.67	0.63
136	653	41	177	1.67	0.62
136.5	648	40	183	1.69	0.62
137	643	40	181	1.67	0.62
137.5	638	41	181	1.66	0.63
138	633	40	174	1.67	0.63
138.5	628	40	175	1.66	0.63
139	622	40	184	1.66	0.63
139.5	617	40	185	1.66	0.63
140	612	40	175	1.66	0.63
140.5	607	40	156	1.66	0.63
141	602	40	125	1.67	0.63
141.5	597	41	125	1.66	0.63
142	591	40	177	1.67	0.62
142.5	586	41	148	1.67	0.63
143	581	40	157	1.67	0.63
143.5	576	40	179	1.67	0.63
144	571	40	166	1.69	0.61
144.5	566	40	152	1.70	0.61
145	561	40	209	1.70	0.61
145.5	555	39	184	1.72	0.60
146	550		193	1.71	0.61
146.5	545	40	196	1.68	0.62
147	540	40	182	1.66	0.63
147.5	535	40	183	1.65	0.64
148	530	40	167	1.65	0.64
148.5	524	40	150	1.66	0.63
149	519	39	150	1.68	0.62
149.5	514	39	201	1.66	0.63
150	509	39	204	1.66	0.63
150.5	504	40	205	1.64	0.64
151	499	39	195	1.67	0.63
151.5	494	39	155	1.66	0.63
152	488	39	202	1.66	0.63
152.5	483	39	222	1.67	0.63
153	478	39	207	1.67	0.62
153.5	473	39	202	1.68	0.62
154	468	39	218	1.67	0.63
154.5	463	39	181	1.67	0.63
155	457	40	159	1.65	0.64
155.5	452	40	159	1.65	0.64
156	447	40	208	1.65	0.64
156.5	442	40	214	1.65	0.64
157	437	41	202	1.65	0.64
157.5	432	40	193	1.67	0.63

continued

Depth [cm]	Year BC/AD	MS-loop [m ³ /kg]	MS-point [m ³ /kg]	Density [g/cm ³]	Porosity
158	427	40	120	1.67	0.63
158.5	421	40	146	1.66	0.63
159	416	40	173	1.68	0.62
159.5	411	41	164	1.67	0.63
160	406	41	155	1.67	0.62
160.5	401	41	203	1.67	0.63
161	396	41	205	1.66	0.63
161.5	390	41	211	1.67	0.63
162	385	41	221	1.67	0.62
162.5	380	41	222	1.68	0.62
163	375	41	180	1.68	0.62
163.5	370	41	194	1.69	0.62
164	365	41	186	1.67	0.63
164.5	360	41	214	1.67	0.63
165	354	40	215	1.71	0.61
165.5	349	40	198	1.70	0.61
166	344	41	165	1.67	0.63
166.5	339	41	206	1.68	0.62
167	334	42	226	1.67	0.62
167.5	329	41	234	1.69	0.62
168	323	41	229	1.68	0.62
168.5	318	41	231	1.68	0.62
169	313	41	221	1.70	0.61
169.5	308	41	201	1.69	0.62
170	303	41	176	1.70	0.61
170.5	298	41	218	1.69	0.62
171	293	41	220	1.69	0.61
171.5	287	41	200	1.68	0.62
172	282	41		1.67	0.62
172.5	277	41	207	1.68	0.62
173	272	42	218	1.65	0.64
173.5	267	40	215	1.66	0.63
174	262	41	197	1.64	0.64
174.5	256	40	172	1.66	0.63
175	251		172	1.65	0.64
175.5	246	41	197	1.63	0.65
176	241	40	208	1.64	0.65
176.5	236	40	205	1.64	0.65
177	231	40	194	1.64	0.64
177.5	226	40	167	1.63	0.65
178	220	40	218	1.64	0.65
178.5	215	40	208	1.63	0.65
179	210	40	208	1.65	0.64
179.5	205	40	192	1.64	0.64
180	200	39	181	1.67	0.63

continued

Depth [cm]	Year BC/AD	MS-loop [m ³ /kg]	MS-point [m ³ /kg]	Density [g/cm ³]	Porosity
180.5	195	40	181	1.64	0.64
181	190	40	202	1.66	0.63
181.5	184	39	202	1.66	0.63
182	179	40	210	1.64	0.65
182.5	174	40	199	1.64	0.64
183	169	40	216	1.65	0.64
183.5	164	40	213	1.66	0.63
184	159	40	197	1.67	0.63
184.5	153	40	189	1.65	0.64
185	148	40	173	1.67	0.63
185.5	143	41	173	1.67	0.63
186	138	40	213	1.67	0.62
186.5	133	40	225	1.69	0.62
187	128	40	230	1.68	0.62
187.5	123	41	207	1.67	0.62
188	117	41	226	1.68	0.62
188.5	112	41	224	1.67	0.62
189	107	40	180	1.70	0.61
189.5	102	40	228	1.70	0.61
190	97	41	237	1.69	0.62
190.5	92		237	1.68	0.62
191	86	41	216	1.70	0.61
191.5	81	41	180	1.69	0.61
192	76	41	231	1.68	0.62
192.5	71	41	233	1.68	0.62
193	66	41	233	1.69	0.62
193.5	61	41	231	1.69	0.62
194	56	41	232	1.68	0.62
194.5	50	41	234	1.68	0.62
195	45	41	227	1.68	0.62
195.5	40	41	213	1.68	0.62
196	35	41	225	1.67	0.63
196.5	30	40	208	1.69	0.61
197	25	40	178	1.68	0.62
197.5	19	41	178	1.67	0.62
198	14	41	63	1.66	0.63
198.5	9	39	117	1.71	0.60
199	4	39	210	1.71	0.60
199.5	-1	39	234	1.70	0.61
200	-6	39	238	1.68	0.62
200.5	-11	39	281	1.68	0.62
201	-17	38	344	1.71	0.60
201.5	-22	38	139	1.68	0.62
202	-27	38	225	1.67	0.63
202.5	-32	38	219	1.67	0.63

continued

Depth [cm]	Year BC/AD	MS-loop [m ³ /kg]	MS-point [m ³ /kg]	Density [g/cm ³]	Porosity
203	-37	38	225	1.68	0.62
203.5	-42	38	165	1.68	0.62
204	-48	38	125	1.68	0.62
204.5	-53	38	216	1.67	0.62
205	-58	37	209	1.66	0.63
205.5	-63	38	197	1.66	0.64
206	-68	38	173	1.65	0.64
206.5	-73	38	128	1.66	0.63
207	-78	38	101	1.67	0.63
207.5	-84	38	193	1.66	0.63
208	-89	38	208	1.66	0.63
208.5	-94	38	211	1.65	0.64
209	-99	38	188	1.66	0.63
209.5	-104	38	165	1.68	0.62
210	-109	38	139	1.66	0.63
210.5	-115	38	100	1.67	0.63
211	-120	39	100	1.66	0.63
211.5	-125	40	233	1.66	0.63
212	-130	40	233	1.67	0.63
212.5	-135	39	225	1.69	0.61
213	-140	40	215	1.68	0.62
213.5	-145	40	186	1.68	0.62
214	-151	40	122	1.69	0.62
214.5	-156	40	231	1.68	0.62
215	-161	41	217	1.67	0.63
215.5	-166	41	201	1.68	0.62
216	-171	41	156	1.67	0.62
216.5	-176	41	156	1.68	0.62
217	-182	40	219	1.69	0.61
217.5	-187	41	173	1.68	0.62
218	-192	40	184	1.69	0.61
218.5	-197	40	150	1.70	0.61
219	-202	41	150	1.68	0.62
219.5	-207	41	217	1.67	0.63
220	-212	41	220	1.66	0.63
220.5	-218	41	225	1.65	0.64
221	-223	41	198	1.66	0.63
221.5	-228	41	176	1.64	0.64
222	-233	40	145	1.65	0.64
222.5	-238	40	109	1.64	0.64
223	-243	40	188	1.64	0.65
223.5	-249	40	192	1.64	0.64
224	-254	40	190	1.64	0.64
224.5	-259	40	177	1.66	0.63
225	-264	39	120	1.66	0.63

continued

Depth [cm]	Year BC/AD	MS-loop [m ³ /kg]	MS-point [m ³ /kg]	Density [g/cm ³]	Porosity
225.5	-269	39	117	1.66	0.63
226	-274	39	224	1.67	0.63
226.5	-279	39	225	1.67	0.63
227	-285	39	230	1.68	0.62
227.5	-290	39	191	1.68	0.62
228	-295	39	145	1.68	0.62
228.5	-300	39	236	1.68	0.62
229	-305	39	242	1.67	0.62
229.5	-310	39	224	1.68	0.62
230	-316	39	170	1.68	0.62
230.5	-321	39	170	1.66	0.63
231	-326	39	218	1.66	0.63
231.5	-331	39	210	1.65	0.64
232	-336	38	156	1.69	0.62
232.5	-341	39	121	1.68	0.62
233	-346	39	111	1.66	0.63
233.5	-352	39	219	1.66	0.63
234	-357	39	223	1.65	0.64
234.5	-362	39	224	1.66	0.63
235	-367	39	201	1.66	0.63
235.5	-372	39	171	1.67	0.63
236	-377	39	138	1.66	0.63
236.5	-382	39	101	1.67	0.63
237	-388	40	226	1.62	0.65
237.5	-393	40	212	1.63	0.65
238	-398	39	197	1.68	0.62
238.5	-403	38	152	1.70	0.61
239	-408	39	111	1.67	0.62
239.5	-413	39	68	1.68	0.62
240	-419	39	186	1.70	0.61
240.5	-424	39	176	1.69	0.61
241	-429	39	178	1.69	0.62
241.5	-434	39	132	1.69	0.62
242	-439	39	250	1.69	0.62
242.5	-444	39	249	1.68	0.62
243	-449	38	200	1.66	0.63
243.5	-455	38	137	1.65	0.64
244	-460	37	221	1.65	0.64
244.5	-465	38	217	1.63	0.65
245	-470	38	190	1.63	0.65
245.5	-475	38	157	1.63	0.65
246	-480	34	137	1.61	0.66
246.5	-486	35	214	1.61	0.66

Appendix D

Geochemical data for gravity cores 2009, Hudson Bay

Appendix D contains geochemical data for the gravity cores 2009 from the Great Whale River study site. The tables list Total Organic Carbon [%], Total Nitrogen [%], C/N-ratios, and $\delta^{13}\text{C}$. Depth intervals are in cm. Time intervals (Years BC/AD) were calculated in cm intervals by interpolating between $^{14}\text{C}_{\text{cal}}$ dates. TOC and TN were measured using a Carlo Erba NA 1500 Series 2 elemental analyzer and $\delta^{13}\text{C}$ was measured using a Thermo Electron Delta V Plus mass spectrometer.

Core-ID: RA09-GW-4-P

Depth [cm]	Year BC/AD	TOC [%]	TN [%]	C/N	$\delta^{13}\text{C}$
0.5	2009	0.752	0.074	10.16	-25.38
5.5	1983	0.721	0.072	10.01	-24.91
10.5	1958	0.674	0.067	10.06	-25.10
15.5	1932	0.622	0.062	10.03	-24.82
20.5	1906	0.617	0.059	10.46	-24.97
25.5	1881	0.662	0.063	10.51	-25.11
30.5	1855	0.621	0.060	10.35	-24.92
35.5	1829	0.626	0.059	10.61	-25.38
40.5	1803	0.600	0.055	10.91	-25.22
45.5	1778	0.649	0.063	10.30	-24.82
50.5	1752	0.636	0.061	10.43	-24.94
55.5	1697	0.621	0.058	10.71	-25.05
60.5	1641	0.657	0.063	10.43	-24.73
65.5	1586	0.584	0.055	10.62	-24.86
70.5	1531	0.603	0.058	10.40	-24.92
75.5	1476	0.621	0.059	10.53	-25.09
80.5	1420	0.668	0.063	10.60	-24.81
85.5	1365	0.687	0.063	10.90	-25.47
90.5	1340	0.665	0.061	10.90	-25.17
95.5	1316	0.653	0.062	10.53	-25.37
100.5	1291	0.617	0.057	10.82	-25.15
105.5	1267	0.637	0.060	10.62	-24.89
110.5	1242	0.610	0.059	10.34	-24.92
115.5	1218	0.594	0.056	10.61	-24.97
120.5	1193	0.629	0.059	10.66	-25.24
125.5	1169	0.622	0.059	10.54	-25.41
130.5	1144	0.631	0.057	11.07	-25.17
135.5	1120	0.620	0.058	10.69	-25.38
140.5	1095	0.616	0.060	10.27	-24.78
145.5	1071	0.600	0.059	10.17	-25.00
150.5	1046	0.635	0.062	10.24	-24.77
155.5	1022	0.649	0.062	10.47	-25.04
160.5	997	0.632	0.062	10.19	-25.08
165.5	973	0.621	0.057	10.89	-25.39
170.5	948	0.572	0.053	10.79	-25.30
175.5	924	0.568	0.054	10.52	-24.83
180.5	900	0.490	0.046	10.65	-25.12
185.5	875	0.587	0.056	10.48	-25.03
190.5	851	0.534	0.051	10.47	-24.85
195.5	827	0.617	0.059	10.46	-24.66

Core-ID: RA09-GW-7-P10

Depth [cm]	Year BC/AD	TOC [%]	TN [%]	C/N	$\delta^{13}\text{C}$
0.5	2009	0.654	0.065	10.06	-25.30
5.5	1968	0.712	0.070	10.17	-24.68
10.5	1927	0.617	0.060	10.28	-25.08
15.5	1886	0.588	0.055	10.69	-25.05
20.5	1845	0.563	0.054	10.43	-24.99
25.5	1804	0.578	0.054	10.70	-25.04
30.5	1764	0.619	0.056	11.05	-25.27
35.5	1723	0.571	0.049	11.65	-25.52
40.5	1682	0.523	0.047	11.13	-25.02
45.5	1641	0.535	0.049	10.92	-25.07
50.5	1600	0.655	0.072	9.10	-24.22
55.5	1559	0.518	0.049	10.57	-24.75
60.5	1506	0.625	0.058	10.78	-24.69
65.5	1453	0.551	0.051	10.80	-24.99
70.5	1401	0.643	0.070	9.19	-24.46
75.5	1348	0.653	0.077	8.48	-24.08
80.5	1295	0.505	0.046	10.98	-25.04
85.5	1242	0.607	0.058	10.47	-24.93
90.5	1189	0.641	0.060	10.68	-24.86
95.5	1136	0.535	0.051	10.49	-25.10
100.5	1072	0.442	0.042	10.52	-25.03
105.5	1031	0.561	0.052	10.79	-25.10
110.5	990	0.603	0.055	10.96	-25.15
115.5	949	0.506	0.050	10.12	-24.71
120.5	908	0.515	0.050	10.30	-25.21
125.5	868	0.436	0.045	9.69	-25.06
130.5	827	0.515	0.052	9.90	-25.20
135.5	786	0.561	0.055	10.20	-25.14
140.5	745	0.561	0.054	10.39	-25.36
145.5	705	0.562	0.055	10.22	-25.05
150.5	664	0.496	0.051	9.73	-24.92
155.5	623	0.504	0.051	9.88	-24.91
160.5	582	0.479	0.044	10.89	-25.39
165.5	541	0.554	0.056	9.89	-24.86
170.5	500	0.601	0.059	10.19	-25.02
175.5	460	0.563	0.054	10.43	-25.03
180.5	419	0.476	0.049	9.71	-24.91
185.5	378	0.529	0.053	9.98	-25.03
190.5	337	0.295	0.027	10.93	-25.61
195.5	296	0.626	0.064	9.78	-24.59
200.5	255	0.585	0.059	9.92	-24.65
205.5	214	0.588	0.057	10.32	-24.73
210.5	174	0.485	0.049	9.90	-24.59

Core-ID: RA09-GW-8-P'

Depth [cm]	Year BC/AD	TOC [%]	TN [%]	C/N	$\delta^{13}\text{C}$
0.5	2009	0.762	0.070	10.89	-25.06
5.5	1957	0.712	0.072	9.89	-25.12
10.5	1905	0.588	0.058	10.14	-25.13
15.5	1853	0.598	0.062	9.65	-25.09
20.5	1801	0.654	0.066	9.91	-25.02
25.5	1749	0.609	0.058	10.50	-25.31
30.5	1697	0.583	0.058	10.05	-24.96
35.5	1645	0.593	0.061	9.72	-25.04
40.5	1593	0.575	0.055	10.45	-25.40
45.5	1541	0.522	0.044	11.86	-24.94
50.5	1489	0.598	0.057	10.49	-25.21
55.5	1438	0.594	0.057	10.42	-24.98
60.5	1389	0.578	0.056	10.32	-24.56
65.5	1341	0.615	0.059	10.42	-25.20
70.5	1293	0.630	0.052	12.12	-25.21
75.5	1244	0.651	0.054	12.06	-25.13
80.5	1196	0.580	0.058	10.00	-24.91
85.5	1148	0.560	0.055	10.18	-25.18
90.5	1100	0.599	0.056	10.70	-24.93
95.5	1051	0.606	0.051	11.88	-25.08
100.5	1003	0.629	0.051	12.33	-25.19
105.5	955	0.560	0.046	12.17	-25.26
110.5	906	0.582	0.055	10.58	-25.49
115.5	858	0.552	0.045	12.27	-25.12
120.5	810	0.717	0.066	10.86	-25.04
125.5	762	0.754	0.057	13.23	-24.99
130.5	710	0.714	0.055	12.98	-25.21
135.5	658	0.673	0.054	12.46	-24.63
140.5	607	0.738	0.058	12.72	-25.08
145.5	555	0.636	0.048	13.25	-24.89
150.5	504	0.699	0.054	12.94	-25.04
155.5	452	0.700	0.054	12.96	-25.26
160.5	401	0.698	0.053	13.17	-25.11
165.5	349	0.635	0.050	12.70	-25.15
170.5	298	0.509	0.036	14.14	-25.39
175.5	246	0.671	0.054	12.43	-25.11
180.5	195	0.705	0.055	12.82	-24.97
185.5	143	0.704	0.055	12.80	-25.15
190.5	92	0.651	0.050	13.02	-24.77
195.5	40	0.666	0.056	11.89	-24.51
200.5	-11	0.643	0.053	12.13	-24.92
205.5	-63	0.696	0.055	12.65	-24.30
210.5	-115	0.629	0.050	12.58	-24.81
215.5	-166	0.620	0.050	12.40	-25.09
220.5	-218	0.659	0.050	13.18	-24.99

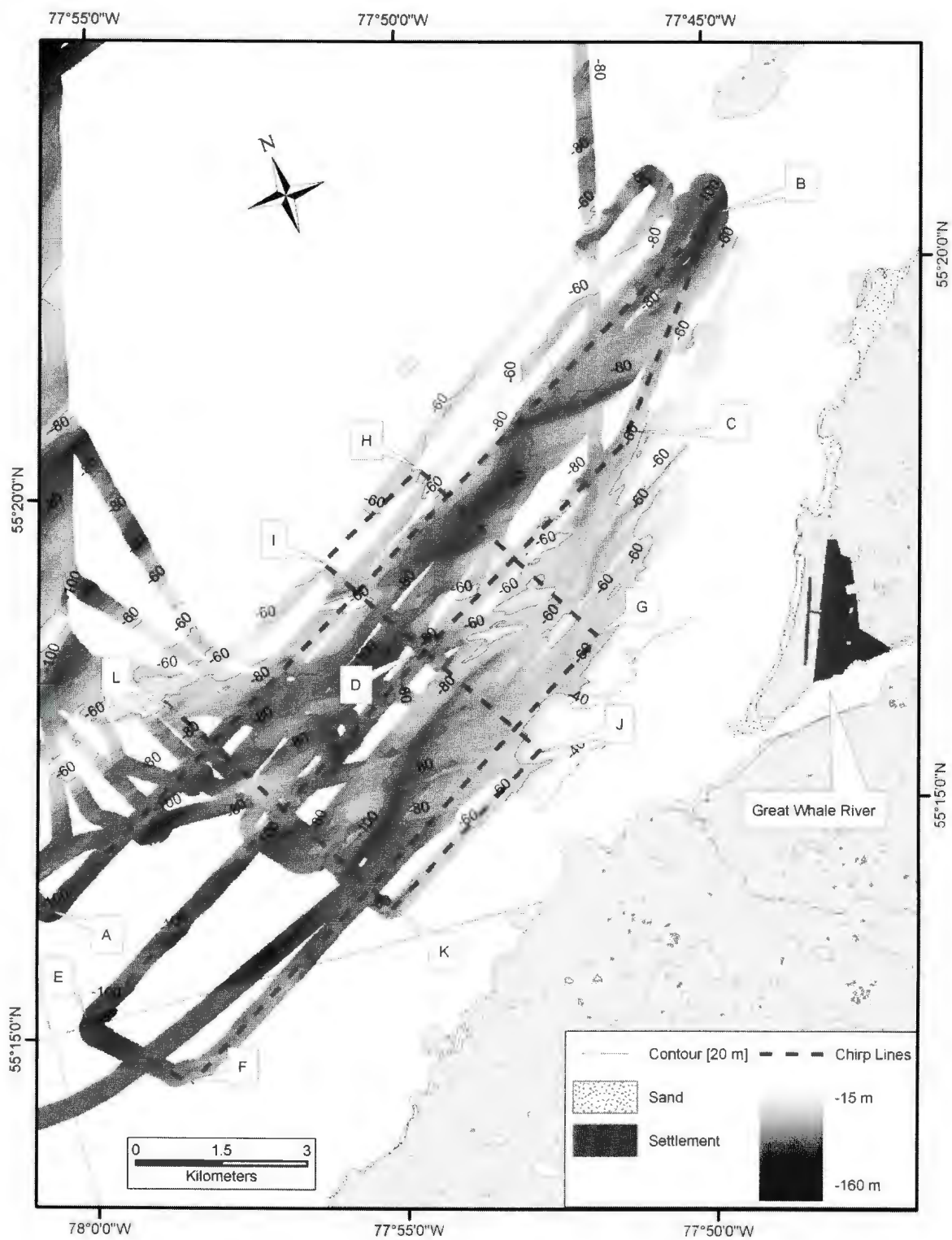
continued

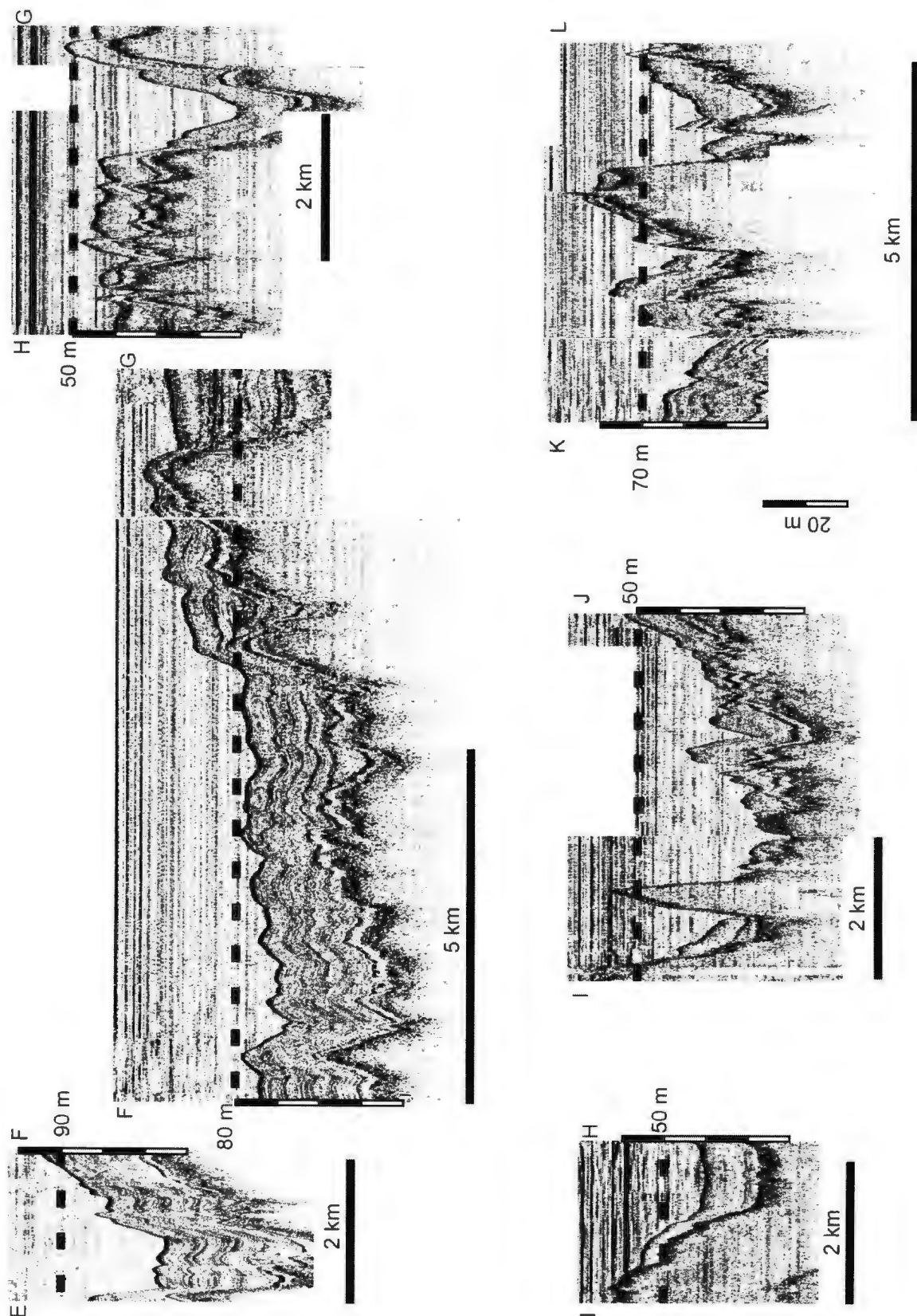
Depth [cm]	Year BC/AD	TOC [%]	TN [%]	C/N	$\delta^{13}\text{C}$
225.5	-269	0.598	0.052	11.50	-25.31
230.5	-321	0.656	0.060	10.93	-25.38
235.5	-372	0.609	0.056	10.88	-25.12
240.5	-424	0.545	0.041	13.29	-24.87
245.5	-475	0.566	0.042	13.48	-25.30

Appendix E

Subbottom profiles, Hudson Bay

Appendix E contains a map displaying the 2007 sub-bottom survey path and the subbottom profiles, that were not displayed in Chapters 2 or 3. Subbottom profiles were collected in summer 2007 using a hull-mounted 3.5 kHz Knudsen Chirp 3200 subbottom profiler.

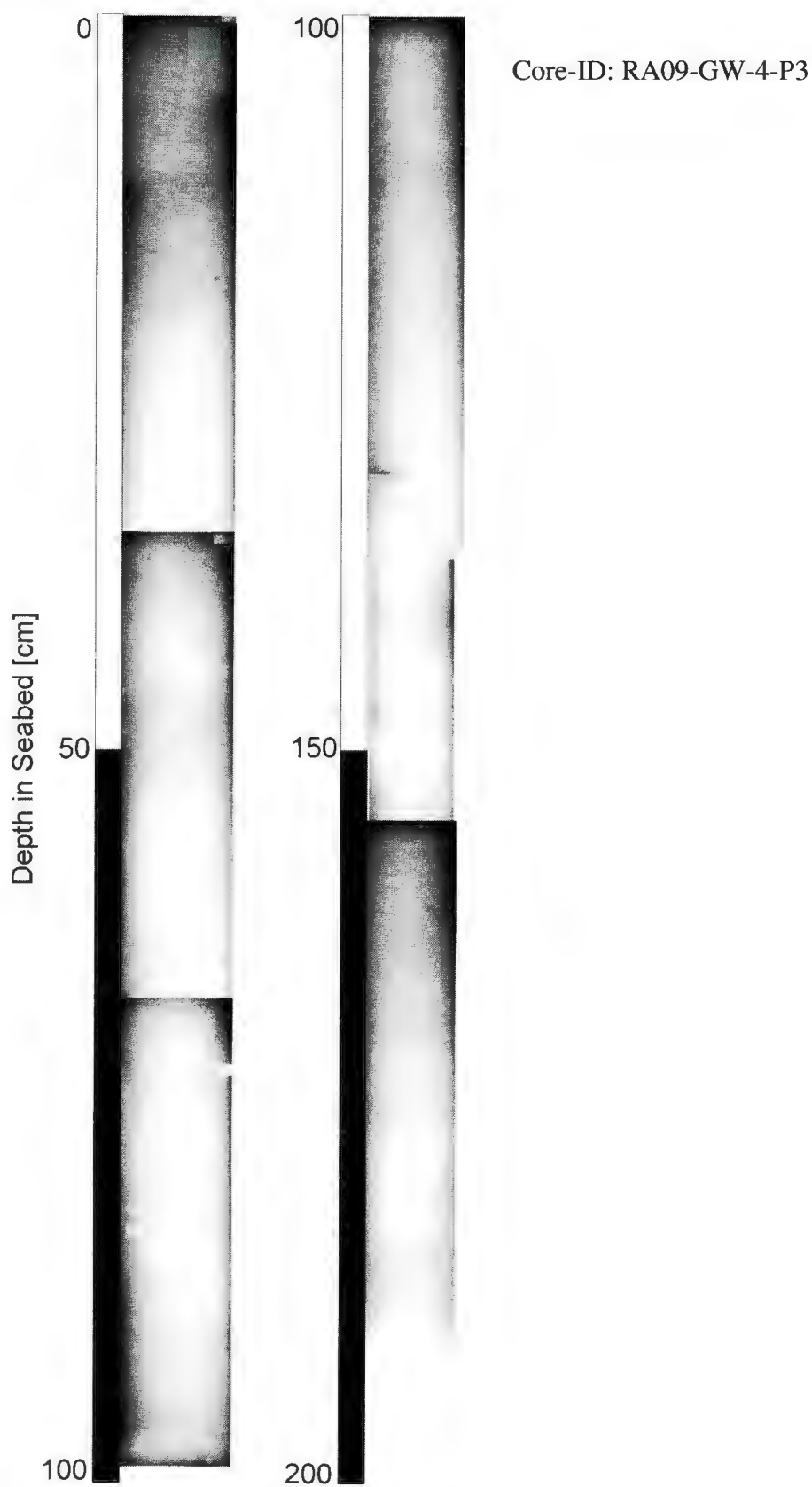


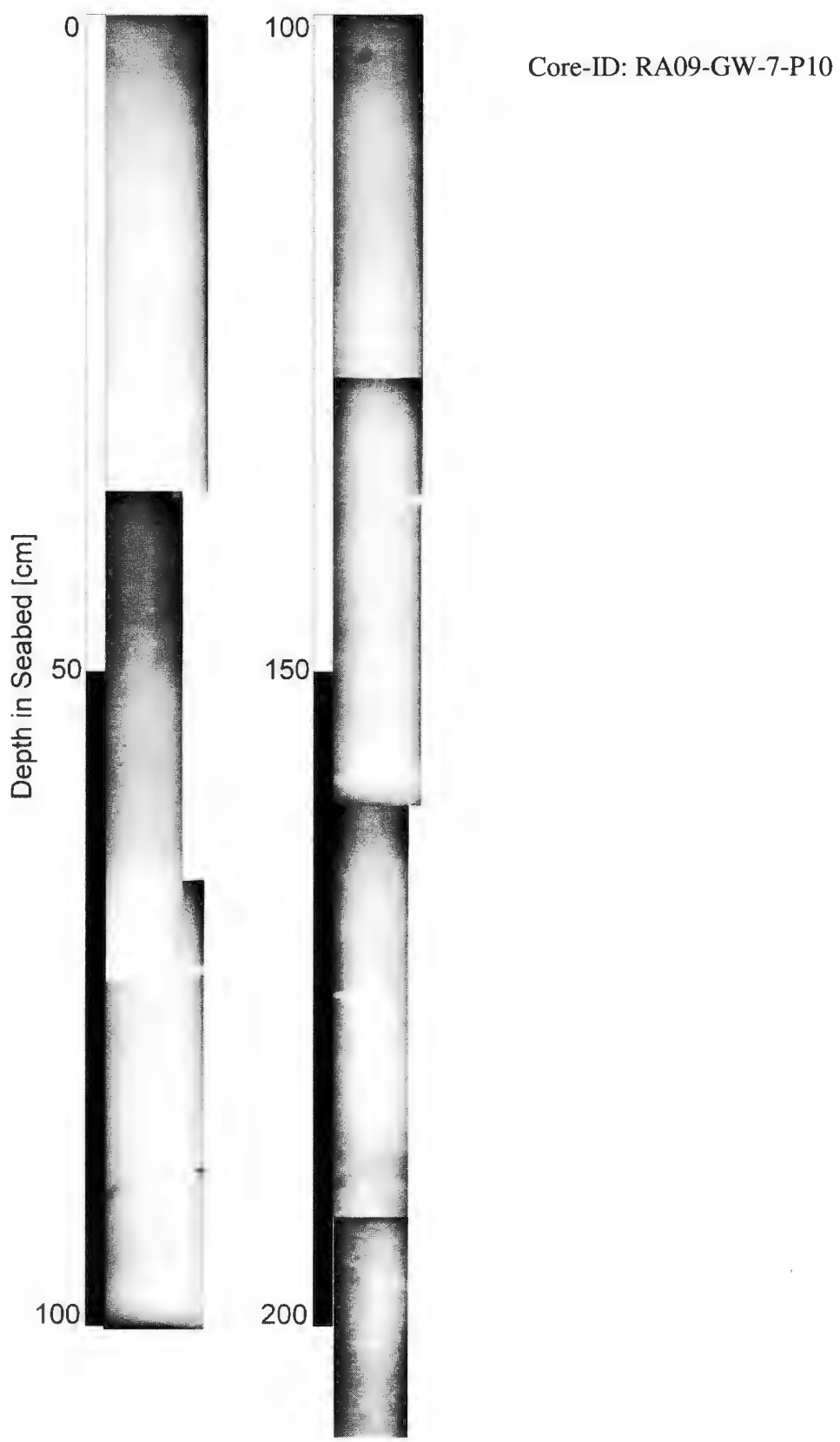


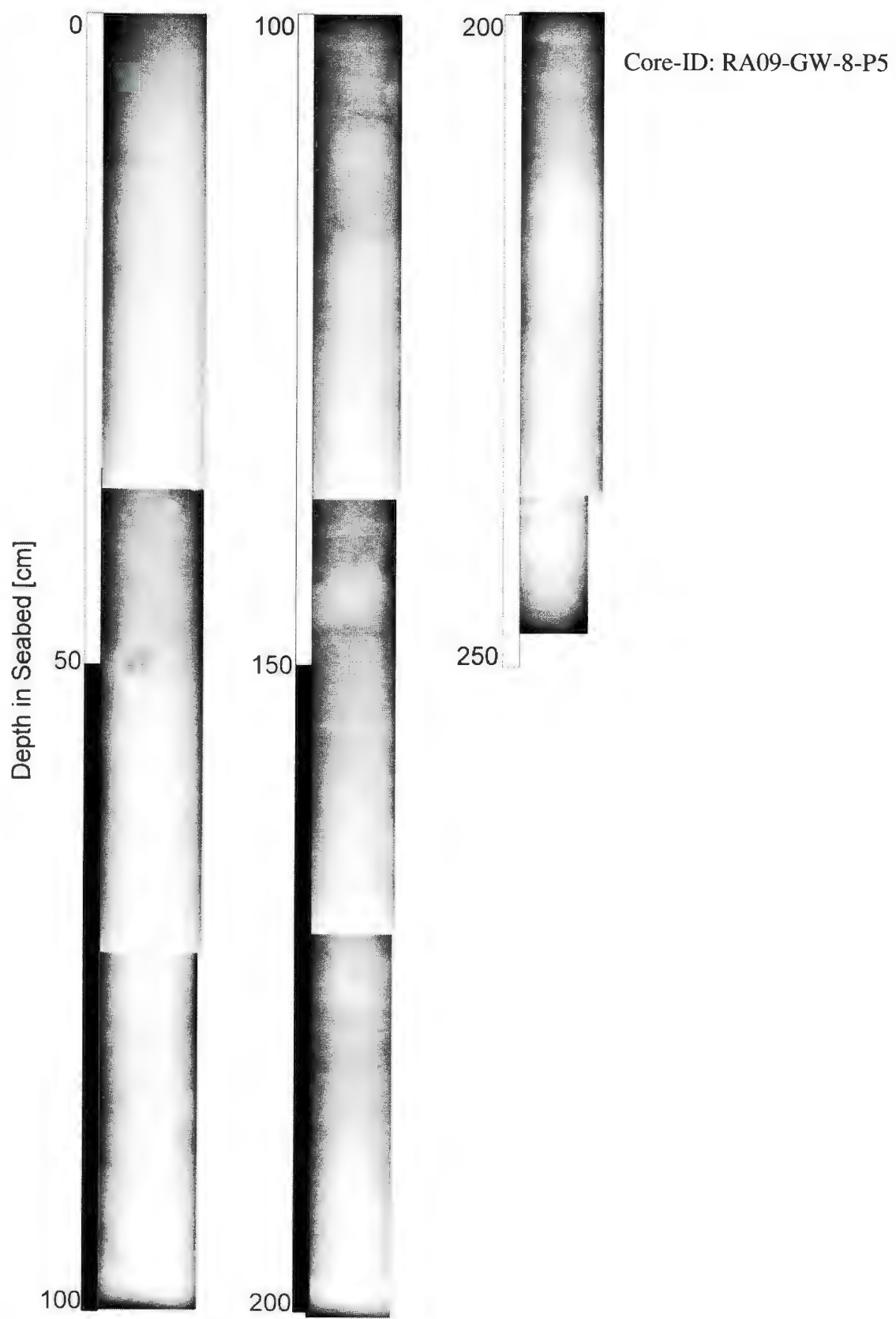
Appendix F

X-radiographic images of gravity cores 2009, Hudson Bay

Appendix F contains x-radiographic images for gravity cores from the Great Whael River study site in Hudson Bay. Sediment cores were imaged x-radiographically using a Thales Flashscan 35 X-ray detector, illuminated with a Lorad LPX 160 X-ray generator. To increase image quality, an aluminum compensator plate was designed to counterbalance decreasing core thickness towards the sides of the core.







Appendix G

Granulometry pistoncores 2009, Labrador

Appendix G contains results of granulometric analyses performed on piston cores cores (2009) collected in Nachvak and Saglek Fjords, Labrador.

The tables list mean grain diameter [μm] (Appendix 11 to 18) and cumulative clay, silt, and sand content [cum. %]. Granulometric measurements were performed using a HORIBA Partica LA-950 laser diffraction particle size analysis system, with a particle size range of 0.1-3000 μm .

Core-ID: AM09-PC-N-606

Depth [cm]	Year BC/AD	Mean grain diameter [μm]	Clay [cum. %]	Silt [cum. %]	Sand [cum. %]
0.5	2009	25.08	0.00	95.51	100.00
5.5	1961	14.34	0.18	99.40	100.00
10.5	1913	14.20	0.14	99.60	100.00
15.5	1865	12.82	0.43	99.94	100.00
20.5	1817	13.49	0.14	100.00	100.00
25.5	1769	12.49	0.58	100.00	100.00
30.5	1721	16.12	0.50	97.94	100.00
35.5	1663	12.49	0.45	100.00	100.00
40.5	1606	12.09	0.46	100.00	100.00
45.5	1548	12.57	0.43	100.00	100.00
50.5	1490	12.44	0.92	99.82	100.00
55.5	1432	12.50	0.43	100.00	100.00
60.5	1375	12.74	0.40	100.00	100.00
65.5	1317	12.71	0.85	99.79	100.00
70.5	1259	12.21	1.10	100.00	100.00
75.5	1202	12.72	0.60	99.81	100.00
80.5	1144	11.62	1.27	100.00	100.00
85.5	1086	17.26	1.80	97.47	100.00
90.5	1028	12.38	0.51	100.00	100.00
95.5	971	12.37	1.11	99.68	100.00
100.5	913	14.26	1.21	98.28	100.00
105.5	855	12.26	0.42	100.00	100.00
110.5	798	8.01	26.35	100.00	100.00
115.5	733	12.45	0.48	100.00	100.00
120.5	668	12.10	0.83	100.00	100.00
125.5	603	14.10	0.41	99.16	100.00
130.5	538	11.94	0.60	100.00	100.00
135.5	473	13.00	0.21	100.00	100.00
140.5	408	15.76	0.20	98.24	100.00
145.5	343	11.96	0.64	100.00	100.00
150.5	278	11.83	0.45	100.00	100.00
155.5	213	12.63	0.49	99.93	100.00
160.5	148	13.19	0.57	99.46	100.00
165.5	83	13.13	0.52	99.94	100.00
170.5	18	12.68	1.07	99.78	100.00
175.5	-47	12.59	0.94	99.81	100.00
180.5	-111	12.47	0.62	99.94	100.00
185.5	-176	13.52	0.91	99.29	100.00
190.5	-241	12.69	0.95	99.81	100.00
195.5	-306	13.30	0.77	99.57	100.00
200.5	-371	12.31	1.09	99.79	100.00
205.5	-436	12.01	1.80	99.93	100.00
210.5	-501	9.01	17.77	100.00	100.00
215.5	-556	12.64	0.53	99.93	100.00
220.5	-612	12.83	0.62	99.80	100.00

continued

Depth [cm]	Year BC/AD	Mean grain diameter [μm]	Clay [cum. %]	Silt [cum. %]	Sand [cum. %]
225.5	-667	14.47	1.27	99.18	100.00
230.5	-722	11.69	1.51	100.00	100.00
235.5	-777	13.00	0.87	99.77	100.00
240.5	-833	13.35	0.41	99.78	100.00
245.5	-888	13.06	0.47	99.70	100.00
250.5	-943	14.95	1.04	98.00	100.00
255.5	-999	12.13	0.84	100.00	100.00
260.5	-1054	11.82	0.66	100.00	100.00
265.5	-1109	12.61	0.83	99.94	100.00
270.5	-1164	13.34	0.51	99.66	100.00
275.5	-1220	12.71	0.87	99.66	100.00
280.5	-1275	12.68	0.52	100.00	100.00
285.5	-1330	12.96	0.46	100.00	100.00
290.5	-1385	12.18	0.78	100.00	100.00
295.5	-1441	11.27	1.86	100.00	100.00
300.5	-1496	12.32	0.57	100.00	100.00
305.5	-1550	13.07	0.22	100.00	100.00
310.5	-1604	12.58	0.61	99.94	100.00
315.5	-1658	12.03	0.52	100.00	100.00
320.5	-1712	12.72	0.50	100.00	100.00
325.5	-1766	11.57	0.78	100.00	100.00
330.5	-1820	11.11	0.90	100.00	100.00
335.5	-1874	11.28	0.59	100.00	100.00
340.5	-1928	11.51	0.57	100.00	100.00
345.5	-1982	11.14	1.16	100.00	100.00
350.5	-2036	12.02	0.52	100.00	100.00
355.5	-2090	13.36	6.31	98.48	100.00
360.5	-2144	14.74	0.97	97.98	100.00
365.5	-2198	15.45	0.98	98.71	100.00
370.5	-2252	12.74	0.46	99.81	100.00
375.5	-2306	20.14	0.18	95.87	100.00
380.5	-2361	18.04	1.30	95.62	100.00
385.5	-2415	11.48	1.35	100.00	100.00
390.5	-2469	12.33	0.44	100.00	100.00
395.5	-2523	9.53	11.28	100.00	100.00
400.5	-2577	854.21	0.15	13.08	100.00
405.5	-2631	12.17	1.64	99.66	100.00
410.5	-2685	11.77	4.11	99.58	100.00
415.5	-2739	12.24	2.24	99.47	100.00
420.5	-2793	11.62	1.21	100.00	100.00
425.5	-2847	18.09	1.29	96.80	100.00
430.5	-2901	17.23	0.50	96.87	100.00
435.5	-2955	15.69	0.44	97.96	100.00
440.5	-3009	18.38	1.55	96.21	100.00
445.5	-3063	16.23	0.79	97.43	100.00

continued

Depth [cm]	Year BC/AD	Mean grain diameter [μm]	Clay [cum. %]	Silt [cum. %]	Sand [cum. %]
450.5	-3117	17.52	0.60	96.79	100.00
455.5	-3171	16.89	1.84	96.47	100.00
460.5	-3226	12.95	1.74	98.88	100.00
465.5	-3280	12.21	0.89	100.00	100.00
470.5	-3334	18.38	0.96	95.96	100.00
475.5	-3388	15.59	0.55	98.16	100.00
480.5	-3442	13.27	0.50	99.79	100.00
485.5	-3496	15.92	0.55	98.04	100.00
490.5	-3550	13.64	0.61	99.62	100.00
495.5	-3604	17.32	0.90	96.79	100.00
500.5	-3659	19.93	1.61	94.73	100.00
505.5	-3761	15.27	1.71	97.78	100.00
510.5	-3863	19.16	4.99	94.70	100.00
515.5	-3966	13.43	3.03	98.80	100.00
520.5	-4068	16.94	3.70	96.35	100.00
525.5	-4171	14.99	5.13	97.15	100.00
530.5	-4273	13.87	2.94	98.29	100.00
535.5	-4376	10.56	14.58	100.00	100.00
540.5	-4478	13.89	3.78	98.19	100.00
545.5	-4581	15.27	9.37	96.71	100.00
550.5	-4683	18.66	4.10	95.46	100.00
555.5	-4786	11.71	4.92	99.81	100.00
560.5	-4888	14.97	10.89	97.05	100.00
565.5	-4990	10.91	7.94	99.82	100.00
570.5	-5093	13.58	7.40	98.08	100.00
575.5	-5195	23.36	6.64	93.08	100.00
580.5	-5298	13.18	6.71	98.37	100.00
585.5	-5400	13.93	4.57	97.86	100.00
590.5	-5503	38.20	11.09	88.91	100.00
595.5	-5605	15.86	12.24	96.94	100.00
600.5	-5708	19.43	10.33	94.71	100.00
605.5	-5810	20.37	11.72	94.09	100.00
610.5	-5913	9.38	23.07	100.00	100.00
615.5	-6015	19.24	17.09	94.06	100.00
620.5	-6118	21.70	15.14	92.11	100.00
625.5	-6220	28.12	14.20	88.53	100.00
630.5	-6322	14.20	16.34	97.03	100.00
635.5	-6425	13.10	16.66	97.79	100.00
640.5	-6527	6.05	23.83	100.00	100.00
645.5	-6630	16.50	17.57	95.83	100.00
650.5	-6732	24.47	13.52	90.89	100.00
655.5	-6835	14.68	16.68	96.75	100.00
660.5	-6937	20.18	13.63	93.62	100.00
665.5	-7040	13.83	18.57	97.46	100.00
670.5	-7142	14.68	19.57	96.84	100.00

continued

Depth [cm]	Year BC/AD	Mean grain diameter [μm]	Clay [cum. %]	Silt [cum. %]	Sand [cum. %]
675.5	-7245	14.78	20.12	96.75	100.00
680.5	-7347	14.51	18.48	96.93	100.00
685.5	-7449	10.39	18.83	99.78	100.00
690.5	-7552	10.67	20.60	99.56	100.00
695.5	-7654	10.38	20.31	99.79	100.00
700.5	-7757	11.09	21.00	99.15	100.00
705.5	-7859	13.57	21.62	97.37	100.00
710.5	-7962	10.19	24.27	99.75	100.00
715.5	-8064	13.04	26.38	97.22	100.00
720.5	-8167	9.51	24.67	100.00	100.00
725.5	-8269	9.06	33.38	99.75	100.00
730.5	-8372	11.87	24.33	98.29	100.00
735.5	-8474	18.02	22.54	95.52	100.00
740.5	-8577	12.21	21.94	98.52	100.00
745.5	-8679	16.61	20.09	95.62	100.00
750.5	-8781	8.46	27.47	100.00	100.00
755.5	-8884	8.31	28.78	100.00	100.00
760.5	-8986	8.32	27.87	100.00	100.00
765.5	-9089	8.16	27.49	100.00	100.00
770.5	-9191	8.64	27.25	100.00	100.00
775.5	-9294	8.21	27.78	100.00	100.00
780.5	-9396	7.91	28.92	100.00	100.00
785.5	-9499	8.35	26.76	100.00	100.00
790.5	-9601	8.89	26.90	99.93	100.00
795.5	-9704	8.14	29.38	100.00	100.00
800.5	-9806	7.63	32.05	100.00	100.00
805.5		8.06	31.94	100.00	100.00
810.5		8.17	31.51	100.00	100.00
815.5		7.99	32.97	100.00	100.00

Core-ID: AM09-PC-S-61

Depth [cm]	Year BC/AD	Mean grain diameter [μm]	Clay [cum. %]	Silt [cum. %]	Sand [cum. %]
0.5	2009	22.40	0.00	94.98	100.00
5.5	1968	21.03	0.00	95.65	100.00
10.5	1928	13.27	0.00	100.00	100.00
15.5	1887	14.25	0.00	99.94	100.00
20.5	1846	14.38	0.00	99.93	100.00
25.5	1806	14.98	0.00	99.19	100.00
30.5	1766	13.61	0.00	100.00	100.00
35.5	1736	14.41	0.00	99.44	100.00
40.5	1706	14.78	0.00	99.13	100.00
45.5	1676	12.94	0.10	100.00	100.00
50.5	1646	13.22	0.10	99.94	100.00
55.5	1616	12.58	0.10	100.00	100.00
60.5	1586	13.27	0.00	99.94	100.00
65.5	1556	13.70	0.00	99.79	100.00
70.5	1526	12.23	0.20	100.00	100.00
75.5	1496	12.57	0.12	100.00	100.00
80.5	1466	12.36	0.17	100.00	100.00
85.5	1436	12.89	0.11	100.00	100.00
90.5	1406	12.68	0.13	100.00	100.00
95.5	1376	15.96	0.00	98.35	100.00
100.5	1346	12.34	0.12	100.00	100.00
105.5	1316	12.91	0.00	100.00	100.00
110.5	1286	13.39	0.17	99.52	100.00
115.5	1245	12.09	0.21	99.90	100.00
120.5	1204	13.14	0.13	99.74	100.00
125.5	1163	13.50	0.00	99.94	100.00
130.5	1122	12.25	0.17	100.00	100.00
135.5	1082	12.41	0.18	100.00	100.00
140.5	1041	15.61	0.12	98.19	100.00
145.5	1000	12.93	0.12	100.00	100.00
150.5	959	12.87	0.11	100.00	100.00
155.5	918	13.86	0.00	99.93	100.00
160.5	877	13.19	0.00	100.00	100.00
165.5	836	13.33	0.00	100.00	100.00
170.5	795	19.25	0.11	95.78	100.00
175.5	754	12.68	0.16	100.00	100.00
180.5	713	12.92	0.00	100.00	100.00
185.5	673	16.92	0.00	97.57	100.00
190.5	632	16.89	0.00	97.60	100.00
195.5	591	27.78	0.00	94.68	100.00
200.5	550	13.62	0.00	99.79	100.00
205.5	509	14.74	0.18	98.40	100.00
210.5	468	12.81	0.16	99.94	100.00
215.5	427	10.77	2.20	100.00	100.00
220.5	385	12.55	0.11	100.00	100.00

continued

Depth [cm]	Year BC/AD	Mean grain diameter [μm]	Clay [cum. %]	Silt [cum. %]	Sand [cum. %]
225.5	344	10.73	1.62	100.00	100.00
230.5	302	12.10	0.17	100.00	100.00
235.5	261	12.89	0.17	99.94	100.00
240.5	219	13.59	0.14	99.62	100.00
245.5	178	12.35	0.14	100.00	100.00
250.5	136	12.38	0.14	100.00	100.00
255.5	95	23.97	0.13	96.97	100.00
260.5	54	12.15	0.18	100.00	100.00
265.5	12	12.08	0.19	100.00	100.00
270.5	-29	12.39	0.14	100.00	100.00
275.5	-71	12.16	0.16	100.00	100.00
280.5	-112	13.08	0.11	100.00	100.00
285.5	-154	12.80	0.12	100.00	100.00
290.5	-195	11.19	2.78	100.00	100.00
295.5	-237	13.27	0.17	99.60	100.00
300.5	-278	10.10	3.13	100.00	100.00
305.5	-311	12.12	0.16	100.00	100.00
310.5	-345	12.30	0.18	100.00	100.00
315.5	-378	12.10	0.21	100.00	100.00
320.5	-412	11.30	0.43	100.00	100.00
325.5	-445	11.47	0.49	100.00	100.00
330.5	-479		0.45	100.00	100.00
335.5	-512	11.51	0.43	100.00	100.00
340.5	-546	11.94	0.36	100.00	100.00
345.5	-579		0.30	100.00	100.00
350.5	-613	12.25	0.20	100.00	100.00
355.5	-646	15.08	0.18	98.30	100.00
360.5	-680	11.47	1.83	100.00	100.00
365.5	-713	11.06	0.55	100.00	100.00
370.5	-747	11.55	0.46	100.00	100.00
375.5	-780	11.97	0.21	100.00	100.00
380.5	-814	12.00	0.23	100.00	100.00
385.5	-847	9.65	10.24	100.00	100.00
390.5	-881	12.61	0.12	100.00	100.00
395.5	-914	12.06	0.19	100.00	100.00
400.5	-948	12.17	0.15	100.00	100.00
405.5	-981	12.12	0.14	100.00	100.00
410.5	-1015	12.49	0.14	100.00	100.00
415.5	-1048	13.94	0.11	99.69	100.00
420.5	-1082	12.73	0.15	100.00	100.00
425.5	-1115	13.03	0.11	100.00	100.00
430.5	-1149	11.70	0.46	100.00	100.00
435.5	-1182	12.75	0.11	100.00	100.00
440.5	-1216	12.30	0.11	100.00	100.00
445.5	-1249	12.64	0.12	100.00	100.00

continued

Depth [cm]	Year BC/AD	Mean grain diameter [μm]	Clay [cum. %]	Silt [cum. %]	Sand [cum. %]
450.5	-1283	12.54	0.12	100.00	100.00
455.5	-1316	12.81	0.16	100.00	100.00
460.5	-1350	12.21	0.21	100.00	100.00
465.5	-1383	12.76	0.13	100.00	100.00
470.5	-1417	12.36	0.15	100.00	100.00
475.5	-1450	11.96	0.23	100.00	100.00
480.5	-1484	11.35	0.41	100.00	100.00
485.5	-1517	11.97	0.21	100.00	100.00
490.5	-1551	12.09	0.21	100.00	100.00
495.5	-1584	11.78	0.45	100.00	100.00
500.5	-1618	11.70	0.38	100.00	100.00
505.5	-1655	12.43	0.84	100.00	100.00
510.5	-1691	13.69	0.12	99.93	100.00
515.5	-1728	13.42	0.12	100.00	100.00
520.5	-1765	19.19	0.42	96.50	100.00
525.5	-1802	13.49	0.16	99.60	100.00
530.5	-1838	13.44	0.18	99.36	100.00
535.5	-1875	18.16	0.64	95.92	100.00
540.5	-1912	12.99	0.16	99.93	100.00
545.5	-1948	15.31	0.18	98.08	100.00
550.5	-1985	14.43	0.20	99.05	100.00
555.5	-2022	13.35	0.11	99.94	100.00
560.5	-2059	12.84	0.17	100.00	100.00
565.5	-2095	11.98	0.45	99.88	100.00
570.5	-2132	11.24	0.64	100.00	100.00
575.5	-2169		0.18	99.87	100.00
580.5	-2206	12.66	0.18	99.90	100.00
585.5	-2242	12.02	0.39	100.00	100.00
590.5	-2279	12.37	0.40	99.82	100.00
595.5	-2316	18.48	0.15	96.14	100.00
600.5	-2352	16.54	0.19	97.41	100.00
605.5	-2389	12.53	0.17	100.00	100.00
610.5	-2426	12.44	0.19	100.00	100.00
615.5	-2463	11.83	0.58	99.77	100.00
620.5	-2499	14.52	0.15	98.89	100.00
625.5	-2536	12.83	0.13	99.89	100.00
630.5	-2573	17.21	0.00	97.47	100.00
635.5	-2609	16.11	0.00	98.56	100.00
640.5	-2646	14.52	0.00	99.50	100.00
645.5	-2683	13.38	0.00	100.00	100.00
650.5	-2720	13.73	0.15	99.59	100.00
655.5	-2756	13.44	0.48	99.16	100.00
660.5	-2793	12.59	0.19	100.00	100.00
665.5	-2830	12.20	0.22	100.00	100.00
670.5	-2866	15.33	0.23	98.26	100.00

continued

Depth [cm]	Year BC/AD	Mean grain diameter [μm]	Clay [cum. %]	Silt [cum. %]	Sand [cum. %]
675.5	-2903	13.20	0.11	100.00	100.00
680.5	-2940	12.29	0.24	100.00	100.00
685.5	-2977	13.63	0.40	99.32	100.00
690.5	-3013	13.45	0.23	99.39	100.00
695.5	-3050	12.42	0.34	100.00	100.00
700.5	-3087	19.61	0.35	95.09	100.00
705.5	-3124	16.48	0.81	96.76	100.00
710.5	-3160	18.77	0.18	95.73	100.00
715.5	-3197	14.83	0.22	98.39	100.00
720.5	-3234	12.43	0.21	100.00	100.00
725.5	-3270	16.20	0.79	97.24	100.00
730.5	-3307	19.15	0.13	96.25	100.00
735.5	-3344	20.18	0.13	95.47	100.00
740.5	-3381	18.86	0.55	96.00	100.00
745.5	-3417	18.20	0.20	96.71	100.00
750.5	-3454	14.86	0.60	98.21	100.00
755.5		17.62	0.23	96.93	100.00
760.5		19.16	0.50	96.84	100.00
765.5		13.52	14.25	97.56	100.00

Appendix H

Physical properties piston cores 2009, Labrador

Appendix H contains data for magnetic susceptibility loop and point sensors (MS-loop, MS-point; m^3/kg), sediment density [g/cm^3], and fractional porosity for each depth interval [cm] for Nachvak and Saglek Fjords. Each depth interval was converted to Year BC/AD using $^{14}\text{C}_{\text{cal}}$ -ages and interpolating between dates. Sediment cores were scanned using a Geotek Multi-Sensor-Core-Logger. Magnetic susceptibility was measured using the Bartington Meter Model MS2 with the loop sensor MS2C and the point sensor MS2E1. Bulk density was measured using the Geotek gamma densitometer, which contains a ^{137}Cs source, that emits a narrow beam of gamma rays. The gamma rays pass through the centre of the core and are recorded on the other side by a detector. Porosity is calculated by the Geotek calibration software directly from gamma density.

Core-ID: AM09-PC-N-60€

Depth [m]	Year BC/AD	MS-loop [m ³ /kg]	Density [g/cm ³]	Porosity
0.005	2009		1.40	
0.010	2004	41	1.43	0.78
0.015	1999	55	1.42	0.77
0.020	1994	61	1.41	0.77
0.025	1989	64	1.40	0.78
0.030	1985	65	1.37	0.78
0.035	1980	67	1.34	0.80
0.040	1975	80	1.35	0.82
0.045	1970	79	1.38	0.81
0.050	1965	83	1.43	0.79
0.055	1960	83	1.42	0.77
0.060	1955	83	1.42	0.77
0.065	1950	91	1.43	0.77
0.070	1946	91	1.44	0.76
0.075	1941	96	1.45	0.76
0.080	1936	96	1.46	0.76
0.085	1931	101	1.45	0.75
0.090	1926	101	1.46	0.75
0.095	1921	101	1.45	0.75
0.100	1916	101	1.45	0.75
0.105	1911	101	1.46	0.75
0.110	1906	100	1.47	0.75
0.115	1902	109	1.46	0.75
0.120	1897	110	1.45	0.75
0.125	1892	110	1.45	0.75
0.130	1887	110	1.45	0.75
0.135	1882	109	1.46	0.76
0.140	1877	111	1.45	0.75
0.145	1872	112	1.44	0.75
0.150	1867	111	1.46	0.76
0.155	1863	112	1.44	0.75
0.160	1858	112	1.44	0.76
0.165	1853	111	1.47	0.76
0.170	1848	111	1.46	0.74
0.175	1843	112	1.46	0.75
0.180	1838	112	1.45	0.75
0.185	1833	111	1.46	0.75
0.190	1828	114	1.48	0.75
0.195	1824	114	1.47	0.74
0.200	1819	115	1.47	0.74
0.205	1814	118	1.46	0.75
0.210	1809		1.46	0.75
0.215	1804		1.46	0.75
0.220	1799		1.44	0.75
0.225	1794		1.44	0.76
0.230	1789		1.44	0.76

0.235	1784	119	1.44	0.76
0.240	1780	118	1.45	0.76
0.245	1775	119	1.43	0.75
0.250	1770	117	1.42	0.77
0.255	1765	114	1.42	0.77
0.260	1760	114	1.42	0.77
0.265	1755	112	1.42	0.77
0.270	1750	112	1.43	0.77
0.275	1745	107	1.47	0.76
0.280	1741	107	1.47	0.74
0.285	1736	108	1.46	0.74
0.290	1731	108	1.43	0.75
0.295	1726	107	1.43	0.77
0.300	1721	107	1.42	0.77
0.305	1715	106	1.43	0.77
0.310	1709	106	1.43	0.77
0.315	1704	106	1.42	0.77
0.320	1698	107	1.42	0.77
0.325	1692	105	1.43	0.77
0.330	1686	101	1.45	0.77
0.335	1681	104	1.43	0.75
0.340	1675	104	1.43	0.76
0.345	1669	105	1.42	0.77
0.350	1663	104	1.42	0.77
0.355	1658	104	1.44	0.77
0.360	1652	102	1.45	0.76
0.365	1646	102	1.46	0.75
0.370	1640	102	1.45	0.75
0.375	1634	104	1.44	0.75
0.380	1629	104	1.44	0.76
0.385	1623	105	1.43	0.76
0.390	1617	103	1.45	0.77
0.395	1611	101	1.47	0.75
0.400	1606	100	1.49	0.74
0.405	1600	102	1.47	0.73
0.410	1594	105	1.43	0.74
0.415	1588	105	1.44	0.76
0.420	1582	105	1.42	0.76
0.425	1577	107	1.42	0.77
0.430	1571	106	1.44	0.77
0.435	1565	105	1.44	0.76
0.440	1559	106	1.43	0.76
0.445	1554	108	1.42	0.77
0.450	1548	106	1.43	0.77
0.455	1542	106	1.43	0.77
0.460	1536	106	1.44	0.77
0.465	1531	108	1.41	0.76
0.470	1525	108	1.42	0.78

0.475	1519	109	1.40	0.77
0.480	1513	109	1.42	0.78
0.485	1507	107	1.44	0.77
0.490	1502	107	1.45	0.76
0.495	1496	109	1.46	0.75
0.500	1490	111	1.44	0.75
0.505	1484	111	1.42	0.76
0.510	1479	111	1.44	0.77
0.515	1473	111	1.43	0.76
0.520	1467	111	1.44	0.76
0.525	1461	112	1.44	0.76
0.530	1455	111	1.46	0.76
0.535	1450	113	1.43	0.75
0.540	1444	115	1.43	0.77
0.545	1438	114	1.44	0.77
0.550	1432	113	1.45	0.76
0.555	1427	113	1.45	0.75
0.560	1421	114	1.44	0.76
0.565	1415	115	1.45	0.76
0.570	1409	114	1.45	0.76
0.575	1404	114	1.45	0.75
0.580	1398	114	1.45	0.75
0.585	1392	115	1.43	0.75
0.590	1386	116	1.42	0.76
0.595	1380	115	1.44	0.77
0.600	1375	114	1.45	0.76
0.605	1369	113	1.46	0.75
0.610	1363	115	1.45	0.75
0.615	1357	113	1.47	0.75
0.620	1352	113	1.47	0.74
0.625	1346	114	1.46	0.74
0.630	1340	117	1.45	0.75
0.635	1334	117	1.47	0.75
0.640	1329	115	1.49	0.75
0.645	1323	116	1.47	0.73
0.650	1317	118	1.45	0.74
0.655	1311	120	1.44	0.75
0.660	1305	121	1.44	0.76
0.665	1300	120	1.45	0.76
0.670	1294	120	1.46	0.75
0.675	1288	118	1.47	0.75
0.680	1282	118	1.46	0.74
0.685	1277	119	1.47	0.75
0.690	1271	119	1.47	0.74
0.695	1265	122	1.47	0.74
0.700	1259	122	1.46	0.75
0.705	1253	123	1.46	0.75
0.710	1248	122	1.48	0.75

0.715	1242	122	1.49	0.74
0.720	1236	122	1.48	0.73
0.725	1230		1.48	0.74
0.730	1225		1.47	0.74
0.735	1219		1.48	0.74
0.740	1213	130	1.46	0.74
0.745	1207	128	1.47	0.75
0.750	1202	127	1.50	0.74
0.755	1196	129	1.49	0.73
0.760	1190	131	1.47	0.73
0.765	1184	129	1.50	0.74
0.770	1178		1.50	0.73
0.775	1173		1.51	0.72
0.780	1167		1.51	0.72
0.785	1161		1.50	0.72
0.790	1155		1.50	0.73
0.795	1150	136	1.50	0.73
0.800	1144	135	1.49	0.73
0.805	1138	136	1.48	0.73
0.810	1132	135	1.49	0.74
0.815	1126	135	1.48	0.73
0.820	1121	133	1.48	0.73
0.825	1115	130	1.49	0.74
0.830	1109	131	1.48	0.73
0.835	1103	128	1.48	0.74
0.840	1098	129	1.47	0.74
0.845	1092	127	1.46	0.74
0.850	1086	126	1.46	0.75
0.855	1080	122	1.49	0.75
0.860	1075		1.48	0.73
0.865	1069		1.47	0.74
0.870	1063	120	1.47	0.74
0.875	1057	119	1.49	0.74
0.880	1051	119	1.47	0.73
0.885	1046	119	1.47	0.74
0.890	1040	118	1.45	0.74
0.895	1034	117	1.46	0.75
0.900	1028	116	1.47	0.75
0.905	1023	116	1.47	0.74
0.910	1017	113	1.47	0.74
0.915	1011	114	1.47	0.74
0.920	1005	114	1.47	0.74
0.925	1000	113	1.47	0.75
0.930	994	112	1.48	0.74
0.935	988	111	1.49	0.74
0.940	982	110	1.50	0.73
0.945	976	109	1.51	0.72
0.950	971	109	1.53	0.72

0.955	965	110	1.52	0.71
0.960	959	109	1.48	0.72
0.965	953	107	1.49	0.74
0.970	948	108	1.48	0.73
0.975	942	107	1.48	0.74
0.980	936	103	1.50	0.74
0.985	930	95	1.52	0.73
0.990	924	93	1.53	0.71
0.995	919	93	1.52	0.71
1.000	913	94	1.52	0.71
1.005	907	96	1.45	0.72
1.010	901	103	1.35	0.76
1.015	896	98	1.40	0.81
1.020	890	95	1.46	0.78
1.025	884	96	1.46	0.75
1.030	878	98	1.45	0.75
1.035	873	97	1.46	0.75
1.040	867	97	1.46	0.75
1.045	861	100	1.46	0.75
1.050	855	101	1.45	0.75
1.055	849	101	1.45	0.76
1.060	844		1.44	0.75
1.065	838	108	1.45	0.76
1.070	832	110	1.45	0.76
1.075	826	109	1.49	0.76
1.080	821	100	1.65	0.73
1.085	815	101	1.63	0.64
1.090	809	108	1.53	0.65
1.095	803	113	1.46	0.71
1.100	798	115	1.44	0.75
1.105	791	114	1.45	0.76
1.110	785	114	1.46	0.75
1.115	778	108	1.46	0.75
1.120	772	107	1.45	0.75
1.125	765	106	1.44	0.75
1.130	759	104	1.47	0.76
1.135	752	105	1.46	0.74
1.140	746	101	1.45	0.75
1.145	739	99	1.46	0.76
1.150	733	96	1.48	0.75
1.155	726	96	1.47	0.73
1.160	720	97	1.47	0.74
1.165	713	95	1.48	0.74
1.170	707	96	1.47	0.74
1.175	700	96	1.47	0.74
1.180	694	97	1.45	0.74
1.185	687	95	1.47	0.75
1.190	681	96	1.46	0.74

1.195	674	94	1.47	0.75
1.200	668	94	1.47	0.74
1.205	661	95	1.47	0.74
1.210	655	96	1.45	0.74
1.215	648	96	1.44	0.75
1.220	642	96	1.44	0.76
1.225	635	95	1.45	0.76
1.230	629	94	1.47	0.75
1.235	622	97	1.44	0.74
1.240	616	95	1.45	0.76
1.245	609	95	1.45	0.75
1.250	603	95	1.46	0.75
1.255	596	96	1.45	0.75
1.260	590	95	1.45	0.75
1.265	583	96	1.45	0.75
1.270	577	96	1.45	0.76
1.275	570	97	1.44	0.75
1.280	564	96	1.46	0.76
1.285	557	96	1.46	0.75
1.290	551	96	1.46	0.75
1.295	544	97	1.46	0.75
1.300	538	95	1.48	0.75
1.305	531	94	1.46	0.74
1.310	525	94	1.46	0.75
1.315	518	94	1.47	0.75
1.320	512	94	1.46	0.74
1.325	505	94	1.46	0.75
1.330	499	95	1.46	0.75
1.335	492	96	1.44	0.75
1.340	486	97	1.44	0.76
1.345	479	99	1.41	0.76
1.350	473	96	1.42	0.78
1.355	466	95	1.43	0.77
1.360	460	94	1.45	0.76
1.365	453	95	1.44	0.75
1.370	447	95	1.44	0.76
1.375	440	101	1.42	0.76
1.380	434	102	1.41	0.77
1.385	427	102	1.41	0.78
1.390	421	101	1.41	0.78
1.395	414	100	1.41	0.78
1.400	408	99	1.42	0.78
1.405	401	98	1.41	0.77
1.410	395	98	1.42	0.77
1.415	388	97	1.43	0.77
1.420	382	95	1.46	0.76
1.425	375	97	1.43	0.75
1.430	369	96	1.44	0.76

1.435	363	100	1.43	0.76
1.440	356	99	1.46	0.77
1.445	350	97	1.48	0.75
1.450	343	96	1.50	0.73
1.455	337	100	1.48	0.72
1.460	330	102	1.46	0.73
1.465	324	101	1.46	0.75
1.470	317	102	1.46	0.75
1.475	311	103	1.46	0.75
1.480	304	103	1.46	0.75
1.485	298	102	1.46	0.75
1.490	291	102	1.47	0.75
1.495	285	102	1.46	0.74
1.500	278		1.46	0.75
1.505	272		1.48	0.75
1.510	265		1.48	0.74
1.515	259		1.48	0.73
1.520	252		1.48	0.74
1.525	246		1.48	0.74
1.530	239	110	1.49	0.74
1.535	233	110	1.48	0.73
1.540	226	110	1.48	0.74
1.545	220	111	1.47	0.74
1.550	213	110	1.48	0.74
1.555	207	111	1.47	0.74
1.560	200	110	1.48	0.74
1.565	194	111	1.47	0.74
1.570	187	110	1.48	0.74
1.575	181	111	1.47	0.74
1.580	174	120	1.48	0.74
1.585	168	120	1.50	0.73
1.590	161	121	1.47	0.73
1.595	155	122	1.47	0.74
1.600	148	121	1.48	0.74
1.605	142	120	1.49	0.74
1.610	135	119	1.49	0.73
1.615	129	121	1.48	0.73
1.620	122	120	1.49	0.74
1.625	116	121	1.48	0.73
1.630	109	120	1.49	0.74
1.635	103	122	1.47	0.73
1.640	96	120	1.48	0.74
1.645	90	120	1.48	0.73
1.650	83	120	1.48	0.74
1.655	77	122	1.46	0.74
1.660	70	120	1.47	0.75
1.665	64	120	1.48	0.74
1.670	57	120	1.48	0.74

1.675	51	120	1.48	0.74
1.680	44	119	1.49	0.74
1.685	38	120	1.48	0.73
1.690	31	122	1.47	0.74
1.695	25	120	1.50	0.74
1.700	18	120	1.50	0.73
1.705	12	122	1.50	0.73
1.710	5	123	1.49	0.73
1.715	-1	123	1.48	0.73
1.720	-8	122	1.49	0.74
1.725	-14	121	1.50	0.73
1.730	-21	126	1.49	0.72
1.735	-27	126	1.50	0.73
1.740	-34	127	1.48	0.72
1.745	-40	127	1.50	0.73
1.750	-47		1.50	0.73
1.755	-53		1.49	0.72
1.760	-60	132	1.46	0.73
1.765	-66	131	1.46	0.75
1.770	-72	130	1.49	0.75
1.775	-79	129	1.49	0.73
1.780	-85	128	1.51	0.73
1.785	-92	129	1.50	0.72
1.790	-98	127	1.52	0.72
1.795	-105	128	1.51	0.71
1.800	-111	130	1.49	0.72
1.805	-118	130	1.51	0.73
1.810	-124	132	1.48	0.72
1.815	-131	129	1.50	0.74
1.820	-137	133	1.48	0.72
1.825	-144	133	1.48	0.73
1.830	-150	133	1.48	0.74
1.835	-157	132	1.49	0.74
1.840	-163	130	1.52	0.73
1.845	-170	129	1.52	0.71
1.850	-176	132	1.51	0.71
1.855	-183	132	1.52	0.72
1.860	-189	135	1.50	0.71
1.865	-196	134	1.52	0.72
1.870	-202	135	1.52	0.72
1.875	-209	135	1.52	0.71
1.880	-215	137	1.52	0.71
1.885	-222	137	1.52	0.71
1.890	-228	142	1.49	0.71
1.895	-235	145	1.46	0.73
1.900	-241	147	1.46	0.75
1.905	-248	146	1.49	0.75
1.910	-254	145	1.50	0.73

1.915	-261		1.51	0.72
1.920	-267		1.51	0.72
1.925	-274		1.49	0.72
1.930	-280	154	1.51	0.73
1.935	-287	152	1.52	0.72
1.940	-293	152	1.53	0.71
1.945	-300	152	1.51	0.71
1.950	-306	153	1.49	0.72
1.955	-313	150	1.51	0.73
1.960	-319	148	1.51	0.72
1.965	-326	147	1.52	0.72
1.970	-332	142	1.51	0.71
1.975	-339	140	1.51	0.72
1.980	-345	141	1.50	0.72
1.985	-352	142	1.49	0.73
1.990	-358	139	1.49	0.73
1.995	-365	137	1.49	0.73
2.000	-371	137	1.49	0.73
2.005	-378	134	1.50	0.73
2.010	-384	135	1.50	0.72
2.015	-391	136	1.51	0.73
2.020	-397	134	1.52	0.72
2.025	-404	130	1.57	0.71
2.030	-410	129	1.60	0.68
2.035	-417	132	1.57	0.66
2.040	-423	135	1.53	0.68
2.045	-430	133	1.56	0.71
2.050	-436	133	1.55	0.69
2.055	-443	135	1.52	0.70
2.060	-449	136	1.52	0.71
2.065	-456	136	1.52	0.72
2.070	-462	134	1.51	0.72
2.075	-469	133	1.51	0.72
2.080	-475	134	1.51	0.72
2.085	-482	132	1.52	0.72
2.090	-488	127	1.54	0.71
2.095	-495	129	1.52	0.70
2.100	-501	129	1.52	0.71
2.105	-507	129	1.51	0.71
2.110	-512	127	1.53	0.72
2.115	-518	128	1.52	0.71
2.120	-523	130	1.51	0.71
2.125	-529	133	1.50	0.72
2.130	-534	133	1.50	0.73
2.135	-540	133	1.50	0.73
2.140	-545	130	1.51	0.73
2.145	-551	130	1.52	0.72
2.150	-556	129	1.52	0.71

2.155	-562	129	1.52	0.71
2.160	-567	127	1.52	0.71
2.165	-573	127	1.52	0.71
2.170	-578	127	1.52	0.71
2.175	-584	128	1.51	0.71
2.180	-589	125	1.51	0.72
2.185	-595	126	1.49	0.72
2.190	-601	126	1.48	0.73
2.195	-606	129	1.45	0.74
2.200	-612	129	1.42	0.76
2.205	-617	125	1.46	0.77
2.210	-623	123	1.49	0.75
2.215	-628	121	1.51	0.73
2.220	-634	121	1.49	0.72
2.225	-639	121	1.49	0.73
2.230	-645	121	1.50	0.73
2.235	-650	120	1.49	0.73
2.240	-656	117	1.50	0.73
2.245	-661	117	1.50	0.73
2.250	-667	116	1.50	0.73
2.255	-672	118	1.48	0.73
2.260	-678	116	1.50	0.74
2.265	-683	115	1.49	0.73
2.270	-689	117	1.48	0.73
2.275	-694	115	1.50	0.74
2.280	-700	115	1.50	0.73
2.285	-706	117	1.48	0.73
2.290	-711	117	1.47	0.73
2.295	-717	116	1.49	0.74
2.300	-722	115	1.50	0.73
2.305	-728	115	1.50	0.73
2.310	-733	116	1.48	0.73
2.315	-739	116	1.48	0.74
2.320	-744	116	1.48	0.73
2.325	-750	115	1.50	0.73
2.330	-755	114	1.53	0.73
2.335	-761	112	1.56	0.71
2.340	-766	114	1.53	0.69
2.345	-772	116	1.50	0.71
2.350	-777	115	1.51	0.73
2.355	-783	118	1.49	0.72
2.360	-788	117	1.49	0.73
2.365	-794	116	1.50	0.73
2.370	-800	117	1.48	0.73
2.375	-805	119	1.46	0.73
2.380	-811	118	1.46	0.75
2.385	-816	116	1.48	0.75
2.390	-822	116	1.48	0.74

2.395	-827	117	1.47	0.74
2.400	-833	117	1.47	0.74
2.405	-838	115	1.46	0.74
2.410	-844	114	1.48	0.75
2.415	-849	114	1.48	0.74
2.420	-855	114	1.50	0.74
2.425	-860	114	1.50	0.72
2.430	-866	114	1.50	0.72
2.435	-871	114	1.51	0.73
2.440	-877		1.50	0.72
2.445	-882	115	1.49	0.73
2.450	-888	115	1.49	0.73
2.455	-893	116	1.48	0.73
2.460	-899	116	1.49	0.74
2.465	-905	117	1.49	0.73
2.470	-910	117	1.49	0.73
2.475	-916	119	1.49	0.73
2.480	-921	121	1.47	0.73
2.485	-927	122	1.47	0.74
2.490	-932	124	1.45	0.74
2.495	-938	122	1.48	0.76
2.500	-943	121	1.50	0.74
2.505	-949	119	1.52	0.72
2.510	-954	121	1.52	0.71
2.515	-960	120	1.54	0.71
2.520	-965	120	1.54	0.70
2.525	-971	121	1.52	0.70
2.530	-976	121	1.52	0.71
2.535	-982	123	1.51	0.71
2.540	-987	124	1.50	0.72
2.545	-993	123	1.50	0.73
2.550	-999	123	1.49	0.72
2.555	-1004	122	1.49	0.73
2.560	-1010	122	1.49	0.73
2.565	-1015	122	1.50	0.73
2.570	-1021	122	1.50	0.73
2.575	-1026	121	1.49	0.73
2.580	-1032	120	1.50	0.73
2.585	-1037	118	1.52	0.73
2.590	-1043	115	1.56	0.72
2.595	-1048	120	1.49	0.69
2.600	-1054	120	1.48	0.73
2.605	-1059	119	1.48	0.74
2.610	-1065	118	1.48	0.74
2.615	-1070	118	1.47	0.74
2.620	-1076	118	1.49	0.74
2.625	-1081	118	1.48	0.73
2.630	-1087	117	1.49	0.74

2.635	-1092	116	1.50	0.73
2.640	-1098	116	1.50	0.73
2.645	-1104	115	1.50	0.73
2.650	-1109	116	1.49	0.73
2.655	-1115	116	1.49	0.73
2.660	-1120	117	1.49	0.73
2.665	-1126	116	1.50	0.73
2.670	-1131	117	1.49	0.73
2.675	-1137	118	1.48	0.73
2.680	-1142	119	1.48	0.73
2.685	-1148	118	1.49	0.74
2.690	-1153	119	1.49	0.73
2.695	-1159	121	1.48	0.73
2.700	-1164	122	1.48	0.73
2.705	-1170	122	1.48	0.74
2.710	-1175	122	1.48	0.74
2.715	-1181	122	1.50	0.73
2.720	-1186	122	1.50	0.73
2.725	-1192	123	1.51	0.72
2.730	-1198	124	1.48	0.72
2.735	-1203	127	1.49	0.74
2.740	-1209	127	1.49	0.73
2.745	-1214	125	1.54	0.73
2.750	-1220	121	1.60	0.70
2.755	-1225	125	1.57	0.67
2.760	-1231	131	1.50	0.68
2.765	-1236	133	1.48	0.72
2.770	-1242	131	1.49	0.74
2.775	-1247	132	1.49	0.73
2.780	-1253	132	1.48	0.73
2.785	-1258	131	1.49	0.74
2.790	-1264	132	1.49	0.73
2.795	-1269	125	1.49	0.73
2.800	-1275	125	1.49	0.73
2.805	-1280	125	1.48	0.73
2.810	-1286	124	1.48	0.73
2.815	-1291	123	1.49	0.73
2.820	-1297	122	1.49	0.73
2.825	-1303	122	1.49	0.73
2.830	-1308	122	1.49	0.73
2.835	-1314	123	1.48	0.73
2.840	-1319	122	1.48	0.74
2.845	-1325	121	1.49	0.74
2.850	-1330	123	1.47	0.73
2.855	-1336	120	1.47	0.74
2.860	-1341	119	1.49	0.74
2.865	-1347	121	1.48	0.73
2.870	-1352	119	1.49	0.74

2.875	-1358	120	1.48	0.73
2.880	-1363	119	1.49	0.74
2.885	-1369	118	1.50	0.73
2.890	-1374	118	1.50	0.73
2.895	-1380	119	1.49	0.73
2.900	-1385	120	1.48	0.73
2.905	-1391	119	1.49	0.74
2.910	-1397	120	1.48	0.73
2.915	-1402	119	1.48	0.74
2.920	-1408	119	1.49	0.74
2.925	-1413	119	1.49	0.73
2.930	-1419	117	1.49	0.73
2.935	-1424	117	1.49	0.73
2.940	-1430	117	1.49	0.73
2.945	-1435	115	1.50	0.73
2.950	-1441	116	1.49	0.72
2.955	-1446	116	1.50	0.73
2.960	-1452	115	1.51	0.73
2.965	-1457	116	1.50	0.72
2.970	-1463	113	1.49	0.73
2.975	-1468	114	1.48	0.73
2.980	-1474	114	1.49	0.73
2.985	-1479	113	1.49	0.73
2.990	-1485	111	1.49	0.73
2.995	-1490	111	1.50	0.73
3.000	-1496	109	1.51	0.73
3.005	-1501	110	1.51	0.72
3.010	-1506	109	1.50	0.72
3.015	-1512	109	1.50	0.72
3.020	-1517	108	1.50	0.72
3.025	-1523	106	1.50	0.72
3.030	-1528	105	1.50	0.73
3.035	-1533	106	1.50	0.72
3.040	-1539	106	1.50	0.72
3.045	-1544	103	1.48	0.73
3.050	-1550	103	1.49	0.73
3.055	-1555	103	1.49	0.73
3.060	-1560	103	1.49	0.73
3.065	-1566	100	1.48	0.73
3.070	-1571	97	1.50	0.74
3.075	-1577	96	1.51	0.73
3.080	-1582	97	1.49	0.72
3.085	-1587	95	1.49	0.73
3.090	-1593	96	1.49	0.73
3.095	-1598		1.40	0.73
3.100	-1604		1.40	0.79
3.105	-1609	95	1.48	0.79
3.110	-1614	94	1.49	0.73

3.115	-1620	94	1.49	0.73
3.120	-1625	94	1.49	0.73
3.125	-1631	93	1.48	0.73
3.130	-1636		1.46	0.74
3.135	-1641		1.46	0.75
3.140	-1647	95	1.46	0.75
3.145	-1652	92	1.48	0.75
3.150	-1658	92	1.48	0.74
3.155	-1663	90	1.48	0.74
3.160	-1669	90	1.48	0.74
3.165	-1674	90	1.48	0.73
3.170	-1679	90	1.48	0.74
3.175	-1685	90	1.47	0.73
3.180	-1690	90	1.48	0.74
3.185	-1696	89	1.47	0.74
3.190	-1701	89	1.48	0.74
3.195	-1706	88	1.49	0.73
3.200	-1712	88	1.48	0.73
3.205	-1717	87	1.49	0.73
3.210	-1723	86	1.49	0.73
3.215	-1728	85	1.48	0.73
3.220	-1733	83	1.50	0.73
3.225	-1739	84	1.49	0.72
3.230	-1744	85	1.48	0.73
3.235	-1750	85	1.48	0.74
3.240	-1755	83	1.48	0.74
3.245	-1760	83	1.48	0.73
3.250	-1766	80	1.50	0.73
3.255	-1771	81	1.49	0.73
3.260	-1777	79	1.49	0.73
3.265	-1782	80	1.48	0.73
3.270	-1787	80	1.49	0.74
3.275	-1793	80	1.49	0.73
3.280	-1798	79	1.51	0.73
3.285	-1804	77	1.54	0.72
3.290	-1809	78	1.53	0.70
3.295	-1814	78	1.52	0.71
3.300	-1820	78	1.53	0.71
3.305	-1825	78	1.52	0.71
3.310	-1831	75	1.49	0.71
3.315	-1836	73	1.51	0.73
3.320	-1842	72	1.51	0.72
3.325	-1847	72	1.50	0.72
3.330	-1852	72	1.47	0.73
3.335	-1858	72	1.47	0.74
3.340	-1863	70	1.48	0.74
3.345	-1869	70	1.48	0.74
3.350	-1874	69	1.46	0.74

3.355	-1879	69	1.45	0.75
3.360	-1885	68	1.46	0.75
3.365	-1890	67	1.47	0.75
3.370	-1896	68	1.45	0.74
3.375	-1901		1.46	0.75
3.380	-1906	65	1.47	0.75
3.385	-1912	63	1.48	0.74
3.390	-1917	63	1.47	0.74
3.395	-1923	63	1.47	0.74
3.400	-1928	63	1.48	0.74
3.405	-1933	63	1.48	0.74
3.410	-1939	65	1.48	0.74
3.415	-1944	64	1.49	0.74
3.420	-1950	64	1.50	0.73
3.425	-1955	64	1.49	0.73
3.430	-1960	68	1.48	0.73
3.435	-1966	67	1.49	0.74
3.440	-1971	67	1.50	0.73
3.445	-1977	68	1.51	0.72
3.450	-1982	67	1.52	0.72
3.455	-1987	67	1.52	0.71
3.460	-1993	67	1.53	0.71
3.465	-1998	66	1.54	0.71
3.470	-2004	67	1.54	0.70
3.475	-2009	67	1.55	0.70
3.480	-2015	69	1.54	0.69
3.485	-2020	70	1.51	0.70
3.490	-2025	70	1.52	0.72
3.495	-2031	71	1.51	0.71
3.500	-2036	71	1.51	0.72
3.505	-2042	71	1.51	0.72
3.510	-2047	71	1.51	0.72
3.515	-2052	72	1.50	0.72
3.520	-2058	72	1.49	0.73
3.525	-2063	70	1.50	0.73
3.530	-2069	70	1.51	0.72
3.535	-2074	70	1.52	0.72
3.540	-2079	69	1.55	0.71
3.545	-2085	70	1.52	0.70
3.550	-2090	70	1.52	0.71
3.555	-2096	68	1.51	0.71
3.560	-2101	67	1.52	0.72
3.565	-2106	65	1.53	0.71
3.570	-2112	66	1.52	0.71
3.575	-2117	63	1.50	0.71
3.580	-2123	62	1.48	0.73
3.585	-2128	61	1.47	0.74
3.590	-2133	61	1.48	0.74

3.595	-2139	61	1.48	0.74
3.600	-2144	56	1.47	0.74
3.605	-2150		1.47	0.74
3.610	-2155	55	1.47	0.74
3.615	-2160	54	1.47	0.74
3.620	-2166	54	1.47	0.74
3.625	-2171	53	1.47	0.74
3.630	-2177	52	1.49	0.74
3.635	-2182	53	1.47	0.73
3.640	-2188	53	1.48	0.74
3.645	-2193	53	1.47	0.74
3.650	-2198		1.48	0.74
3.655	-2204		1.47	0.74
3.660	-2209		1.48	0.74
3.665	-2215	52	1.48	0.74
3.670	-2220	52	1.48	0.74
3.675	-2225	52	1.47	0.74
3.680	-2231	52	1.46	0.74
3.685	-2236	52	1.47	0.75
3.690	-2242	49	1.47	0.74
3.695	-2247	49	1.46	0.74
3.700	-2252	49	1.45	0.75
3.705	-2258	50	1.45	0.75
3.710	-2263	49	1.44	0.76
3.715	-2269	48	1.46	0.76
3.720	-2274	49	1.45	0.75
3.725	-2279	49	1.45	0.75
3.730	-2285	48	1.49	0.76
3.735	-2290	49	1.47	0.73
3.740	-2296	50	1.45	0.74
3.745	-2301	52	1.43	0.75
3.750	-2306	51	1.45	0.77
3.755	-2312	51	1.45	0.76
3.760	-2317	55	1.43	0.75
3.765	-2323	55	1.44	0.76
3.770	-2328	55	1.44	0.76
3.775	-2333	54	1.46	0.76
3.780	-2339	54	1.47	0.75
3.785	-2344	54	1.47	0.74
3.790	-2350	61	1.47	0.75
3.795	-2355	60	1.48	0.74
3.800	-2361	60	1.50	0.73
3.805	-2366	59	1.53	0.73
3.810	-2371		1.52	0.71
3.815	-2377		1.51	0.71
3.820	-2382	59	1.53	0.72
3.825	-2388	58	1.53	0.71
3.830	-2393	57	1.53	0.71

3.835	-2398	58	1.51	0.71
3.840	-2404	57	1.50	0.72
3.845	-2409	57	1.50	0.73
3.850	-2415	56	1.51	0.72
3.855	-2420	56	1.49	0.72
3.860	-2425	56	1.49	0.73
3.865	-2431	57	1.49	0.73
3.870	-2436	55	1.48	0.73
3.875	-2442	54	1.48	0.73
3.880	-2447	54	1.47	0.73
3.885	-2452	54	1.47	0.74
3.890	-2458	54	1.47	0.74
3.895	-2463	54	1.48	0.74
3.900	-2469	53	1.48	0.74
3.905	-2474	54	1.47	0.73
3.910	-2479	55	1.45	0.74
3.915	-2485	54	1.46	0.75
3.920	-2490	55	1.45	0.75
3.925	-2496	55	1.46	0.75
3.930	-2501	55	1.45	0.75
3.935	-2506	56	1.45	0.75
3.940	-2512	56	1.46	0.75
3.945	-2517	57	1.45	0.75
3.950	-2523	57	1.45	0.76
3.955	-2528	56	1.47	0.75
3.960	-2534	56	1.49	0.74
3.965	-2539	55	1.50	0.73
3.970	-2544	58	1.54	0.72
3.975	-2550	56	1.60	0.70
3.980	-2555	55	1.61	0.66
3.985	-2561	58	1.54	0.66
3.990	-2566	59	1.52	0.70
3.995	-2571	60	1.50	0.71
4.000	-2577	60	1.49	0.73
4.005	-2582	60	1.48	0.73
4.010	-2588	60	1.49	0.74
4.015	-2593	60	1.49	0.73
4.020	-2598	59	1.49	0.73
4.025	-2604	60	1.48	0.73
4.030	-2609	60	1.49	0.74
4.035	-2615	60	1.49	0.73
4.040	-2620	60	1.50	0.73
4.045	-2625	59	1.50	0.73
4.050	-2631	59	1.50	0.72
4.055	-2636	59	1.52	0.72
4.060	-2642	59	1.51	0.71
4.065	-2647	62	1.51	0.72
4.070	-2652	62	1.51	0.72

4.075	-2658	60	1.53	0.72
4.080	-2663	60	1.53	0.71
4.085	-2669	60	1.52	0.71
4.090	-2674	68	1.35	0.71
4.095	-2679	93	0.98	0.81
4.100	-2685	71	1.29	1.03
4.105	-2690	60	1.53	0.85
4.110	-2696	61	1.52	0.71
4.115	-2701	60	1.53	0.71
4.120	-2707	59	1.53	0.71
4.125	-2712	60	1.52	0.71
4.130	-2717	60	1.54	0.71
4.135	-2723	61	1.52	0.70
4.140	-2728	60	1.53	0.71
4.145	-2734	59	1.53	0.71
4.150	-2739	59	1.53	0.71
4.155	-2744	58	1.55	0.71
4.160	-2750	58	1.55	0.70
4.165	-2755	58	1.54	0.70
4.170	-2761	58	1.53	0.70
4.175	-2766	58	1.53	0.71
4.180	-2771	58	1.53	0.71
4.185	-2777	58	1.52	0.71
4.190	-2782	57	1.52	0.71
4.195	-2788	57	1.52	0.71
4.200	-2793	58	1.50	0.71
4.205	-2798	55	1.51	0.72
4.210	-2804	54	1.51	0.72
4.215	-2809	54	1.51	0.72
4.220	-2815	52	1.51	0.72
4.225	-2820	54	1.50	0.72
4.230	-2825	52	1.52	0.72
4.235	-2831	51	1.51	0.71
4.240	-2836	52	1.49	0.72
4.245	-2842	50	1.49	0.73
4.250	-2847	50	1.48	0.73
4.255	-2852	49	1.47	0.74
4.260	-2858	49	1.47	0.74
4.265	-2863	48	1.46	0.74
4.270	-2869	47	1.47	0.75
4.275	-2874	47	1.46	0.74
4.280	-2880	47	1.46	0.75
4.285	-2885	47	1.46	0.75
4.290	-2890	48	1.44	0.75
4.295	-2896	48	1.44	0.76
4.300	-2901	48	1.45	0.76
4.305	-2907	47	1.46	0.76
4.310	-2912	46	1.45	0.75

4.315	-2917	46	1.45	0.75
4.320	-2923	46	1.46	0.75
4.325	-2928	47	1.48	0.75
4.330	-2934	47	1.48	0.74
4.335	-2939	47	1.49	0.74
4.340	-2944	48	1.47	0.73
4.345	-2950	48	1.45	0.75
4.350	-2955	53	1.46	0.75
4.355	-2961	51	1.48	0.75
4.360	-2966	51	1.50	0.74
4.365	-2971	51	1.51	0.72
4.370	-2977	50	1.51	0.72
4.375	-2982	50	1.53	0.72
4.380	-2988	58	1.51	0.71
4.385	-2993	58	1.51	0.72
4.390	-2998	58	1.52	0.72
4.395	-3004	58	1.50	0.72
4.400	-3009	60	1.50	0.73
4.405	-3015	61	1.50	0.72
4.410	-3020	60	1.52	0.73
4.415	-3025	59	1.54	0.72
4.420	-3031	59	1.54	0.70
4.425	-3036	60	1.52	0.70
4.430	-3042	60	1.52	0.71
4.435	-3047	60	1.53	0.72
4.440	-3053	62	1.51	0.71
4.445	-3058	63	1.49	0.72
4.450	-3063	63	1.49	0.73
4.455	-3069	63	1.48	0.73
4.460	-3074	63	1.48	0.74
4.465	-3080	61	1.49	0.73
4.470	-3085	60	1.49	0.73
4.475	-3090	60	1.49	0.73
4.480	-3096	61	1.48	0.73
4.485	-3101	60	1.50	0.74
4.490	-3107	62	1.49	0.72
4.495	-3112	62	1.50	0.73
4.500	-3117	64	1.51	0.72
4.505	-3123	64	1.51	0.72
4.510	-3128	65	1.51	0.72
4.515	-3134	65	1.51	0.72
4.520	-3139	68	1.51	0.72
4.525	-3144	68	1.51	0.72
4.530	-3150	68	1.51	0.72
4.535	-3155	68	1.51	0.72
4.540	-3161	69	1.51	0.72
4.545	-3166	69	1.51	0.72
4.550	-3171	69	1.52	0.72

4.555	-3177	69	1.51	0.71
4.560	-3182	69	1.53	0.72
4.565	-3188	68	1.53	0.71
4.570	-3193	67	1.56	0.71
4.575	-3198	69	1.55	0.69
4.580	-3204	69	1.53	0.70
4.585	-3209	69	1.54	0.71
4.590	-3215	68	1.56	0.70
4.595	-3220	67	1.57	0.69
4.600	-3226	67	1.57	0.68
4.605	-3231	68	1.56	0.68
4.610	-3236	68	1.54	0.69
4.615	-3242	68	1.55	0.70
4.620	-3247	66	1.53	0.70
4.625	-3253	65	1.52	0.71
4.630	-3258	63	1.51	0.71
4.635	-3263	62	1.51	0.72
4.640	-3269	63	1.50	0.72
4.645	-3274	58	1.50	0.73
4.650	-3280	56	1.51	0.73
4.655	-3285		1.49	0.72
4.660	-3290		1.49	0.73
4.665	-3296	54	1.48	0.73
4.670	-3301	53	1.48	0.74
4.675	-3307	54	1.47	0.74
4.680	-3312	54	1.47	0.74
4.685	-3317	51	1.47	0.74
4.690	-3323	51	1.48	0.74
4.695	-3328	50	1.47	0.74
4.700	-3334	49	1.47	0.74
4.705	-3339	49	1.46	0.74
4.710	-3344	50	1.45	0.75
4.715	-3350	49	1.45	0.75
4.720	-3355	49	1.45	0.75
4.725	-3361	49	1.46	0.75
4.730	-3366	49	1.46	0.75
4.735	-3371	48	1.46	0.75
4.740	-3377	48	1.47	0.75
4.745	-3382	49	1.45	0.74
4.750	-3388	49	1.45	0.75
4.755	-3393	49	1.45	0.75
4.760	-3399	49	1.45	0.75
4.765	-3404		1.45	0.75
4.770	-3409	47	1.46	0.76
4.775	-3415	46	1.46	0.75
4.780	-3420	47	1.45	0.75
4.785	-3426	46	1.47	0.75
4.790	-3431	46	1.47	0.74

4.795	-3436	44	1.50	0.74
4.800	-3442	46	1.46	0.73
4.805	-3447	46	1.46	0.75
4.810	-3453	46	1.46	0.75
4.815	-3458	47	1.45	0.75
4.820	-3463	47	1.46	0.75
4.825	-3469	47	1.47	0.75
4.830	-3474	47	1.47	0.74
4.835	-3480	47	1.46	0.75
4.840	-3485	49	1.46	0.75
4.845	-3490	48	1.47	0.75
4.850	-3496	49	1.46	0.74
4.855	-3501	50	1.48	0.75
4.860	-3507	50	1.48	0.74
4.865	-3512	50	1.47	0.74
4.870	-3517	50	1.48	0.74
4.875	-3523	50	1.49	0.74
4.880	-3528	49	1.49	0.73
4.885	-3534		1.49	0.73
4.890	-3539	50	1.49	0.73
4.895	-3544	51	1.49	0.73
4.900	-3550	51	1.49	0.73
4.905	-3555	51	1.49	0.73
4.910	-3561	53	1.49	0.73
4.915	-3566	53	1.50	0.73
4.920	-3572	53	1.48	0.73
4.925	-3577	53	1.48	0.74
4.930	-3582	54	1.47	0.74
4.935	-3588	54	1.48	0.74
4.940	-3593	55	1.46	0.74
4.945	-3599	54	1.47	0.75
4.950	-3604	54	1.47	0.74
4.955	-3609	58	1.49	0.74
4.960	-3615	58	1.49	0.73
4.965	-3620	59	1.50	0.73
4.970	-3626	61	1.50	0.73
4.975	-3631	63	1.48	0.73
4.980	-3636	63	1.49	0.73
4.985	-3642	62	1.50	0.73
4.990	-3647	62	1.50	0.73
4.995	-3653	71	1.50	0.73
5.000	-3659	74	1.50	0.73
5.005	-3669	74	1.50	0.73
5.010	-3679	80	1.52	0.72
5.015	-3689	83	1.52	0.72
5.020	-3699	87	1.52	0.71
5.025	-3710	88	1.60	0.71
5.030	-3720	78	1.87	0.67

5.035	-3730	68	2.22	0.51
5.040	-3740	65	2.38	0.31
5.045	-3751	65	2.40	0.21
5.050	-3761	67	2.34	0.20
5.055	-3771	79	1.98	0.24
5.060	-3781	92	1.68	0.45
5.065	-3792	98	1.57	0.62
5.070	-3802	100	1.54	0.69
5.075	-3812	101	1.54	0.70
5.080	-3822	99	1.56	0.70
5.085	-3833	84	1.57	0.69
5.090	-3843	84	1.52	0.68
5.095	-3853	82	1.51	0.71
5.100	-3863	79	1.51	0.72
5.105	-3874	76	1.51	0.72
5.110	-3884	76	1.52	0.72
5.115	-3894	73	1.51	0.72
5.120	-3904	71	1.49	0.72
5.125	-3915	70	1.51	0.73
5.130	-3925	68	1.49	0.72
5.135	-3935	67	1.49	0.73
5.140	-3945	67	1.49	0.73
5.145	-3956	67	1.50	0.73
5.150	-3966	65	1.49	0.73
5.155	-3976	65	1.50	0.73
5.160	-3986	64	1.52	0.73
5.165	-3997	64	1.52	0.72
5.170	-4007	68	1.45	0.71
5.175	-4017	68	1.46	0.76
5.180	-4027	68	1.47	0.75
5.185	-4038	69	1.47	0.74
5.190	-4048	70	1.47	0.74
5.195	-4058	69	1.48	0.74
5.200	-4068	70	1.49	0.74
5.205	-4079	71	1.48	0.73
5.210	-4089	72	1.48	0.73
5.215	-4099	72	1.48	0.74
5.220	-4109	73	1.47	0.73
5.225	-4120	73	1.48	0.74
5.230	-4130		1.47	0.74
5.235	-4140	76	1.49	0.74
5.240	-4150	76	1.48	0.73
5.245	-4161	77	1.49	0.73
5.250	-4171	77	1.51	0.73
5.255	-4181	77	1.51	0.72
5.260	-4191	78	1.51	0.72
5.265	-4202	79	1.51	0.72
5.270	-4212	80	1.50	0.72

5.275	-4222	80	1.49	0.73
5.280	-4232	80	1.49	0.73
5.285	-4243	80	1.50	0.73
5.290	-4253	83	1.50	0.72
5.295	-4263	85	1.50	0.72
5.300	-4273	85	1.49	0.72
5.305	-4283	84	1.52	0.73
5.310	-4294	88	1.50	0.71
5.315	-4304	87	1.51	0.72
5.320	-4314	88	1.51	0.72
5.325	-4324	88	1.50	0.72
5.330	-4335	87	1.52	0.73
5.335	-4345	91	1.52	0.71
5.340	-4355	91	1.51	0.71
5.345	-4365	91	1.53	0.72
5.350	-4376	92	1.52	0.71
5.355	-4386	91	1.55	0.71
5.360	-4396	93	1.53	0.69
5.365	-4406	93	1.53	0.71
5.370	-4417		1.54	0.71
5.375	-4427	94	1.54	0.70
5.380	-4437	95	1.52	0.70
5.385	-4447	95	1.52	0.72
5.390	-4458	97	1.51	0.71
5.395	-4468	95	1.53	0.72
5.400	-4478	96	1.54	0.71
5.405	-4488	96	1.52	0.70
5.410	-4499	97	1.51	0.71
5.415	-4509	98	1.51	0.72
5.420	-4519	97	1.52	0.72
5.425	-4529	98	1.52	0.72
5.430	-4540	97	1.53	0.72
5.435	-4550	99	1.50	0.71
5.440	-4560	99	1.53	0.72
5.445	-4570	100	1.51	0.71
5.450	-4581		1.51	0.72
5.455	-4591		1.52	0.72
5.460	-4601	104	1.53	0.71
5.465	-4611	105	1.52	0.71
5.470	-4622	104	1.53	0.71
5.475	-4632	104	1.53	0.71
5.480	-4642	110	1.53	0.71
5.485	-4652	112	1.53	0.71
5.490	-4663	112	1.52	0.71
5.495	-4673	112	1.52	0.71
5.500	-4683	118	1.52	0.71
5.505	-4693	120	1.51	0.71
5.510	-4704	121	1.52	0.72

5.515	-4714	121	1.52	0.71
5.520	-4724	124	1.54	0.71
5.525	-4734	124	1.54	0.70
5.530	-4745	128	1.56	0.70
5.535	-4755	129	1.56	0.69
5.540	-4765	129	1.57	0.69
5.545	-4775	134	1.57	0.68
5.550	-4786	135	1.57	0.69
5.555	-4796	138	1.56	0.68
5.560	-4806	137	1.57	0.69
5.565	-4816	136	1.58	0.68
5.570	-4827	143	1.57	0.68
5.575	-4837	145	1.57	0.68
5.580	-4847	144	1.58	0.68
5.585	-4857	147	1.57	0.68
5.590	-4868	148	1.56	0.69
5.595	-4878	148	1.56	0.69
5.600	-4888	149	1.58	0.69
5.605	-4898	148	1.58	0.68
5.610	-4908	149	1.58	0.68
5.615	-4919	149	1.58	0.68
5.620	-4929	150	1.58	0.68
5.625	-4939	149	1.58	0.68
5.630	-4949	150	1.57	0.68
5.635	-4960	150	1.58	0.68
5.640	-4970	149	1.58	0.68
5.645	-4980	148	1.58	0.68
5.650	-4990	147	1.59	0.68
5.655	-5001	150	1.57	0.67
5.660	-5011	150	1.57	0.69
5.665	-5021		1.56	0.69
5.670	-5031	152	1.54	0.69
5.675	-5042	150	1.56	0.70
5.680	-5052	149	1.57	0.69
5.685	-5062	148	1.57	0.69
5.690	-5072	148	1.57	0.69
5.695	-5083	148	1.57	0.69
5.700	-5093		1.57	0.69
5.705	-5103	148	1.57	0.68
5.710	-5113		1.59	0.68
5.715	-5124	148	1.57	0.67
5.720	-5134	148	1.57	0.68
5.725	-5144	147	1.58	0.68
5.730	-5154	147	1.58	0.68
5.735	-5165	147	1.58	0.68
5.740	-5175	144	1.60	0.68
5.745	-5185	140	1.65	0.67
5.750	-5195	140	1.63	0.64

5.755	-5206	144	1.57	0.65
5.760	-5216	144	1.55	0.68
5.765	-5226	141	1.57	0.70
5.770	-5236	141	1.55	0.68
5.775	-5247	141	1.56	0.69
5.780	-5257	142	1.55	0.69
5.785	-5267	138	1.54	0.70
5.790	-5277	138	1.54	0.70
5.795	-5288	137	1.54	0.70
5.800	-5298	136	1.55	0.70
5.805	-5308	134	1.56	0.70
5.810	-5318	135	1.56	0.69
5.815	-5329	136	1.54	0.69
5.820	-5339	135	1.55	0.70
5.825	-5349	135	1.55	0.70
5.830	-5359	140	1.55	0.69
5.835	-5370	139	1.56	0.70
5.840	-5380	140	1.57	0.69
5.845	-5390	142	1.56	0.69
5.850	-5400	141	1.57	0.69
5.855	-5411	145	1.54	0.69
5.860	-5421	144	1.56	0.70
5.865	-5431	144	1.56	0.69
5.870	-5441	144	1.56	0.69
5.875	-5452	143	1.57	0.69
5.880	-5462	143	1.56	0.68
5.885	-5472	142	1.56	0.69
5.890	-5482	143	1.56	0.69
5.895	-5493	142	1.56	0.69
5.900	-5503	141	1.57	0.69
5.905	-5513	141	1.57	0.69
5.910	-5523	142	1.56	0.69
5.915	-5533	141	1.57	0.69
5.920	-5544	140	1.57	0.69
5.925	-5554	140	1.57	0.68
5.930	-5564	141	1.56	0.68
5.935	-5574	140	1.55	0.69
5.940	-5585	141	1.55	0.69
5.945	-5595	139	1.56	0.69
5.950	-5605	139	1.56	0.69
5.955	-5615	140	1.56	0.69
5.960	-5626	139	1.56	0.69
5.965	-5636	139	1.56	0.69
5.970	-5646	140	1.56	0.69
5.975	-5656	139	1.57	0.69
5.980	-5667	139	1.57	0.68
5.985	-5677	139	1.57	0.69
5.990	-5687		1.57	0.68

5.995	-5697	138	1.59	0.68
6.000	-5708	140	1.57	0.67
6.005	-5718	144	1.54	0.68
6.010	-5728	144	1.55	0.70
6.015	-5738	146	1.55	0.70
6.020	-5749	147	1.56	0.69
6.025	-5759	147	1.58	0.69
6.030	-5769	149	1.56	0.68
6.035	-5779	148	1.57	0.69
6.040	-5790	148	1.57	0.69
6.045	-5800	158	1.59	0.68
6.050	-5810	159	1.62	0.67
6.055	-5820	142	1.81	0.66
6.060	-5831	130	1.98	0.54
6.065	-5841	130	1.98	0.44
6.070	-5851	158	1.77	0.45
6.075	-5861	174	1.61	0.57
6.080	-5872	176	1.59	0.66
6.085	-5882	176	1.60	0.67
6.090	-5892	173	1.62	0.67
6.095	-5902	173	1.62	0.66
6.100	-5913	205	1.65	0.65
6.105	-5923	205	1.72	0.64
6.110	-5933	204	1.75	0.60
6.115	-5943	206	1.78	0.58
6.120	-5954	208	1.79	0.56
6.125	-5964	214	1.75	0.56
6.130	-5974	220	1.69	0.58
6.135	-5984	221	1.64	0.61
6.140	-5995	224	1.62	0.64
6.145	-6005	213	1.62	0.65
6.150	-6015	206	1.62	0.65
6.155	-6025	201	1.61	0.66
6.160	-6036	216	1.50	0.66
6.165	-6046	285	1.13	0.72
6.170	-6056	222	1.34	0.94
6.175	-6066	185	1.61	0.82
6.180	-6077	182	1.63	0.66
6.185	-6087	177	1.63	0.65
6.190	-6097	174	1.64	0.65
6.195	-6107	174	1.64	0.64
6.200	-6118	175	1.63	0.64
6.205	-6128	173	1.64	0.65
6.210	-6138	172	1.65	0.64
6.215	-6148	175	1.62	0.64
6.220	-6158	173	1.63	0.66
6.225	-6169	174	1.62	0.65
6.230	-6179	175	1.61	0.65

6.235	-6189	168	1.63	0.66
6.240	-6199	168	1.62	0.65
6.245	-6210	164	1.64	0.66
6.250	-6220	158	1.70	0.64
6.255	-6230	158	1.69	0.61
6.260	-6240	164	1.63	0.61
6.265	-6251	162	1.60	0.65
6.270	-6261	160	1.60	0.66
6.275	-6271	159	1.61	0.66
6.280	-6281	157	1.60	0.66
6.285	-6292	155	1.62	0.67
6.290	-6302	155	1.62	0.66
6.295	-6312	153	1.61	0.66
6.300	-6322	153	1.60	0.66
6.305	-6333	152	1.60	0.67
6.310	-6343	151	1.60	0.67
6.315	-6353	151	1.60	0.67
6.320	-6363	150	1.60	0.67
6.325	-6374	148	1.62	0.67
6.330	-6384	149	1.61	0.65
6.335	-6394	149	1.61	0.66
6.340	-6404	149	1.62	0.66
6.345	-6415	150	1.61	0.66
6.350	-6425	150	1.61	0.66
6.355	-6435	149	1.63	0.66
6.360	-6445	150	1.61	0.65
6.365	-6456	150	1.61	0.66
6.370	-6466	150	1.63	0.66
6.375	-6476	151	1.62	0.65
6.380	-6486	152	1.62	0.66
6.385	-6497	155	1.61	0.66
6.390	-6507	153	1.64	0.66
6.395	-6517	156	1.63	0.65
6.400	-6527	157	1.62	0.65
6.405	-6538	157	1.63	0.65
6.410	-6548	156	1.66	0.65
6.415	-6558	152	1.71	0.63
6.420	-6568	153	1.71	0.61
6.425	-6579	157	1.66	0.60
6.430	-6589	161	1.62	0.63
6.435	-6599	163	1.63	0.65
6.440	-6609	162	1.63	0.65
6.445	-6620	163	1.63	0.65
6.450	-6630	162	1.63	0.65
6.455	-6640	162	1.63	0.65
6.460	-6650	164	1.63	0.65
6.465	-6661	163	1.64	0.65
6.470	-6671	164	1.63	0.64

6.475	-6681	164	1.64	0.65
6.480	-6691	164	1.64	0.65
6.485	-6702	165	1.64	0.65
6.490	-6712	162	1.66	0.64
6.495	-6722	163	1.65	0.63
6.500	-6732	164	1.66	0.64
6.505	-6742	165	1.64	0.63
6.510	-6753	165	1.64	0.64
6.515	-6763	165	1.63	0.65
6.520	-6773	165	1.63	0.65
6.525	-6783	167	1.62	0.65
6.530	-6794	166	1.61	0.66
6.535	-6804	163	1.61	0.66
6.540	-6814	163	1.61	0.66
6.545	-6824	161	1.62	0.66
6.550	-6835	160	1.63	0.65
6.555	-6845	160	1.64	0.65
6.560	-6855	159	1.64	0.65
6.565	-6865	163	1.61	0.64
6.570	-6876	163	1.62	0.66
6.575	-6886	164	1.61	0.66
6.580	-6896	163	1.61	0.66
6.585	-6906	162	1.62	0.66
6.590	-6917	164	1.63	0.65
6.595	-6927	166	1.62	0.65
6.600	-6937	166	1.63	0.65
6.605	-6947	165	1.64	0.65
6.610	-6958	167	1.62	0.64
6.615	-6968	165	1.64	0.66
6.620	-6978	166	1.62	0.64
6.625	-6988	172	1.62	0.65
6.630	-6999	171	1.63	0.65
6.635	-7009	171	1.64	0.65
6.640	-7019	169	1.66	0.65
6.645	-7029	170	1.65	0.63
6.650	-7040	169	1.66	0.64
6.655	-7050	171	1.64	0.63
6.660	-7060	170	1.66	0.64
6.665	-7070	171	1.65	0.63
6.670	-7081	171	1.65	0.64
6.675	-7091	171	1.66	0.64
6.680	-7101	172	1.65	0.63
6.685	-7111	173	1.64	0.64
6.690	-7122	172	1.64	0.64
6.695	-7132	170	1.66	0.64
6.700	-7142	171	1.65	0.63
6.705	-7152	171	1.65	0.64
6.710	-7163	171	1.65	0.64

6.715	-7173	170	1.66	0.64
6.720	-7183	171	1.65	0.63
6.725	-7193	171	1.65	0.64
6.730	-7204	170	1.66	0.64
6.735	-7214	172	1.64	0.63
6.740	-7224	172	1.64	0.64
6.745	-7234	171	1.65	0.64
6.750	-7245	170	1.66	0.64
6.755	-7255	169	1.66	0.63
6.760	-7265	170	1.66	0.63
6.765	-7275	170	1.66	0.63
6.770	-7286	172	1.66	0.63
6.775	-7296	172	1.67	0.63
6.780	-7306	173	1.65	0.63
6.785	-7316	174	1.64	0.64
6.790	-7327	172	1.64	0.64
6.795	-7337	171	1.64	0.64
6.800	-7347	172	1.64	0.64
6.805	-7357	172	1.63	0.65
6.810	-7367	170	1.66	0.65
6.815	-7378	165	1.64	0.63
6.820	-7388	165	1.64	0.64
6.825	-7398	163	1.65	0.64
6.830	-7408	162	1.66	0.64
6.835	-7419	161	1.65	0.63
6.840	-7429	161	1.63	0.64
6.845	-7439	160	1.64	0.65
6.850	-7449	161	1.63	0.64
6.855	-7460	160	1.64	0.65
6.860	-7470	161	1.62	0.65
6.865	-7480	161	1.62	0.65
6.870	-7490	162	1.61	0.66
6.875	-7501	160	1.63	0.66
6.880	-7511	158	1.63	0.65
6.885	-7521	158	1.63	0.65
6.890	-7531	158	1.64	0.65
6.895	-7542	157	1.66	0.65
6.900	-7552	157	1.66	0.63
6.905	-7562	159	1.64	0.64
6.910	-7572	713	1.64	0.64
6.915	-7583	159	1.65	0.64
6.920	-7593	158	1.66	0.64
6.925	-7603	158	1.66	0.63
6.930	-7613	157	1.66	0.63
6.935	-7624	156	1.67	0.63
6.940	-7634	157	1.67	0.63
6.945	-7644	159	1.66	0.63
6.950	-7654	156	1.67	0.63

6.955	-7665	155	1.68	0.62
6.960	-7675	156	1.67	0.62
6.965	-7685	159	1.65	0.63
6.970	-7695	156	1.68	0.64
6.975	-7706	156	1.68	0.62
6.980	-7716	154	1.68	0.62
6.985	-7726	155	1.67	0.62
6.990	-7736	155	1.68	0.62
6.995	-7747	154	1.69	0.62
7.000	-7757	153	1.69	0.62
7.005	-7767	151	1.70	0.62
7.010	-7777	150	1.70	0.61
7.015	-7788	152	1.68	0.61
7.020	-7798	150	1.69	0.62
7.025	-7808	150	1.69	0.61
7.030	-7818	149	1.70	0.61
7.035	-7829	150	1.70	0.61
7.040	-7839	150	1.69	0.61
7.045	-7849	151	1.68	0.62
7.050	-7859	151	1.68	0.62
7.055	-7870	263	1.67	0.62
7.060	-7880	152	1.68	0.63
7.065	-7890	152	1.68	0.62
7.070	-7900	153	1.67	0.62
7.075	-7911	155	1.67	0.63
7.080	-7921	155	1.68	0.62
7.085	-7931	157	1.67	0.62
7.090	-7941	156	1.68	0.63
7.095	-7952	157	1.69	0.62
7.100	-7962	157	1.68	0.62
7.105	-7972	158	1.68	0.62
7.110	-7982	157	1.71	0.62
7.115	-7992	158	1.71	0.60
7.120	-8003	159	1.69	0.61
7.125	-8013	159	1.70	0.62
7.130	-8023	159	1.69	0.61
7.135	-8033	159	1.70	0.61
7.140	-8044	160	1.70	0.61
7.145	-8054	159	1.71	0.61
7.150	-8064	158	1.72	0.60
7.155	-8074	158	1.72	0.60
7.160	-8085	160	1.70	0.59
7.165	-8095	164	1.66	0.61
7.170	-8105	161	1.69	0.63
7.175	-8115	161	1.70	0.61
7.180	-8126	161	1.70	0.61
7.185	-8136	163	1.69	0.61
7.190	-8146	165	1.68	0.61

7.195	-8156	164	1.69	0.62
7.200	-8167	164	1.69	0.62
7.205	-8177	164	1.69	0.61
7.210	-8187	165	1.69	0.62
7.215	-8197	167	1.67	0.61
7.220	-8208	166	1.68	0.63
7.225	-8218	165	1.70	0.62
7.230	-8228	165	1.70	0.61
7.235	-8238	165	1.70	0.61
7.240	-8249	165	1.70	0.61
7.245	-8259	164	1.71	0.61
7.250	-8269	170	1.69	0.60
7.255	-8279	170	1.69	0.61
7.260	-8290	170	1.71	0.61
7.265	-8300	170	1.71	0.61
7.270	-8310	173	1.70	0.61
7.275	-8320	172	1.72	0.61
7.280	-8331	172	1.72	0.60
7.285	-8341	174	1.71	0.60
7.290	-8351	176	1.70	0.60
7.295	-8361	177	1.70	0.61
7.300	-8372	176	1.70	0.61
7.305	-8382	178	1.70	0.61
7.310	-8392	175	1.73	0.61
7.315	-8402	175	1.73	0.59
7.320	-8413	176	1.72	0.59
7.325	-8423	176	1.72	0.60
7.330	-8433	175	1.74	0.59
7.335	-8443	176	1.73	0.59
7.340	-8454	176	1.73	0.59
7.345	-8464	176	1.73	0.59
7.350	-8474	177	1.72	0.59
7.355	-8484	176	1.73	0.60
7.360	-8495	177	1.72	0.59
7.365	-8505	178	1.71	0.60
7.370	-8515	178	1.72	0.60
7.375	-8525	178	1.72	0.60
7.380	-8536	178	1.72	0.59
7.385	-8546	180	1.70	0.60
7.390	-8556	180	1.73	0.61
7.395	-8566	180	1.72	0.59
7.400	-8577	181	1.73	0.60
7.405	-8587	184	1.72	0.59
7.410	-8597	181	1.75	0.60
7.415	-8607	187	1.73	0.58
7.420	-8617	187	1.72	0.59
7.425	-8628	191	1.73	0.59
7.430	-8638	194	1.73	0.59

7.435	-8648	197	1.72	0.59
7.440	-8658	197	1.72	0.60
7.445	-8669	195	1.74	0.60
7.450	-8679	208	1.72	0.59
7.455	-8689	209	1.72	0.60
7.460	-8699	212	1.69	0.60
7.465	-8710	212	1.70	0.61
7.470	-8720	211	1.71	0.61
7.475	-8730	208	1.72	0.61
7.480	-8740	203	1.77	0.59
7.485	-8751	233	1.80	0.57
7.490	-8761	232	1.80	0.55
7.495	-8771	234	1.81	0.55
7.500	-8781	233	1.82	0.55
7.505	-8792	234	1.77	0.54
7.510	-8802	233	1.75	0.57
7.515	-8812	233	1.75	0.58
7.520	-8822	222	1.72	0.58
7.525	-8833	222	1.72	0.60
7.530	-8843	204	1.73	0.60
7.535	-8853	202	1.75	0.59
7.540	-8863	202	1.74	0.58
7.545	-8874	202	1.74	0.59
7.550	-8884	173	1.73	0.59
7.555	-8894	170	1.72	0.59
7.560	-8904	171	1.71	0.60
7.565	-8915	170	1.72	0.60
7.570	-8925	169	1.73	0.60
7.575	-8935	153	1.74	0.59
7.580	-8945	155	1.72	0.59
7.585	-8956	156	1.71	0.60
7.590	-8966	150	1.73	0.60
7.595	-8976	150	1.72	0.59
7.600	-8986	150	1.71	0.60
7.605	-8997		1.71	0.60
7.610	-9007		1.70	0.60
7.615	-9017		1.69	0.61
7.620	-9027	148	1.68	0.62
7.625	-9038	147	1.69	0.62
7.630	-9048	146	1.69	0.61
7.635	-9058	146	1.68	0.62
7.640	-9068	147	1.67	0.62
7.645	-9079	145	1.68	0.63
7.650	-9089	147	1.66	0.62
7.655	-9099	146	1.66	0.63
7.660	-9109	147	1.65	0.63
7.665	-9120	146	1.65	0.64
7.670	-9130	147	1.64	0.64

7.675	-9140	148	1.63	0.64
7.680	-9150	145	1.66	0.65
7.685	-9161	146	1.65	0.64
7.690	-9171	146	1.63	0.64
7.695	-9181	146	1.64	0.65
7.700	-9191	146	1.64	0.64
7.705	-9201	146	1.64	0.65
7.710	-9212	145	1.66	0.64
7.715	-9222	145	1.65	0.64
7.720	-9232	145	1.65	0.64
7.725	-9242	144	1.64	0.64
7.730	-9253	146	1.63	0.64
7.735	-9263	144	1.64	0.65
7.740	-9273	142	1.64	0.64
7.745	-9283	142	1.64	0.64
7.750	-9294	140	1.64	0.64
7.755	-9304	139	1.65	0.64
7.760	-9314	140	1.64	0.64
7.765	-9324	139	1.64	0.65
7.770	-9335	137	1.65	0.64
7.775	-9345	137	1.65	0.64
7.780	-9355	137	1.65	0.64
7.785	-9365	138	1.65	0.64
7.790	-9376	138	1.65	0.64
7.795	-9386	139	1.64	0.64
7.800	-9396		1.65	0.64
7.805	-9406		1.64	0.64
7.810	-9417		1.65	0.65
7.815	-9427	138	1.66	0.64
7.820	-9437	139	1.65	0.63
7.825	-9447	138	1.66	0.64
7.830	-9458	138	1.67	0.63
7.835	-9468	139	1.65	0.63
7.840	-9478	139	1.65	0.64
7.845	-9488	143	1.66	0.64
7.850	-9499	143	1.66	0.63
7.855	-9509	145	1.66	0.63
7.860	-9519	146	1.66	0.63
7.865	-9529	146	1.66	0.64
7.870	-9540	145	1.67	0.63
7.875	-9550	146	1.68	0.63
7.880	-9560	145	1.68	0.62
7.885	-9570	146	1.67	0.62
7.890	-9581	147	1.68	0.62
7.895	-9591	149	1.67	0.62
7.900	-9601	148	1.69	0.63
7.905	-9611	149	1.69	0.61
7.910	-9622	149	1.68	0.61

7.915	-9632	151	1.69	0.62
7.920	-9642	153	1.68	0.61
7.925	-9652	152	1.68	0.62
7.930	-9663	152	1.70	0.62
7.935	-9673	155	1.70	0.61
7.940	-9683	155	1.70	0.61
7.945	-9693	158	1.69	0.61
7.950	-9704	158	1.70	0.62
7.955	-9714	158	1.70	0.61
7.960	-9724	160	1.70	0.61
7.965	-9734	161	1.70	0.61
7.970	-9745	159	1.72	0.61
7.975	-9755	162	1.71	0.60
7.980	-9765	161	1.71	0.60
7.985	-9775	161	1.72	0.60
7.990	-9786	163	1.72	0.60
7.995	-9796	165	1.70	0.60
8.000	-9806	163	1.72	0.61

Core-ID: AM09-PC-N-606

Depth [m]	Year BC/AD	MS-point [m ³ /kg]	Depth [m]	Year BC/AD	MS-point [m ³ /kg]
0.01	2009	5	0.46	1548	149
0.02	1999	130	0.47	1536	163
0.03	1990	146	0.48	1525	175
0.04	1980	145	0.49	1513	165
0.05	1971	166	0.5	1502	140
0.06	1961	174	0.51	1490	155
0.07	1951	169	0.52	1479	156
0.08	1942	194	0.53	1467	137
0.09	1932		0.54	1455	189
0.10	1923	204	0.55	1444	171
0.11	1913	185	0.56	1432	173
0.12	1903	186	0.57	1421	141
0.13	1894	167	0.58	1409	142
0.14	1884	162	0.59	1398	178
0.15	1875	178	0.6	1386	172
0.16	1865	167	0.61	1375	127
0.17	1855	169	0.62	1363	201
0.18	1846	184	0.63	1352	141
0.19	1836	217	0.64	1340	172
0.20	1827	216	0.65	1329	174
0.21	1817	194	0.66	1317	166
0.22	1807	184	0.67	1305	166
0.23	1798	191	0.68	1294	165
0.24	1788	175	0.69	1282	254
0.25	1779	156	0.7	1271	183
0.26	1769	170	0.71	1259	185
0.27	1759	163	0.72	1248	158
0.28	1750	165	0.73	1236	185
0.29	1740	140	0.74	1225	191
0.30	1731	160	0.75	1213	188
0.31	1721	165	0.76	1202	202
0.32	1709	153	0.77	1190	206
0.33	1698	151	0.78	1178	185
0.34	1686	167	0.79	1167	186
0.35	1675	168	0.8	1155	177
0.36	1663	158	0.81	1144	190
0.37	1652	149	0.82	1132	182
0.38	1640	153	0.83	1121	183
0.39	1629	146	0.84	1109	192
0.40	1617	152	0.85	1098	188
0.41	1606	154	0.86	1086	186
0.42	1594	157	0.87	1075	172
0.43	1582	161	0.88	1063	164
0.44	1571	140	0.89	1051	162
0.45	1559	150	0.9	1040	165

continued

Depth [m]	Year BC/AD	MS-point [m ³ /kg]	Depth [m]	Year BC/AD	MS-point [m ³ /kg]
0.91	1028	158	1.36	473	121
0.92	1017	145	1.37	460	115
0.93	1005	165	1.38	447	95
0.94	994	187	1.39	434	117
0.95	982	169	1.40	421	129
0.96	971	145	1.41	408	95
0.97	959	95	1.42	395	134
0.98	948	140	1.43	382	136
0.99	936	95	1.44	369	140
1.00	924		1.45	356	140
1.01	913		1.46	343	135
1.02	901		1.47	330	133
1.03	890	12	1.48	317	92
1.04	878	160	1.49	304	118
1.05	867	162	1.50	291	137
1.06	855	144	1.51	278	140
1.07	844	152	1.52	265	143
1.08	832	162	1.53	252	145
1.09	821	183	1.54	239	138
1.10	809	196	1.55	226	175
1.11	798	137	1.56	213	160
1.12	785	148	1.57	200	173
1.13	772	147	1.58	187	161
1.14	759	115	1.59	174	168
1.15	746	132	1.60	161	233
1.16	733	140	1.61	148	169
1.17	720	206	1.62	135	171
1.18	707	126	1.63	122	173
1.19	694	132	1.64	109	172
1.20	681	147	1.65	96	142
1.21	668	136	1.66	83	170
1.22	655	140	1.67	70	165
1.23	642	129	1.68	57	168
1.24	629	131	1.69	44	133
1.25	616	117	1.70	31	48
1.26	603	127	1.71	18	150
1.27	590	109	1.72	5	57
1.28	577	106	1.73	-8	45
1.29	564	131	1.74	-21	70
1.30	551	133	1.75	-34	85
1.31	538	136	1.76	-47	131
1.32	525	136	1.77	-60	69
1.33	512	110	1.78	-72	36
1.34	499	134	1.79	-85	156
1.35	486	125	1.80	-98	149

continued

Depth [m]	Year BC/AD	MS-point [m ³ /kg]	Depth [m]	Year BC/AD	MS-point [m ³ /kg]
1.81	-111	120	2.26	-667	179
1.82	-124	173	2.27	-678	174
1.83	-137	181	2.28	-689	184
1.84	-150	128	2.29	-700	173
1.85	-163	163	2.30	-711	180
1.86	-176	212	2.31	-722	159
1.87	-189	214	2.32	-733	29
1.88	-202	197	2.33	-744	41
1.89	-215	211	2.34	-755	68
1.90	-228	211	2.35	-766	56
1.91	-241	203	2.36	-777	153
1.92	-254	205	2.37	-788	162
1.93	-267	207	2.38	-800	157
1.94	-280	205	2.39	-811	155
1.95	-293	206	2.40	-822	150
1.96	-306	209	2.41	-833	137
1.97	-319	208	2.42	-844	160
1.98	-332	193	2.43	-855	194
1.99	-345	184	2.44	-866	153
2.00	-358	190	2.45	-877	156
2.01	-371	199	2.46	-888	159
2.02	-384	191	2.47	-899	154
2.03	-397	183	2.48	-910	113
2.04	-410	140	2.49	-921	159
2.05	-423	126	2.50	-932	165
2.06	-436	126	2.51	-943	146
2.07	-449	319	2.52	-954	93
2.08	-462	188	2.53	-965	128
2.09	-475	125	2.54	-976	151
2.10	-488	10	2.55	-987	182
2.11	-501	58	2.56	-999	157
2.12	-512	68	2.57	-1010	156
2.13	-523	79	2.58	-1021	176
2.14	-534	206	2.59	-1032	171
2.15	-545	193	2.60	-1043	171
2.16	-556	191	2.61	-1054	175
2.17	-567	183	2.62	-1065	166
2.18	-578	118	2.63	-1076	148
2.19	-589	128	2.64	-1087	156
2.20	-601	164	2.65	-1098	162
2.21	-612	158	2.66	-1109	167
2.22	-623	161	2.67	-1120	168
2.23	-634	153	2.68	-1131	164
2.24	-645	169	2.69	-1142	161
2.25	-656	171	2.70	-1153	170

continued

Depth [m]	Year BC/AD	MS-point [m ³ /kg]	Depth [m]	Year BC/AD	MS-point [m ³ /kg]
2.71	-1164	118	3.16	-1658	149
2.72	-1175	178	3.17	-1669	140
2.73	-1186	134	3.18	-1679	187
2.74	-1198	167	3.19	-1690	136
2.75	-1209	189	3.20	-1701	119
2.76	-1220	225	3.21	-1712	127
2.77	-1231	176	3.22	-1723	128
2.78	-1242	173	3.23	-1733	123
2.79	-1253	140	3.24	-1744	117
2.80	-1264	166	3.25	-1755	122
2.81	-1275	187	3.26	-1766	106
2.82	-1286	202	3.27	-1777	107
2.83	-1297	185	3.28	-1787	109
2.84	-1308	181	3.29	-1798	110
2.85	-1319	177	3.30	-1809	100
2.86	-1330	169	3.31	-1820	101
2.87	-1341	160	3.32	-1831	94
2.88	-1352	185	3.33	-1842	113
2.89	-1363	188	3.34	-1852	89
2.90	-1374	175	3.35	-1863	85
2.91	-1385	163	3.36	-1874	89
2.92	-1397	180	3.37	-1885	88
2.93	-1408	163	3.38	-1896	82
2.94	-1419	185	3.39	-1906	79
2.95	-1430	198	3.40	-1917	70
2.96	-1441	191	3.41	-1928	82
2.97	-1452	335	3.42	-1939	92
2.98	-1463	177	3.43	-1950	79
2.99	-1474	167	3.44	-1960	89
3.00	-1485	175	3.45	-1971	90
3.01	-1496	161	3.46	-1982	83
3.02	-1506	168	3.47	-1993	21
3.03	-1517	164	3.48	-2004	6
3.04	-1528	172	3.49	-2015	22
3.05	-1539	164	3.50	-2025	51
3.06	-1550	173	3.51	-2036	43
3.07	-1560	156	3.52	-2047	24
3.08	-1571	169	3.53	-2058	88
3.09	-1582	171	3.54	-2069	96
3.10	-1593	153	3.55	-2079	101
3.11	-1604	2	3.56	-2090	82
3.12	-1614		3.57	-2101	127
3.13	-1625	7	3.58	-2112	64
3.14	-1636	27	3.59	-2123	95
3.15	-1647	145	3.60	-2133	95

continued

Depth [m]	Year BC/AD	MS-point [m ³ /kg]	Depth [m]	Year BC/AD	MS-point [m ³ /kg]
3.61	-2144	85	4.06	-2631	51
3.62	-2155	77	4.07	-2642	50
3.63	-2166	64	4.08	-2652	52
3.64	-2177	65	4.09	-2663	65
3.65	-2188	57	4.10	-2674	65
3.66	-2198	60	4.11	-2685	85
3.67	-2209	66	4.12	-2696	80
3.68	-2220	62	4.13	-2707	
3.69	-2231	72	4.14	-2717	
3.70	-2242	63	4.15	-2728	
3.71	-2252	62	4.16	-2739	99
3.72	-2263	5	4.17	-2750	97
3.73	-2274	61	4.18	-2761	91
3.74	-2285	49	4.19	-2771	100
3.75	-2296	57	4.20	-2782	90
3.76	-2306	60	4.21	-2793	88
3.77	-2317	47	4.22	-2804	93
3.78	-2328	54	4.23	-2815	83
3.79	-2339	62	4.24	-2825	76
3.80	-2350	35	4.25	-2836	70
3.81	-2361	8	4.26	-2847	57
3.82	-2371	40	4.27	-2858	8
3.83	-2382	40	4.28	-2869	
3.84	-2393	41	4.29	-2880	37
3.85	-2404	53	4.30	-2890	22
3.86	-2415	79	4.31	-2901	47
3.87	-2425	42	4.32	-2912	43
3.88	-2436	65	4.33	-2923	49
3.89	-2447	59	4.34	-2934	53
3.90	-2458	66	4.35	-2944	55
3.91	-2469	75	4.36	-2955	46
3.92	-2479	52	4.37	-2966	72
3.93	-2490	56	4.38	-2977	
3.94	-2501	69	4.39	-2988	70
3.95	-2512	66	4.40	-2998	57
3.96	-2523	57	4.41	-3009	55
3.97	-2534	59	4.42	-3020	67
3.98	-2544	59	4.43	-3031	35
3.99	-2555	62	4.44	-3042	10
4.00	-2566	12	4.45	-3053	18
4.01	-2577	42	4.46	-3063	20
4.02	-2588	36	4.47	-3074	53
4.03	-2598	14	4.48	-3085	82
4.04	-2609	40	4.49	-3096	82
4.05	-2620	52	4.50	-3107	71

continued

Depth [m]	Year BC/AD	MS-point [m ³ /kg]	Depth [m]	Year BC/AD	MS-point [m ³ /kg]
4.51	-3117	73	4.96	-3604	72
4.52	-3128	102	4.97	-3615	62
4.53	-3139	65	4.98	-3626	67
4.54	-3150	53	4.99	-3636	61
4.55	-3161	66	5.00	-3647	67
4.56	-3171	76	5.01	-3659	99
4.57	-3182	87	5.02	-3679	108
4.58	-3193	94	5.03	-3699	75
4.59	-3204	87	5.04	-3720	81
4.60	-3215	61	5.05	-3740	80
4.61	-3226	78	5.06	-3761	82
4.62	-3236	84	5.07	-3781	32
4.63	-3247	68	5.08	-3802	54
4.64	-3258	77	5.09	-3822	
4.65	-3269	72	5.10	-3843	
4.66	-3280	54	5.11	-3863	39
4.67	-3290	67	5.12	-3884	90
4.68	-3301	69	5.13	-3904	137
4.69	-3312	62	5.14	-3925	94
4.70	-3323	57	5.15	-3945	90
4.71	-3334	32	5.16	-3966	91
4.72	-3344	52	5.17	-3986	98
4.73	-3355	52	5.18	-4007	87
4.74	-3366	53	5.19	-4027	77
4.75	-3377	37	5.20	-4048	71
4.76	-3388	39	5.21	-4068	13
4.77	-3399	55	5.22	-4089	
4.78	-3409	37	5.23	-4109	17
4.79	-3420	39	5.24	-4130	
4.80	-3431	36	5.25	-4150	61
4.81	-3442	45	5.26	-4171	103
4.82	-3453	55	5.27	-4191	106
4.83	-3463	63	5.28	-4212	83
4.84	-3474	56	5.29	-4232	94
4.85	-3485	57	5.30	-4253	114
4.86	-3496	54	5.31	-4273	115
4.87	-3507	67	5.32	-4294	110
4.88	-3517	55	5.33	-4314	115
4.89	-3528	65	5.34	-4335	94
4.90	-3539	65	5.35	-4355	136
4.91	-3550	78	5.36	-4376	118
4.92	-3561	54	5.37	-4396	134
4.93	-3572	68	5.38	-4417	132
4.94	-3582	71	5.39	-4437	185
4.95	-3593	67	5.40	-4458	164

continued

Depth [m]	Year BC/AD	MS-point [m ³ /kg]	Depth [m]	Year BC/AD	MS-point [m ³ /kg]
5.41	-4478	127	5.86	-5400	197
5.42	-4499	141	5.87	-5421	200
5.43	-4519	160	5.88	-5441	198
5.44	-4540	172	5.89	-5462	203
5.45	-4560	158	5.90	-5482	207
5.46	-4581	158	5.91	-5503	197
5.47	-4601	128	5.92	-5523	183
5.48	-4622	144	5.93	-5544	176
5.49	-4642	146	5.94	-5564	162
5.50	-4663	128	5.95	-5585	228
5.51	-4683	131	5.96	-5605	211
5.52	-4704	156	5.97	-5626	219
5.53	-4724	161	5.98	-5646	224
5.54	-4745	173	5.99	-5667	162
5.55	-4765	147	6.00	-5687	205
5.56	-4786	159	6.01	-5708	204
5.57	-4806	135	6.02	-5728	216
5.58	-4827	166	6.03	-5749	214
5.59	-4847	239	6.04	-5769	108
5.60	-4868	224	6.05	-5790	148
5.61	-4888	234	6.06	-5810	173
5.62	-4908	260	6.07	-5831	172
5.63	-4929	225	6.08	-5851	177
5.64	-4949	236	6.09	-5872	188
5.65	-4970	245	6.10	-5892	99
5.66	-4990	226	6.11	-5913	188
5.67	-5011	235	6.12	-5933	222
5.68	-5031	223	6.13	-5954	42
5.69	-5052	199	6.14	-5974	142
5.70	-5072	188	6.15	-5995	226
5.71	-5093	208	6.16	-6015	171
5.72	-5113	208	6.17	-6036	190
5.73	-5134	199	6.18	-6056	277
5.74	-5154	210	6.19	-6077	248
5.75	-5175	210	6.20	-6097	226
5.76	-5195	242	6.21	-6118	71
5.77	-5216	237	6.22	-6138	16
5.78	-5236	231	6.23	-6158	15
5.79	-5257	243	6.24	-6179	33
5.80	-5277	244	6.25	-6199	8
5.81	-5298	228	6.26	-6220	117
5.82	-5318	206	6.27	-6240	313
5.83	-5339	221	6.28	-6261	303
5.84	-5359	163	6.29	-6281	295
5.85	-5380	192	6.30	-6302	296

continued

Depth [m]	Year BC/AD	MS-point [m ³ /kg]	Depth [m]	Year BC/AD	MS-point [m ³ /kg]
6.31	-6322	185	6.76	-7245	275
6.32	-6343	248	6.77	-7265	199
6.33	-6363	258	6.78	-7286	220
6.34	-6384	267	6.79	-7306	246
6.35	-6404	258	6.80	-7327	240
6.36	-6425	298	6.81	-7347	265
6.37	-6445	245	6.82	-7367	214
6.38	-6466	212	6.83	-7388	205
6.39	-6486	228	6.84	-7408	232
6.40	-6507	236	6.85	-7429	224
6.41	-6527	247	6.86	-7449	267
6.42	-6548	182	6.87	-7470	237
6.43	-6568	231	6.88	-7490	217
6.44	-6589	226	6.89	-7511	241
6.45	-6609	253	6.90	-7531	243
6.46	-6630	250	6.91	-7552	262
6.47	-6650	243	6.92	-7572	195
6.48	-6671	234	6.93	-7593	204
6.49	-6691	260	6.94	-7613	210
6.50	-6712	285	6.95	-7634	172
6.51	-6732	265	6.96	-7654	222
6.52	-6753	260	6.97	-7675	222
6.53	-6773	268	6.98	-7695	192
6.54	-6794	221	6.99	-7716	75
6.55	-6814	269	7.00	-7736	163
6.56	-6835	280	7.01	-7757	178
6.57	-6855	284	7.02	-7777	162
6.58	-6876	259	7.03	-7798	252
6.59	-6896	245	7.04	-7818	197
6.60	-6917	150	7.05	-7839	199
6.61	-6937	245	7.06	-7859	202
6.62	-6958	195	7.07	-7880	210
6.63	-6978	243	7.08	-7900	226
6.64	-6999	246	7.09	-7921	249
6.65	-7019	252	7.10	-7941	239
6.66	-7040	256	7.11	-7962	224
6.67	-7060	275	7.12	-7982	239
6.68	-7081	288	7.13	-8003	216
6.69	-7101	267	7.14	-8023	218
6.70	-7122	285	7.15	-8044	227
6.71	-7142	239	7.16	-8064	207
6.72	-7163	287	7.17	-8085	136
6.73	-7183	305	7.18	-8105	194
6.74	-7204	313	7.19	-8126	217
6.75	-7224	293	7.20	-8146	229

continued

Depth [m]	Year BC/AD	MS-point [m ³ /kg]	Depth [m]	Year BC/AD	MS-point [m ³ /kg]
7.21	-8167	229	7.66	-9089	151
7.22	-8187	192	7.67	-9109	141
7.23	-8208		7.68	-9130	157
7.24	-8228	34	7.69	-9150	155
7.25	-8249	26	7.70	-9171	39
7.26	-8269	265	7.71	-9191	126
7.27	-8290	180	7.72	-9212	166
7.28	-8310	84	7.73	-9232	173
7.29	-8331	126	7.74	-9253	171
7.30	-8351	126	7.75	-9273	52
7.31	-8372	227	7.76	-9294	223
7.32	-8392	244	7.77	-9314	218
7.33	-8413	218	7.78	-9335	214
7.34	-8433	208	7.79	-9355	227
7.35	-8454	227	7.80	-9376	233
7.36	-8474	164	7.81	-9396	196
7.37	-8495	66	7.82	-9417	181
7.38	-8515	22	7.83	-9437	211
7.39	-8536	48	7.84	-9458	192
7.40	-8556	186	7.85	-9478	191
7.41	-8577	207	7.86	-9499	201
7.42	-8597	191	7.87	-9519	82
7.43	-8617	185	7.88	-9540	130
7.44	-8638	213	7.89	-9560	145
7.45	-8658	223	7.90	-9581	133
7.46	-8679	208	7.91	-9601	134
7.47	-8699	201	7.92	-9622	126
7.48	-8720	260	7.93	-9642	95
7.49	-8740	264	7.94	-9663	106
7.50	-8761	262	7.95	-9683	123
7.51	-8781	263	7.96	-9704	127
7.52	-8802	255	7.97	-9724	138
7.53	-8822	236	7.98	-9745	116
7.54	-8843	206	7.99	-9765	136
7.55	-8863	227	8.00	-9786	178
7.56	-8884	426			
7.57	-8904	441			
7.58	-8925	383			
7.59	-8945	360			
7.60	-8966	194			
7.61	-8986	168			
7.62	-9007	188			
7.63	-9027	188			
7.64	-9048	124			
7.65	-9068	118			

Core-ID: AM09-PC-S-618

Depth [m]	Year BC/AD	MS-loop [m ³ /kg]	Density [g/cm ³]	Porosity
0.005	2009	28	1.29	
0.010	2005	28	1.29	0.85
0.015	2001	27	1.30	0.84
0.020	1997	28	1.31	0.84
0.025	1992	28	1.29	0.84
0.030	1988	40	1.27	0.85
0.035	1984	40	1.25	0.86
0.040	1980	42	1.28	0.87
0.045	1976	42	1.29	0.85
0.050	1972	44	1.29	0.84
0.055	1968	44	1.30	0.85
0.060	1964	45	1.28	0.84
0.065	1959	45	1.28	0.85
0.070	1955	47	1.29	0.85
0.075	1951		1.29	0.85
0.080	1947		1.28	0.85
0.085	1943	47	1.28	0.85
0.090	1939	47	1.28	0.85
0.095	1935	47	1.29	0.85
0.100	1930	47	1.28	0.85
0.105	1926	47	1.28	0.85
0.110	1922	47	1.28	0.85
0.115	1918		1.29	0.85
0.120	1914		1.28	0.85
0.125	1910		1.26	0.85
0.130	1906		1.28	0.86
0.135	1901	47	1.28	0.85
0.140	1897		1.29	0.85
0.145	1893	48	1.29	0.85
0.150	1889	49	1.29	0.85
0.155	1885	48	1.28	0.85
0.160	1881	49	1.28	0.85
0.165	1877	48	1.28	0.85
0.170	1873	48	1.30	0.85
0.175	1868	48	1.29	0.84
0.180	1864	49	1.30	0.85
0.185	1860	48	1.28	0.84
0.190	1856	48	1.29	0.85
0.195	1852	48	1.29	0.85
0.200	1848	49	1.29	0.85
0.205	1844	50	1.29	0.85
0.210	1839	49	1.27	0.85
0.215	1835	50	1.29	0.86
0.220	1831	51	1.28	0.85
0.225	1827	51	1.29	0.85
0.230	1823	51	1.31	0.85

0.235	1819	51	1.31	0.83
0.240	1815	49	1.32	0.83
0.245	1810	51	1.37	0.83
0.250	1806	53	1.35	0.80
0.255	1802	53	1.32	0.81
0.260	1798	52	1.31	0.83
0.265	1794	52	1.31	0.84
0.270	1790	52	1.31	0.83
0.275	1786	53	1.30	0.84
0.280	1782	53	1.30	0.84
0.285	1777	53	1.32	0.84
0.290	1773	52	1.30	0.83
0.295	1769	52	1.30	0.84
0.300	1765	52	1.31	0.84
0.305	1762	52	1.32	0.83
0.310	1759	52	1.32	0.83
0.315	1756	53	1.32	0.83
0.320	1753	54	1.32	0.83
0.325	1750	54	1.32	0.83
0.330	1747	54	1.32	0.83
0.335	1744	55	1.32	0.83
0.340	1741	53	1.31	0.83
0.345	1738	50	1.33	0.84
0.350	1735	49	1.40	0.82
0.355	1732	51	1.47	0.78
0.360	1729	54	1.44	0.74
0.365	1726	55	1.35	0.76
0.370	1723	54	1.33	0.81
0.375	1720	53	1.36	0.83
0.380	1717	57	1.39	0.81
0.385	1714	58	1.35	0.79
0.390	1711	58	1.33	0.81
0.395	1708	58	1.33	0.83
0.400	1705	59	1.34	0.82
0.405	1702	59	1.34	0.82
0.410	1699	59	1.34	0.82
0.415	1696	60	1.35	0.82
0.420	1693	61	1.34	0.81
0.425	1690	61	1.34	0.82
0.430	1687		1.36	0.82
0.435	1684		1.35	0.81
0.440	1681		1.34	0.81
0.445	1678		1.34	0.82
0.450	1675	62	1.35	0.82
0.455	1672	61	1.35	0.81
0.460	1669	62	1.36	0.81
0.465	1666	63	1.36	0.81
0.470	1663	63	1.36	0.81

0.475	1660	63	1.35	0.81
0.480	1657	63	1.37	0.81
0.485	1654	64	1.37	0.80
0.490	1651	64	1.35	0.80
0.495	1648	63	1.36	0.81
0.500	1645	63	1.36	0.81
0.505	1642	63	1.37	0.81
0.510	1639	63	1.37	0.80
0.515	1636	63	1.36	0.80
0.520	1633	63	1.36	0.80
0.525	1630	63	1.37	0.81
0.530	1627	63	1.36	0.80
0.535	1624	65	1.36	0.80
0.540	1621	63	1.36	0.81
0.545	1618	63	1.37	0.81
0.550	1615	62	1.37	0.80
0.555	1612	62	1.37	0.80
0.560	1609	64	1.38	0.80
0.565	1606	63	1.34	0.80
0.570	1603	62	1.35	0.82
0.575	1600	61	1.37	0.81
0.580	1597	61	1.39	0.80
0.585	1594	61	1.37	0.79
0.590	1591	62	1.38	0.80
0.595	1588	62	1.37	0.80
0.600	1585	61	1.37	0.80
0.605	1582	61	1.37	0.80
0.610	1579	60	1.36	0.80
0.615	1576	60	1.36	0.81
0.620	1573	60	1.37	0.81
0.625	1570	59	1.36	0.80
0.630	1567	59	1.36	0.81
0.635	1564	59	1.35	0.80
0.640	1561	57	1.35	0.81
0.645	1558	54	1.33	0.81
0.650	1555		1.38	0.82
0.655	1552		1.56	0.79
0.660	1549		1.72	0.69
0.665	1546	42	1.73	0.60
0.670	1543	47	1.62	0.59
0.675	1540	49	1.44	0.66
0.680	1537	49	1.36	0.76
0.685	1534	47	1.35	0.81
0.690	1531	51	1.33	0.81
0.695	1528	57	1.25	0.83
0.700	1526	55	1.15	0.87
0.705	1523	54	1.20	0.93
0.710	1520	53	1.29	0.90

0.715	1517	54	1.34	0.85
0.720	1514	53	1.33	0.82
0.725	1511	56	1.35	0.82
0.730	1508	56	1.36	0.81
0.735	1505	57	1.36	0.81
0.740	1502	57	1.37	0.81
0.745	1499	60	1.37	0.80
0.750	1496	59	1.37	0.80
0.755	1493	59	1.39	0.80
0.760	1490	62	1.38	0.79
0.765	1487	62	1.38	0.80
0.770	1484	64	1.37	0.80
0.775	1481		1.38	0.80
0.780	1478	65	1.38	0.80
0.785	1475	66	1.38	0.80
0.790	1472	65	1.37	0.79
0.795	1469	65	1.38	0.80
0.800	1466	65	1.38	0.80
0.805	1463	64	1.39	0.80
0.810	1460	64	1.38	0.79
0.815	1457	64	1.38	0.80
0.820	1454	65	1.39	0.80
0.825	1451	66	1.38	0.79
0.830	1448	65	1.38	0.79
0.835	1445	64	1.38	0.80
0.840	1442	63	1.38	0.80
0.845	1439	63	1.38	0.80
0.850	1436	64	1.37	0.80
0.855	1433	63	1.37	0.80
0.860	1430	63	1.38	0.80
0.865	1427	63	1.37	0.80
0.870	1424	64	1.37	0.80
0.875	1421	63	1.37	0.80
0.880	1418	63	1.38	0.80
0.885	1415	64	1.38	0.80
0.890	1412	64	1.37	0.80
0.895	1409	64	1.37	0.80
0.900	1406	64	1.37	0.80
0.905	1403	61	1.38	0.80
0.910	1400	61	1.37	0.80
0.915	1397	61	1.38	0.80
0.920	1394	61	1.38	0.79
0.925	1391	61	1.36	0.80
0.930	1388	61	1.36	0.80
0.935	1385	61	1.37	0.80
0.940	1382	60	1.37	0.80
0.945	1379	59	1.36	0.80
0.950	1376	60	1.38	0.81

0.955	1373	60	1.36	0.80
0.960	1370	60	1.37	0.80
0.965	1367	60	1.37	0.80
0.970	1364	60	1.37	0.80
0.975	1361	60	1.37	0.80
0.980	1358	60	1.37	0.80
0.985	1355	60	1.36	0.80
0.990	1352	58	1.37	0.81
0.995	1349	60	1.35	0.80
1.000	1346	58	1.32	0.81
1.005	1343	57	1.35	0.83
1.010	1340	57	1.38	0.81
1.015	1337	57	1.38	0.79
1.020	1334	58	1.37	0.80
1.025	1331	58	1.35	0.80
1.030	1328	58	1.36	0.81
1.035	1325	56	1.36	0.81
1.040	1322	58	1.36	0.81
1.045	1319	58	1.35	0.81
1.050	1316	58	1.37	0.81
1.055	1313	57	1.35	0.80
1.060	1310	57	1.37	0.81
1.065	1307	56	1.37	0.80
1.070	1304	57	1.37	0.80
1.075	1301	57	1.36	0.80
1.080	1298	56	1.37	0.81
1.085	1295	57	1.36	0.80
1.090	1292	57	1.36	0.80
1.095	1289	55	1.37	0.81
1.100	1286	55	1.36	0.80
1.105	1282	55	1.36	0.81
1.110	1278	56	1.37	0.81
1.115	1274	56	1.36	0.80
1.120	1270	56	1.37	0.81
1.125	1266	55	1.35	0.80
1.130	1261	55	1.35	0.81
1.135	1257	55	1.36	0.81
1.140	1253	56	1.36	0.80
1.145	1249	55	1.35	0.81
1.150	1245	55	1.36	0.81
1.155	1241	56	1.36	0.81
1.160	1237	57	1.36	0.81
1.165	1233	55	1.35	0.80
1.170	1229	55	1.36	0.81
1.175	1225	55	1.36	0.80
1.180	1221	55	1.36	0.81
1.185	1216	56	1.37	0.81
1.190	1212	56	1.37	0.80

1.195	1208	55	1.37	0.80
1.200	1204	54	1.39	0.80
1.205	1200	55	1.41	0.79
1.210	1196	56	1.42	0.78
1.215	1192	56	1.40	0.77
1.220	1188	57	1.39	0.78
1.225	1184	57	1.36	0.79
1.230	1180	57	1.36	0.80
1.235	1176	57	1.36	0.80
1.240	1171	56	1.37	0.81
1.245	1167	56	1.38	0.80
1.250	1163	57	1.37	0.80
1.255	1159	57	1.37	0.80
1.260	1155	58	1.37	0.80
1.265	1151	57	1.37	0.80
1.270	1147	57	1.37	0.80
1.275	1143	57	1.38	0.80
1.280	1139	58	1.37	0.80
1.285	1135	58	1.36	0.80
1.290	1131	56	1.36	0.80
1.295	1126	56	1.38	0.80
1.300	1122	56	1.39	0.80
1.305	1118	56	1.40	0.79
1.310	1114	56	1.39	0.79
1.315	1110	57	1.38	0.79
1.320	1106	56	1.38	0.79
1.325	1102	56	1.39	0.80
1.330	1098	55	1.39	0.79
1.335	1094		1.39	0.79
1.340	1090		1.38	0.79
1.345	1086	56	1.38	0.80
1.350	1082	56	1.38	0.79
1.355	1077	57	1.39	0.79
1.360	1073	57	1.37	0.79
1.365	1069	56	1.38	0.80
1.370	1065	55	1.38	0.80
1.375	1061	55	1.38	0.79
1.380	1057	55	1.38	0.79
1.385	1053		1.39	0.79
1.390	1049	54	1.38	0.79
1.395	1045	54	1.38	0.79
1.400	1041	55	1.38	0.79
1.405	1037	54	1.38	0.79
1.410	1032	53	1.39	0.79
1.415	1028	53	1.38	0.79
1.420	1024	53	1.38	0.80
1.425	1020	54	1.38	0.79
1.430	1016	54	1.37	0.80

1.435	1012	53	1.37	0.80
1.440	1008	54	1.37	0.80
1.445	1004	54	1.37	0.80
1.450	1000	54	1.36	0.80
1.455	996	54	1.37	0.81
1.460	992	53	1.36	0.80
1.465	987	53	1.37	0.80
1.470	983	53	1.37	0.80
1.475	979	53	1.37	0.80
1.480	975	53	1.36	0.80
1.485	971	52	1.37	0.80
1.490	967	53	1.38	0.80
1.495	963	52	1.37	0.80
1.500	959	53	1.38	0.80
1.505	955	53	1.38	0.80
1.510	951	53	1.37	0.80
1.515	947	53	1.37	0.80
1.520	942	53	1.37	0.80
1.525	938	52	1.36	0.80
1.530	934	52	1.37	0.81
1.535	930	52	1.37	0.80
1.540	926	52	1.38	0.80
1.545	922	53	1.37	0.79
1.550	918	50	1.37	0.80
1.555	914	51	1.38	0.80
1.560	910	51	1.37	0.79
1.565	906	51	1.37	0.80
1.570	902	51	1.37	0.80
1.575	897	51	1.38	0.80
1.580	893	51	1.36	0.80
1.585	889	52	1.38	0.80
1.590	885	50	1.35	0.80
1.595	881	52	1.37	0.81
1.600	877	50	1.36	0.80
1.605	873	51	1.38	0.80
1.610	869	51	1.37	0.80
1.615	865	52	1.38	0.80
1.620	861	49	1.37	0.80
1.625	857	50	1.39	0.80
1.630	852	51	1.38	0.79
1.635	848	51	1.38	0.79
1.640	844	50	1.38	0.79
1.645	840	51	1.39	0.79
1.650	836	50	1.37	0.79
1.655	832	50	1.37	0.80
1.660	828	49	1.37	0.80
1.665	824	48	1.38	0.80
1.670	820	48	1.38	0.80

1.675	816	48	1.38	0.79
1.680	812	45	1.38	0.79
1.685	807	43	1.39	0.79
1.690	803	43	1.39	0.79
1.695	799	47	1.37	0.79
1.700	795		1.25	0.80
1.705	791		0.79	0.87
1.710	787		0.38	1.13
1.715	783		0.31	1.38
1.720	779		0.30	1.41
1.725	775		0.31	1.42
1.730	771		0.30	1.42
1.735	767		0.31	1.42
1.740	762		0.32	1.42
1.745	758		0.40	1.41
1.750	754	39	0.74	1.36
1.755	750	38	1.20	1.16
1.760	746	38	1.36	0.90
1.765	742	42	1.39	0.81
1.770	738	44	1.40	0.79
1.775	734	44	1.38	0.78
1.780	730	44	1.38	0.79
1.785	726	43	1.38	0.79
1.790	722	43	1.40	0.79
1.795	717	50	1.40	0.78
1.800	713	50	1.38	0.78
1.805	709	49	1.38	0.80
1.810	705	49	1.38	0.80
1.815	701	50	1.39	0.79
1.820	697	51	1.38	0.79
1.825	693	50	1.39	0.80
1.830	689	50	1.39	0.79
1.835	685	50	1.39	0.79
1.840	681	51	1.38	0.79
1.845	677	50	1.39	0.79
1.850	673	50	1.40	0.79
1.855	668	51	1.40	0.78
1.860	664	51	1.39	0.79
1.865	660	51	1.40	0.79
1.870	656	51	1.39	0.79
1.875	652	50	1.40	0.79
1.880	648	50	1.41	0.78
1.885	644	51	1.40	0.78
1.890	640	51	1.39	0.78
1.895	636	51	1.41	0.79
1.900	632	51	1.41	0.78
1.905	628	52	1.40	0.78
1.910	623	52	1.40	0.78

1.915	619	52	1.40	0.78
1.920	615	51	1.39	0.78
1.925	611	52	1.39	0.79
1.930	607	51	1.38	0.79
1.935	603	52	1.39	0.79
1.940	599	52	1.40	0.79
1.945	595	52	1.40	0.78
1.950	591	51	1.40	0.78
1.955	587	51	1.40	0.78
1.960	583	52	1.40	0.79
1.965	578	53	1.40	0.78
1.970	574	52	1.39	0.78
1.975	570	54	1.40	0.79
1.980	566	54	1.39	0.78
1.985	562	54	1.39	0.79
1.990	558	54	1.40	0.79
1.995	554	54	1.40	0.79
2.000	550	53	1.39	0.78
2.005	546	52	1.40	0.79
2.010	542	52	1.42	0.78
2.015	538	52	1.41	0.77
2.020	533	53	1.41	0.78
2.025	529	53	1.40	0.78
2.030	525	53	1.41	0.78
2.035	521	53	1.41	0.78
2.040	517	52	1.41	0.78
2.045	513	52	1.43	0.78
2.050	509	52	1.41	0.77
2.055	505	51	1.39	0.78
2.060	501	51	1.41	0.79
2.065	497	51	1.42	0.78
2.070	493	52	1.42	0.77
2.075	488	50	1.40	0.77
2.080	484	51	1.40	0.78
2.085	480	50	1.40	0.78
2.090	476	50	1.40	0.78
2.095	472	50	1.41	0.78
2.100	468	50	1.39	0.78
2.105	464	50	1.40	0.79
2.110	460	51	1.39	0.79
2.115	456	51	1.39	0.79
2.120	451	52	1.39	0.79
2.125	447	51	1.39	0.79
2.130	443	51	1.39	0.79
2.135	439	51	1.38	0.79
2.140	435	51	1.39	0.79
2.145	431	52	1.38	0.79
2.150	427	52	1.39	0.79

2.155	422	52	1.38	0.79
2.160	418		1.37	0.80
2.165	414	50	1.38	0.80
2.170	410	50	1.43	0.80
2.175	406	54	1.43	0.76
2.180	402	56	1.38	0.77
2.185	398	56	1.37	0.80
2.190	393	62	1.37	0.80
2.195	389		1.36	0.80
2.200	385	64	1.37	0.80
2.205	381	61	1.37	0.80
2.210	377	58	1.36	0.80
2.215	373	55	1.37	0.80
2.220	369	55	1.37	0.80
2.225	364	50	1.37	0.80
2.230	360	50	1.37	0.80
2.235	356	51	1.36	0.80
2.240	352	47	1.36	0.81
2.245	348	47	1.36	0.81
2.250	344	45	1.36	0.81
2.255	340	45	1.36	0.81
2.260	335	45	1.37	0.81
2.265	331	44	1.36	0.80
2.270	327	43	1.37	0.80
2.275	323	43	1.37	0.80
2.280	319	44	1.37	0.80
2.285	315	44	1.36	0.80
2.290	311	43	1.36	0.81
2.295	306	43	1.37	0.80
2.300	302	44	1.36	0.80
2.305	298	45	1.36	0.81
2.310	294	44	1.35	0.80
2.315	290		1.36	0.81
2.320	286	43	1.36	0.81
2.325	282	44	1.36	0.81
2.330	277	43	1.37	0.80
2.335	273	44	1.38	0.80
2.340	269	43	1.37	0.79
2.345	265	43	1.38	0.80
2.350	261	43	1.37	0.79
2.355	257	43	1.37	0.80
2.360	252	42	1.38	0.80
2.365	248	42	1.37	0.79
2.370	244	42	1.37	0.80
2.375	240	42	1.37	0.80
2.380	236	43	1.37	0.80
2.385	232	43	1.38	0.80
2.390	228	44	1.37	0.80

2.395	223	44	1.37	0.80
2.400	219	44	1.38	0.80
2.405	215	42	1.38	0.79
2.410	211	43	1.39	0.80
2.415	207	43	1.38	0.79
2.420	203	43	1.37	0.79
2.425	199	43	1.37	0.80
2.430	194	43	1.37	0.80
2.435	190	43	1.38	0.80
2.440	186	43	1.38	0.80
2.445	182	43	1.37	0.79
2.450	178	44	1.37	0.80
2.455	174	44	1.38	0.80
2.460	170	44	1.38	0.80
2.465	165	43	1.38	0.80
2.470	161	43	1.38	0.80
2.475	157	43	1.40	0.79
2.480	153	43	1.39	0.78
2.485	149	44	1.39	0.79
2.490	145	43	1.38	0.79
2.495	141	43	1.39	0.79
2.500	136	44	1.39	0.79
2.505	132	44	1.39	0.79
2.510	128	43	1.39	0.79
2.515	124	45	1.38	0.79
2.520	120	45	1.37	0.79
2.525	116	43	1.37	0.80
2.530	112	43	1.37	0.80
2.535	107	43	1.38	0.80
2.540	103	43	1.39	0.80
2.545	99	43	1.38	0.79
2.550	95	43	1.38	0.79
2.555	91	44	1.39	0.80
2.560	87	44	1.38	0.79
2.565	83	44	1.39	0.79
2.570	78	44	1.38	0.79
2.575	74	43	1.38	0.80
2.580	70	43	1.37	0.79
2.585	66	43	1.37	0.80
2.590	62	43	1.39	0.80
2.595	58	43	1.38	0.79
2.600	54	42	1.39	0.79
2.605	49	44	1.40	0.79
2.610	45	44	1.39	0.78
2.615	41	44	1.39	0.79
2.620	37	44	1.38	0.79
2.625	33	46	1.38	0.79
2.630	29	45	1.37	0.80

2.635	25	45	1.36	0.80
2.640	20	44	1.39	0.80
2.645	16	44	1.38	0.79
2.650	12	44	1.38	0.80
2.655	8	45	1.37	0.80
2.660	4	44	1.37	0.80
2.665	0	44	1.39	0.80
2.670	-4	45	1.39	0.79
2.675	-9	44	1.37	0.79
2.680	-13	44	1.38	0.80
2.685	-17	44	1.38	0.79
2.690	-21	44	1.39	0.79
2.695	-25	45	1.39	0.79
2.700	-29	44	1.38	0.79
2.705	-33	44	1.39	0.79
2.710	-38	44	1.39	0.79
2.715	-42	44	1.39	0.79
2.720	-46	43	1.39	0.79
2.725	-50	47	1.38	0.79
2.730	-54	49	1.30	0.79
2.735	-58	46	1.24	0.84
2.740	-62	44	1.34	0.88
2.745	-67	45	1.37	0.82
2.750	-71	45	1.37	0.80
2.755	-75	46	1.33	0.80
2.760	-79	44	1.35	0.82
2.765	-83	44	1.38	0.81
2.770	-87	44	1.38	0.79
2.775	-92	44	1.39	0.79
2.780	-96		1.38	0.79
2.785	-100		1.38	0.80
2.790	-104	44	1.38	0.79
2.795	-108	44	1.38	0.80
2.800	-112	44	1.37	0.80
2.805	-116	44	1.37	0.80
2.810	-121	44	1.37	0.80
2.815	-125	44	1.38	0.80
2.820	-129	45	1.38	0.80
2.825	-133	45	1.38	0.80
2.830	-137	45	1.37	0.80
2.835	-141	48	1.36	0.80
2.840	-145	48	1.37	0.80
2.845	-150	49	1.36	0.80
2.850	-154	51	1.38	0.80
2.855	-158	50	1.37	0.80
2.860	-162	51	1.38	0.80
2.865	-166	56	1.37	0.80
2.870	-170	56	1.36	0.80

2.875	-174	55	1.37	0.80
2.880	-179	55	1.36	0.80
2.885	-183	54	1.35	0.81
2.890	-187	56	1.37	0.81
2.895	-191	55	1.38	0.80
2.900	-195	54	1.38	0.80
2.905	-199	56	1.38	0.80
2.910	-203	55	1.37	0.80
2.915	-208	54	1.38	0.80
2.920	-212	54	1.38	0.79
2.925	-216	53	1.39	0.80
2.930	-220	53	1.38	0.79
2.935	-224	52	1.37	0.80
2.940	-228	52	1.38	0.80
2.945	-232	50	1.39	0.79
2.950	-237	49	1.38	0.79
2.955	-241	49	1.38	0.80
2.960	-245	51	1.40	0.79
2.965	-249	51	1.38	0.79
2.970	-253	49	1.38	0.80
2.975	-257	49	1.39	0.80
2.980	-261	49	1.40	0.79
2.985	-266	49	1.40	0.78
2.990	-270	50	1.39	0.78
2.995	-274	50	1.38	0.79
3.000	-278	50	1.40	0.80
3.005	-281	50	1.39	0.78
3.010	-284	50	1.40	0.79
3.015	-288	51	1.40	0.79
3.020	-291	52	1.39	0.78
3.025	-294	51	1.39	0.79
3.030	-298	51	1.41	0.79
3.035	-301	52	1.40	0.78
3.040	-304	52	1.41	0.78
3.045	-308	52	1.40	0.78
3.050	-311	52	1.41	0.78
3.055	-314	52	1.42	0.77
3.060	-318	51	1.42	0.77
3.065	-321	51	1.44	0.77
3.070	-324	51	1.43	0.76
3.075	-328	52	1.43	0.77
3.080	-331	51	1.42	0.77
3.085	-334	51	1.43	0.77
3.090	-338	51	1.42	0.76
3.095	-341	52	1.42	0.77
3.100	-345	53	1.41	0.77
3.105	-348	53	1.39	0.78
3.110	-351	52	1.41	0.79

3.115	-355	52	1.40	0.78
3.120	-358	52	1.41	0.78
3.125	-361	52	1.41	0.78
3.130	-365	52	1.40	0.78
3.135	-368	51	1.40	0.78
3.140	-371	52	1.42	0.78
3.145	-375	51	1.41	0.77
3.150	-378	50	1.40	0.78
3.155	-381	50	1.42	0.78
3.160	-385	51	1.43	0.77
3.165	-388	52	1.41	0.77
3.170	-391	52	1.39	0.78
3.175	-395	51	1.39	0.79
3.180	-398	51	1.41	0.79
3.185	-401	51	1.40	0.78
3.190	-405	50	1.41	0.78
3.195	-408	50	1.40	0.78
3.200	-412	49	1.40	0.78
3.205	-415	49	1.40	0.78
3.210	-418	49	1.41	0.78
3.215	-422	50	1.41	0.78
3.220	-425	50	1.40	0.78
3.225	-428	49	1.39	0.78
3.230	-432	49	1.39	0.79
3.235	-435	49	1.39	0.79
3.240	-438	48	1.40	0.79
3.245	-442	49	1.41	0.78
3.250	-445	49	1.40	0.78
3.255	-448	49	1.39	0.79
3.260	-452	50	1.38	0.79
3.265	-455	49	1.38	0.80
3.270	-458	50	1.41	0.79
3.275	-462	49	1.40	0.78
3.280	-465	48	1.41	0.78
3.285	-468	49	1.40	0.78
3.290	-472	49	1.40	0.78
3.295	-475	50	1.38	0.79
3.300	-479	50	1.38	0.79
3.305	-482	49	1.39	0.79
3.310	-485	49	1.42	0.79
3.315	-489	50	1.40	0.77
3.320	-492	50	1.38	0.78
3.325	-495	51	1.39	0.80
3.330	-499	50	1.35	0.79
3.335	-502	49	1.39	0.81
3.340	-505	50	1.41	0.79
3.345	-509	49	1.41	0.78
3.350	-512	50	1.41	0.78

3.355	-515	50	1.40	0.78
3.360	-519	50	1.38	0.78
3.365	-522	51	1.41	0.80
3.370	-525	51	1.37	0.78
3.375	-529	50	1.38	0.80
3.380	-532	49	1.41	0.80
3.385	-535	50	1.41	0.78
3.390	-539	51	1.39	0.78
3.395	-542	50	1.38	0.79
3.400	-546	50	1.41	0.80
3.405	-549	50	1.40	0.78
3.410	-552	50	1.41	0.78
3.415	-556	50	1.40	0.78
3.420	-559	49	1.40	0.78
3.425	-562	50	1.41	0.78
3.430	-566	50	1.41	0.77
3.435	-569	51	1.41	0.78
3.440	-572	52	1.39	0.78
3.445	-576	51	1.37	0.79
3.450	-579	49	1.40	0.80
3.455	-582	49	1.44	0.79
3.460	-586	50	1.43	0.76
3.465	-589	52	1.41	0.77
3.470	-592	51	1.37	0.78
3.475	-596	48	1.39	0.80
3.480	-599	49	1.42	0.79
3.485	-602	49	1.40	0.77
3.490	-606	50	1.38	0.78
3.495	-609	48	1.40	0.80
3.500	-613	48	1.42	0.79
3.505	-616	49	1.40	0.77
3.510	-619	48	1.40	0.78
3.515	-623	48	1.41	0.78
3.520	-626	46	1.43	0.78
3.525	-629	44	1.47	0.77
3.530	-633	46	1.54	0.74
3.535	-636	49	1.48	0.70
3.540	-639	49	1.39	0.74
3.545	-643	48	1.38	0.79
3.550	-646	48	1.41	0.79
3.555	-649	50	1.41	0.78
3.560	-653	50	1.40	0.77
3.565	-656	50	1.38	0.78
3.570	-659	49	1.37	0.79
3.575	-663	49	1.40	0.80
3.580	-666	48	1.41	0.78
3.585	-669	47	1.41	0.78
3.590	-673	49	1.43	0.78

3.595	-676	50	1.40	0.77
3.600	-680	48	1.38	0.79
3.605	-683	48	1.39	0.80
3.610	-686	48	1.40	0.79
3.615	-690	48	1.42	0.78
3.620	-693	48	1.43	0.77
3.625	-696	47	1.43	0.77
3.630	-700	49	1.42	0.76
3.635	-703	48	1.41	0.77
3.640	-706	47	1.40	0.78
3.645	-710	47	1.42	0.78
3.650	-713	47	1.40	0.77
3.655	-716	49	1.40	0.78
3.660	-720	49	1.36	0.78
3.665	-723	47	1.35	0.80
3.670	-726	46	1.39	0.81
3.675	-730		1.40	0.79
3.680	-733		1.40	0.78
3.685	-736		1.42	0.78
3.690	-740	46	1.39	0.77
3.695	-743	46	1.39	0.79
3.700	-747	45	1.43	0.79
3.705	-750	45	1.42	0.77
3.710	-753	46	1.42	0.77
3.715	-757	46	1.41	0.77
3.720	-760	46	1.41	0.78
3.725	-763	46	1.41	0.78
3.730	-767	46	1.42	0.78
3.735	-770	45	1.42	0.77
3.740	-773	44	1.43	0.77
3.745	-777	44	1.45	0.76
3.750	-780	46	1.47	0.76
3.755	-783	46	1.47	0.74
3.760	-787	47	1.44	0.74
3.765	-790	48	1.41	0.76
3.770	-793	47	1.40	0.78
3.775	-797	47	1.40	0.78
3.780	-800	46	1.41	0.79
3.785	-803	46	1.40	0.78
3.790	-807	45	1.41	0.78
3.795	-810	45	1.41	0.78
3.800	-814	45	1.41	0.77
3.805	-817	45	1.41	0.78
3.810	-820	45	1.42	0.78
3.815	-824	46	1.42	0.77
3.820	-827	46	1.39	0.77
3.825	-830	46	1.39	0.79
3.830	-834	46	1.38	0.79

3.835	-837		1.40	0.80
3.840	-840	45	1.40	0.78
3.845	-844	44	1.41	0.78
3.850	-847	44	1.41	0.78
3.855	-850	46	1.41	0.78
3.860	-854	46	1.37	0.78
3.865	-857	46	1.35	0.80
3.870	-860	44	1.37	0.81
3.875	-864	45	1.38	0.80
3.880	-867	43	1.36	0.80
3.885	-870	43	1.38	0.80
3.890	-874	42	1.37	0.80
3.895	-877	43	1.39	0.80
3.900	-881	43	1.38	0.79
3.905	-884	42	1.36	0.80
3.910	-887	42	1.39	0.81
3.915	-891	42	1.40	0.79
3.920	-894	44	1.38	0.78
3.925	-897	43	1.34	0.79
3.930	-901	43	1.35	0.82
3.935	-904	42	1.37	0.81
3.940	-907	42	1.38	0.80
3.945	-911	42	1.36	0.80
3.950	-914	43	1.38	0.81
3.955	-917	43	1.41	0.80
3.960	-921	42	1.40	0.78
3.965	-924	42	1.39	0.78
3.970	-927	43	1.37	0.79
3.975	-931	44	1.36	0.80
3.980	-934	43	1.35	0.80
3.985	-937	43	1.38	0.81
3.990	-941	44	1.38	0.79
3.995	-944	43	1.34	0.79
4.000	-948	43	1.35	0.82
4.005	-951	43	1.37	0.81
4.010	-954	43	1.36	0.80
4.015	-958	42	1.36	0.81
4.020	-961	42	1.36	0.81
4.025	-964	41	1.38	0.81
4.030	-968	41	1.39	0.80
4.035	-971	42	1.37	0.79
4.040	-974	42	1.37	0.80
4.045	-978	42	1.36	0.80
4.050	-981	40	1.35	0.81
4.055	-984	41	1.39	0.81
4.060	-988	41	1.36	0.79
4.065	-991	41	1.36	0.81
4.070	-994	40	1.37	0.81

4.075	-998	41	1.38	0.80
4.080	-1001	41	1.36	0.79
4.085	-1004	42	1.36	0.81
4.090	-1008	42	1.33	0.81
4.095	-1011	41	1.34	0.82
4.100	-1015	41	1.38	0.82
4.105	-1018	41	1.38	0.79
4.110	-1021	42	1.38	0.79
4.115	-1025	43	1.36	0.80
4.120	-1028	43	1.33	0.81
4.125	-1031	44	1.33	0.82
4.130	-1035	43	1.34	0.82
4.135	-1038	43	1.35	0.82
4.140	-1041	42	1.37	0.81
4.145	-1045	41	1.37	0.80
4.150	-1048	43	1.38	0.80
4.155	-1051	43	1.35	0.80
4.160	-1055	43	1.36	0.81
4.165	-1058	43	1.36	0.81
4.170	-1061	42	1.34	0.81
4.175	-1065	41	1.34	0.82
4.180	-1068	42	1.34	0.82
4.185	-1071		1.29	0.82
4.190	-1075	39	1.33	0.85
4.195	-1078	40	1.39	0.82
4.200	-1082	40	1.38	0.79
4.205	-1085	40	1.38	0.80
4.210	-1088	40	1.34	0.80
4.215	-1092	39	1.33	0.82
4.220	-1095	38	1.35	0.82
4.225	-1098	38	1.38	0.81
4.230	-1102	39	1.37	0.80
4.235	-1105	38	1.35	0.80
4.240	-1108	38	1.39	0.81
4.245	-1112	38	1.41	0.79
4.250	-1115	38	1.37	0.78
4.255	-1118	38	1.37	0.80
4.260	-1122	38	1.38	0.80
4.265	-1125	38	1.39	0.79
4.270	-1128	39	1.35	0.79
4.275	-1132	39	1.33	0.81
4.280	-1135	38	1.34	0.82
4.285	-1138	39	1.38	0.82
4.290	-1142	39	1.34	0.80
4.295	-1145	37	1.34	0.82
4.300	-1149	38	1.35	0.82
4.305	-1152	38	1.34	0.81
4.310	-1155	37	1.35	0.82

4.315	-1159	39	1.38	0.81
4.320	-1162	39	1.35	0.80
4.325	-1165	39	1.35	0.81
4.330	-1169	38	1.36	0.81
4.335	-1172	37	1.36	0.81
4.340	-1175	38	1.38	0.81
4.345	-1179	38	1.39	0.79
4.350	-1182	38	1.38	0.79
4.355	-1185	38	1.38	0.79
4.360	-1189	38	1.39	0.79
4.365	-1192	39	1.40	0.79
4.370	-1195	39	1.39	0.78
4.375	-1199	39	1.40	0.79
4.380	-1202	38	1.38	0.78
4.385	-1205	39	1.37	0.79
4.390	-1209	39	1.38	0.80
4.395	-1212	38	1.37	0.79
4.400	-1216	39	1.35	0.80
4.405	-1219	37	1.36	0.81
4.410	-1222	38	1.37	0.80
4.415	-1226	38	1.38	0.80
4.420	-1229	39	1.38	0.79
4.425	-1232	39	1.38	0.80
4.430	-1236	38	1.38	0.80
4.435	-1239	38	1.38	0.79
4.440	-1242	39	1.37	0.79
4.445	-1246	39	1.39	0.80
4.450	-1249	39	1.38	0.79
4.455	-1252	39	1.38	0.79
4.460	-1256	38	1.39	0.79
4.465	-1259	38	1.39	0.79
4.470	-1262	38	1.39	0.79
4.475	-1266	38	1.38	0.79
4.480	-1269	37	1.39	0.79
4.485	-1272	39	1.40	0.79
4.490	-1276	39	1.38	0.78
4.495	-1279	39	1.36	0.79
4.500	-1283	39	1.38	0.80
4.505	-1286	40	1.36	0.79
4.510	-1289	38	1.36	0.81
4.515	-1293	39	1.40	0.80
4.520	-1296	39	1.41	0.78
4.525	-1299	38	1.41	0.78
4.530	-1303	40	1.42	0.78
4.535	-1306	40	1.41	0.77
4.540	-1309	40	1.39	0.78
4.545	-1313	41	1.39	0.79
4.550	-1316	41	1.37	0.79

4.555	-1319	41	1.38	0.80
4.560	-1323	41	1.37	0.80
4.565	-1326	41	1.38	0.80
4.570	-1329	41	1.38	0.80
4.575	-1333	41	1.38	0.79
4.580	-1336	41	1.37	0.79
4.585	-1339	41	1.38	0.80
4.590	-1343	40	1.38	0.79
4.595	-1346	40	1.39	0.79
4.600	-1350	40	1.40	0.79
4.605	-1353	40	1.39	0.78
4.610	-1356	40	1.40	0.79
4.615	-1360	41	1.41	0.78
4.620	-1363	41	1.40	0.78
4.625	-1366	41	1.41	0.78
4.630	-1370	41	1.42	0.78
4.635	-1373	42	1.42	0.77
4.640	-1376	44	1.39	0.77
4.645	-1380	42	1.37	0.79
4.650	-1383	42	1.39	0.80
4.655	-1386	42	1.40	0.79
4.660	-1390	42	1.41	0.78
4.665	-1393	42	1.41	0.78
4.670	-1396		1.40	0.78
4.675	-1400		1.39	0.78
4.680	-1403		1.38	0.79
4.685	-1406		1.39	0.79
4.690	-1410		1.40	0.79
4.695	-1413	43	1.40	0.78
4.700	-1417	42	1.41	0.79
4.705	-1420	42	1.40	0.78
4.710	-1423	42	1.41	0.78
4.715	-1427	42	1.40	0.78
4.720	-1430	42	1.40	0.78
4.725	-1433	42	1.41	0.78
4.730	-1437	43	1.41	0.78
4.735	-1440	44	1.40	0.78
4.740	-1443	43	1.39	0.78
4.745	-1447	43	1.40	0.79
4.750	-1450	43	1.41	0.78
4.755	-1453	43	1.42	0.78
4.760	-1457	43	1.42	0.77
4.765	-1460	43	1.42	0.77
4.770	-1463	43	1.40	0.77
4.775	-1467	43	1.41	0.78
4.780	-1470	43	1.42	0.78
4.785	-1473	43	1.42	0.77
4.790	-1477	43	1.41	0.77

4.795	-1480	43	1.42	0.78
4.800	-1484	44	1.42	0.77
4.805	-1487	44	1.42	0.77
4.810	-1490	47	1.41	0.77
4.815	-1494	47	1.37	0.78
4.820	-1497	45	1.37	0.80
4.825	-1500	44	1.42	0.80
4.830	-1504	45	1.43	0.77
4.835	-1507	44	1.42	0.77
4.840	-1510		1.46	0.77
4.845	-1514		1.59	0.75
4.850	-1517	46	1.57	0.67
4.855	-1520	49	1.52	0.68
4.860	-1524	49	1.44	0.71
4.865	-1527	49	1.42	0.76
4.870	-1530	49	1.42	0.77
4.875	-1534	49	1.42	0.77
4.880	-1537	49	1.42	0.77
4.885	-1540	46	1.42	0.77
4.890	-1544	46	1.41	0.77
4.895	-1547	46	1.41	0.77
4.900	-1551	45	1.40	0.78
4.905	-1554	45	1.40	0.78
4.910	-1557	45	1.41	0.78
4.915	-1561	45	1.41	0.78
4.920	-1564	45	1.41	0.78
4.925	-1567	45	1.41	0.78
4.930	-1571	45	1.40	0.78
4.935	-1574	45	1.41	0.78
4.940	-1577	44	1.41	0.78
4.945	-1581	44	1.42	0.78
4.950	-1584	44	1.41	0.77
4.955	-1587	43	1.41	0.78
4.960	-1591	43	1.40	0.77
4.965	-1594	42	1.42	0.78
4.970	-1597	42	1.43	0.77
4.975	-1601	44	1.43	0.76
4.980	-1604	44	1.40	0.77
4.985	-1607	44	1.40	0.78
4.990	-1611	43	1.41	0.78
4.995	-1614	43	1.42	0.78
5.000	-1618	43	1.42	0.77
5.005	-1622	44	1.42	0.77
5.010	-1625	45	1.41	0.77
5.015	-1629	44	1.41	0.78
5.020	-1633	44	1.41	0.78
5.025	-1636	45	1.43	0.78
5.030	-1640	45	1.41	0.77

5.035	-1644	45	1.40	0.78
5.040	-1647	44	1.41	0.78
5.045	-1651	44	1.43	0.78
5.050	-1655	44	1.43	0.77
5.055	-1658	45	1.45	0.77
5.060	-1662	45	1.43	0.75
5.065	-1666	45	1.42	0.76
5.070	-1669	45	1.41	0.77
5.075	-1673	44	1.41	0.78
5.080	-1677	44	1.43	0.78
5.085	-1680	45	1.43	0.77
5.090	-1684	44	1.42	0.77
5.095	-1688	45	1.43	0.77
5.100	-1691	45	1.40	0.77
5.105	-1695	45	1.41	0.78
5.110	-1699	44	1.41	0.78
5.115	-1702	43	1.40	0.78
5.120	-1706	44	1.40	0.78
5.125	-1710	44	1.40	0.78
5.130	-1713	43	1.41	0.78
5.135	-1717	43	1.40	0.77
5.140	-1721	44	1.41	0.78
5.145	-1724	43	1.41	0.78
5.150	-1728	42	1.40	0.78
5.155	-1732	43	1.41	0.78
5.160	-1736		1.41	0.78
5.165	-1739	43	1.41	0.78
5.170	-1743	43	1.41	0.78
5.175	-1747	43	1.41	0.78
5.180	-1750	42	1.41	0.78
5.185	-1754	44	1.41	0.78
5.190	-1758	44	1.40	0.78
5.195	-1761	42	1.40	0.78
5.200	-1765	43	1.42	0.78
5.205	-1769	43	1.40	0.77
5.210	-1772	42	1.39	0.78
5.215	-1776	42	1.41	0.79
5.220	-1780	42	1.40	0.78
5.225	-1783	42	1.41	0.78
5.230	-1787	42	1.40	0.78
5.235	-1791	41	1.40	0.78
5.240	-1794	40	1.40	0.78
5.245	-1798	41	1.40	0.78
5.250	-1802	41	1.40	0.78
5.255	-1805	41	1.40	0.78
5.260	-1809	43	1.41	0.78
5.265	-1813	41	1.41	0.78
5.270	-1816	42	1.41	0.78

5.275	-1820	42	1.40	0.78
5.280	-1824	42	1.40	0.78
5.285	-1827	41	1.41	0.78
5.290	-1831	42	1.41	0.78
5.295	-1835	42	1.41	0.78
5.300	-1838	43	1.40	0.78
5.305	-1842	42	1.39	0.78
5.310	-1846	43	1.41	0.79
5.315	-1849	42	1.41	0.78
5.320	-1853	43	1.41	0.78
5.325	-1857	42	1.42	0.78
5.330	-1860	42	1.42	0.77
5.335	-1864	42	1.42	0.77
5.340	-1868	42	1.40	0.77
5.345	-1871	42	1.39	0.79
5.350	-1875	42	1.41	0.79
5.355	-1879	43	1.42	0.78
5.360	-1882	41	1.41	0.77
5.365	-1886	41	1.41	0.78
5.370	-1890	42	1.41	0.78
5.375	-1893	42	1.40	0.77
5.380	-1897	41	1.39	0.78
5.385	-1901	41	1.40	0.79
5.390	-1904	41	1.41	0.78
5.395	-1908	42	1.40	0.78
5.400	-1912	43	1.40	0.78
5.405	-1915	42	1.40	0.78
5.410	-1919		1.41	0.78
5.415	-1923	44	1.40	0.78
5.420	-1926	42	1.40	0.78
5.425	-1930	42	1.42	0.78
5.430	-1934	43	1.43	0.77
5.435	-1937	44	1.41	0.77
5.440	-1941	43	1.42	0.78
5.445	-1945	45	1.42	0.77
5.450	-1948	44	1.41	0.77
5.455	-1952	44	1.42	0.78
5.460	-1956	43	1.42	0.77
5.465	-1959	43	1.48	0.77
5.470	-1963	46	1.50	0.74
5.475	-1967	46	1.42	0.72
5.480	-1971	47	1.41	0.77
5.485	-1974	47	1.40	0.78
5.490	-1978	46	1.40	0.79
5.495	-1982	46	1.40	0.78
5.500	-1985	45	1.40	0.78
5.505	-1989	43	1.40	0.78
5.510	-1993	43	1.40	0.78

5.515	-1996	43	1.40	0.78
5.520	-2000	41	1.40	0.78
5.525	-2004	40	1.40	0.78
5.530	-2007	40	1.40	0.78
5.535	-2011	40	1.40	0.79
5.540	-2015	40	1.40	0.78
5.545	-2018	39	1.40	0.78
5.550	-2022	38	1.40	0.79
5.555	-2026	38	1.39	0.78
5.560	-2029	37	1.39	0.79
5.565	-2033	37	1.39	0.79
5.570	-2037	37	1.41	0.79
5.575	-2040	38	1.40	0.78
5.580	-2044	38	1.39	0.78
5.585	-2048	38	1.41	0.79
5.590	-2051	37	1.39	0.78
5.595	-2055	37	1.39	0.79
5.600	-2059	38	1.40	0.79
5.605	-2062	38	1.38	0.79
5.610	-2066	38	1.40	0.79
5.615	-2070	38	1.38	0.78
5.620	-2073	37	1.37	0.79
5.625	-2077	37	1.38	0.80
5.630	-2081	37	1.38	0.79
5.635	-2084	39	1.38	0.80
5.640	-2088	38	1.39	0.79
5.645	-2092	38	1.40	0.79
5.650	-2095	38	1.40	0.79
5.655	-2099	38	1.40	0.78
5.660	-2103	39	1.40	0.78
5.665	-2106	39	1.41	0.79
5.670	-2110	38	1.41	0.78
5.675	-2114	38	1.40	0.78
5.680	-2117	38	1.42	0.78
5.685	-2121	38	1.40	0.77
5.690	-2125	38	1.40	0.78
5.695	-2128	38	1.41	0.78
5.700	-2132	38	1.40	0.78
5.705	-2136	38	1.41	0.78
5.710	-2139	39	1.41	0.78
5.715	-2143	38	1.40	0.77
5.720	-2147	38	1.41	0.78
5.725	-2150	38	1.41	0.78
5.730	-2154	38	1.41	0.77
5.735	-2158	38	1.40	0.78
5.740	-2161	38	1.40	0.78
5.745	-2165	38	1.39	0.79
5.750	-2169	37	1.39	0.79

5.755	-2172	37	1.39	0.79
5.760	-2176	37	1.41	0.79
5.765	-2180	38	1.40	0.78
5.770	-2183	38	1.38	0.78
5.775	-2187	36	1.38	0.79
5.780	-2191	36	1.39	0.80
5.785	-2195	36	1.39	0.79
5.790	-2198	36	1.39	0.79
5.795	-2202	36	1.40	0.79
5.800	-2206	35	1.41	0.78
5.805	-2209	35	1.40	0.78
5.810	-2213	36	1.41	0.78
5.815	-2217	36	1.38	0.78
5.820	-2220	37	1.34	0.80
5.825	-2224	36	1.38	0.82
5.830	-2228	36	1.41	0.80
5.835	-2231	35	1.43	0.78
5.840	-2235	35	1.43	0.77
5.845	-2239	36	1.44	0.77
5.850	-2242	36	1.41	0.76
5.855	-2246	36	1.42	0.78
5.860	-2250	35	1.42	0.77
5.865	-2253	36	1.42	0.77
5.870	-2257	36	1.40	0.77
5.875	-2261	37	1.40	0.78
5.880	-2264	36	1.39	0.78
5.885	-2268	36	1.39	0.79
5.890	-2272		1.39	0.79
5.895	-2275		1.39	0.79
5.900	-2279	35	1.38	0.79
5.905	-2283	35	1.38	0.79
5.910	-2286	35	1.39	0.80
5.915	-2290	34	1.39	0.79
5.920	-2294	35	1.39	0.79
5.925	-2297	34	1.40	0.79
5.930	-2301	34	1.39	0.79
5.935	-2305	34	1.40	0.79
5.940	-2308	34	1.40	0.78
5.945	-2312	34	1.41	0.78
5.950	-2316	34	1.40	0.78
5.955	-2319	34	1.40	0.78
5.960	-2323	34	1.41	0.79
5.965	-2327	34	1.40	0.78
5.970	-2330	34	1.41	0.78
5.975	-2334	34	1.41	0.78
5.980	-2338	35	1.41	0.78
5.985	-2341	34	1.42	0.78
5.990	-2345	35	1.41	0.77

5.995	-2349	35	1.41	0.78
6.000	-2352	35	1.42	0.78
6.005	-2356	36	1.41	0.77
6.010	-2360	35	1.42	0.77
6.015	-2363	35	1.41	0.77
6.020	-2367	36	1.41	0.78
6.025	-2371	36	1.42	0.78
6.030	-2374	36	1.41	0.77
6.035	-2378	35	1.40	0.78
6.040	-2382	35	1.40	0.79
6.045	-2385	35	1.40	0.78
6.050	-2389	35	1.41	0.78
6.055	-2393	35	1.39	0.78
6.060	-2396	35	1.41	0.79
6.065	-2400	35	1.41	0.78
6.070	-2404	34	1.40	0.78
6.075	-2407	34	1.40	0.78
6.080	-2411	34	1.41	0.78
6.085	-2415	35	1.40	0.78
6.090	-2418	35	1.39	0.78
6.095	-2422	35	1.40	0.79
6.100	-2426	35	1.39	0.79
6.105	-2430	33	1.40	0.79
6.110	-2433	34	1.40	0.79
6.115	-2437	34	1.39	0.78
6.120	-2441	34	1.39	0.79
6.125	-2444	34	1.39	0.79
6.130	-2448	34	1.39	0.79
6.135	-2452	33	1.39	0.79
6.140	-2455	33	1.40	0.79
6.145	-2459	33	1.40	0.78
6.150	-2463	34	1.40	0.79
6.155	-2466	35	1.39	0.78
6.160	-2470	34	1.39	0.79
6.165	-2474	34	1.39	0.79
6.170	-2477	33	1.40	0.79
6.175	-2481	34	1.40	0.79
6.180	-2485	34	1.41	0.78
6.185	-2488	34	1.40	0.78
6.190	-2492	34	1.40	0.78
6.195	-2496	36	1.40	0.78
6.200	-2499	35	1.39	0.78
6.205	-2503	36	1.41	0.79
6.210	-2507	35	1.39	0.78
6.215	-2510	35	1.39	0.79
6.220	-2514	36	1.39	0.79
6.225	-2518	36	1.39	0.79
6.230	-2521	35	1.39	0.79

6.235	-2525	36	1.45	0.79
6.240	-2529	36	1.42	0.75
6.245	-2532	37	1.40	0.77
6.250	-2536	37	1.39	0.78
6.255	-2540	37	1.37	0.79
6.260	-2543	36	1.38	0.80
6.265	-2547	37	1.39	0.79
6.270	-2551	36	1.38	0.79
6.275	-2554	36	1.40	0.79
6.280	-2558	35	1.41	0.78
6.285	-2562	35	1.40	0.78
6.290	-2565	35	1.39	0.78
6.295	-2569	36	1.38	0.79
6.300	-2573	35	1.38	0.79
6.305	-2576	35	1.40	0.80
6.310	-2580	34	1.40	0.78
6.315	-2584	34	1.38	0.78
6.320	-2587	34	1.38	0.79
6.325	-2591	34	1.38	0.79
6.330	-2595	34	1.39	0.80
6.335	-2598	34	1.39	0.79
6.340	-2602	35	1.38	0.79
6.345	-2606	35	1.38	0.80
6.350	-2609	34	1.37	0.80
6.355	-2613	35	1.39	0.80
6.360	-2617	35	1.38	0.79
6.365	-2620	34	1.39	0.80
6.370	-2624	34	1.39	0.79
6.375	-2628	34	1.39	0.79
6.380	-2631	34	1.38	0.79
6.385	-2635	33	1.39	0.79
6.390	-2639	34	1.38	0.79
6.395	-2642	33	1.38	0.80
6.400	-2646	34	1.40	0.79
6.405	-2650	34	1.39	0.78
6.410	-2654	34	1.38	0.79
6.415	-2657	34	1.38	0.80
6.420	-2661	35	1.38	0.80
6.425	-2665	34	1.38	0.80
6.430	-2668	34	1.39	0.79
6.435	-2672	35	1.41	0.79
6.440	-2676	35	1.39	0.78
6.445	-2679	35	1.39	0.79
6.450	-2683	35	1.38	0.79
6.455	-2687	35	1.39	0.79
6.460	-2690	35	1.37	0.79
6.465	-2694		1.38	0.80
6.470	-2698	34	1.38	0.80

6.475	-2701	35	1.38	0.80
6.480	-2705	34	1.38	0.79
6.485	-2709	34	1.39	0.79
6.490	-2712	35	1.38	0.79
6.495	-2716	35	1.38	0.80
6.500	-2720	34	1.39	0.79
6.505	-2723	34	1.39	0.79
6.510	-2727	34	1.38	0.79
6.515	-2731	34	1.39	0.79
6.520	-2734	34	1.38	0.79
6.525	-2738		1.39	0.80
6.530	-2742	34	1.40	0.79
6.535	-2745	34	1.39	0.78
6.540	-2749	34	1.39	0.79
6.545	-2753	34	1.38	0.79
6.550	-2756	33	1.40	0.80
6.555	-2760	34	1.41	0.78
6.560	-2764	34	1.39	0.78
6.565	-2767	35	1.40	0.79
6.570	-2771	34	1.39	0.78
6.575	-2775	34	1.40	0.79
6.580	-2778	35	1.40	0.78
6.585	-2782	34	1.38	0.78
6.590	-2786	35	1.40	0.79
6.595	-2789	35	1.40	0.78
6.600	-2793	36	1.41	0.78
6.605	-2797	36	1.41	0.78
6.610	-2800	36	1.41	0.78
6.615	-2804	36	1.41	0.78
6.620	-2808	36	1.41	0.78
6.625	-2811	36	1.42	0.78
6.630	-2815	36	1.41	0.77
6.635	-2819	36	1.41	0.78
6.640	-2822	36	1.42	0.78
6.645	-2826	36	1.42	0.77
6.650	-2830	35	1.42	0.77
6.655	-2833	35	1.43	0.77
6.660	-2837	35	1.42	0.77
6.665	-2841	35	1.42	0.77
6.670	-2844	35	1.42	0.77
6.675	-2848	35	1.41	0.77
6.680	-2852	35	1.41	0.78
6.685	-2855	34	1.40	0.77
6.690	-2859	34	1.41	0.78
6.695	-2863	34	1.40	0.78
6.700	-2866	34	1.40	0.78
6.705	-2870	34	1.40	0.78
6.710	-2874	34	1.40	0.78

6.715	-2877	33	1.39	0.78
6.720	-2881	34	1.41	0.79
6.725	-2885		1.40	0.78
6.730	-2889		1.41	0.78
6.735	-2892	34	1.41	0.78
6.740	-2896	33	1.40	0.78
6.745	-2900	34	1.41	0.78
6.750	-2903	34	1.39	0.78
6.755	-2907	34	1.40	0.79
6.760	-2911	34	1.40	0.78
6.765	-2914	34	1.39	0.78
6.770	-2918	35	1.39	0.79
6.775	-2922	34	1.40	0.79
6.780	-2925	34	1.41	0.78
6.785	-2929	35	1.42	0.78
6.790	-2933	36	1.41	0.77
6.795	-2936	36	1.39	0.78
6.800	-2940	35	1.40	0.79
6.805	-2944	35	1.39	0.78
6.810	-2947	36	1.40	0.79
6.815	-2951	39	1.37	0.78
6.820	-2955	39	1.31	0.80
6.825	-2958	37	1.30	0.84
6.830	-2962	36	1.38	0.84
6.835	-2966	37	1.39	0.80
6.840	-2969	38	1.38	0.79
6.845	-2973	38	1.40	0.79
6.850	-2977	38	1.40	0.78
6.855	-2980	38	1.40	0.78
6.860	-2984	38	1.41	0.78
6.865	-2988	39	1.41	0.78
6.870	-2991	39	1.41	0.78
6.875	-2995	38	1.40	0.78
6.880	-2999	38	1.42	0.78
6.885	-3002	39	1.42	0.77
6.890	-3006	39	1.42	0.77
6.895	-3010	39	1.41	0.77
6.900	-3013	38	1.41	0.78
6.905	-3017	40	1.42	0.78
6.910	-3021	40	1.41	0.77
6.915	-3024	39	1.40	0.78
6.920	-3028	40	1.40	0.78
6.925	-3032	40	1.39	0.78
6.930	-3035	40	1.39	0.79
6.935	-3039	41	1.38	0.79
6.940	-3043	42	1.40	0.79
6.945	-3046	42	1.39	0.78
6.950	-3050	43	1.39	0.79

6.955	-3054	43	1.40	0.79
6.960	-3057	42	1.39	0.78
6.965	-3061	44	1.40	0.79
6.970	-3065	44	1.39	0.78
6.975	-3068	44	1.42	0.79
6.980	-3072	44	1.41	0.77
6.985	-3076	44	1.41	0.78
6.990	-3079	44	1.41	0.78
6.995	-3083	43	1.41	0.78
7.000	-3087	44	1.42	0.78
7.005	-3090	43	1.41	0.77
7.010	-3094		1.42	0.78
7.015	-3098		1.40	0.77
7.020	-3101	40	1.42	0.78
7.025	-3105	40	1.42	0.77
7.030	-3109	40	1.42	0.77
7.035	-3113	40	1.42	0.77
7.040	-3116	40	1.42	0.77
7.045	-3120	40	1.42	0.77
7.050	-3124	40	1.41	0.77
7.055	-3127	39	1.43	0.77
7.060	-3131	39	1.43	0.77
7.065	-3135	39	1.42	0.77
7.070	-3138	38	1.42	0.77
7.075	-3142	39	1.41	0.77
7.080	-3146	39	1.41	0.77
7.085	-3149	39	1.40	0.78
7.090	-3153	40	1.42	0.79
7.095	-3157		1.41	0.77
7.100	-3160		1.42	0.77
7.105	-3164		1.42	0.77
7.110	-3168		1.43	0.77
7.115	-3171	41	1.42	0.76
7.120	-3175	41	1.42	0.77
7.125	-3179	41	1.43	0.77
7.130	-3182	42	1.43	0.77
7.135	-3186	43	1.43	0.77
7.140	-3190	42	1.44	0.77
7.145	-3193	43	1.46	0.76
7.150	-3197	43	1.44	0.75
7.155	-3201	45	1.44	0.76
7.160	-3204	45	1.46	0.76
7.165	-3208	45	1.46	0.75
7.170	-3212	43	1.47	0.75
7.175	-3215	43	1.52	0.74
7.180	-3219	44	1.54	0.71
7.185	-3223	45	1.49	0.70
7.190	-3226	45	1.48	0.73

7.195	-3230	44	1.47	0.74
7.200	-3234	45	1.44	0.74
7.205	-3237		1.42	0.76
7.210	-3241	41	1.43	0.77
7.215	-3245	41	1.43	0.77
7.220	-3248	41	1.44	0.76
7.225	-3252	40	1.42	0.76
7.230	-3256	39	1.42	0.77
7.235	-3259	39	1.42	0.77
7.240	-3263	38	1.42	0.77
7.245	-3267	38	1.43	0.77
7.250	-3270	38	1.43	0.76
7.255	-3274	38	1.42	0.77
7.260	-3278	38	1.42	0.77
7.265	-3281	37	1.42	0.77
7.270	-3285	38	1.43	0.77
7.275	-3289	38	1.43	0.76
7.280	-3292	38	1.43	0.77
7.285	-3296	38	1.42	0.77
7.290	-3300	39	1.43	0.77
7.295	-3303	38	1.42	0.77
7.300	-3307	38	1.42	0.77
7.305	-3311	40	1.41	0.77
7.310	-3314	38	1.42	0.77
7.315	-3318	38	1.43	0.77
7.320	-3322	39	1.43	0.77
7.325	-3325	39	1.43	0.77
7.330	-3329	39	1.43	0.77
7.335	-3333	39	1.43	0.77
7.340	-3336	40	1.44	0.76
7.345	-3340	39	1.42	0.76
7.350	-3344	39	1.43	0.77
7.355	-3348	39	1.44	0.77
7.360	-3351		1.45	0.76
7.365	-3355	43	1.44	0.76
7.370	-3359	43	1.44	0.76
7.375	-3362	42	1.44	0.76
7.380	-3366	42	1.45	0.76
7.385	-3370	42	1.46	0.76
7.390	-3373	42	1.47	0.75
7.395	-3377	42	1.47	0.75
7.400	-3381	46	1.47	0.74
7.405	-3384	47	1.46	0.74
7.410	-3388	46	1.45	0.75
7.415	-3392	47	1.45	0.76
7.420	-3395	48	1.44	0.76
7.425	-3399	48	1.44	0.76
7.430	-3403	49	1.44	0.76

7.435	-3406	48	1.45	0.76
7.440	-3410	49	1.45	0.75
7.445	-3414	50	1.45	0.75
7.450	-3417	50	1.47	0.75
7.455	-3421	50	1.46	0.74
7.460	-3425	50	1.47	0.75
7.465	-3428	52	1.46	0.75
7.470	-3432	51	1.45	0.75
7.475	-3436	51	1.46	0.76
7.480	-3439	50	1.46	0.75
7.485	-3443	50	1.49	0.75
7.490	-3447	51	1.47	0.73
7.495	-3450	51	1.46	0.74
7.500	-3454	51	1.48	0.75
7.505		51	1.48	0.74
7.510		50	1.47	0.74
7.515		52	1.47	0.74
7.520		51	1.46	0.74
7.525		51	1.47	0.75
7.530		51	1.47	0.74
7.535		50	1.46	0.74
7.540		50	1.46	0.75
7.545		50	1.46	0.75
7.550		49	1.47	0.75
7.555		50	1.47	0.74
7.560		49	1.44	0.75
7.565		50	1.47	0.76
7.570		47	1.44	0.74
7.575		48	1.44	0.76
7.580		47	1.43	0.76
7.585		46	1.44	0.76
7.590		44	1.43	0.76
7.595		43	1.45	0.76
7.600		44	1.45	0.76
7.605		44	1.44	0.75
7.610		43	1.43	0.76
7.615		43	1.43	0.76
7.620		43	1.44	0.76
7.625		43	1.45	0.76
7.630		43	1.45	0.76
7.635		43	1.44	0.76
7.640		43	1.45	0.76
7.645		43	1.45	0.76
7.650			1.46	0.75
7.655			1.45	0.75
7.660		45	1.45	0.75
7.665		45	1.43	0.75
7.670		45	1.45	0.76

7.675	47	1.45	0.76
7.680	47	1.44	0.75
7.685	47	1.43	0.76
7.690	47	1.43	0.77
7.695	46	1.44	0.76
7.700	46	1.45	0.76
7.705	46	1.46	0.75
7.710	46	1.46	0.75
7.715	46	1.47	0.75
7.720	46	1.48	0.75
7.725	45	1.48	0.74
7.730	45	1.48	0.74
7.735	45	1.47	0.74
7.740	45	1.46	0.74
7.745	44	1.46	0.75
7.750	44	1.47	0.75
7.755	45	1.48	0.74
7.760	45	1.46	0.74
7.765	45	1.46	0.75
7.770		1.45	0.75
7.775		1.43	0.76
7.780	40	1.43	0.77
7.785	45	1.38	0.77
7.790	65	1.15	0.79

Core-ID: AM09-PC-S-618

Depth [m]	Year BC/AD	MS-point [m ³ /kg]	Depth [m]	Year BC/AD	MS-point [m ³ /kg]
0.01	2009	13	0.46	1676	71
0.02	2001	62	0.47	1670	72
0.03	1993	59	0.48	1664	75
0.04	1985	66	0.49	1658	74
0.05	1976	58	0.5	1652	80
0.06	1968	57	0.51	1646	74
0.07	1960	54	0.52	1640	69
0.08	1952	52	0.53	1634	74
0.09	1944	64	0.54	1628	71
0.1	1936	62	0.55	1622	74
0.11	1928	60	0.56	1616	77
0.12	1920	59	0.57	1610	71
0.13	1911	52	0.58	1604	79
0.14	1903	58	0.59	1598	78
0.15	1895	59	0.6	1592	75
0.16	1887	57	0.61	1586	71
0.17	1879	59	0.62	1580	71
0.18	1871	59	0.63	1574	72
0.19	1863	58	0.64	1568	70
0.2	1854	53	0.65	1562	70
0.21	1846	48	0.66	1556	43
0.22	1838	60	0.67	1550	34
0.23	1830	56	0.68	1544	25
0.24	1822	69	0.69	1538	
0.25	1814	71	0.7	1532	
0.26	1806	65	0.71	1526	
0.27	1798	63	0.72	1520	
0.28	1789	49	0.73	1514	75
0.29	1781	54	0.74	1508	81
0.3	1773	52	0.75	1502	85
0.31	1766	60	0.76	1496	78
0.32	1760	67	0.77	1490	82
0.33	1754	48	0.78	1484	78
0.34	1748	43	0.79	1478	79
0.35	1742	58	0.8	1472	80
0.36	1736	64	0.81	1466	89
0.37	1730	66	0.82	1460	77
0.38	1724	67	0.83	1454	77
0.39	1718	68	0.84	1448	79
0.4	1712	74	0.85	1442	76
0.41	1706	70	0.86	1436	79
0.42	1700	35	0.87	1430	74
0.43	1694	72	0.88	1424	72
0.44	1688	66	0.89	1418	70
0.45	1682	51	0.9	1412	72

continued

Depth [m]	Year BC/AD	MS-point [m^3/kg]	Depth [m]	Year BC/AD	MS-point [m^3/kg]
0.91	1406	68	1.36	1082	70
0.92	1400		1.37	1073	66
0.93	1394	68	1.38	1065	61
0.94	1388	69	1.39	1057	63
0.95	1382	68	1.4	1049	64
0.96	1376	68	1.41	1041	61
0.97	1370	58	1.42	1032	60
0.98	1364	68	1.43	1024	66
0.99	1358	67	1.44	1016	
1	1352	66	1.45	1008	59
1.01	1346	66	1.46	1000	58
1.02	1340	69	1.47	992	59
1.03	1334	67	1.48	983	61
1.04	1328	61	1.49	975	61
1.05	1322	66	1.5	967	64
1.06	1316	67	1.51	959	63
1.07	1310	65	1.52	951	59
1.08	1304	63	1.53	942	60
1.09	1298	59	1.54	934	61
1.1	1292	63	1.55	926	57
1.11	1286	60	1.56	918	58
1.12	1278	61	1.57	910	61
1.13	1270	62	1.58	902	58
1.14	1261	63	1.59	893	54
1.15	1253	61	1.6	885	60
1.16	1245	64	1.61	877	59
1.17	1237	62	1.62	869	56
1.18	1229	55	1.63	861	58
1.19	1221	65	1.64	852	65
1.2	1212	64	1.65	844	66
1.21	1204	63	1.66	836	65
1.22	1196	63	1.67	828	66
1.23	1188	63	1.68	820	66
1.24	1180	61	1.69	812	62
1.25	1171	64	1.7	803	
1.26	1163	64	1.71	795	
1.27	1155	63	1.72	787	
1.28	1147	61	1.73	779	
1.29	1139	64	1.74	771	
1.3	1131	66	1.75	762	
1.31	1122	65	1.76	754	
1.32	1114	56	1.77	746	57
1.33	1106	67	1.78	738	58
1.34	1098	65	1.79	730	57
1.35	1090	65	1.8	722	58

continued

Depth [m]	Year BC/AD	MS-point [m ³ /kg]	Depth [m]	Year BC/AD	MS-point [m ³ /kg]
1.81	713	61	2.26	344	53
1.82	705	59	2.27	335	48
1.83	697	60	2.28	327	53
1.84	689	60	2.29	319	54
1.85	681	62	2.3	311	52
1.86	673	60	2.31	302	52
1.87	664	63	2.32	294	57
1.88	656	64	2.33	286	54
1.89	648	63	2.34	277	53
1.9	640	61	2.35	269	54
1.91	632	62	2.36	261	52
1.92	623	59	2.37	252	54
1.93	615		2.38	244	57
1.94	607	63	2.39	236	53
1.95	599	63	2.4	228	54
1.96	591	62	2.41	219	55
1.97	583	62	2.42	211	47
1.98	574	66	2.43	203	38
1.99	566	67	2.44	194	42
2	558	67	2.45	186	46
2.01	550	65	2.46	178	48
2.02	542	68	2.47	170	51
2.03	533	66	2.48	161	52
2.04	525	60	2.49	153	41
2.05	517	63	2.5	145	55
2.06	509	64	2.51	136	52
2.07	501	75	2.52	128	57
2.08	493	73	2.53	120	56
2.09	484	63	2.54	112	56
2.1	476	57	2.55	103	57
2.11	468	59	2.56	95	65
2.12	460	60	2.57	87	55
2.13	451	59	2.58	78	52
2.14	443	61	2.59	70	45
2.15	435	57	2.6	62	37
2.16	427	59	2.61	54	55
2.17	418	58	2.62	45	53
2.18	410	57	2.63	37	47
2.19	402	52	2.64	29	51
2.2	393	54	2.65	20	52
2.21	385	57	2.66	12	55
2.22	377	56	2.67	4	53
2.23	369	55	2.68	-4	
2.24	360	52	2.69	-13	51
2.25	352	52	2.7	-21	

continued

Depth [m]	Year BC/AD	MS-point [m ³ /kg]	Depth [m]	Year BC/AD	MS-point [m ³ /kg]
2.71	-29		3.16	-378	67
2.72	-38		3.17	-385	65
2.73	-46		3.18	-391	62
2.74	-54	52	3.19	-398	63
2.75	-62	62	3.2	-405	63
2.76	-71	57	3.21	-412	60
2.77	-79	54	3.22	-418	64
2.78	-87	52	3.23	-425	61
2.79	-96	53	3.24	-432	60
2.8	-104	53	3.25	-438	58
2.81	-112	53	3.26	-445	61
2.82	-121	54	3.27	-452	65
2.83	-129	53	3.28	-458	65
2.84	-137	52	3.29	-465	67
2.85	-145	53	3.3	-472	67
2.86	-154	56	3.31	-479	66
2.87	-162	55	3.32	-485	64
2.88	-170	22	3.33	-492	69
2.89	-179	25	3.34	-499	69
2.9	-187	36	3.35	-505	71
2.91	-195	19	3.36	-512	66
2.92	-203	21	3.37	-519	63
2.93	-212	43	3.38	-525	65
2.94	-220	58	3.39	-532	67
2.95	-228	65	3.4	-539	64
2.96	-237	62	3.41	-546	62
2.97	-245	66	3.42	-552	68
2.98	-253	68	3.43	-559	68
2.99	-261	65	3.44	-566	57
3	-270	71	3.45	-572	67
3.01	-278	62	3.46	-579	62
3.02	-284	70	3.47	-586	64
3.03	-291	69	3.48	-592	65
3.04	-298	69	3.49	-599	66
3.05	-304	69	3.5	-606	66
3.06	-311	73	3.51	-613	70
3.07	-318	70	3.52	-619	69
3.08	-324	66	3.53	-626	63
3.09	-331	66	3.54	-633	61
3.1	-338	56	3.55	-639	65
3.11	-345	67	3.56	-646	60
3.12	-351	68	3.57	-653	67
3.13	-358	67	3.58	-659	68
3.14	-365	69	3.59	-666	67
3.15	-371	69	3.6	-673	68

continued

Depth [m]	Year BC/AD	MS-point [m ³ /kg]	Depth [m]	Year BC/AD	MS-point [m ³ /kg]
3.61	-680	68	4.06	-981	51
3.62	-686	66	4.07	-988	53
3.63	-693	64	4.08	-994	55
3.64	-700	74	4.09	-1001	51
3.65	-706	63	4.1	-1008	58
3.66	-713	54	4.11	-1015	52
3.67	-720	64	4.12	-1021	49
3.68	-726	59	4.13	-1028	54
3.69	-733	65	4.14	-1035	50
3.7	-740	61	4.15	-1041	51
3.71	-747	59	4.16	-1048	51
3.72	-753	47	4.17	-1055	48
3.73	-760		4.18	-1061	50
3.74	-767		4.19	-1068	49
3.75	-773		4.2	-1075	49
3.76	-780	61	4.21	-1082	46
3.77	-787	63	4.22	-1088	48
3.78	-793	54	4.23	-1095	46
3.79	-800	57	4.24	-1102	47
3.8	-807	58	4.25	-1108	49
3.81	-814	58	4.26	-1115	45
3.82	-820	58	4.27	-1122	47
3.83	-827	55	4.28	-1128	50
3.84	-834	59	4.29	-1135	50
3.85	-840	55	4.3	-1142	51
3.86	-847	56	4.31	-1149	47
3.87	-854	65	4.32	-1155	49
3.88	-860	57	4.33	-1162	52
3.89	-867	56	4.34	-1169	49
3.9	-874	56	4.35	-1175	51
3.91	-881	56	4.36	-1182	51
3.92	-887	59	4.37	-1189	51
3.93	-894		4.38	-1195	50
3.94	-901	56	4.39	-1202	49
3.95	-907	56	4.4	-1209	46
3.96	-914	55	4.41	-1216	48
3.97	-921		4.42	-1222	47
3.98	-927	47	4.43	-1229	49
3.99	-934	54	4.44	-1236	48
4	-941	57	4.45	-1242	44
4.01	-948	53	4.46	-1249	43
4.02	-954	54	4.47	-1256	41
4.03	-961	55	4.48	-1262	39
4.04	-968	52	4.49	-1269	41
4.05	-974	53	4.5	-1276	40

continued

Depth [m]	Year BC/AD	MS-point [m ³ /kg]	Depth [m]	Year BC/AD	MS-point [m ³ /kg]
4.51	-1283	42	4.96	-1584	61
4.52	-1289	48	4.97	-1591	57
4.53	-1296	33	4.98	-1597	55
4.54	-1303	17	4.99	-1604	53
4.55	-1309	30	5	-1611	58
4.56	-1316	39	5.01	-1618	59
4.57	-1323	42	5.02	-1625	60
4.58	-1329	49	5.03	-1633	57
4.59	-1336	45	5.04	-1640	56
4.6	-1343	39	5.05	-1647	60
4.61	-1350	42	5.06	-1655	59
4.62	-1356	43	5.07	-1662	56
4.63	-1363	41	5.08	-1669	60
4.64	-1370	41	5.09	-1677	63
4.65	-1376	46	5.1	-1684	59
4.66	-1383	47	5.11	-1691	61
4.67	-1390	47	5.12	-1699	
4.68	-1396	48	5.13	-1706	62
4.69	-1403	49	5.14	-1713	58
4.7	-1410	51	5.15	-1721	57
4.71	-1417	53	5.16	-1728	55
4.72	-1423	47	5.17	-1736	58
4.73	-1430		5.18	-1743	58
4.74	-1437	48	5.19	-1750	56
4.75	-1443	49	5.2	-1758	55
4.76	-1450	53	5.21	-1765	57
4.77	-1457	46	5.22	-1772	53
4.78	-1463	43	5.23	-1780	58
4.79	-1470	39	5.24	-1787	54
4.8	-1477	27	5.25	-1794	55
4.81	-1484	18	5.26	-1802	56
4.82	-1490	15	5.27	-1809	56
4.83	-1497	65	5.28	-1816	56
4.84	-1504	48	5.29	-1824	56
4.85	-1510	61	5.3	-1831	62
4.86	-1517	43	5.31	-1838	62
4.87	-1524	57	5.32	-1846	65
4.88	-1530	60	5.33	-1853	59
4.89	-1537	62	5.34	-1860	59
4.9	-1544	59	5.35	-1868	66
4.91	-1551	59	5.36	-1875	58
4.92	-1557	57	5.37	-1882	56
4.93	-1564	65	5.38	-1890	56
4.94	-1571	70	5.39	-1897	56
4.95	-1577	59	5.4	-1904	56

continued

Depth [m]	Year BC/AD	MS-point [m ³ /kg]	Depth [m]	Year BC/AD	MS-point [m ³ /kg]
5.41	-1912	58	5.86	-2242	50
5.42	-1919	54	5.87	-2250	47
5.43	-1926	55	5.88	-2257	48
5.44	-1934	61	5.89	-2264	59
5.45	-1941	62	5.9	-2272	33
5.46	-1948	68	5.91	-2279	14
5.47	-1956	34	5.92	-2286	17
5.48	-1963	30	5.93	-2294	43
5.49	-1971	26	5.94	-2301	42
5.5	-1978	37	5.95	-2308	39
5.51	-1985	46	5.96	-2316	36
5.52	-1993	51	5.97	-2323	33
5.53	-2000	53	5.98	-2330	32
5.54	-2007	53	5.99	-2338	30
5.55	-2015	52	6	-2345	28
5.56	-2022	50	6.01	-2352	28
5.57	-2029	51	6.02	-2360	31
5.58	-2037	47	6.03	-2367	28
5.59	-2044	47	6.04	-2374	28
5.6	-2051	29	6.05	-2382	27
5.61	-2059	46	6.06	-2389	28
5.62	-2066	50	6.07	-2396	30
5.63	-2073	52	6.08	-2404	30
5.64	-2081	54	6.09	-2411	28
5.65	-2088	58	6.1	-2418	34
5.66	-2095	57	6.11	-2426	39
5.67	-2103	55	6.12	-2433	37
5.68	-2110	60	6.13	-2441	40
5.69	-2117	57	6.14	-2448	33
5.7	-2125	53	6.15	-2455	39
5.71	-2132	50	6.16	-2463	31
5.72	-2139	46	6.17	-2470	30
5.73	-2147	51	6.18	-2477	34
5.74	-2154	41	6.19	-2485	35
5.75	-2161	52	6.2	-2492	40
5.76	-2169	48	6.21	-2499	21
5.77	-2176	48	6.22	-2507	34
5.78	-2183		6.23	-2514	34
5.79	-2191	45	6.24	-2521	40
5.8	-2198	41	6.25	-2529	43
5.81	-2206	39	6.26	-2536	47
5.82	-2213	13	6.27	-2543	47
5.83	-2220	8	6.28	-2551	48
5.84	-2228	32	6.29	-2558	48
5.85	-2235	52	6.3	-2565	49

continued

Depth [m]	Year BC/AD	MS-point [m ³ /kg]	Depth [m]	Year BC/AD	MS-point [m ³ /kg]
6.31	-2573	48	6.76	-2903	37
6.32	-2580	47	6.77	-2911	36
6.33	-2587	48	6.78	-2918	38
6.34	-2595	46	6.79	-2925	38
6.35	-2602	44	6.8	-2933	40
6.36	-2609	45	6.81	-2940	34
6.37	-2617	29	6.82	-2947	28
6.38	-2624	47	6.83	-2955	49
6.39	-2631	46	6.84	-2962	2
6.4	-2639	26	6.85	-2969	10
6.41	-2646	49	6.86	-2977	19
6.42	-2654	45	6.87	-2984	52
6.43	-2661	47	6.88	-2991	50
6.44	-2668	45	6.89	-2999	37
6.45	-2676	48	6.9	-3006	46
6.46	-2683	47	6.91	-3013	60
6.47	-2690	44	6.92	-3021	33
6.48	-2698	45	6.93	-3028	47
6.49	-2705	46	6.94	-3035	50
6.5	-2712	23	6.95	-3043	46
6.51	-2720	35	6.96	-3050	48
6.52	-2727	39	6.97	-3057	54
6.53	-2734	39	6.98	-3065	52
6.54	-2742	43	6.99	-3072	54
6.55	-2749	41	7	-3079	50
6.56	-2756	42	7.01	-3087	23
6.57	-2764	44	7.02	-3094	17
6.58	-2771	43	7.03	-3101	29
6.59	-2778	42	7.04	-3109	48
6.6	-2786	43	7.05	-3116	51
6.61	-2793	48	7.06	-3124	53
6.62	-2800	49	7.07	-3131	52
6.63	-2808	50	7.08	-3138	47
6.64	-2815	50	7.09	-3146	49
6.65	-2822	23	7.1	-3153	50
6.66	-2830	22	7.11	-3160	57
6.67	-2837	31	7.12	-3168	53
6.68	-2844	44	7.13	-3175	47
6.69	-2852	36	7.14	-3182	57
6.7	-2859	40	7.15	-3190	54
6.71	-2866	31	7.16	-3197	55
6.72	-2874	23	7.17	-3204	60
6.73	-2881	35	7.18	-3212	61
6.74	-2889	42	7.19	-3219	69
6.75	-2896	38	7.2	-3226	

continued

Depth [m]	Year BC/AD	MS-point [m ³ /kg]
7.21	-3234	70
7.22	-3241	56
7.23	-3248	48
7.24	-3256	51
7.25	-3263	50
7.26	-3270	46
7.27	-3278	47
7.28	-3285	51
7.29	-3292	48
7.3	-3300	51
7.31	-3307	50
7.32	-3314	50
7.33	-3322	48
7.34	-3329	47
7.35	-3336	46
7.36	-3344	49
7.37	-3351	48
7.38	-3359	55
7.39	-3366	55
7.4	-3373	61
7.41	-3381	73
7.42	-3388	72
7.43	-3395	69
7.44	-3403	63
7.45	-3410	68
7.46	-3417	73
7.47	-3425	70
7.48	-3432	75
7.49	-3439	75
7.5	-3447	75
7.51	-3454	79

Appendix I

Geochemistry data for piston cores 2009, Labrador

Appendix I contains geochemical data for the piston cores 2009 from Nachvak and Saglek Fjords. The tables list Total Organic Carbon [%], Total Nitrogen [%], C/N-ratios, and $\delta^{13}\text{C}$. Depth intervals are in cm. Time intervals (Years BC/AD) were calculated in cm intervals by interpolating between $^{14}\text{C}_{\text{cal}}$ dates. TOC and TN were measured using a Carlo Erba NA 1500 Series 2 elemental analyzer and $\delta^{13}\text{C}$ was measured using a Thermo Electron Delta V Plus mass spectrometer.

Core-ID: AM09-PC-N-606

Depth [cm]	Year BC/AD	TOC [%]	TN [%]	C/N	$\delta^{13}\text{C}$
0.5	2009	2.24	0.20	11.21	-24.21
5.5	1961	1.46	0.17	8.60	-22.03
10.5	1913	1.31	0.15	8.73	-21.94
15.5	1865	1.37	0.16	8.78	-22.04
20.5	1817	1.30	0.15	8.78	-21.99
25.5	1769	1.42	0.16	8.94	-22.07
30.5	1721	1.33	0.15	8.74	-22.30
35.5	1663	1.33	0.15	8.79	-21.95
40.5	1606	1.35	0.15	8.93	-21.98
45.5	1548	1.33	0.15	8.89	-21.96
50.5	1490	1.21	0.14	8.80	-22.16
55.5	1432	1.23	0.14	8.94	-22.15
60.5	1375	1.17	0.13	8.72	-22.10
65.5	1317	1.14	0.13	8.73	-22.14
70.5	1259	1.28	0.14	9.09	-22.04
75.5	1202	1.22	0.15	8.43	-21.92
80.5	1144	1.17	0.13	8.91	-22.00
85.5	1086	1.21	0.14	8.86	-22.04
90.5	1028	1.19	0.13	8.91	-21.87
95.5	971	1.26	0.14	8.90	-22.16
100.5	913	1.36	0.15	8.98	-22.65
105.5	855	1.29	0.14	8.99	-22.23
110.5	798	1.34	0.15	8.96	-22.00
115.5	733	1.34	0.15	9.05	-22.08
120.5	668	1.30	0.15	8.81	-21.90
125.5	603	1.32	0.15	8.95	-22.05
130.5	538	1.34	0.15	8.95	-22.35
135.5	473	1.46	0.16	9.14	-22.02
140.5	408	1.39	0.15	9.11	-22.27
145.5	343	1.36	0.15	8.98	-21.81
150.5	278	1.26	0.14	8.94	-21.88
155.5	213	1.24	0.14	9.08	-22.09
160.5	148	1.15	0.13	9.09	-21.99
165.5	83	1.25	0.14	9.09	-22.29
170.5	18	1.14	0.13	9.12	-22.16
175.5	-47	1.20	0.13	9.14	-22.42
180.5	-111	1.18	0.13	9.25	-22.48
185.5	-176	1.18	0.13	9.09	-22.22
190.5	-241	1.18	0.13	9.24	-22.51
195.5	-306	1.16	0.13	9.17	-22.56
200.5	-371	1.18	0.13	9.11	-22.31
205.5	-436	1.28	0.14	9.23	-22.36
210.5	-501	1.22	0.13	9.13	-22.52
215.5	-556	1.19	0.13	9.03	-22.34
220.5	-612	1.23	0.14	9.10	-22.48

continued

Depth [cm]	Year BC/AI	TOC [%]	TN [%]	C/N	$\delta^{13}\text{C}$
225.5	-667	1.22	0.13	9.26	-22.38
230.5	-722	1.23	0.13	9.27	-22.42
235.5	-777	1.33	0.14	9.39	-22.31
240.5	-833	1.27	0.14	9.08	-22.33
245.5	-888	1.23	0.14	8.94	-22.39
250.5	-943	1.20	0.13	9.16	-22.37
255.5	-999	1.21	0.13	9.16	-22.63
260.5	-1054	1.24	0.14	9.12	-22.08
265.5	-1109	1.29	0.14	9.39	-22.71
270.5	-1164	1.25	0.13	9.31	-22.68
275.5	-1220	1.25	0.14	9.15	-22.40
280.5	-1275	1.29	0.14	9.27	-22.47
285.5	-1330	1.24	0.14	9.12	-22.40
290.5	-1385	1.34	0.14	9.31	-22.24
295.5	-1441	1.27	0.14	9.24	-22.47
300.5	-1496	1.18	0.15	7.76	-22.30
305.5	-1550	1.18	0.15	7.66	-22.38
325.5	-1550	1.30	0.18	7.42	-22.16
350.5	-1766	1.15	0.15	7.62	-22.21
375.5	-2036	1.18	0.15	7.82	-22.63
400.5	-2306	1.25	0.16	7.64	-22.38
425.5	-2577	1.30	0.18	7.40	-22.35
450.5	-2847	1.13	0.15	7.57	-22.45
475.5	-3117	1.11	0.15	7.66	-22.59
500.5	-3388	0.88	0.11	8.11	-22.63
525.5	-3658	0.96	0.12	7.95	-22.92
550.5	-4170	0.82	0.10	8.29	-22.96
575.5	-4683	0.81	0.09	8.59	-22.76
600.5	-5195	0.81	0.09	8.75	-23.35
625.5	-5707	0.76	0.08	9.22	-23.42
650.5	-6219	0.71	0.07	9.54	-23.53
675.5	-6732	0.64	0.06	10.16	-23.77
700.5	-7244	0.71	0.08	9.52	-23.53
725.5	-7756	0.65	0.07	10.05	-23.74
750.5	-8269	0.67	0.06	10.76	-24.02
775.5	-8781	0.76	0.07	10.20	-23.82
800.5	-9293	0.68	0.06	10.83	-23.93

Core-ID: AM09-PC-N-606

Depth [cm]	Year BC/AD	TOC [%]	TN [%]	C/N	$\delta^{13}\text{C}$
0.5	2009	1.98	0.32	6.29	-22.65
5.5	1968	1.88	0.30	6.38	-22.45
10.5	1928	1.88	0.29	6.43	-22.53
15.5	1887	2.27	0.36	6.23	-23.90
20.5	1846	1.81	0.27	6.66	-22.44
25.5	1806	1.77	0.26	6.75	-22.23
30.5	1766	1.80	0.27	6.80	-22.35
35.5	1736	1.78	0.26	6.82	-22.13
40.5	1706	2.04	0.22	9.11	-21.90
45.5	1676	2.09	0.24	8.86	-21.99
50.5	1646	2.05	0.23	8.87	-22.06
55.5	1616	2.04	0.23	8.90	-22.09
60.5	1586	2.01	0.23	8.89	-22.19
65.5	1556	2.04	0.23	8.78	-22.25
70.5	1526	2.10	0.23	9.26	-22.66
75.5	1496	1.97	0.22	8.86	-22.24
80.5	1466	2.13	0.24	8.74	-21.89
85.5	1436	2.10	0.24	8.84	-21.92
90.5	1406	2.14	0.24	8.81	-21.93
95.5	1376	2.13	0.24	8.84	-21.90
100.5	1346	2.13	0.24	8.76	-22.05
105.5	1316	2.17	0.24	8.87	-22.06
110.5	1286	2.12	0.24	8.68	-21.99
115.5	1245	2.13	0.24	8.72	-22.06
120.5	1204	2.00	0.23	8.65	-21.89
125.5	1163	1.98	0.23	8.75	-22.28
130.5	1122	2.15	0.24	8.84	-21.86
135.5	1082	2.05	0.23	9.04	-22.02
140.5	1041	2.12	0.24	8.83	-21.91
145.5	1000	2.04	0.23	9.04	-21.92
150.5	959	2.18	0.25	8.85	-22.03
155.5	918	2.17	0.24	9.15	-21.97
160.5	877	2.16	0.24	8.84	-22.05
165.5	836	2.07	0.24	8.79	-22.36
170.5	795	2.03	0.23	9.02	-22.04
175.5	754	2.10	0.23	8.97	-22.04
180.5	713	2.15	0.24	8.82	-21.99
185.5	673	2.11	0.24	8.95	-21.83
190.5	632	2.31	0.23	9.97	-21.87
195.5	591	2.24	0.23	9.94	-22.20
200.5	550	2.23	0.22	10.15	-22.22
205.5	509	2.24	0.22	10.08	-22.16
210.5	468	2.23	0.22	10.10	-22.32
215.5	427	2.23	0.22	10.19	-22.27
220.5	385	2.24	0.22	10.09	-22.22

Core-ID: AM09-PC-N-606

Depth [cm]	Year BC/AD	TOC [%]	TN [%]	C/N	$\delta^{13}\text{C}$
225.5	344	2.26	0.23	10.02	-22.38
230.5	302	2.27	0.23	9.90	-22.33
235.5	261	2.29	0.22	10.41	-22.29
240.5	219	2.33	0.23	10.30	-22.27
245.5	178	2.21	0.22	10.24	-22.49
250.5	136	2.33	0.23	10.13	-22.35
255.5	95	2.41	0.24	10.08	-22.38
260.5	54	2.39	0.24	10.10	-22.24
265.5	12	2.45	0.24	10.25	-22.53
270.5	-29	2.28	0.23	9.97	-22.26
275.5	-71	2.31	0.23	9.94	-22.21
280.5	-112	2.23	0.22	10.21	-22.12
285.5	-154	2.14	0.22	9.92	-22.59
290.5	-195	2.15	0.22	9.94	-22.50
295.5	-237	2.27	0.23	9.93	-23.86
300.5	-278	2.04	0.20	10.12	-22.43
325.5	-445	1.94	0.20	9.96	-22.34
350.5	-613	2.08	0.21	10.02	-22.32
375.5	-780	2.08	0.20	10.24	-22.26
400.5	-948	2.16	0.21	10.26	-22.08
425.5	-1115	2.29	0.22	10.59	-22.63
450.5	-1283	2.25	0.21	10.56	-22.46
475.5	-1450	2.04	0.20	10.18	-22.55
500.5	-1618	2.01	0.23	8.75	-22.53
525.5	-1802	2.06	0.24	8.56	-22.49
550.5	-1985	2.18	0.26	8.50	-22.43
575.5	-2169	2.33	0.27	8.61	-22.33
600.5	-2352	2.11	0.25	8.46	-22.40
625.5	-2536	2.11	0.24	8.71	-22.43
650.5	-2720	1.90	0.22	8.72	-22.59
675.5	-2903	2.05	0.24	8.55	-22.65
700.5	-3087	1.90	0.22	8.61	-22.69
725.5	-3270	1.84	0.21	8.62	-22.40
750.5	-3454	1.86	0.22	8.59	-22.52

Appendix J

X-radiographic images piston cores 2009, Labrador

Appendix J contains x-radiographic images for piston cores from Nachvak and Saglek Fjords, Labrador. Sediment cores were imaged x-radiographically using a Thales Flashscan 35 X-ray detector, illuminated with a Lorad LPX 160 X-ray generator. To increase image quality, an aluminum compensator plate was designed to counterbalance decreasing core thickness towards the sides of the core.

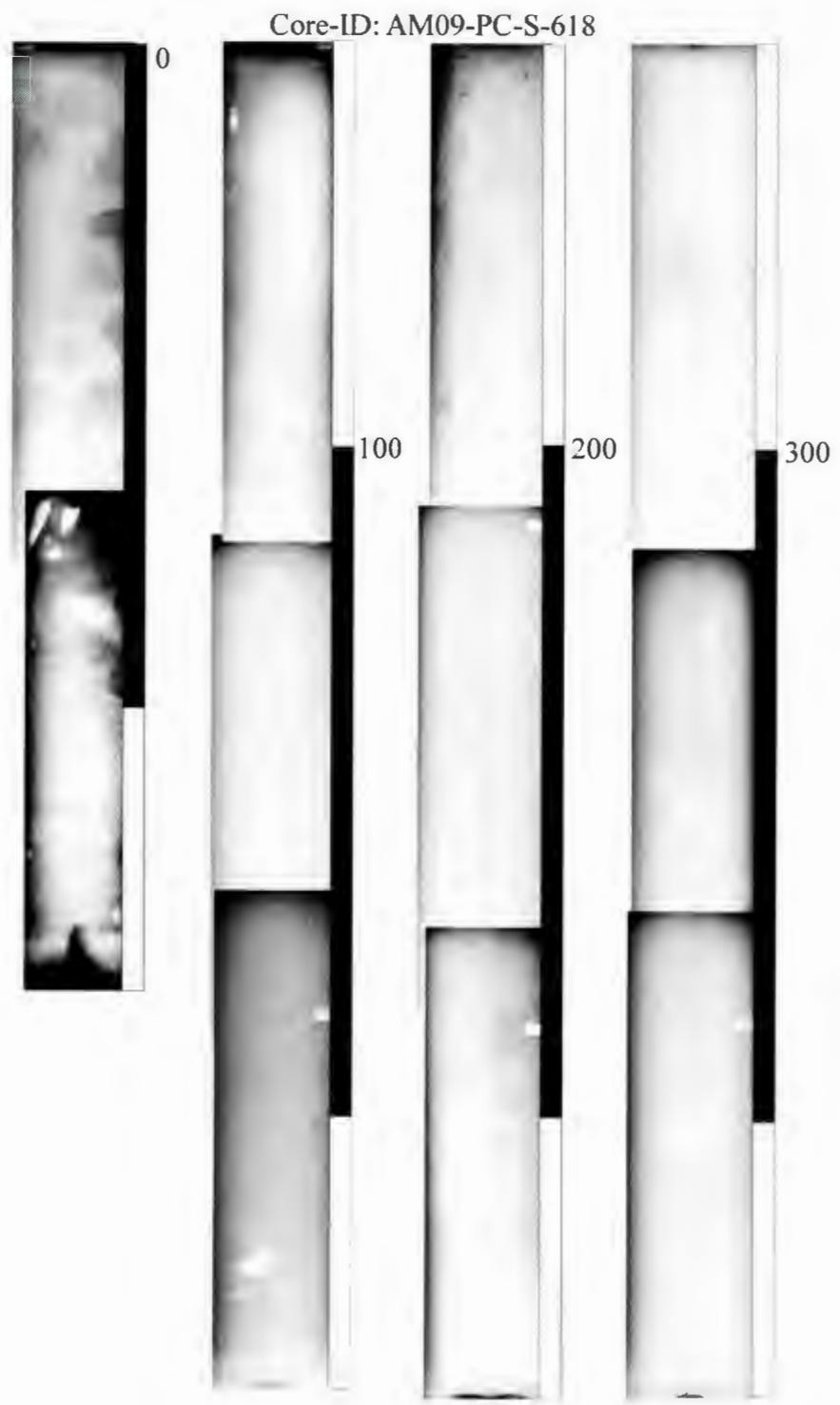
Core-ID: AM09-PC-N-606



continued



Depth in Seabed [cm]



continued

